



Università degli Studi di Cagliari

PHD DEGREE IN LIFE, ENVIRONMENTAL, AND DRUG SCIENCES

XXXII cycle

TITLE OF THE PHD THESIS

ULTRA CLOSE-RANGE DIGITAL PHOTOGRAMMETRY AS A TOOL  
TO PRESERVE, STUDY, AND SHARE SKELETAL REMAINS

Scientific disciplinary sector      BIO/08 – Anthropology

PhD Student      [Paolo Lussu](#)

Coordinator of the PhD Programme      [Simona Distinto](#)

Supervisor      [Elisabetta Marini](#)

Final exam. Academic Year 2018 – 2019

Thesis defence: June - July 2020 Session

To my loved ones.

*“Admiral, how can you speak of failure?”*

*You must look at what you have done: your whole life has been a triumph!*

*What did God do more, for Moses – or for David, his servant – than he did for you?*

*The barriers of the Ocean Sea – which were closed with such mighty chains – have been opened by you!*

*You have given us a whole new world. A world without limits. From it will come the wealth to make Spain the most powerful nation on Earth. Within it, Christianity will grow and flourish. New and great peoples will be found. Splendid new cities will rise into the Heavens.*

*You have given us – all of humanity – a future. Rejoice in your life, admiral! Rejoice in it!”*

Faye Dunaway plays Queen Isabella of Spain in *Christopher Columbus*, TV mini-series, 1985.

# CONTENTS

<b>INTRODUCTION .....</b>	<b>6</b>
Digital technologies for skeletal collections management: opportunities and issues .....	6
The role of virtual anthropology .....	11
Techniques for three-dimensional reconstruction .....	18
Principles and methods of digital photogrammetry .....	20
Historical development of digital photogrammetry .....	24
Three-dimensional data description and storage .....	28
The skeletal collection at the University of Cagliari .....	36
Aim of the research .....	37
<b>THE STATE OF THE ART: UCR-DP IN SKELETAL ANTHROPOLOGY ...</b>	<b>40</b>
The necessity for a systematic review .....	40
Review protocol – Search strategy and eligibility criteria.....	42
Review protocol – Data collection and paper analysis .....	43
Search yield and bibliographic characteristics .....	43
Applications.....	49
Technical implementation.....	51
Accuracy and reliability .....	62
Limits .....	67
Conclusions.....	68

<b>A NEW APPROACH: CLOUD-BASED UCR-DP .....</b>	<b>70</b>
Offline versus cloud computing for UCR-DP .....	70
Materials and methods .....	72
Results .....	79
Discussion .....	98
Copyright issues.....	106
Limits .....	107
Conclusions.....	108
<b>THE DIGITALISED SAMPLE .....</b>	<b>109</b>
The Osteological Collection.....	109
The reconstructed sample.....	110
The Prehistoric Collection .....	113
The Historical Collection.....	115
The Modern Collection.....	116
Other reconstructed material .....	117
<b>UCR-DP APPLICATIONS AND CASE STUDIES .....</b>	<b>120</b>
Skeletal three-dimensional dataset applications.....	120
Digital skeletal collections to serve comparative and population studies.....	121
Guiding principles for preserving and disseminating digital collections .....	122
Planning durable online use and reuse .....	133
Values-led participatory designs to share skeletal collections .....	138



Open science and FAIR case study: the Teaching Collection of the University .....	139
Open science and FAIR reuse case study: a virtual laboratory of physical anthropology .....	140
Open science and FAIR case study: the sharing of the San Benedetto Collection .....	145
Value led participatory design case study: the MuSAE.....	147
<b>CONCLUSIONS.....</b>	<b>154</b>
<b>APPENDIX: UCR-DP PROTOCOL.....</b>	<b>157</b>
Software setup .....	157
Autodesk ReCap Pro and ReCap Photo .....	157
digiCamControl.....	160
Hardware setup.....	161
Preliminary settings.....	162
Data acquisition.....	164
Data processing and post-processing .....	166
<b>ACKNOWLEDGEMENTS.....</b>	<b>169</b>
<b>REFERENCES .....</b>	<b>170</b>
Bibliography.....	170
Figure index .....	191
Table index .....	199

## INTRODUCTION

### *Digital technologies for skeletal collections management: opportunities and issues*

As a result of the scientific knowledge cumulated in the fields of cultural heritage, Cultural and Biological Anthropology mainly after the discovery of the Americas, several institutions around the world are host to anthropological collections of specimens. Preserved specimens range from various types of artefacts – including tools, pieces of art, and religious expressions – to human remains. Among the latter, skeletal remains are the most represented since they are less prone to being altered by environmental conditions than any other biological structure.

Such collections are particularly stimulating because they tickle the anthropological curiosity we feel (1) for our own kind, our past, and our destiny, feeding the introspective thoughts that make us human; an interest confirmed by the vastness of the research on the human biological and cultural past published yearly, some of which will be discussed here, and by the attention of the public for related science communication essays (2–5), sites such as Pompeii (6,7), and exhibits, e.g. the Museo Archeologico di Bolzano which is host to the remains of Ötzi the glacier mummy (8–10).

However, some challenging problems arise with skeletal collection management and, despite their potential value in society, they are still difficult to be valued, i.e. making the specimens available for research and enjoyment by the public. The problems above fall into three main categories: preservation and organisation, study, and communication and dissemination.

#### *Preservation and organisation*

concern the necessity of conserving, protecting, and indexing the specimens and all related data for current and future use. It comprises specimen storage and restoration, along with data acquisition and structuring to allow efficient retrieval and interpretation. Detailed and accurate specimen documentation is of great help in case of damage or definitive loss of the collection,

preventing data loss whenever such unlikely events occur. Often, in the past, such topics have been addressed by finding an appropriate site to preserve the specimens, restoring them when possible, and indexing their data in a catalogue.

Nowadays, digital technologies enable much broader possibilities, the most intriguing of which entail three-dimensional reconstructions of the specimens to achieve their indefinitely long-lasting preservation and potential future use and reuse. To this purpose it is essential to associate metadata and paradata – i.e. any relevant information on how data was generated, is structured, and can be used – and to plan current and future data findability, accessibility, and interoperability to facilitate new applications for research and communication (11).

#### *Research*

is the first way in which skeletal collections are generally used. In particular, extensive skeletal collections potentially allow for robust anatomical (12,13), functional, and population studies (13–15). However, although many institutions preserve remarkable collections, their physical access is limited by practical issues – this is not only because of the rarity of the most ancient specimens.

Indeed, gathering a representative and possibly vast sample is still very difficult even for recent specimens as they are scattered among different institutions around the world, with insufficient information available online and, therefore, the need for study variables to be recorded measuring the specimen *in situ*.

Lastly, even when scientists succeed in gaining access to the specimens, it is not always possible to manipulate them because of conservation rules. Every time a specimen is manipulated, it is also damaged to some extent, which should be avoided to preserve significant and fragile remains.

As a result, population studies on skeletal features are relatively scanty and limited to small samples, particularly for early ones, where comparisons often include just a couple of specimens and even a sample of 10 is the exception.

Digitalising skeletal collections could help to achieve significant samples by gathering specimens around the world without any activity in the presence (12). Furthermore, a comprehensive online availability of extensive and open access collections of digital specimens would be of great help in reducing the scientific output gap between high-income, on one side, and middle- and low-income countries on the other.

#### *Communication and dissemination*

constitute the second way in which skeletal collections could – and definitely should – be used and reused. It is, actually, the most important way of use as the ultimate mission of science is not only to produce reliable information to be kept in ivory towers, but to share information and make humanity capable of enjoying and exploiting it, thus improving their living conditions (16) and ultimately the survival chances of the species, at least for the near future. Therefore, skeletal collections could play a key role in making humanity aware of its past.

Nevertheless, significant issues limiting the open access to 3D models are related to the intensive resources associated with their scanning and post-production (17), and the constraints deriving from intellectual property rights (18,19).

The most widely used techniques for digitising skeletal specimens are CT and laser scanning (20–24), with CT-scanning being recognised as the gold standard (21,25). Such techniques are both resource-intensive in terms of hardware, labour, and therefore overall cost (13).

Indeed, some 3D surface scanners based on structured light – e.g. the [Spider](#) (Artec 3D, Luxembourg) (26) – have recently become extremely handy and relatively fast in achieving high-resolution three-dimensional reconstructions with photorealistic textures. However, the scanning and reconstruction times are still considerable and so is the cost of the hardware. Hence, other alternatives could be preferable when documenting extensive collections or samples.

Limitations in accessing skeletal collection for research purposes are not only technical. As highlighted in a recent *Nature* analysis, scientists are reluctant to share their three-dimensional data (19), and even when some form of sharing occurs, it happens upon request, or temporarily, during short-term exhibitions or meetings (17,27–30). Researchers traditionally do not share data about their ongoing or future work because of their fear of receiving insufficient acknowledgement by scientists who use it. Museums are also concerned with sharing data from the collections in their care because of economic reasons and copyright policies.

Lastly, the sharing of anthropological remains is also limited by ethical and political reasons, e.g. in the case of remains from indigenous people, who generally do not approve their publication (19).

The restrictions surrounding the free sharing of three-dimensional data reduce the opportunities for communication within science, and hence the potential for scientific knowledge evolution. However, many limitations could be overcome by using more straightforward techniques for 3D reconstruction – such as, for instance, ultra close-range digital photogrammetry (UCR-DP), discussed in the present thesis – and by following open science principles and FAIR guidelines

Open science is a way of doing and communicating research collaboratively, using computer networks for the free production, validation and diffusion of knowledge to make it accessible to all. Such approach would benefit scientific knowledge development, particularly in middle- and low-income countries which usually lack research funding for high-end hardware and sample collection activities, and therefore would benefit from the online availability of freely accessible data.

FAIR guidelines were developed to improve the impact of digital assets by enhancing their Findability, Accessibility, Interoperability, and Reuse (11).

Examples of how this could be done include the indexing by an online repository and the use of DOIs and ORCIDs; [Creative Commons](#) licensing; interactive online visualisation; use of common

thesauruses for cultural heritage, geographic names, period terms, and dating, and adoption of an open, well documented and widespread file format.

The durability of the published data should also be considered, e.g. by choosing repositories that – for being open access, multi-national or internationally recognised, and publicly owned and funded – are more likely to last.

Indeed, there is a clear tendency towards an increase of palaeontological 3D data sharing: journals and professional societies are encouraging it (19), and, for instance, the [Archaeology Data Service](#) of the United Kingdom, which is the national repository for archaeology data of the country, has developed [guidelines](#) detailing the good practices for preservation and documentation of 3D models in Archaeology (31,32). What is more, several museums have recently rewritten their policies to favour 3D data sharing (19) and started digitisation programs for their collections.

This is well exemplified by the [Smithsonian Institution](#), which is currently carrying out a mass digitisation project to publish their collections online as comprehensively, quickly, and cost-effectively as possible.

As explained by the project managers: *“with more than 155 million objects and specimens, volumes, and archives, distributed across 19 museums, nine research centers, a zoo, and numerous storage facilities, the scale and diversity of Smithsonian collections present a unique digitization challenge. [...] We feel a great sense of urgency in bringing our collections online. With less than 1% of the collections on display at any one time, our digital collections provide building blocks and entryways to new journeys of discovery.”*

Indeed, such effort is one way to accomplish what has been defined above as science’s ultimate mission. However, when communication and dissemination are directed to the general public, ways of making them useful, understandable, and enjoyable (33), as well as public engagement (34), should also be taken into account.

Here, the application of values-led participatory design principles and practices (33,35–39) to human osteo-archaeological materials could play a fundamental role in taking advantage of the digital data to value them further and help to build visitors' engagement for museums, universities, and other cultural institutions.

This could be done, for instance, by developing interactive exhibitions usable in situ, and re-usable online, raising awareness of how it is possible to learn about humans in the past through their skeletal remains. Following such communication and sharing, feedback could be studied to assess user experience and even deepen our understanding of the nature and limits of the individual perception of the osteoarchaeological knowledge (1,40,41).

### The role of virtual anthropology

Virtual anthropology is best characterised as an interdisciplinary field of research, mainly developed over the past two decades to study anatomical data representations in three dimensions (20), (42), thus addressing questions in physical, evolutionary, and forensic anthropology, and facilitating insights into human body features.

Its major benefits relate to the application of non-invasive procedures to obtain virtual specimens for many purposes, including preservation, powerful descriptive (43), comparative and functional morphological studies (12,15,20,22,23,44–47), and communication.

In contrast to 2D raster images, 3D digital datasets present several key advantages with 3D data being easily scaled, rotated, measured, and viewed from any direction and angle. Such potential enables a wide use within the scientific community and the public, including preservation, documentation, and dissemination (13,20,44).

Some of the most significant applications are briefly described below.

### *Digitisation and conservation*

The digitisation process relates to the conversion of the specimen's data from analogue to digital, thus preserving the information about its size, shape, bulk, structure, and appearance for an indefinite time and making it usable with computer systems.

The gold standard to digitise a human subject or remain without destroying it is CT-scanning (21,25). CT-scan information is organised in a [DICOM](#) dataset (48), commonly used in the storage and exchange of medical data. Such kind of information can be treated with open-source and free of charge software such as [3D Slicer](#) to visualise it in a three-dimensional and interactive way (Figure 1, Figure 2, and Figure 3).

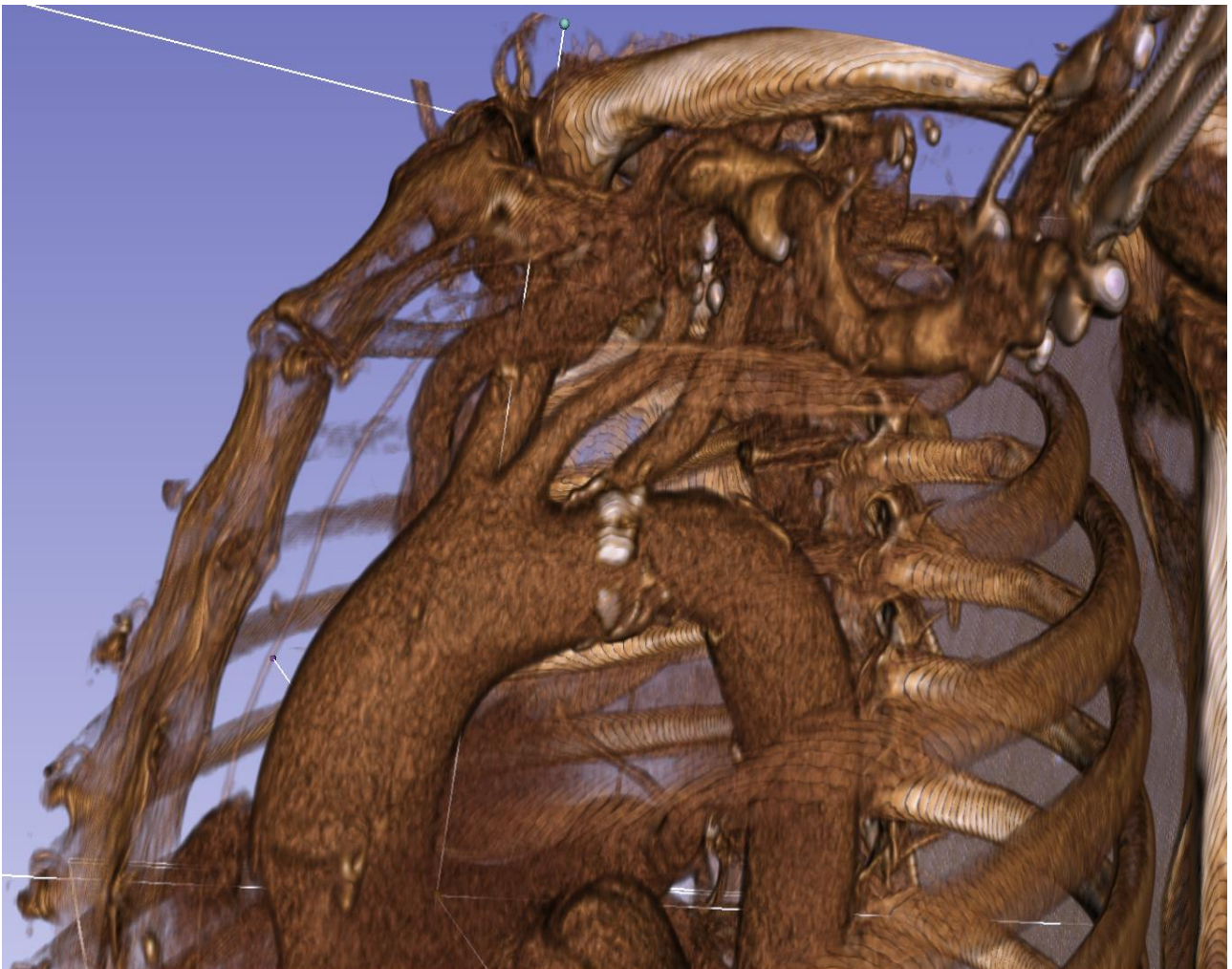


**Figure 1.** Interactive visualisation of the ascending aorta from CT-scanning data of a living subject who gave explicit consent to this image publication.



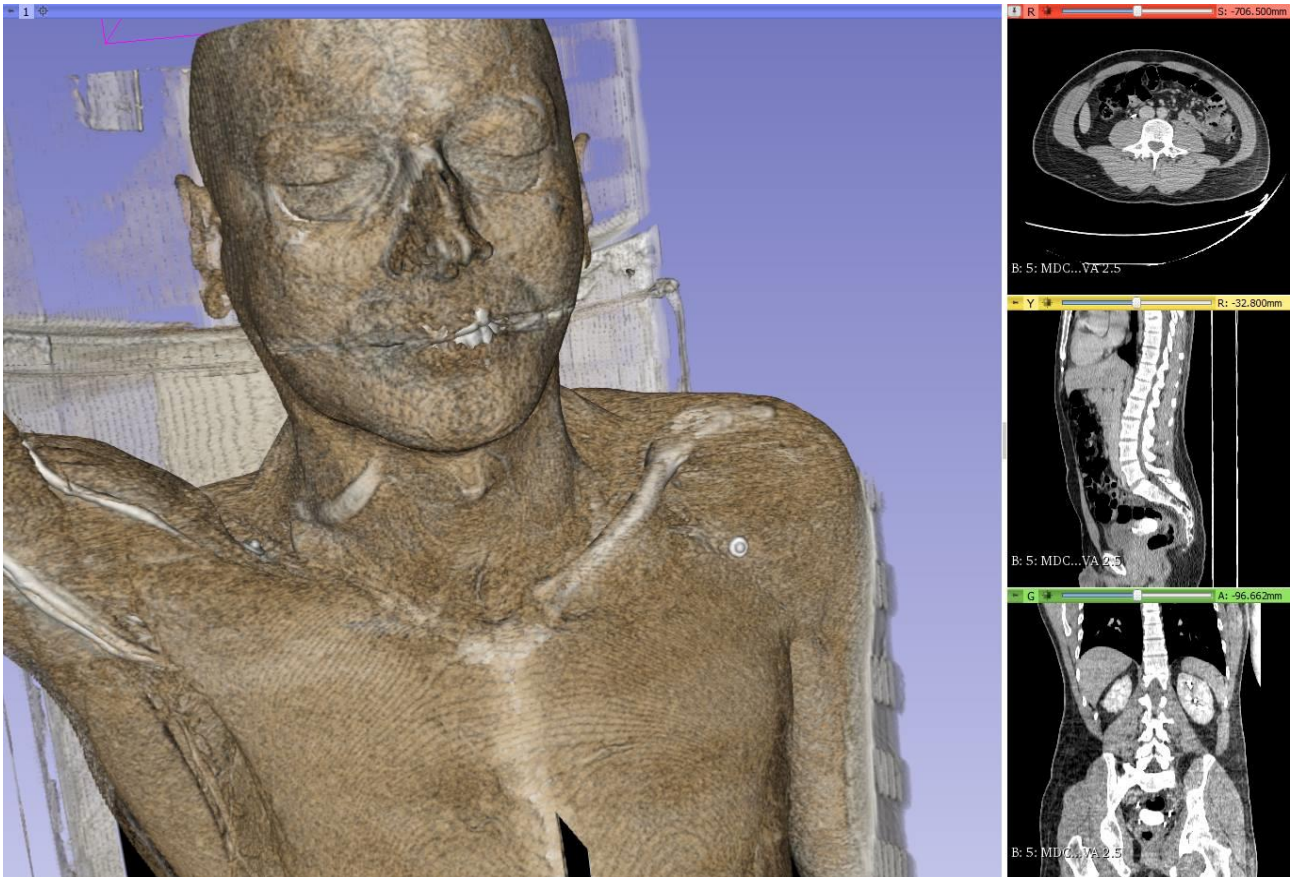


**Figure 2.** Interactive visualisation of three-dimensional data from a total-body CT-scan of a living subject: the author.

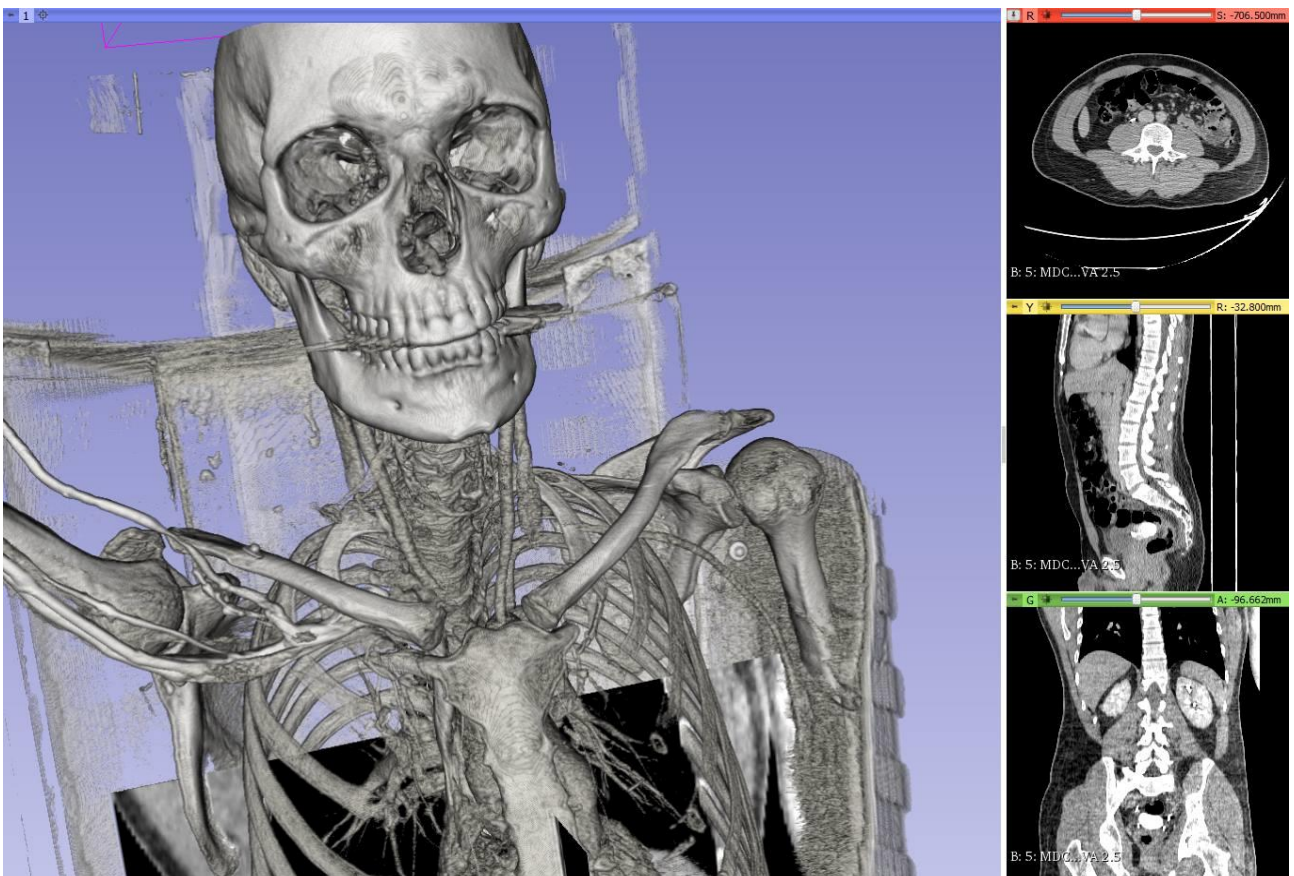


**Figure 3.** Interactive visualisation of the skeletal system from a total-body CT-scan of a living subject: the author.

### *Segmentation and exposure*

Once a digital replica of the specimen is produced, virtual anthropology enables anatomical data segmentation, i.e. the isolation of specific features, tissues, organs, and apparatuses to be studied separately.

Virtual dissection of the specimen is possible to preserve its integrity while exposing features that would be inaccessible otherwise (Figure 4).

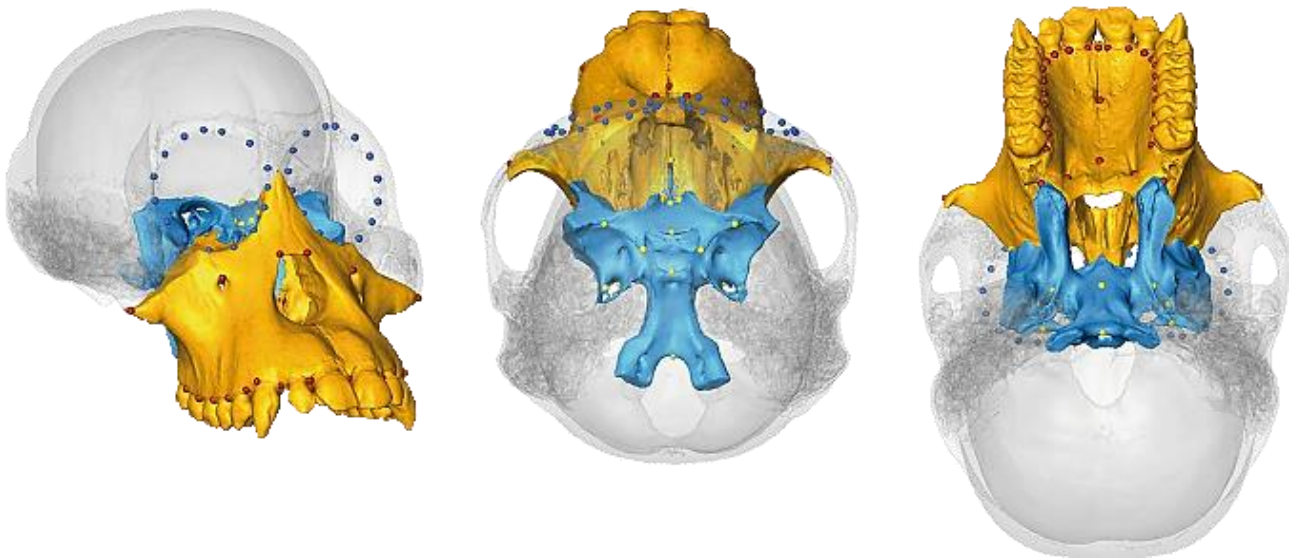


**Figure 4.** Anatomical modules in a cranium of *Pongo pygmaeus pygmaeus* (Northwest Bornean orangutan). Blue surface and yellow landmarks: cranial base (sphenoid bone including basion); blue landmarks: orbital outline; orange surface and red landmarks: maxillary bone (49). Image by [Sascha Senck](#) and [Michael Coquerelle](#). Reprinted with the authors' permission.

### *Reconstruction and comparison*

By working with digital three-dimensional representations, it is also possible to repair, since simple assumptions, e.g. bilateral symmetry, a lack of geometric information in the actual specimen. In this way, an incomplete or deformed specimen could be virtually reconstructed before being studied.

Furthermore, the application of virtual anthropology enables influential comparative studies concerning skeletal anatomy and function, species evolution, and population biological characteristics and ancestry (47) (Figure 5).





**Figure 5.** Side-by-side comparison of Neanderthal and modern human skulls from the [Cleveland Museum of Natural History](#). Original photo by Matt Celeskey, licensed under [CC BY-SA 2.0](#); modified by [DrMikeBaxter](#) and [Paolo Lussu](#).

Methodologies for comparing 3D models include the well-established geometric morphometrics (50–52), which is a landmark-based approach, and the recent new dense cloud and mesh-to-mesh approaches (47,50), in which the entire surfaces of the 3D models are compared to assess specimens morphological distance.

This latter approach allows researchers to study a higher amount of morphological data (47,50) with less effort, and therefore could be useful when dealing with large samples. Indeed, geometric morphometric studies are, in general, limited to small skeletal samples.

However, since geometric morphometrics is a well-established framework, and recent research comparing the approaches in a study on hominin mandibular variation (50) returned slightly different group membership estimates for this technique compared to alternative approaches, further research is definitely needed on this subject.

### *Materialisation, share and fruition*

Materialisation could be suggested as the opposite process to digitisation, bringing back to the real and tangible world an object that had already been digitised and transferred to the virtual one, which could be useful both for research and dissemination purposes.

A remarkable example is the reproduction of Ötzi, the Similaun glacier mummy found in South Tyrol, at the border with Austria, and dated between 3300 and 3100 BC (8–10). The mummy is preserved at the [Südtiroler Archäologiemuseum](#) (Museo Archeologico dell'Alto Adige, Bolzano/Bozen, Italy) in a cold room and visibly live through a 30 × 40 cm window (Figure 6). However, a 3D-printed copy was obtained from CT-scanning data and finished by Gary Staab (53,54). The replica is currently on display at the [DNA Learning Center](#) (New York, U.S.A.). In such a way an extraordinary specimen preserved in Europe has been made accessible to the public of another continent (Figure 7).



**Figure 6.** Ötzi the Iceman's mummified corpse, as preserved in a cold room at the [Südtiroler Archäologiemuseum](#) (Museo Archeologico dell'Alto Adige, Bolzano/Bozen, Italy). Image credit: [Südtiroler Archäologiemuseum](#). Public domain.



**Figure 7.** Gary Staab's recreation of Ötzi the Iceman's mummified corpse on display at the [DNA Learning Center](#) (Cold Spring Harbor, New York, the United States). Public domain.

### *Exemplificative studies*

As a result of such an unprecedented range of possibilities, three-dimensional datasets have become commonplace in many anthropological projects (13,19,21,22,31,55), allowing easy data integration with other data sources (17,29,30,56,57). From this perspective, virtual anthropology provides several effective ways to manage, study, and value skeletal collections.

In Italy, exemplificative studies were conceived by several authors. Profico et al. (2018) reviewed, from a general perspective, the applications of virtual anthropology techniques to cultural heritage studies (22).

As for the most recent applicative studies, Santoro et al. (2017) set up a new body identification technique for use in case of missing people (58). Profico et al. (2018) reported the reconstruction of the *Altamura skull*, whose posterior side could be accessed only using close-range photogrammetry (23).

Furthermore, Trizio et al. (2018) performed a survey of a burial during the archaeological excavation in the medieval site of Amiternum (L'Aquila, Italy) (59). Buzi et al. (2018) obtained the 3D model of the Neanderthal cranium *Saccopastore 1* (46). Di Vincenzo et al. (2019) Studied the morphology of the scapula of the *Neanderthal skeleton from Altamura, Italy*, and compared it with other individuals of the same species (23). Galletta et al. (2019) used geometric morphometrics to compare the articular surface of the first metacarpal in extant and fossil hominines (12). Gunz et al. (2020) reconstructed the skull of the fossil hominid *Rudapithecus hungaricus* (45). Lastly, Sorrentino et al. (2020) used geometric morphometrics to study sexual dimorphism in human talus (15).

### Techniques for three-dimensional reconstruction

Several different techniques and procedures have been developed to achieve accurate and reliable 3D models of anthropological specimens, in association with various software (13,20,21,55).

The main distinction is between volume – such as computed tomography (CT) and magnetic resonance imaging (MRI) – and surface techniques, e.g. laser scanning, structured light scanning, and digital photogrammetry (13,60–62).

Volume and surface scanning are both based on non-contact data acquisition and therefore respond to increasing requirements in conservation (13). While volume scanning provides information about the entire volume of the specimen, including all internal structures, data acquired with surface scanning techniques are limited to the outer surface of the specimen.

However, when studying dry bones, outer surface data returns a satisfactory geometric description of the specimen when inner structures are not subject to investigation. Accordingly, because volume techniques and laser scanning involve much more expensive equipment, intricate workflows, and trained operators, and are resource-intensive (13,21,22,24,60), surface techniques could be more indicated in describing extensive osteological samples (13).

Besides, it is worth mentioning that, producing 3D models from CT-scanning data, a segmentation step is required (63). Regrettably, segmentation is prone to a still poorly investigated *segmentation threshold effect* which limits the resulting 3D model accuracy (see Discussion in chapter A NEW APPROACH: CLOUD-BASED UCR-DP, page 98). Conversely, laser scanning requires the prior alignment of the partial 3D scans (24), a cumbersome task which can cause artifacts in the outcome, and structured light scanning shows insufficient accuracy for skeletal anthropology applications when implemented through low-cost hardware and software (64,65), although some middle-cost solutions appear promising (26).

Digital photogrammetry enables 3D reconstructions from digital photographs of the object (55,61) (see *Principles and methods of digital photogrammetry*, page 20, and *Historical development of digital photogrammetry*, page 24). Different from satellite and aerial photogrammetry, respectively based on remote sensing images and aerial photographs, it is applied in terrestrial contexts, with a wide range of potential subjects. When the camera-object distance is under 300 m, it is generally referred to as close-range digital photogrammetry (CR-DP) (61). The denomination of ultra close-range digital photogrammetry (UCR-DP) has been suggested (27) for cases within a working distance of 10 m, suitable for anthropological subjects and their in situ documentation.

UCR-DP is emerging as a robust technique for 3D model generation and represents a convenient and low-cost solution for rapid data acquisition (27,50,66). In fact, some methodological studies reported the best practices (60,67–69), and UCR-DP has already been widely applied in fields closely related to anthropological research, such as archaeology and cultural heritage – for the surveying, interpretation and virtual reconstruction of excavation sites, caves, buildings, monuments (50,55,70,71), documenting statues, bas-relief and mosaics (72,73), building 3D repositories of museum collections (74) – and palaeontology, particularly for site interpretation and track site documentation (67,75,76), or for digitising bones from mounted skeletons (77).

Such extensive applications are rarely limited by the size, or scale, of a given object. Relatively small objects include pottery, osteological or lithic pieces and, at the other end of the spectrum, historic buildings or archaeologically significant structures. Some of the most extensive applications for CR-DP include entire archaeological excavations, mounds or tel sites (31).



## Principles and methods of digital photogrammetry

Photogrammetry encompasses mathematical methods in order to derive information concerning the size, shape, and location of an object from one or more photographs.

Following the mathematical model of the central projection imaging, the coordinates of the object surface are estimated by identifying the homologous features in two or more images taken from different perspectives (61).

Each point  $x$  of the surface of the object is projected into a point  $p_1, p_2, p_3...$  of the corresponding image 1, 2, 3... taken from different perspectives views (Figure 8). The projected point, together with the corresponding *camera perspective centre*  $o_1, o_2, o_3...$ , define the spatial direction of the image ray to the corresponding object point. From the intersection of at least two homologous and spatially separated image rays, the position in the three-dimensional space of an object point is then calculated (61).

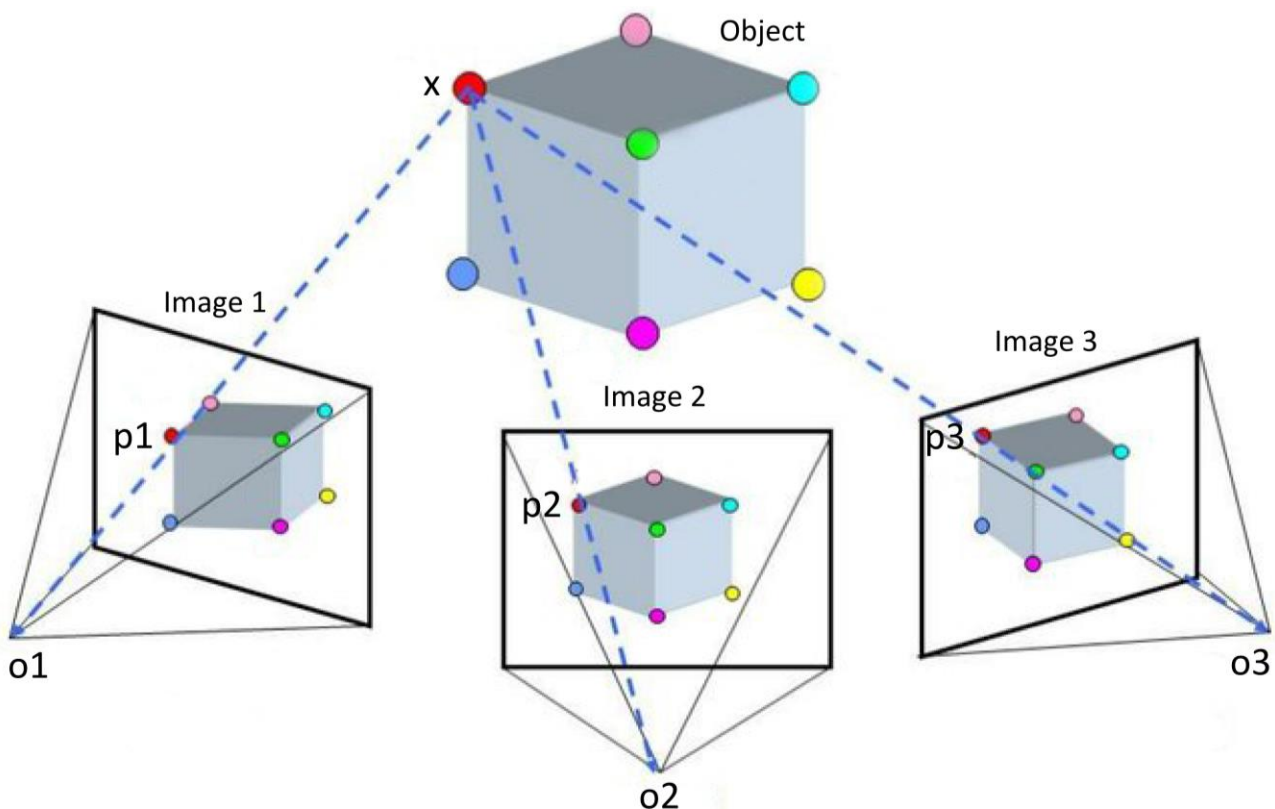


**Figure 8.** Application of the mathematical model of the central projection imaging to calculate the spatial coordinates of object point  $x$  from its projected image points  $p_1, p_2$ , and  $p_3$  and camera perspective centres  $o_1, o_2$ , and  $o_3$ .



Because photogrammetry uses light as the information carrier, it is included within non-contact, optical measurement methods, in the class of triangulation techniques, which provide information only related to the external surface of an object (61).

Unlike terrestrial laser scanning or structured light scanning, photogrammetry is a passive technique that relies on the ambient light reflected by the specimen rather than actively obtaining range data (55,69). When applied to produce computer representations, photogrammetry falls into the field of digital image-based modelling (IBM) techniques, allowing the creation of 3D models using data from two-dimensional images (55).

The actual implementation of the technique can be categorised in several ways.

- By the *number of images*: single-image, stereo and multi-image photogrammetry (61).
- By *camera position* and *object distance*: satellite, aerial, terrestrial, close-range, and ultra close-range photogrammetry (27,61).
- By *where the processing logic resides*: offline and cloud-based photogrammetry (27).

Satellite and aerial photogrammetry are respectively based on remote sensing images or aerial photographs and have been employed for a long time in topographic applications. Likewise, for terrestrial photogrammetry, using images taken from a fixed terrestrial location.

Close-range digital photogrammetry (CR-DP), instead, deals with terrestrial subjects which are within 300 m range, such as archaeological sites and buildings (55). For skeletal applications, it has been recently proposed to call the technique Ultra close-range digital photogrammetry (UCR-DP) when applied to subjects about the size of the human body, recorded within a 10 m range (27).

CR-DP and UCR-DP can be further categorised depending on where the software for their implementation resides. Offline photogrammetry relies on locally installed software and on the hardware provided by the user, while cloud-based software environments host the processing logic and data storage capabilities into remote servers operated by a third-party services provider.

UCR-DP is particularly convenient for most of SA applications, given the scale of the specimens. It can be applied with standard, close-up or macro-lenses following the desired reproduction scale factor and accuracy of the resulting 3D models.

CR-DP and UCR-DP workflow encompass three main phases: shooting, mesh processing (including sparse and dense point cloud generation; mesh and texture construction (55)), and mesh post-processing.

### *Shooting*

relates to the photographic documentation of each specimen. The shooting protocol should be carefully planned (44,67), in accordance with both photographic principles (69,78) and specimen characteristics. In fact, improper shooting affects the quality of the outcome, causing noise or topological artifact because the geometric information acquired from the specimen is insufficient or that from the background is excessive (79).

Therefore, precautions should be taken so as to capture the maximum amount of the geometry of the specimen by enhancing the image resolution and depth of field, and by ensuring an adequate image coverage, framing, and shooting environment.

To enhance the image resolution, digital single-lens reflex (DSLR) cameras with a full-frame sensor and high definition prime lenses are best; ISO sensitivity should be set to the minimum, and precautions for image stabilisation should be taken, such as a tripod mount, a remote shutter release, or a self-timer (78).

For achieving an adequate depth of field, the lens diaphragm should be closed by increasing the f-numbers until the whole specimen is in focus, as any further increase would only reduce image resolution. Then, the camera should be set to aperture priority mode (A or Av), where the desired f-number is given, and the shutter speed is chosen accordingly, based on the lighting conditions (78).

Moreover, it is good practice to match the specimen's apparent maximum dimensions with the frame size, while taking the necessary precautions to avoid any cropping. In fact, the closer the camera is positioned to the object, the more detail can be obtained (65,67). On the other hand, if the specimen dimensions are too small compared to the frame size, its geometric features could be ignored by UCR-DP algorithms, and the use of macro-lenses and short shooting distance is necessary. As UCR-DP algorithms extract geometrical features from their perspective change, the specimen should be oriented to maximise the detectable change.

Concerning the shooting environment, a well-conceived plain and out of focus background isolates the subject, reducing the need for time-demanding masking interventions in the following phases. Moreover, regular and diffused illumination abates the areas of shade over the specimen's surface, thus preventing the loss of geometric information and non-corresponding image features between the perspective views. Lastly, an appropriate setting of the white balance is necessary to render colours and texture appearance successfully.

#### *Mesh processing*

starts with feature correspondence and structure-from-motion algorithms matching the homologous points between the images, calculating the camera pose and calibration without prior information, and generating a sparse point cloud which describes the main geometric features of the specimen surface. From this data, multi-view stereo algorithms build a dense point cloud representing the external surface of the object in detail (55). Then, the geometry of the specimen is built connecting the dense points and generating a polygon mesh of millions of faces. The appearance and colours of the object are obtained as a texture from the source images and superimposed to the mesh to originate a photorealistic 3D model (55,66).

UCR-DP meshes need to be carefully scaled to embed absolute dimensions to them. This step will affect the accuracy of all subsequent measurements. One or more linear lengths should be

measured on the actual specimen, and then the measured value should be referred to the same length on the 3D model. Alternatively, scaling could also be achieved through calibration markers or millimetric scale bars being recorded in the shots, as some offline commercial software packages allow to scale the model through reference lengths located on the input photographs.

#### *Mesh post-processing*

concerns itself with the improvement of the quality of the 3D models to make them usable for research and communication. In particular, post-processing is useful to simplify the geometric representation of the mesh to make it easy to be visualised, studied, or materialised.

#### Historical development of digital photogrammetry

Photogrammetry applications started as early as photography itself when, in the 1840s and 1850s, Aimé Laussedat succeeded in measuring buildings from perspective views (80,81). The technique was then introduced into cartography, topography, architecture and archaeology, mainly for landscape surveys (50), and passed through four main phases of technical development – *plane-table*, *analogue*, *analytical and digital* (61). However, only the latter two phases saw applications in skeletal anthropology.

#### *Plane-table photogrammetry*

began in Italy in the 1860s, following the introduction of *phototheodolite* by Ignazio Porro (in 1865) and Pio Paganini (in 1884) (61,82). The new instrument, a combination of a metric photo camera and theodolite, allowed to record the precise orientation of the optical axis of the photo camera when taking a photograph. Because of the lack of efficient computing machines, object reconstruction was based on graphical evaluation of analogue images, following the laws of the perspective that had been developed during the Italian Renaissance. The technique allowed the reconstruction of horizontal bundles of rays from photographs, with two or more images permitting a point-by-point survey using intersecting rays. Plane-table photogrammetry was applied until ca. the 1930s (61,82).

### *Analogue photogrammetry*

began in 1901, with the introduction of the *stereocomparator* by Carl Pulfrich (in Germany) and Henry Georges Fourcade (in South Africa). The basic principle behind this technique is the use of parallax between two photographs or x-rays taken from different positions to produce a terrain elevation map where contour lines connect all the points that have the same elevation (61,82).

The stereocomparator – later *stereoplotter* – is an opto-mechanical measurement system in which two light sources are used to project two photographs of the same object taken from different angles of view (83). One photo is projected using a cyan or blue filter and the other with a red one.

Wearing glasses that have the same colour filter for lenses, the resultant overlapping image, called anaglyph, shows a three-dimensional model of the terrain. The operator records the elevations on the terrain by *flying* a light spot along the contours. Analogue photogrammetry was applied until ca. the 1980s (61,82,84).

The possibility of the application of analogue photogrammetry in medicine was first pointed out by M. Mannsbach in 1922 (85,86).

Following the cartographic applications of the technique, pioneering works in medicine and anthropology were carried out. In 1939 Max Zeller published a 10 mm contour interval map of a man's face (86).

In 1956 H.T.E. Hertzberg et al., studying the design of form-fitting, protective garments to ensure pilot survival at high altitudes, used two K-17 aerial cameras and a Kelsh Type stereoplotter to produce elevation contour maps of the human body (Figure 9) (85).

Other pioneering applications of the technique involved facial swellings volume measurement related to postoperative edemas or infections (87).

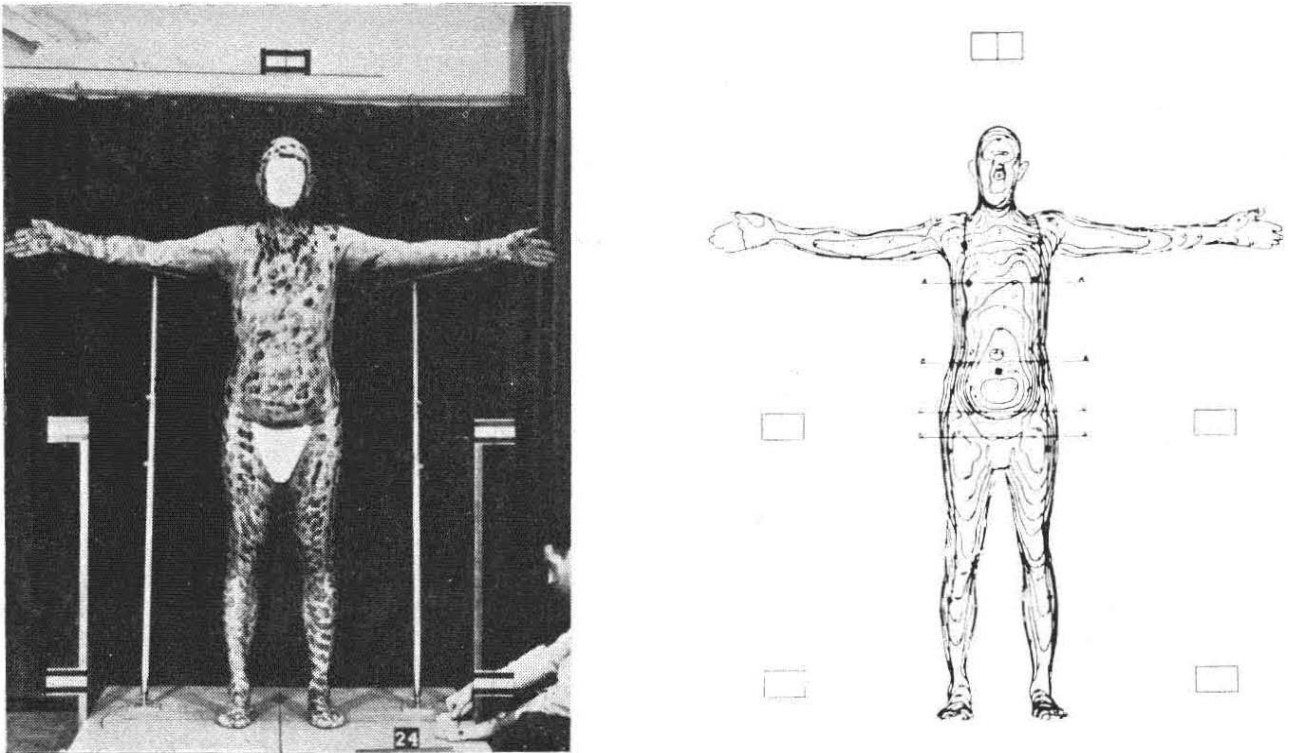


**Figure 9.** The pioneering work of Hertzberg et al. (1956) (85) produced elevation contour maps of the human body.

### *Analytical photogrammetry*

took place past the 1950s by employing the first generations of programmable digital computers. A *stereocomparator* was used to measure the parallax between corresponding points in two photographs or X-rays taken from different perspectives.

Point coordinates were then inputted into an electronic computer returning the data to produce elevation maps where contour lines connected points with the same elevation (61,82). Afterwards, computers were incorporated into stereoplotters themselves, resulting in *analytical stereoplotters*.

Analytical stereoplotters were applied to the living population for the analysis of body form and shape. Validation of the technique was achieved in the early 1970s on the whole body volume of living subject, with respect to the water displacement gold standard (88).

Applications included: the estimation of the volume of amputated stumps as an aid in fitting prostheses; the assessment of the efficacy of lymphedema therapies as a result of surgical removal of the breast; the early detection of changes in the curvature of the spine of children in anticipation of preventing the development of idiopathic scoliosis; the monitoring of breast volume changes during the ovarian cycle (89), and the analysis of surgically corrected facial morphology (90).

In 1980 the first application to skeletal anthropology was illustrated by Burkhard Jacobshagen (84,91). Human skulls were photographed from various perspectives using an analytical stereocomparator; data was then integrated into a coordinate system by means of a computer – Approximately 300 points were measured on each skull.

Jacobshagen recognised that the use of a contact-free measuring technique, which also involves temporal and spatial separation between the primary scanning of the object (data collection phase) and the actual measurement phase, improves study flexibility and work efficiency (84).

Indeed, instead of taking selective measurements, the entire object is surveyed *in toto*, transferring the problem of data selection from the early study level of collecting the objects to the more mature stage of dealing with the collected evidence.

Such advantages were generalised to anthropometry, as the access to the whole external morphology of a living being could be gained through a series of synchronised photographs, and therefore the subjects were no more required to be present for their actual measurements (84).

Once the data collection is complete, measurements can be reproduced as often as necessary, or even changed or extended without the need for the availability of the original specimens.

### *Digital photogrammetry*

Implementations and procedures changed dramatically after the introduction of *Digital photogrammetry*, involving fast, digital image processing.

In 1993 an early example of UCR-DP application to skeletal anthropology involved the capture of the 3D surface of bone metaphyses and joints from image pairs acquired with 256x256 pixel resolution through an 8-bit digitiser. Dedicated software was developed to process the data and display the three-dimensional surfaces (92). Just a few years later the availability of significantly more powerful graphic workstations led to a dramatic increase in the complexity of processable data. In 1998 and 1999 UCR-DP was used to reconstruct parts of the glacier mummy known as *Ötzi the Iceman* (93).

The development of sophisticated structure-from-motion and multi-view stereo algorithms represented a major breakthrough which allowed the extraction of 3D data and texture from unordered images of unknown calibration and poses (55).

More recently, cloud-based digital photogrammetry has allowed 3D models to be obtained via the Internet.

### Three-dimensional data description and storage

The constitutive elements of digital 3D representations fall into three main categories: geometry, appearance, and scene information (94). From such properties, which can be stored in many different file formats, the object visualisation is computed through a procedure called *rendering* and results in either static raster graphics, or videos, or interactive models (31).

### *Geometry*

In computer graphics methods used to store 3D geometric information include the following ones (31).



- *Parametric Equations*, describing the three-dimensional representation mathematically through parameters and equations which, once solved, identify its point coordinates, e.g. Non-Uniform Rational B-Splines or NURBS. While the use of mathematically described curves and surfaces allows scalability without any loss of detail, the latter is lost when trying to describe objects whose geometry is particularly complex, e.g. where describing human skulls.

- *Constructive Solid Geometry (CSG)*, using Boolean operators to combine simple geometric solids into much more complex representations by adding, subtracting, and intersecting their volumes or executing other logical operations on them.

- *Boundary Representation (B-rep or BREP)*, representing solids through their limits, described by elementary surface elements. While B-rep is able to represent complex objects, its data structure is memory-intensive.

- *Vertex-based representations*, which are the most common type of 3D models and consist of vertices expressed by three-dimensional coordinates. Apart from hardware specifications, the achievable level of detail for such geometries is only limited by the number of vertexes used to represent an object. Vertex-based representations include both *point clouds* and *wireframes (aka polygon meshes)*. While point clouds only consist of unconnected vertices (Figure 10) placed in a Cartesian coordinate system on an x-, y- and z-axis, polygon meshes also represent the connecting edges between the vertices (Figure 11) using (straight) lines or curves. Therefore In a polygon mesh, the three-dimensional coordinates of the vertices correspond to the corners of polygons commonly created through the subdivision of the surface into triangular or quadrilateral faces (Figure 11).

Point clouds are commonly generated by techniques such as 3D laser scanning, structured light scanning, and close-range digital photogrammetry (CR-DP) and are often further processed to form a mesh model.



**Figure 10.** Point cloud with colour information. Public domain original image modified by [Paolo Lussu](#).

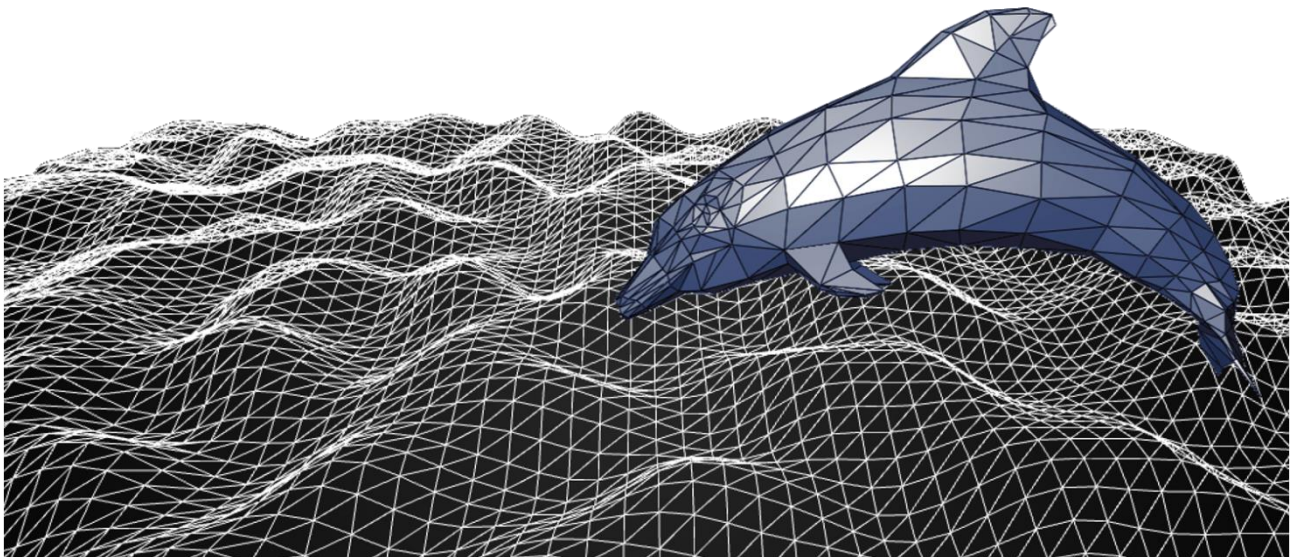


**Figure 11.** Two over imposed triangular polygon meshes. Public domain original images modified by [Paolo Lussu](#).

In the cultural heritage field, due to the complexity of the objects being represented, the most used three-dimensional representations consider vertex-based geometries. Indeed, sites, buildings, other artefacts, and human remains are way too difficult to be described in detail by mathematical equations or logical operators.

Furthermore, these latter descriptions suffer problems related to their preservation and future reuse because their format is highly dependent on the software used.

On the other hand, point clouds and polygon meshes enable a detailed description of the object or specimen, and the related information can be stored straightforwardly.

### *Appearance*

In addition to 3D model geometry, surface properties need to be stored to describe the complete appearance of an object. The combination of colour information, textures, and material properties can create a highly photorealistic 3D model.

At an elementary level, vertex-based datasets from laser scanning or digital photogrammetry can have intensity or colour (RGB) values associated with each vertex. For instance, the colour information contained in a photographic sampling can be projected back on to the point cloud or triangle mesh by assigning a single colour value (95).

Alternatively, a texture image (Figure 12) can be projected onto the three-dimensional surface applied and wrapped around a model using texture coordinates (Figure 12) A texture can then be resampled from the input set of images, at the proper resolution required by the specific application, and used at the rendering stage (95).

In addition to textures, other properties could be used to describe the appearance of the object, e.g. materials modelled to assign the correct reflectance properties, e.g. a wooden table will have different reflective properties to that of a glass table. This is done using parameters to describe reflection and refraction of diffuse light, specular light, ambient light, transparency, and emissive light.

However, a discussion of these techniques goes beyond the scope of the present research.



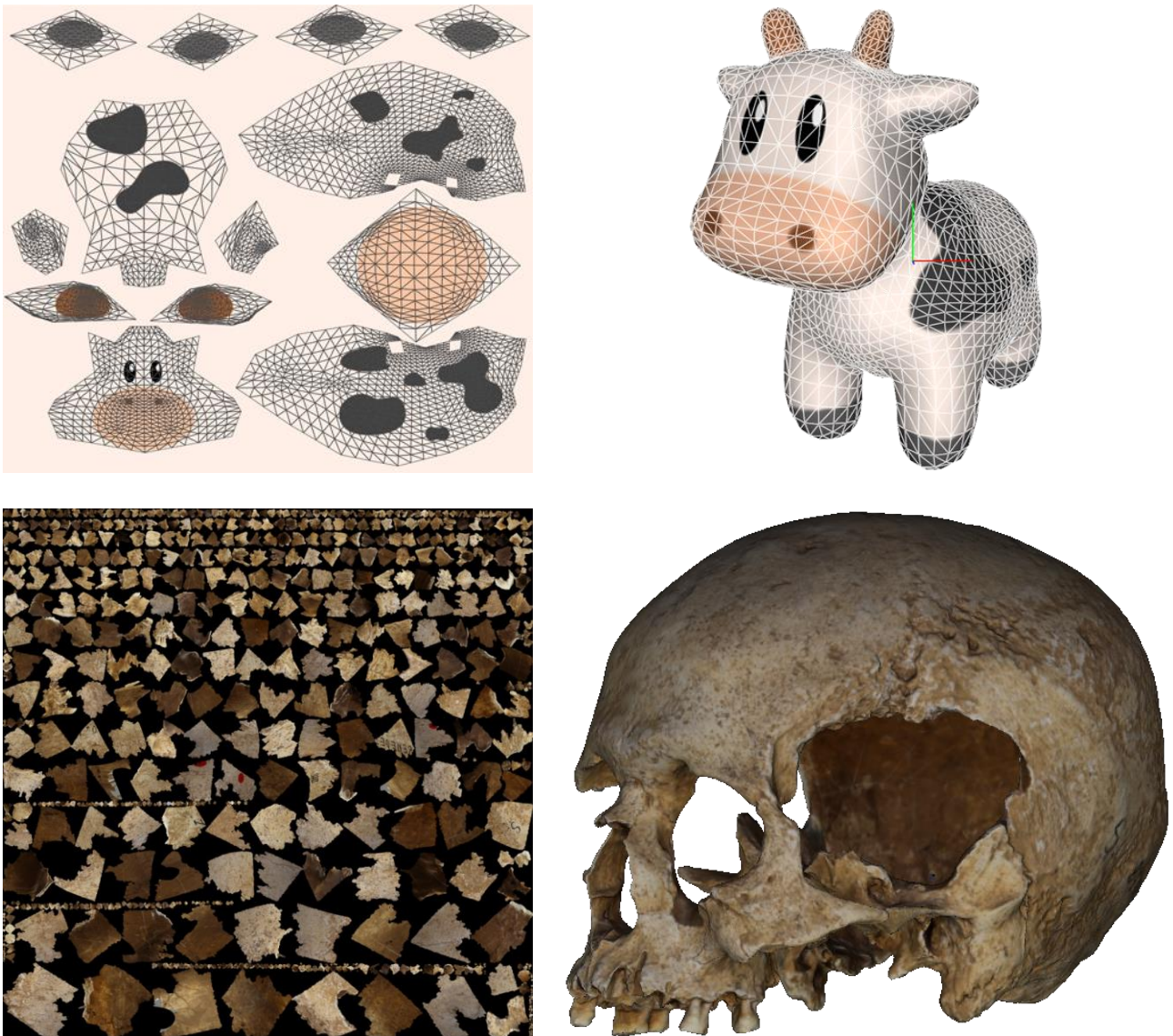


**Figure 12.** Texture images (left) and their projection on a polygon mesh 3D model (right). In this way textures map point-to-point the colour of the object, as represented for the three-dimensional models of a toy (above) and of cranium MSAE-6230, reconstructed with digital photogrammetry (Museo Sardo di Antropologia ed Etnografia, [MuSAE](#)). Upper 3D model provided by [Keenan Crane](#). Upper images by [Warren Moore](#), modified by [Paolo Lussu](#). Reprinted with the author's permission.

### *Scene information*

The way a 3D model is displayed depends on the scene settings and elements, including the size of the viewport, the positioning of the model, the position of the camera and light sources (31). The viewport is comparable to a stage, defining a frame for the model in terms of height, width and depth. For the camera, not only the position but also the viewing direction needs to be stored.

If rendered without light, only a black image of the 3D model is created so light settings, i.e. correctly positioned and configured light sources, are necessary to illuminate 3D scenes. Without this information it is up to the user to determine new settings although they may be automatically pre-set by the software.

A scene can contain one or multiple models which in turn can consist of any number of object groups. Grouping is necessary when a model consists of several individual parts or objects. When a group is set, the positioning of the parts also must be stored and can be described by transformations such as the shifting, rotating, or scaling of objects.

3D scanning devices or image-based techniques produce vast amounts of data and it is quite easy to produce 3D models so complex that it is impossible to fit them in RAM or to display in real-time. This complexity is usually reduced in a controlled manner, either by producing discrete Level Of Details (LOD) or multi-resolution representations (96).

For large and complex scenes it can be useful to store different LOD for individual objects to increase the efficiency of the rendering phase (97). Adopting a LOD representation means that every single object in the scene is represented using several different models. An object in the foreground of the scene, close to the camera, would be displayed at a high level of detail whereas trees or other objects in the background would be displayed using a lower resolution level. LOD representations can be easily built using geometric simplification algorithms, provided by many geometry processing tools (e.g. see the simplification features of [MeshLab](#) (98,99)). The level of detail for 3D models is dependent on the number of polygons.

By definition, LOD representations are characterised by a small number of different models. Conversely, multi-resolution approaches allow the production of a very large number of different models from a single representation and in real-time, adopting view-dependent criteria.

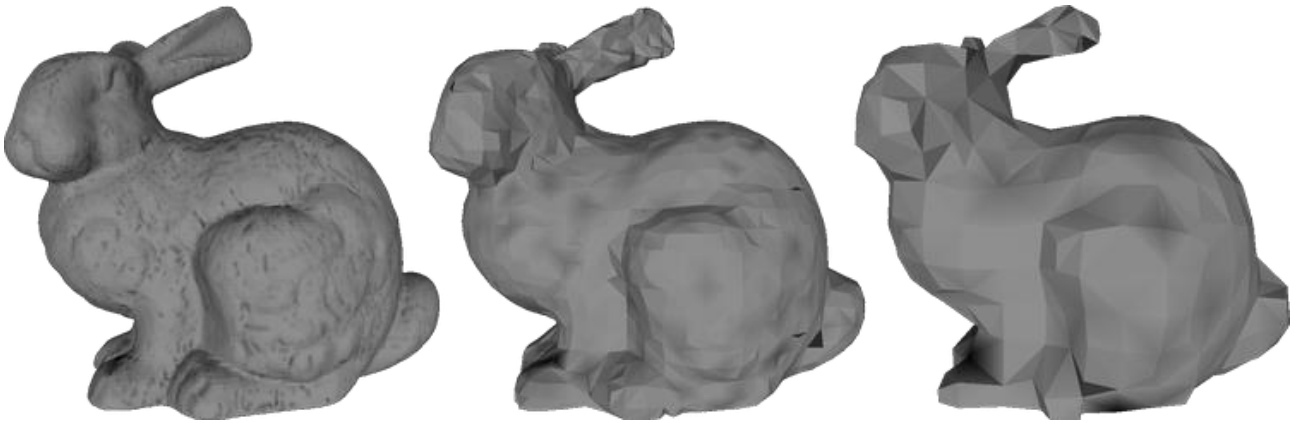


**Figure 13.** Figure 5: Effects of different Levels of Detail applied to the Stanford Bunny 3D model (left to right: 69451, 3851 and 948 polygons). Image by [Federico Ponchio](#) (100). Reprinted with the author's permission.

### *3D data file formats*

A vast array of file formats exists for 3D data, each with varying properties and capabilities concerning how they store geometry, textures, light sources, viewport and cameras. A somewhat complete overview of common formats has been submitted (94), although some of the therein mentioned file types have become obsolete. Here we consider file formats enabling the storage of vertex-based information, which are the most useful for cultural heritage applications.

- *.PDF (Adobe Portable Document Format)*. The PDF format is self-contained and allows basic operations such as measuring, cross-sections, light sources, wireframe views. While convenient for viewing data without specialist software the format is mostly a 'dead-end' in that data cannot easily be extracted.

- *.OBJ (Wavefront OBJ file)*. The open OBJ format was first developed by Wavefront Technologies around 1990 and a specification was published to encourage interoperability. Currently, it is supported by a large user community. The format stores both geometry and textures separately. The OBJ file represents the geometrical information in ASCII or binary format. When in ASCII

format the information is represented in human-readable text lines, a characteristic which allows for long-lasting preservation and the possibility of use and reuse possibly even in the far future. Together with the OBJ file, there are an optional MTL file, describing the material constituting the object, and image JPG file, storing the actual texture. The OBJ file format is suitable for preservation of wire frame or textured models, and the ASCII format is preferred for such aim.

- *.PLY (Stanford PoLYgon file format)*. The PLY format, also known as the Stanford Triangle Format, is a simple format with ASCII and binary versions developed at [Stanford University](#) in the mid-90s by Greg Turk and others, primarily for 3D scanning data. The format is inspired by OBJ but allows extensions to incorporate a variety of properties including colour and transparency, surface normals, texture coordinates and data confidence values. The format also allows different properties for the front and reverse of a polygon. While the addition of certain extensions will not make the format unreadable, not all software supports all extensions so data may at best be unread or, in a worst-case scenario, be discarded when files are resaved. Suitable for preservation (ASCII version) although file content should be clearly documented.

- *.X3D (eXtensible 3D graphics)*. The X3D is an ISO standard XML-based file format whose specification was developed by the [Web3D Consortium](#) and first approved by the ISO in 2004. It is an evolution of the previous VRML format and has been ISO certified since 2006. The format is suitable for the storage of single 3D models as well as of complex 3D content such as virtual reality.

- *.NXS (NeXuS)*. Nexus is an open-source multi-resolution format developed by [ISTI-CNR \(Pisa, Italy\)](#) in the late 2000s. The Nexus software package includes a format specification alongside tools for the conversion of .OBJ and .PLY files to the multi-resolution format and a visualisation library aimed at the interactive rendering of very large surface models. The format is used by [3DHOP](#) (96),

an open-source platform for web-based visualisation of large 3D meshes. While OBJ is suitable for preservation, the NXS is not. However, it is suitable for the online interactive visualisation of complex three-dimensional content derived from OBJ and PLY sources.

- *.STL (STereoLithography or Standard Tessellation Language)*. The STL was developed by [3D Systems](#) as early as 1987 and is prevalent in the field of 3D printers and digital fabrication. However, the ASCII version of STL only stores 3D model geometry (no textures) whereas the binary version, with the help of an extension, also saves colour information and requires less storage space. While an old format, STL is still well supported, particularly by 3D scanners, and is easy to transfer data due to its simple structure and human-readable format. However, this format is not suitable for the photorealistic preservation or visualisation of complex objects.

Recommended formats for anthropological subjects are discussed in more detail in chapter UCR-DP APPLICATIONS AND CASE STUDIES.

### [The skeletal collection at the University of Cagliari](#)

The Università degli Studi di Cagliari ([UniCa](#)) hosts a wide collection of human skeletal remains (101) including some 12,000 specimens dating from Neolithic to modern times, mainly established by Carlo Maxia (1907–1996).

Former Professor of Human Anatomy at the Faculty of Medicine and Surgery and full Professor of Anthropology at the Faculty of Sciences, Maxia spent his academic life studying paleopathological, paleobiological and cultural aspects of the Sardinian population and founded the Institute of Anthropology and the Museo Sardo di Antropologia ed Etnografia ([MuSAE](#)) in 1953.



During the time, the osteological collection grew and was subject to several studies, particularly by Giovanni Floris (101,102), Emanuele Sanna (102,103), and Rosalba Floris (101). Finally, in 2011 Sarigu et al. (101) performed a census of its specimens and reorganised the collection

The skeletal remains are currently housed at the Anthropology Laboratory annexed to the Museum. They are divided in specific collections which are of two types: the ones of so-called *property*, related to archaeological excavations, donations and exchanges between researchers, and those obtained in the early 2000s from the Soprintendenza Archeologica della Sardegna for research purposes.

However, as long as up to 2016, little had been done to digitally preserve the specimens or to apply virtual anthropology techniques to value and share the collection. Indeed, at the time only a small part (~ 0.2%) of the collection had been physically put on display at the [MuSAE](#). Furthermore, no actions had been taken to ensure findability, access, interoperability, and reusability of the related data per FAIR (11), and open science principles.

An exception is represented by the [Anthroponet](#) project (104), which in 2008 made available an online platform to share any information relating to Sardinian skeletal remains and their retrieval sites from Prehistory to the start of the Middle Ages, along with 3D models of relevant specimens and artefacts.

### [Aim of the research](#)

Despite their undoubtful utility for scientific knowledge advancement and dissemination, extensive osteological collections have never been digitised nor shared comprehensively due to technical, economical, ethical, and attitudinal criticality within the scientific community.

Furthermore, the role played by geographical and cultural factors in determining Sardinian prehistoric and historic settlement is still a matter of debate. Despite some insightful contributions

(101–103,105), the changes in the biological characteristics of the Sardinians from Neolithic to modern times have never been investigated using a large sample with a virtual anthropology approach, for instance to demonstrate the patterns of morphological variation, in space and time, of the skeletal features in the Sardinian population and environmental and the cultural factors which influenced them throughout the time.

To establish a foundation to answer such research question, the present study aimed to find new technologies and protocols for collecting digital three-dimensional data effectively, thus helping the preservation, study, and appreciation of wide osteological collections, such as those hosted at the Museo Sardo di Antropologia ed Etnografia ([MuSAE, Università degli Studi di Cagliari](#), Italy) (101).

The research was first directed at analysing the state of the art. Close-range digital photogrammetry was selected as the most suitable technique for three-dimensional reconstruction and a new protocol to enable fast and effective data collection from osteological samples was proposed and validated.

After that, the new protocol was used to collect an unprecedented quantity of three-dimensional data, with a view at achieving the sample to address a future population study with virtual anthropology techniques.

Virtual anthropology was also used to find new ways to engage university students and museum visitors, thus helping to build awareness of the past in the society and valuing [MuSAE](#) collections.

The role played by geographical and cultural factors in determining Sardinian prehistoric and historic settlement is still a matter of debate. Despite some insightful contributions (101–103,105), the changes in the biological characteristics of the Sardinians from Neolithic to modern times have never been investigated using a large sample with a virtual anthropology approach. Furthermore, no population has been directed to demonstrate the patterns of morphological variation, in space

and time, of the skeletal features in the Sardinian population and environmental and cultural factors which influenced them throughout the time.

The research was carried out with the intent to help a future, deeper, understanding of the matter: a goal that for the time being could not be achieved due to the sudden emergence of unpredictable environmental and cultural conditions.

# THE STATE OF THE ART: UCR-DP IN SKELETAL ANTHROPOLOGY

## The necessity for a systematic review

In fields closely related to skeletal anthropology, such as archaeology, cultural heritage and palaeontology, close- and ultra close-range digital photogrammetry (CR-DP and UCR-DP, respectively) are already widely employed for 3D model generation in many applications, from the surveying, interpretation and virtual reconstruction of entire sites to the documentation of a single palaeontological specimen (50,55,67,70–77). Some methodological studies reported the best practices for the application of the technique (60,67–69). Several applications have also been developed in anthropology, e.g. for documenting rock art (106–110), artefacts (111,112), cut and percussion marks due to human activity (113–117), and hominin footprints (118).

However, in skeletal anthropology, UCR-DP represents the least used method. Probably due to the novelty of its application, research is quite heterogeneous concerning methods and quality of results. Moreover, it is mainly of methodological concern, aimed at describing or comparing procedures or new possible applications, while application study numbers remain inadequate and do not show a relevant increase over the time (28,42,52,59,65,119). However, some pieces of research, mainly dealing with methodological aspects, include the application of the procedure to real cases (47,51,56).

Regrettably, there is a lack of standardisation in terminology, as the term *photogrammetry* itself could also refer to linear measurements obtained from photographs (120–122) or, inexactly, to active structured light techniques (123–125) (Figure 14). More confusion is arising as the expressions *structure from motion*, and *dense image matching* – which identify peculiar algorithms applied in the geometry reconstruction – and *computer vision* are becoming increasingly used to refer to the technique itself (57,65,68,126).

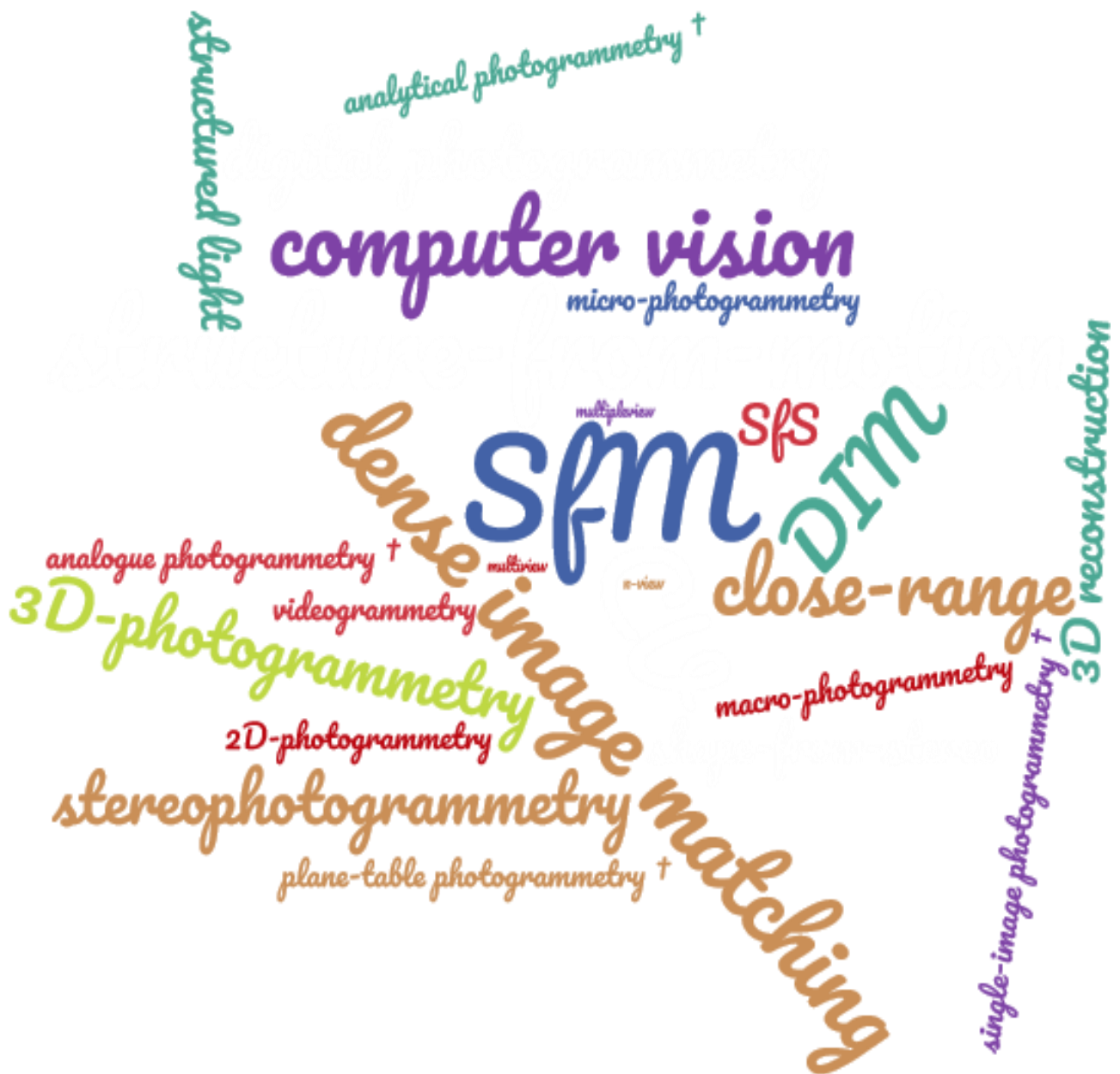


**Figure 14.** Some terms and acronyms variably associated with the photogrammetric technique, including obsolete (†) ones.

The present chapter aims to analyse technical implementation, applications and performance of UCR-DP in virtual anthropology, focusing on skeletal anthropology. There are no systematic reviews on this specific subject. However, a few studies have summarised selected literature including photogrammetry among other 3D techniques concerning the application of advanced techniques in virtual anthropology (22), forensic anthropology and taphonomy (21,60), and in situ documentation of skeletal remains (55).

## Review protocol – Search strategy and eligibility criteria

The literature review was carried out following the *Preferred Reporting Items for Systematic reviews and Meta-Analyses* (PRISMA) guidelines (127). Inclusion criteria considered the source type, incorporating peer-reviewed studies related to UCR-DP and skeletal anthropology, accessible in English full-text. The bibliographic search was performed on March 1<sup>st</sup>, 2019, using Scopus and MEDLINE online databases.

The search query was applied to the source title, abstract, and keywords, and included combinations of at least one of the terms identifying the field of application (i.e., *anthropology*, *anthropometry*, *paleoanthropology*, and *palaeoanthropology*) with at least one of the terms correctly identifying the technique (i.e., *photogrammetry*, *photogrammetric*, *stereophotogrammetry*, and *stereophotogrammetric*). Furthermore, in order to reduce the risk of bias due to the use of imprecise terminology, the following terms were also included in the query: *structure from motion*, *SFM*, *dense image matching*, *DIM*, *shape from stereo*, *SFS*, and *videogrammetry*. The resulting search query was:

(\*ANTHROPO\*) AND ((\*PHOTOGRAMM\*) OR ("STRUCTURE FROM MOTION") OR ("SFM") OR ("DENSE IMAGE MATCHING") OR ("DIM") OR ("SHAPE FROM STEREO") OR ("SFS") OR ("VIDEOGRAMMETRY"))

An iterative process was followed to identify progressively, in greater and greater detail, the scientific papers relevant to the review (Figure 15). After duplicates removal, the first screening considered the source type and title of the publications retrieved by the search query and classified them as relevant or not. To confirm that sources fitted with eligibility criteria, the second screening considered their abstract and the third involved full-text reading.

Finally, to widen the analysis, both a backward citation analysis (i.e., the screening of selected articles references) and forward citation analysis (i.e., the screening of the latest studies quoting

the selected articles, using Google scholar) were performed. The newly identified articles underwent, recursively, the same citation analysis. At any step, two authors worked independently to select the articles meeting inclusion criteria, upon discussion.

### Review protocol – Data collection and paper analysis

Relevant articles were analysed to extract details on:

- bibliographic features: authors, journal, journal area and category (according to SCImago), year and country of publication, research group countries, scientific journal ranking (SJR, for studies which appear in SCImago);
- study type: methodological (including reviews) or application studies;
- study characteristics: aim, the field of application, sample, technical implementation (photogrammetric technique; hardware and software; shooting protocol; mesh processing, post-processing, and analysis), quality of results (3D model characteristics and accuracy; data validation procedures and results; statistics), availability or online sharing of 3D models.

Relevant studies underwent a qualitative synthesis considering the following key questions.

- 1) What are the applications of UCR-DP in skeletal anthropology?
- 2) What are the most used technical implementations?
- 3) What is the accuracy and reliability of the technique, and how was it assessed?

### Search yield and bibliographic characteristics

The bibliographic search retrieved 758 documents from the Scopus online database (Figure 15). MedLine did not contribute any additional documents. Three duplicates were removed before continuing the analysis. Following the examination of source type, title and keywords, 95 articles were found to be possibly relevant. Based on the abstract content, 54 articles underwent full-text

reading; of them, 15 were found to fulfil the eligibility criteria. Nine additional records were identified through *backward-* and 3 through *forward-citation analysis*. Therefore, a total of 26 articles were included in the review.

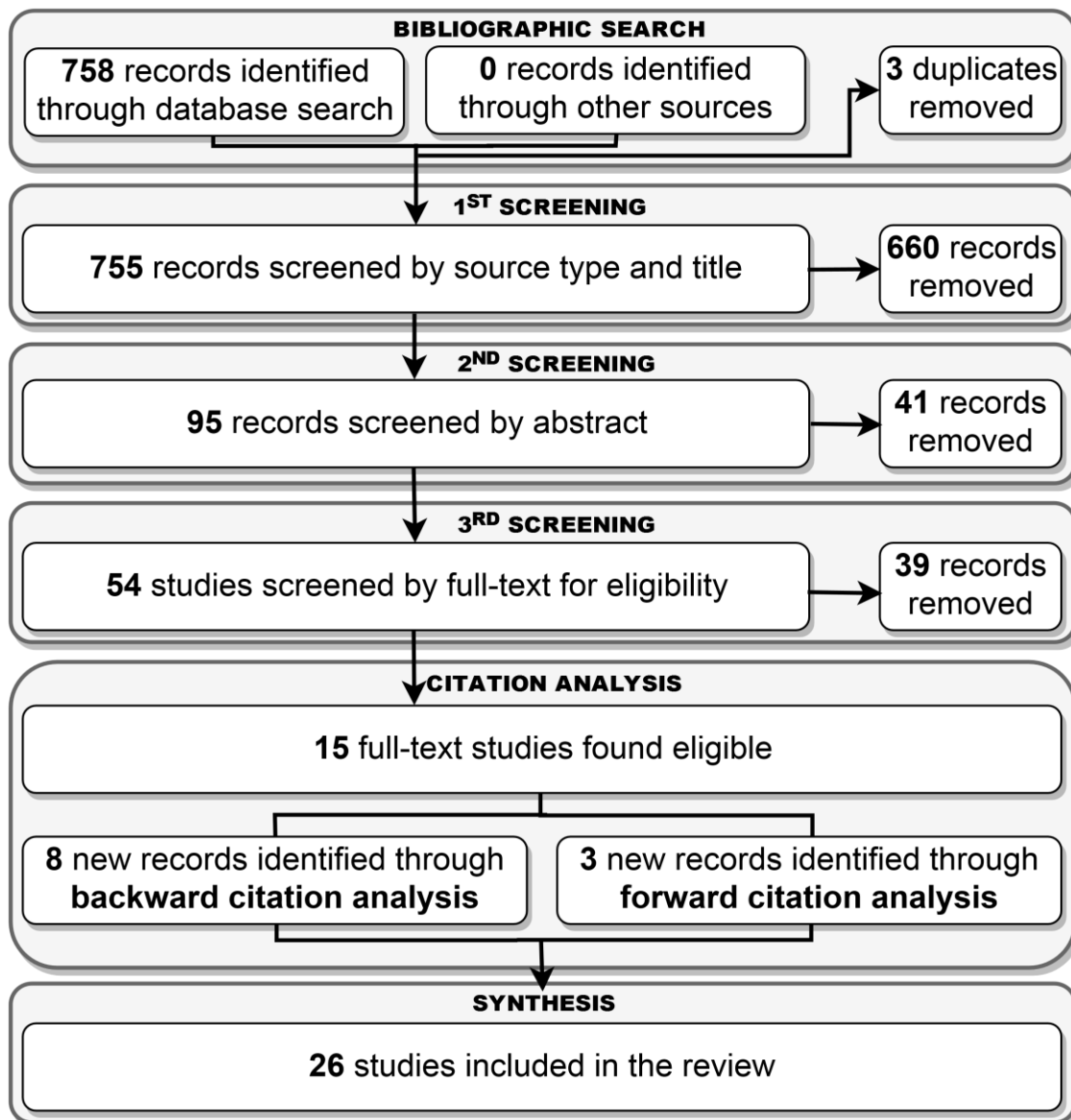


**Figure 15.** Flow chart for the study identification.

The articles included in the review were published from 2010 to 2019 (Table 1). The majority of them appeared in 2016 or after. Most of the research was conducted in Europe (especially in the United Kingdom and in Italy) and the Americas (especially in the United States).



Table 1. Summary of the reviewed articles.

Journal areas (and category) <sup>a</sup>	Field of application (study type) – main aim	Sample	Authors' countries	Reference
Medicine (Pathology and Forensic Medicine)	<b>Human biology (Methodological)</b> – Introducing a methodology for diaphyseal cross-sectional measurement	<b>1 humerus, 1 femur, and 1 tibia</b> <i>Modern skeletal collection (Athens, Greece)</i>	Greece	<b>Bertsatos &amp; Chovalopoulou (2019) (128)</b>
Medicine (Anatomy) Social Sciences (Anthropology)	<b>Human biology (Methodological)</b> – Assessing best practices for producing 3D digital cranial models	–	United Kingdom	<b>Morgan et al. (2019) (68)</b>
Engineering (Electrical and Electronic Engineering; Mechanical Engineering); Physics and Astronomy (Instrumentation)	<b>Palaeoanthropology (Methodological)</b> – Improving 3D data acquisition via a micro-controlled turntable	<b>Saccopastore 1 Neanderthal skull</b> <i>Museo di Antropologia della Sapienza (Roma, Italy)</i>	Italy	<b>Buzi et al. (2018) (46)</b>
Medicine (Pathology and Forensic Medicine) Biochemistry, Genetics and Molecular Biology (Genetics)	<b>Forensic anthropology (Methodological)</b> – Assessing different 3D printers and software settings in reproducing cranial traumas	<b>1 human and 1 pig crania</b>	Canada	<b>Edwards &amp; Rogers (2018) (79)</b>
Arts and Humanities (Conservation)	<b>Human biology (Methodological)</b> – Reviewing 3D imaging techniques in virtual anthropology	–	Italy	<b>Profico et al. (2018) (22)</b>
–	<b>Taphonomy (Methodological)</b> – Reviewing techniques in taphonomy	<b>Human and non-human skeletal remains</b>	United Kingdom South Africa	<b>Randolph-Quinney et al. (2018) <sup>b</sup> (60)</b>
Computer Science (Information Systems) Social Sciences (Geography, Planning and Development)	<b>Prehistoric and historic anthropology (Application)</b> Documenting a finding and its excavation process	<b>Skeletal remains from 3 burials</b> <i>Amiternum medieval site (L'Aquila, Italy)</i>	Italy	<b>Trizio et al. (2018) (59)</b>
Agricultural and Biological Sciences (Ecology, Evolution, Behavior and Systematics); Earth and Planetary Sciences (Earth-Surface Processes, Oceanography, Palaeontology)	<b>Palaeoanthropology (Methodological   Application)</b> – Introducing a methodology for identifying the agent of carnivore tooth pits	<b>OH8 and OH35 hominids</b> <i>Olduvai Gorge (Tanzania)</i>	Spain South Africa	<b>Aramendi et al. (2017) (51)</b>
Arts and Humanities (Archaeology, History) Social Sciences (Archaeology)	<b>Prehistoric and historic anthropology (Application)</b> Documenting a finding	<b>L2A skeleton</b> <i>Cussac cave (France)</i>	France	<b>Guyomarc'h et al. (2017) (52)</b>
Arts and Humanities (History) Social Sciences (Archaeology)	<b>Palaeoanthropology (Methodological)</b> – Comparing landmark- and high-density point clouds-based approaches to describe morphology	<b>9 mandible casts from the <i>Homo</i> lineage</b>	United Kingdom	<b>Hassett &amp; Lewis-Bale (2017) (50)</b>
Medicine (Pathology and Forensic Medicine)	<b>Forensic anthropology (Methodological)</b> – Introducing a technique for human body identification	<b>13 skulls</b>	Italy	<b>Santoro et al. (2017) (58)</b>
–	<b>Human biology (Methodological)</b> – Reviewing the application of digital-based modelling to the recording of in situ human remains	–	United Kingdom	<b>Ulguim (2017) <sup>b</sup> (55)</b>
Medicine (Pathology and Forensic Medicine)	<b>Forensic anthropology   Taphonomy (Methodological)</b> Proposing a new approach in mass grave documentation and study	<b>6 teaching skeletons</b>	United Kingdom	<b>Baier &amp; Rando (2016) (57)</b>
Computer Science (Applications; miscellaneous)	<b>Human biology (Methodological   Application)</b> – Producing a 3D dataset of the lumbar spine vertebrae, and validating the method	<b>86 human lumbar vertebrae (10 for the validation)</b> <i>Trotter Anatomy Museum (Dunedin, New Zealand)</i>	New Zealand	<b>Bennani et al. (2016) (65)</b>

Journal areas (and category) <sup>a</sup>	Field of application (study type) – main aim	Sample	Authors' countries	Reference
–	<b>Forensic anthropology (Methodological)</b> – Reviewing the applications of digital imaging in forensic anthropology	–	United States	<b>Garvin &amp; Stock (2016) <sup>c</sup></b> (21)
<b>Nursing</b> (Issues, Ethics and Legal Aspects) <b>Medicine</b> (Pathology and Forensic Medicine)	<b>Human biology (Methodological   Application)</b> – Testing the landmark and mesh-to-mesh approaches in assessing sex and ancestry	<b>80 human adult crania</b>	Czech Republic	<b>Jurda &amp; Urbanová (2016b)</b> (47)
<b>Social Sciences</b> (Anthropology)	<b>Prehistoric and historic anthropology (Methodological)</b> Addressing issues and limitations in photogrammetry and laser scanning	<b>Skeletal elements from 3 Upper Palaeolithic individuals</b> ( <i>Dolní Věstonice, Czech Republic</i> )	Czech Republic	<b>Jurda &amp; Urbanová (2016a)</b> (43)
<b>Medicine</b> (Anatomy) <b>Social Sciences</b> (Anthropology)	<b>Prehistoric and historic anthropology (Methodological   Application)</b> Integrating excavation and post-processing data from archaeological and osteological contexts	<b>2 skeletons from the Migration Period</b> ( <i>AD 400-550, Sandby ring fort, Öland island, Sweden</i> )	Sweden	<b>Wilhelmson &amp; Dell'Unto (2015)</b> (56)
<b>Arts and Humanities</b> (Arts and Humanities (miscellaneous)); <b>Social Sciences</b> (Archaeology)	<b>Prehistoric and historic anthropology (Methodological)</b> Summarising the development of reflexive methods at Çatalhöyük	<b>Various skeletal remains from unspecified burials</b> ( <i>Çatalhöyük, Konya, Turkey</i> )	Sweden United States United Kingdom	<b>Berggren et al. (2015)</b> (17)
–	<b>Prehistoric and historic anthropology (Methodological)</b> Integrating tools and methods to make the excavation process virtually reversible, thus helping human burials interpretation	<b>Various skeletal remains from unspecified burials</b> ( <i>Çatalhöyük, Konya, Turkey</i> )	United States Sweden	<b>Forte et al. (2015) <sup>c</sup></b> (30)
–	<b>Forensic anthropology (Methodological)</b> Demonstrating a protocol for forensic facial reconstruction	<b>1 cranium</b>	Italy Brazil	<b>Morales et al. (2014) <sup>c</sup></b> (129)
–	<b>Prehistoric and historic anthropology (Methodological)</b> Integrating tools and methods to make the excavation process virtually reversible, thus helping human burials interpretation	<b>Various skeletal remains from unspecified burials</b> ( <i>Çatalhöyük, Konya, Turkey</i> )	United States	<b>Forte (2014) <sup>d</sup></b> (29)
<b>Medicine</b> (Anatomy) <b>Social Sciences</b> (Anthropology)	<b>Human biology (Methodological)</b> – Assessing UCR-DP in capturing and quantifying human skull morphology	<b>4 modern crania of Mongolian origin</b> <i>Musée de l'Homme (Paris, France)</i>	United States France	<b>Katz &amp; Friess (2014)</b> (66)
–	<b>Palaeoanthropology (Application)</b> – Capturing National Museums of Kenya and Turkana Basin Institute's collections in digital format to be accessed on-line and interacted with	<b>Various specimens of the <i>Homo</i> lineage</b> <i>National Museums of Kenya and Turkana Basin (Kenya)</i>	Kenya United States	<b>Leakey &amp; Dzambazova (2013) <sup>b</sup></b> (42)
<b>Computer Science</b> (Computer Graphics and Computer-Aided Design; Human-Computer Interaction) <b>Engineering</b> (miscellaneous)	<b>Prehistoric and historic anthropology (Application)</b> – Documenting a finding	<b>51 skulls and associated skeletons from the Anglo-Saxon period</b> ( <i>AD 910-1030, Weymouth, United Kingdom</i> )	United Kingdom	<b>Ducke et al. (2011)</b> (28)
<b>Medicine</b> (Anatomy) <b>Social Sciences</b> (Anthropology)	<b>Compared anatomy (Application)</b> – Studying trapeziometacarpal joint curvature among five extant Primates genera, including <i>Homo</i>	<b>58 trapezia and 58 first metacarpals</b> , plus other specimens from other present and past species	United States	<b>Marzke et al. (2010)</b> (119)

<sup>a</sup> According to Scimago. <sup>b</sup> Peer-reviewed book chapter. <sup>c</sup> Study published in a peer-reviewed journal not indexed in Scopus or Scimago. <sup>d</sup> Study published in a peer-reviewed journal indexed in Scopus or Scimago after 2017.

According to SJR, the journals where the studies have been published are of medium or high impact. The areas of the journals were quite heterogeneous, with the majority of them falling into the SCImago areas of *Social sciences* (mostly *Anthropology* and *Archaeology* categories) and *Medicine* (mostly *Pathology and Forensic Medicine* and *Anatomy* categories) (Figure 16).

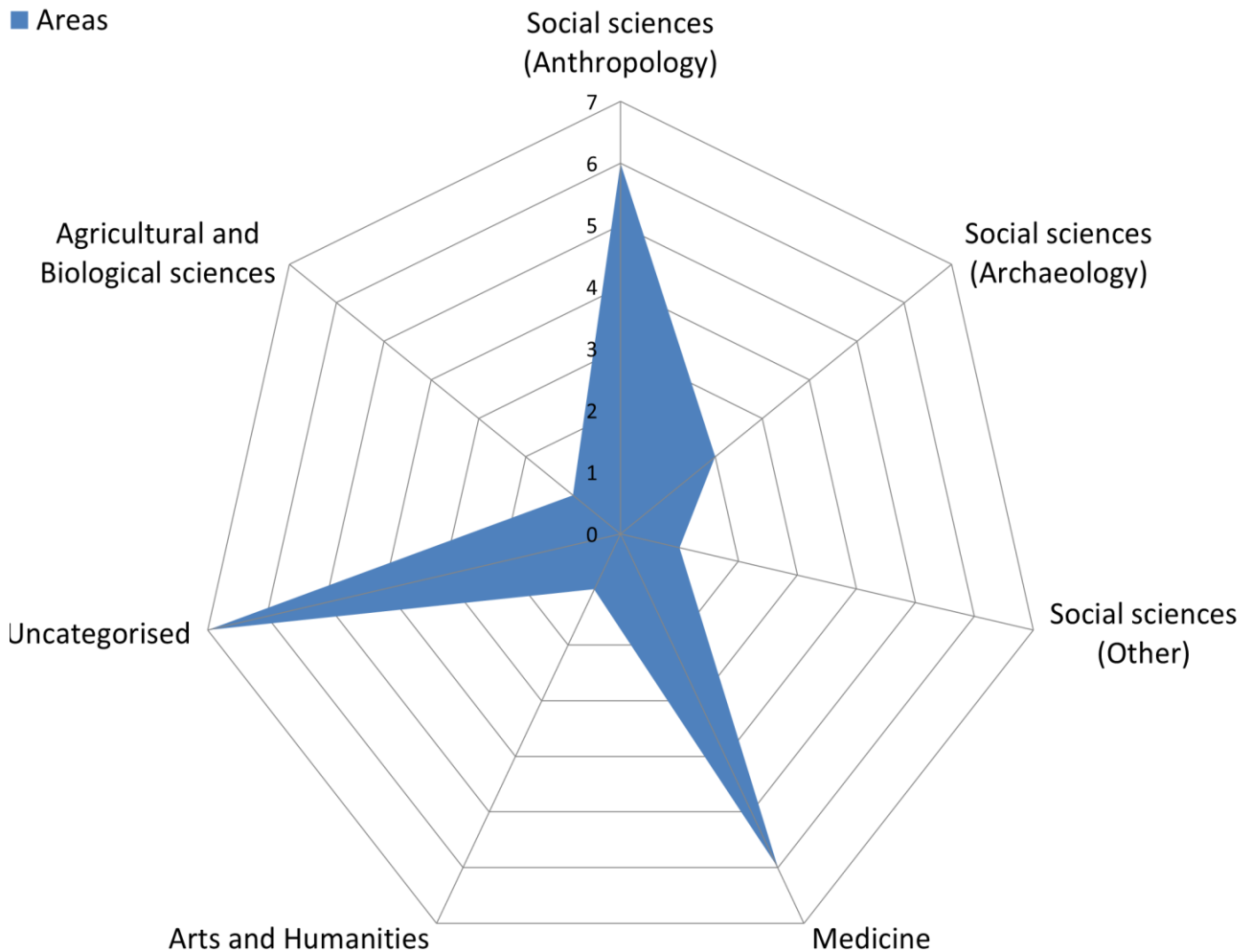


**Figure 16.** Distribution of the publication journals within SCImago disciplinary areas.

The majority of studies (77%) were primarily of methodological concern, including book chapters and narrative reviews. Despite an increasing trend in the most recent years (Figure 17), studies applying UCR-DP in skeletal anthropology remain scarce, as the most widely used techniques for 3D reconstruction continue to be CT and laser scanning (20–23).

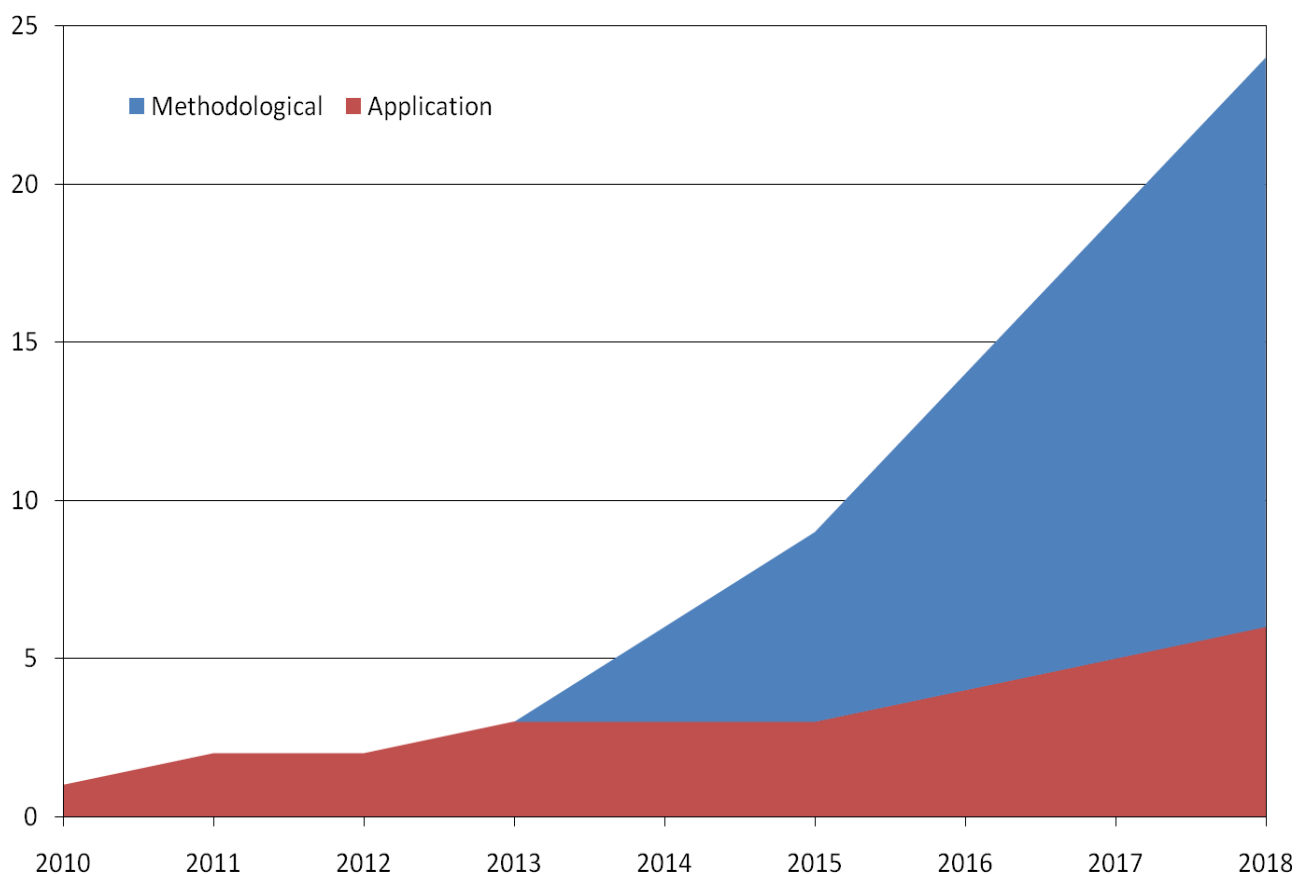


**Figure 17.** Classification of reviewed studies according to their aim. Data up to December 31st, 2018.

Methodological research included:

- comparative studies against various alternative methods (46,52,65,66,68,129);
- comparison of different approaches for morphological analysis (47,50);
- introduction of new procedures with specific purposes: integrating archaeological and osteological data (17,29,30,56,57); identifying carnivore agents on skeletal remains (51); body identification and forensic facial reconstruction (58,129); diaphyseal cross-sectional measurement (128); automatising data acquisition via a microcontrolled turntable (46);
- realisation of a dataset for diagnostic purposes (65).

The narrative reviews and book chapters were related to the general application of different 3D imaging and reconstruction methods in different fields (physical anthropology (22); forensic anthropology and taphonomy (21,60); in situ human remains recording (17,55)).

## Applications

The applicative studies mainly dealt with the documentation of skeletal findings (28,52,59), including their taphonomy (56,57); the identification or comparison of anatomical features and trauma (47,51,65,119); the use of three-dimensional printing techniques for communication and educational purposes (42).

Their focus was related to fossil remains within the human lineage until the early development of anatomically modern humans, hence falling into the field of Palaeoanthropology (42,46,50,51), prehistoric and historic samples (17,28–30,43,52,56,59), or with contemporary skeletal remains (21,47,58,60,65,66,68,79,119,128,129).

### *In situ documentation*

The field in which UCR-DP has been more frequently employed is in situ documentation of skeletal remains (55), aiming to describe the specimen (52), the taphonomic processes (56), and the phases of the excavation process (17,29,30,56,57), or for communication purposes (28). Such a privileged application is attributable to the higher versatility and reduced time requirements of UCR-DP, compared to other surface scanning or range techniques (27). Photogrammetry is more practical in sites presenting access limitations for physical or normative reasons (52) and enables 3D reconstructions even when such application has not been planned (28).

Skeletal remains have been contextualised within their environment, be it a burial (28,56,59), an entire settlement (17,29,30), or a cave with access restrictions (52). In this context, UCR-DP has sometimes been used to reconstruct skeletal remains (30,52), while other technologies, such as laser scanning, were used for a broader scale survey of the site (17,29). However, UCR-DP itself is suitable for both purposes (55,69), as exemplified by studies reconstructing remains altogether with their burial using site photographic documentation taken ad hoc (17,29,56,59) or making the most of a pre-existing photographic archive (28).

### *Integration within geographic information systems*

UCR-DP data has also been contextualised with other three-dimensional or archaeological data sources, within the framework of geographic information systems (GIS) (17,29,30,56,59), which is particularly useful in documenting complex sites, e.g. Catalhöyük (17,29,30).

### *Forensic analyses*

Other research focused on forensic and taphonomic applications, where UCR-DP's ability to capture the surface texture and colour is invaluable to complete the description of the specimen, e.g. in accurately documenting fracture patterns or modifications such as sun bleaching and soil staining (21).

Forensic and taphonomic analyses have also been directed to diagnose sex (47), reconstruct facial morphology (129), help in human body identification (58), document trauma (79), point post-mortem bone fracture patterns out (56,59), and identify aspects of past human life and environment, e.g. the carnivore agent who caused death or looted the corpse afterwards (51). Indeed, UCR-DP 3D models are suitable in a criminal investigation. However, the lack of standardised and validated protocols still negatively affects their probative value as court evidence in legal proceedings (21,60).

### *Anatomical, functional and population studies*

Another field of application includes comparative studies, aimed at determining the individual's ancestry group (47) or the similarities among fossil hominins and extant catarrhine genera (119). Indeed, this is promising, although almost unexplored, application of photogrammetry in skeletal anthropology.

Indeed, while comparative studies have already been performed on 3D models reconstructed from CT and laser scanning data, sometimes comparing them with UCR-DP-derived data obtained from other studies (23), the extensive application of UCR-DP would enable researchers to study considerably wider samples because of the technique's reduced resource requirements associated with the sampling.

## Technical implementation

### Shooting

Sixteen studies (43,46,47,50–52,57–60,65,66,68,79,119,129) – over 23 producing 3D models – specified the shooting protocol, while other studies provided fragmentary information (Table 2).

**Table 2.** Shooting protocol summary.

Cameras		
Type	<b>APS-C DSRL</b> (42,43,47,50–52,57–60,65,66,129) – of which, with integrated GPS: (59)	<b>Other</b> (ultra-compact (79); tablet PC camera (29); C-mount microscope camera (119))
Number	<b>One</b> (29,42,43,47,50–52,57–60,65,66,79,119,129)	
Lenses		
Type	<b>Zoom</b> (standard (46,50,52,79,129))	<b>Prime</b> (standard (65); macro (43,47,51))
Focal length	<b>Fixed</b> (<50mm (52,65); 50mm (50); >50mm (43,47,129))	<b>Variable</b> (60,66,79)
Shot settings		
Exposure	<b>Given ISO</b> (100 (46), 400 (65))	<b>Variable ISO</b> (60,66,79); (68) <sup>a</sup>
	<b>Given diaphragm aperture</b> (f/8 (65), f/10 (46), f/22 (43), f/27 (47), f/32 (129))	<b>Variable or automatic diaphragm aperture</b> (50–52,57,58,60,66,79); (68) <sup>a</sup>
	<b>Given time</b> 1/30s (65), 1/2s (46), 3s (47)	<b>Variable time</b> (68) <sup>a</sup>
Shooting environment		
Specimen installation	<b>Turntable</b> (manually operated (50,60,65,66,68,79); microcontrolled (46))	<b>Fixed support</b> (styrofoam ring (129)) or <b>in situ documentation</b> (28,52,57,59)
	<b>A distance</b> of 45 cm (46), 50 cm (68) cm from the camera lens	
Background	<b>Plain and uniform</b> (46,60,65,68) – of which, with pre-shooting masking (68)	
Illumination	<b>Constant</b> (46,47,51,58,60,65,68,129) – of which, with a lightbox (46)	<b>Variable</b> (flash (68) <sup>a</sup> )
Stabilisation	<b>Tripod mount</b> (46,47,51,58,65,129)	<b>Other</b> (Remote shutter release (47,129); self-timer (47))
Shooting procedure		
Shooting sessions	All studies reported sequential shooting sessions, i.e. the production of consecutive shots	
	<b>Continuous</b> <sup>b</sup> (28,29,42,43,47,50,57–60,66,68,79,119)	<b>Discrete</b> <sup>c</sup> (manual mesh merging (43,51,65,129); automatic mesh merging (46,52))
Shot n°	< 85 (43,50,58,66,79,119)	85–120 (47,51,128)
Image overlap	<b>Horizontal</b> (7° (46), 10° (65,79), 12° (129), 15° (51), no more than 30° (28), 30° (119))	<b>Vertical</b> (15° (65), 20° (51), 30° (46), 35° (129))
Perspective change	<b>Specimen rotation</b> (46,50,60,65,66,68,79)	<b>Camera movement</b> (rotation around the specimen (47,51,129); other (119); in situ <sup>d</sup> (28,29,52,57,59))
Duration	<b>10 minutes</b> (66), <b>30 minutes</b> (43), <b>60 minutes</b> (129)	

<sup>a</sup> Used automatic camera mode, although recommending aperture priority mode. <sup>b</sup> I.e. a continuous series of shots to obtain a single complete mesh directly. <sup>c</sup> I.e. discrete series of shots to obtain several partial meshes to be merged. <sup>d</sup> No study specified the pattern followed for in situ documentation.

The shooting protocol should be planned carefully (see *Principles and methods of digital photogrammetry*, page 20) as any mistake in this phase cannot be rectified without repeating the data acquisition (60). Instead, within the 16 studies reporting the shooting protocol, only a few described it in detail. Most of them limited the information to the type and number of the cameras applied, the number of shooting sessions and shots, and the way of changing the specimen's perspective view. Hence, the appropriateness of the procedures used for enhancing image resolution and depth of field, fitting the specimen image to the frame size, and installing a suitable light environment, was frequently difficult to ascertain.

As for the resolution, no author reported the use of a DSLR with a full-frame sensor, a few studies mentioned the adoption of prime lenses (43,47,51,65), ISO sensitivity was set to the minimum in one case only (46), and precautions for image stabilisation were rarely declared (46,47,51,58,65,129). Some authors declared the use of zoom lenses (46,50,52,79,129), even if they usually show higher optical aberrations and lower optical resolution than the prime ones (78).

As for the depth of field, only a few authors set a narrow diaphragm aperture (43,47,129). Others left the choice to the camera (50–52,57,58,60,66,68,79), a sub-optimal option that enhances image resolution at the expense of the achievable depth of field (78). However, it should be noted that wide diaphragm settings could be used without contraindications for in situ documentation (28,52,56,57,59), where the wider distance between the subject and the lens allows for sufficient depth of field regardless of the diaphragm aperture (78).

As for the framing, among the reviewed studies, only two specified the distance between the camera lens and the specimen (46,68), and three specified the use of macro-lenses (43,47,51).

The shooting environment also implies appropriate specimen installation, background, illumination, and image stabilisation. To hold a skeletal specimen, a convenient option, frequently used in the reviewed studies, is that of a turntable (46,50,60,65,66,68,79), i.e. a rotating platform facilitating the shooting phase and improving its repeatability. Such platforms should be of



uniform colour and texture, matching those of the background, so as not to provide additional geometric information, and could be operated either manually or automatically. Specimen installation could also be facilitated by the use of a styrofoam ring, as done in one study (129).

Despite their relevance, only a minority of the authors declared their concerns with assuring an appropriate light environment (46,47,51,58,60,65,68,129) and a plain uniform background (46,60,65,68), using, for instance, a lightbox (46) or a white cloth placed underneath the rotating platform (68). One of the reviewed studies found that 3D models outcomes were not affected by the use of an inconstant light source, such as a camera-mounted flash (68). Besides, no research declared the use of white balancing procedures nor specified light source colour temperature.

Another fundamental issue concerns image stabilisation, i.e. the prevention of any specimen or camera shake, so as to avoid motion blurs that cause a loss of detail and incorrect shot alignment (79,130). Among the reviewed studies, clearer images were achieved by mounting the camera on a tripod (46,47,51,58,65,129), and using a remote shutter release (47,129), or a self-timer (47).

*Alternative approaches to shooting.* All studies reported sequential shooting sessions, instead of simultaneous ones, i.e. the production of shots from different perspectives using multiple cameras, that would have sped up the image acquisition process (Table 2).

Some of the reviewed studies (28,29,42,43,47,50,57–60,66,68,79,119) performed sequential shooting sessions with a continuous approach, whereas others used the discrete procedure. In the latter case a subsequent manual (28,29,42,43,47,50,57–60,66,68,79,119), or automatic (46,52) alignment and merging of the partial meshes was needed, thus implying a longer procedure.

*Factors affecting the outcome quality.* Besides requiring more time, the discrete approach has been found associated with a decay in the quality of the outcomes (43). Indeed, the fusion of partial meshes introduces additional sources of error due to the higher degree of subjectivity in the alignment, thus resulting in a less accurate 3D model (43,65,79). Furthermore, using the

Poisson remeshing algorithm to merge the partial meshes produced extensively smoothed surfaces with localised defects (43). For the reasons mentioned above, the discrete approach should be avoided whenever possible (60).

Another relevant factor affecting the quality of the final product is the number of photos used to generate the model. This aspect was highly variable within the reviewed literature, as the shots taken for a specimen ranged from 3 to 320. According to a recent technical note, the optimal number for the cranium is around 150 (68). In fact, beyond this number, there is a significant increase in model creation time and no detectable improvement. On the other hand, while using as few as 50 images is sufficient to reconstruct a complete cranium, the corresponding 3D models showed poor quality (68).

During the present research it was found that 100 shots are sufficient for the purpose where the protocol is conceived to achieve additional perspective views from the regions showing higher geometrical complexity. Orienting the specimen's axis of symmetry with the lowest order, perpendicularly to the horizontal camera plane, enables it to capture the maximum geometric information when changing the perspective view, and thus reduces the required number of poses.

However, a large image overlapping should be ensured. Indeed, this is achievable by using an angular difference between consecutive shots generally not greater than  $15^\circ$  along the horizontal plane (46,51,65,79,129) and  $35^\circ$  along the vertical one (46,51,65,129). It should be noted that in situ documentation generally requires a higher number of shots, due to the extent of the recorded area (59).

*Shooting session automation.* Remarkably, no author controlled the data acquisition via software. The open-source software package [digiCamControl](#) enables multiple camera management for simultaneous or sequential shooting sessions, and automatic image indexing and storage, thus reducing the possibility of errors and the time demand and cost of the process.

### Mesh processing

All but one (42) study used a dedicated 3D model production computer hardware. Powerful graphic workstations (43,57,65,66,68,79,129), up to a set of 64 cores and 512 GB RAM (65), were used.

Studies employed offline software packages, with a single exception in which a cloud-based environment was adopted, **ReCap Photo** (Autodesk Inc., USA) (42) (Table 3).

**Table 3.** Software used for mesh processing, post-processing, and analysis.

Software (Producer, author or reference)	Licence		Application and references	
<b>PhotoModeler</b> (EOS Systems, Canada)	Commercial		<b>Offline 3D reconstruction</b> (58,119)	
<b>GRAPHOS</b> ((131))	Open-source		<b>Offline 3D reconstruction</b> (50,51)	
<b>Patch-Based Multi-View Stereo</b> ((132))	–		<b>Offline 3D reconstruction</b> (28,52)	
<b>Bundler</b> (Snavely, Noah)	Open-source		<b>Offline 3D reconstruction</b> (sparse point cloud generation) (28)	
<b>PPT-GUI</b> ((133))	Open-source		<b>Offline 3D reconstruction</b> (dense point cloud generation) (129)	
<b>PhotoScan</b> (AgiSoft, Russia)	Commercial	Processing	<b>Offline 3D reconstruction</b> (17,29,30,43,46,50,52,56,57,59,60,65,66,68,79) <b>Decimation, remeshing and hole filling</b> (59); <b>Scaling</b> (66,68)	
<b>ReCap Photo</b> (Autodesk Inc., United States)	Free for academic use		<b>Cloud-based 3D reconstruction</b> (42)	
<b>MeshLab</b> (Visual Computing Lab, ISTI-CNR, Italy (98,99))	Open-source		<b>Offline 3D reconstruction</b> (in support of) (129)	
			<b>Noise reduction, cleaning and hole-filling</b> (28,43,47,65,129); <b>Optimisation</b> (29)	
			<b>Partial meshes alignment and fusion</b> (43,129)	
<b>CloudCompare</b> (Girardeau-Montaut et al.)	Open-source		<b>Scaling</b> (43,79,129); <b>Data analysis</b> (30,57)	
			<b>Visualisation, manipulation</b> (28,56,58)	
<b>Geomagic Studio</b> (3D Systems Inc., United States)	Commercial		Post-processing	<b>Offline 3D reconstruction</b> (in support of) (50,51)
<b>Geomagic Wrap</b> (3D Systems, Inc., United States)	Commercial			<b>Mesh alignment and mesh comparison</b> (42,47,50,57,79,129)
				<b>Data analysis</b> (30,57)
<b>ArcScene</b> (Esri, United States)	Commercial	<b>Noise reduction, and hole-filling</b> (66)		
		<b>Scaling</b> (66); <b>Segmentation</b> (66)		
		<b>Segmentation</b> (43,52)		
<b>Avizo Software</b> (Thermo Scientific, United States)	Commercial	<b>Visualisation and manipulation, in situ</b> (56)		
		<b>Landmarking and measurement, in situ</b> (56)		
<b>TVMII</b> (PACEA lab, Université Bordeaux 1, France)	–	Analysis		<b>3D georeferencing and geo-spatial analysis</b> (56)
<b>FIDENTIS Analyst</b> ((134))	Open-source			<b>Landmarking and measurement</b> (21,29,51)
<b>Morphologika</b> (O'Higgins and Jones, 2006)	–		<b>Landmarking and measurement</b> (43,52,66)	
			<b>Mesh comparison</b> (47)	
			<b>Mesh comparison</b> (50)	

Most authors used a commercial solution – mainly PhotoScan (now [MetaShape](#), Agisoft, Russia) (17,29,30,43,46,50,52,56,57,59,60,65,66,68,79) or [PhotoModeler](#) (EOS Systems, Canada) (58,119).

Others used a combination of commercial and open-source or free for academic use software packages, such as PhotoScan and [PMVS](#) (Patch-Based Multi-View Stereo Software (132)) (52), or applied open-source or free for academic use solutions, such as GRAPHOS (inteGRated PHOtogrammetric Suite (131)) (50,51); [Bundler](#) and [MeshLab](#) (Visual Computing Lab, [ISTI-CNR](#), Italy (98,99)) (28), or [PPT-GUI](#) (Python Photogrammetry Toolbox with Graphic User Interface (133)) and [MeshLab](#) (129), or did not provide any information (128).

Within the studies adopting discrete shooting sessions (Table 2), the alignment and merging of the partial meshes were realised using [MeshLab](#) (43,129), PhotoScan (46,52), or [CloudCompare](#) (51).

Different algorithms were applied, such as the least-squares optimisation (51) and the iterative closest point (ICP) (43,50,65) for the alignment, and the Poisson remeshing algorithm (43) for the fusion.

*Input file format.* The file format for the input photographs was declared in a few studies and was mainly JPEG (42,46,68,129); in one case this was accompanied by the occasional use of lossless camera proprietary RAW (42). Regarding the input images, it has been shown that UCR-DP algorithms are very good at dealing with differences in resolution, exposure or lighting conditions (68). Indeed, algorithms return the best performance in reproducing fine details when using lossless file formats, including TIFF or camera proprietary RAW (28,67,68).

However, photographs should never be cropped, as this would change the relative scale of the image features retrieved from different shots (28). Raw input images have their drawbacks in requiring more computational resources, and therefore, when the maximum accuracy is not the priority, such as for dissemination, high-quality JPEG input is justifiable (67), and suitable to create accurate photogrammetric models (129).

*Processing software.* Almost all the studies used an offline approach based on commercial software, while the use of open-source (28,50–52,129) or cloud-based free for academic use (42) software were the exceptions. This has several disadvantages that go beyond the cost of software acquisition and updates. Offline computing requires powerful computational hardware with high-end processors and a considerable amount of working memory. Furthermore, the use of offline software packages is time-demanding, as they engage the processing capabilities of the local hardware for several hours, and follow many steps to generate a mesh and its texture.

Even where open-source solutions were employed, this was usually done through a combination of offline software packages, each specific for any of the reconstruction steps (28,50–52,129), sometimes requiring the use of additional general-purpose software, such as [MeshLab](#) (129) or [CloudCompare](#) (50,51), for completing mesh reconstruction.

A few free and open-source software packages are available for offline processing – such as [Regard3D](#) and [MeshRecon](#) – even if they have not been validated in skeletal anthropology yet, and hence their suitability is unknown.

*Scaling.* Among the reviewed studies, the scaling of 3D models has been based on calibration scales and markers (43,47,51,52,119) or on linear lengths on the specimen (46,50,66,129). In the latter case, as suggested by Hassett & Lewis-Bale (50), a length between arbitrary reference stickers is preferable to standard osteological measurements whose landmarks can be more challenging to be accurately and precisely localised (50).

Once the measurements had been taken, scaling was usually achieved via the 3D reconstruction software, although other software, such as [Geomagic Studio](#) (3D Systems Inc., the United States) (66) or [MeshLab](#) (43,79,129) was occasionally used. Regrettably, mesh scaling based on an arbitrary length is cumbersome with [MeshLab](#), while other software packages, such as [ReCap Photo](#), can identify the landmarks more easily and precisely.

To increase the accuracy of the scaled meshes, only two studies (50,66) took repeated measurements, while no study applied a separate scaling factor for each of the three orthogonal axes. A differential scaling along the axes is achievable with [MeshLab](#). However, during the present research it was found that it produces only minor variations.

*Output file format.* For the final 3D processing outcome PLY (28,129), OBJ (58,128), and 3D PDF (29) file formats were employed.

The suitability of a file format for storing 3D models depends on their intended use. Where the main application is research, the choice of PLY or OBJ file formats, which are open access and supported by the most used software packages for geometric data analysis, is advisable.

Indeed, other formats, such as 3D PDF, are not readable by most software for 3D models analysis. On the other hand, widespread file formats not supporting the embedding of texture, such as STL, should be avoided when dealing with UCR-DP data.

Where the main application is dissemination, it should be taken into account whether to allow the download and reuse of the 3D models, or only their online display and use. In fact, to use the locally downloaded 3D models, the installation of specific software, such as [MeshLab](#) (28,56,58), is needed. The 3D PDF file format could represent an effective solution (29), as it can be read by Adobe Reader DC, a globally widespread software package. However, a commercial software licence is needed to generate 3D PDF files, (e.g. Adobe Acrobat Pro, Adobe Photoshop, 3Dsystems [Geomagic Studio](#), 3Dsystems [Geomagic Design X](#)).

Where only online visualisation and manipulation is planned, the NXZ file format is more suitable, having been specifically designed for the efficient web-based fruition of extensive 3D reconstructions, and supporting their lossless compression, embedding, and streaming, i.e. their visualisation and manipulation while the download is still in progress.

If 3D models are intended both for research and dissemination purposes, again the PLY and OBJ file formats are suitable. For instance, the [ARIADNE Visual Media Service](#) (135) (Table 10) supports the upload of both PLY or OBJ files, and they are automatically converted to NXZ for their online display.

Further detail on 3D model file formats is provided in *Planning durable online use and reuse*, page 133.

*Versatility and scalability.* The wide range of technical implementations available for implementing UCR-DP, the possibility of automating data flow for handling a variable number of cameras depending on the specimen and sample characteristics, alongside the availability of diverse outputs in accordance with the planned data usage, all demonstrate the versatility and scalability of UCR-DP compared to other volume or range scanning techniques.

*Shooting and processing time.* As for the 3D model production time for a single specimen, the shooting session required up to 60 minutes (129), while the manual correction of the photographic masks took on average about 1 minute per image (66).

The mesh processing required a minimum of 70-80 minutes (51), between 110 and 300 minutes (65,66), and up to 540 minutes (129). The time required for the offline mesh processing of a single specimen (from 70 to 540 minutes, among the reviewed studies) depends on the complexity of the geometry to be rebuilt, the local hardware specifications, the image number, and the protocol type. For instance, discrete shooting sessions take much longer because they generate several partial meshes of the specimen (43).

It is noteworthy that, as opposed to the offline approach, the cloud-based one only requires users to upload the photographs, without prior masking, and to download the three-dimensional outcome at the end of the processing, enabling effective 3D reconstruction in less than 20 minutes, including the shooting session, scaling and post-processing.

### *Mesh post-processing*

Post-processing issues were discussed by some authors from a general perspective, highlighting the problems that may arise and the best practices to prevent them (43,47,60,66,129). A wide variety of software was applied (Table 3). Open-source software packages such as [MeshLab](#) (28–30,43,47,65,129) and [CloudCompare](#) (42,47,50,129) were the most used in many contexts. Some studies used commercial software for specific tasks: PhotoScan (59); [Geomagic Studio](#) (66), and [Geomagic Wrap](#) (3D Systems Inc., the United States) (43,52).

In order to improve the quality of the 3D models, remove artifacts, and simplify mesh geometry, the open-source software [MeshLab](#) was the most used in the reviewed literature for its flexibility and broad application capability to cleaning, trimming, noise reduction, hole-filling, decimation, and remeshing (28–30,43,47,65,129). Commercial software was rarely used for the purpose (59,66).

Despite the recognised benefits of 3D post-processing, an excessive level of intervention should be avoided as it would introduce errors in the final 3D model (28), such as filling authentic holes or smoothing and down-sampling complex mesh data.

However, as highlighted by some authors (22,79), specific applications such as 3D printing require a so-called watertight mesh, i.e. a mesh whose surface is continuous, and therefore even actual holes, e.g. the foramen magnum, may need filling.

### *Mesh analysis*

Depending on the aim, the 3D model analysis was carried out using several software packages (Table 3). Open-source solutions such as [CloudCompare](#) (42,47,50,129) were widely applied for mesh orientation and comparison (42,47,50,79,129), and for data analysis (30,57,79). [MeshLab](#) was used similarly for visualisation and manipulation (28,56,58), and, along with [CloudCompare](#), for data analysis (30,57). For landmarking and measurement [Avizo Software](#) (Thermo Fisher Scientific, the



United States) (51), [ArcScene](#) (Esri, the United States), and NewFaceComp (which was developed *ad hoc* for the study) (58) were used. TIVMI (PACEA laboratory, [Université Bordeaux 1](#), France), developed explicitly for skeletal anthropology applications, was frequently applied for the same tasks.

The analyses carried out on the 3D models involved visual assessment (28,56,58), segmentation (43,52,66), landmarking and measurement (21,29,43,51,52,56,66), mesh alignment, comparison and inter-3D model distance calculation (42,47,50,57,79,129), and data analysis (30,57).

As for the software packages for 3D model analysis, although the most frequently used were [CloudCompare](#) (30,42,47,50,57,79,129) and [MeshLab](#) (28,30,56–58), some dedicated software could be more adequate for specific tasks. For instance, [ReCap Photo](#) allows users to identify landmarks more easily and precisely, despite lacking the variety of functions of [MeshLab](#). Moreover, specific software for landmarking and measurement was used by some authors (21,29,43,51,52,66).

For comparative analyses, [Morphologika](#) (50), a free software package, was used to calculate geometric morphometric distances while open-source software packages [MeshLab](#) (79), FIDENTIS Analyst (47) and [CloudCompare](#) (50,57,79,129), along with commercial [Geomagic Studio](#) (66), were all used for mesh-to-mesh and mesh-to-point cloud comparisons.

Methodologies for comparing 3D models included the well-established geometric morphometrics, (50–52) which is a landmark-based approach, and the new dense cloud and mesh-to-mesh approaches (47,50), in which the entire surfaces of the 3D models are compared to each-other to assess specimens distance. This latter approach allows researchers to study a greater amount of morphological data (47,50). The two approaches have been compared in a study on hominin mandibular variation (50), returning slightly different group membership estimates.

## Accuracy and reliability

Although no study was openly aimed at validating UCR-DP in skeletal anthropology, some authors provided quantitative data on its outcome assessment, with respect to other techniques such as osteometry (29,52,65,68); 3D coordinate digitiser (65); laser scanning (66,129), or microtomography (46) (Table 4).

**Table 4.** Summary of literature on UCR-DP accuracy and reliability.

STUDY MODEL			RESULTS		Reference
Sample and measurement	Reference techniques	Statistical techniques	Accuracy	Reliability	
3 crania – 50 measures 3 repetitions – 1 rater	Osteometry	Bland–Altman	Bias < 2 mm (2%) <sup>a</sup> Bias range: 0.11 to 1.93 mm <sup>bc</sup> Bias range %: 0.84 to 2.82 <sup>bc</sup> LOA (best): -0.96 to 1.74 mm <sup>c</sup> LOA (worst): -1.14 to 1.87 mm <sup>c</sup>	–	Morgan et al. (2019) (68)
1 cranium – 16 landmarks No repetition – 1 rater	CT-scanning	Geometric morphometrics	Bias: 1.6 mm Bias range: 0.43 to 3.08 mm <sup>d</sup>	–	Buzi et al. (2018) (46)
1 cranium – 30 measures No repetition – 1 rater	Osteometry (in situ)	–	Bias: 2.4% (0.01-7.9%)	–	Guyomarc'h et al. (2017) (52)
10 vertebrae – 5 measures No repetition – 1 rater	Osteometry Arm-scanning	Bland–Altman	Bias: 5.2% <sup>e</sup> , 4.7% <sup>f</sup> Bias < 3.5 mm <sup>fg</sup> LoA: 4.4-5.4mm <sup>e</sup> LoA: 4.8-5.0mm <sup>f</sup>	–	Bennani et al. (2016) (65)
–	Osteometry (in situ)	–	Bias: ~5 mm	–	Forte (2014) (29)
4 crania – 16 landmarks 2 surface areas 4 repetitions – 1 rater	Laser scanning	Geometric morphometrics ANOVA	Bias < 2 mm <sup>h</sup> Bias + 1.2% <sup>ij</sup>	112 mm <sup>2</sup> <sup>ij</sup> 9.6 mm <sup>2</sup> <sup>ik</sup>	Katz & Friess (2014) (66)
1 cranium No repetition – 1 rater	Laser scanning	–	Bias: ± 1 mm	–	Morales et al. (2014) (129)

<sup>a</sup> In most cases. <sup>b</sup> Data for 3D models created using 150 or more photographs. <sup>c</sup> Data for 3D models created on high- or ultra-high alignment and dense point cloud software settings. <sup>d</sup> Range of the absolute landmark displacement between UCR-DP and CT-scanning. <sup>e</sup> Data referred to osteometry. <sup>f</sup> Data referred to arm scanning. <sup>g</sup> In 95% of measures. <sup>h</sup> Data relative to linear measurements. <sup>i</sup> Data relative to surface area measurements. <sup>j</sup> Replication error in measuring parietal bone area. <sup>k</sup> Replication error in measuring nasal bone area.

The study aim included the assessment of UCR-DP performance in describing the human cranium (66,68) and vertebrae (65); in situ measurement (29,52), and facial reconstruction (129). The suitability of specific procedures, such as the use of a micro-controlled turntable (46), was also considered. Furthermore, a study validating 3D printing procedures using different hardware and software settings included data produced via UCR-DP (79), among other techniques. However, in this latter case, as all the data sources were evaluated altogether, no specific result for UCR-DP was recognisable.

Study models varied. When declared, the sample included 1 (46,52,129) to 10 (65) specimens, while measured variables ranged from 5 (65) to 50 (68). Only in three cases did authors declare that measurements had been taken under osteological criteria (52,66,68).

Most studies provided data on accuracy, where UCR-DP showed similar results compared to osteometry (68), laser scanning (66) (129) and CT-scanning (46). The bias in relation to the reference technique was generally under 2 mm and 2% (Table 4; Figure 19).

The performance was slightly worse when the technique was applied to relatively small specimens such as vertebrae (65) (Figure 18) and in situ (29,52). In this latter case high-end laser scanners have been found to outperform UCR-DP for surveys (29).



**Figure 18.** Cloud-based UCR-DP (27) 3D model of a human vertebra obtained with macro lenses (left) compared with a specimen digitized with  $\mu$ CT (right), the recognised standard for three-dimensional reconstruction of skeletal remains (60).



**Figure 19.** Cloud UCR-DP 3D model compared to: offline UCR-DP 3D model of *Saccopastore 1* from Buzi et al. (2018) (46) (top of the page); 3D model segmented from a standard CT-scan with 0.7 mm slice thickness (bottom of the page).

As for the reliability, only two studies included repeated measurements in their model (66) (68), while the coefficient of variation, intraclass correlation coefficient, standard error of measurement, combined standard uncertainty of measurement (136,137), along with interrater data, have not been investigated yet.

Moreover, while a few studies provided the standard deviation for the whole sample (52,66), reliability comparing repeated measurements of the same variable on the same specimen was rarely studied, and only one study provided some data on UCR-DP reliability in measuring bone surface areas (66), showing a slightly better performance of UCR-DP compared to laser scanning.

Most studies (29,46,52,65,66,68,79,129), with only one exception (43), agree that UCR-DP results are comparable to those produced by osteometry (65,66,68), CT-scanning (46,68), laser scanning (66,68,79,129), or structured light scanning (79) (Table 4). The bias was generally below the 2 mm threshold, that is considered an acceptable error in osteometry (138). Moreover, frequency histograms produced for UCR-DP 3D models measurements were unimodal and normally distributed, meaning that errors were fundamentally random (68).

UCR-DP has been acknowledged to reproduce fully recognisable anatomical traits, although some skeletal areas are more prone to having artifacts (66,68). Moreover, differently to CT, MRI, and some range techniques, the presence of a photorealistic texture is of invaluable help in locating landmarks and fine structures (Figure 20, a1-a2). However, when acquiring a human cranium with standard lenses, meshes obtainable via UCR-DP are less dense than those derived from a CT-scanning (Figure 20, b1-b2). Therefore, although the detail appears adequate in describing the human cranium, it could be insufficient to study smaller structures. More research is needed on the subject. In fact, the sub-optimal performance reported by some authors on relatively small specimens could be due to their size compared to that of the frame, particularly where macro lenses have not been adopted (65), or due to the use of discrete shooting sessions (51,65).



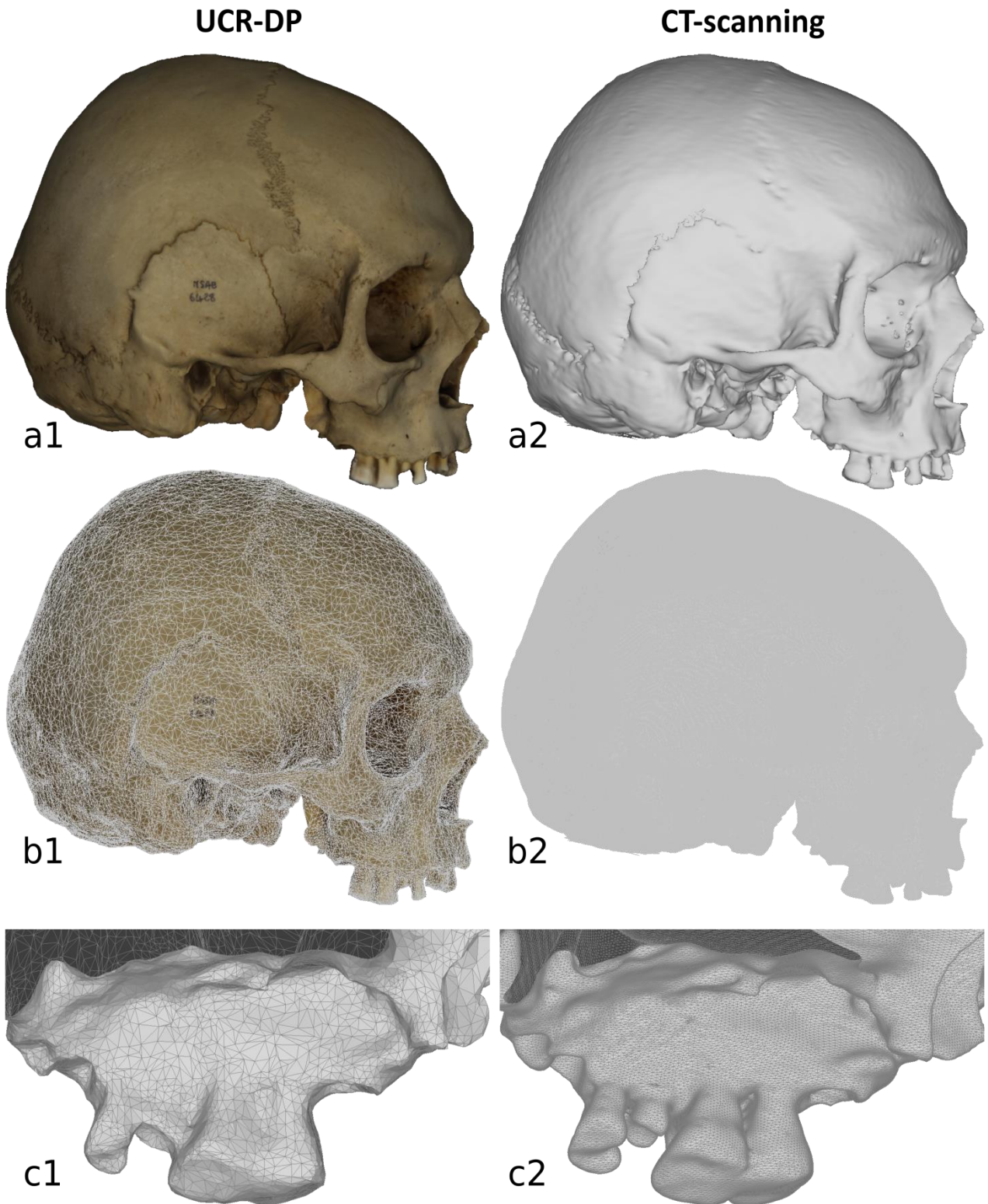


**Figure 20.** Comparison between UCR-DP (left) and CT-scanning (right) in describing the cranium MSAE-6428 ([MuSAE, Università degli Studi di Cagliari, Italy](#)). a1-a2. Visual restitution of the whole specimen. b1-b2. Mesh density for the whole specimen. c1-c2. Mesh density detailing the geometry. UCR-DP data collection with two Canon EOS 1200D DSLRs at 100 ISO, using prime 50 mm f/1.8 lenses, 50 cm shooting distance, 5500 K light sources; 3D reconstruction via [ReCap Photo](#) cloud-based environment. CT data collection with a Siemens SOMATOM Definition Flash CT-scanner and 0.75 mm slice thickness; segmentation via [3D Slicer](#).

In the case of in-situ documentation, in which the geometric features of the site are recorded jointly with those of the skeletal remains, the scale of the resulting 3D model is so small that accuracy error is likely to rise over the acceptable threshold for osteometric applications (29,52). In such context, if accuracy is a priority, it is perhaps advisable to use a multimodal method of data collection, using UCR-DP for capturing the skeletal remains at a larger scale and laser scanning for capturing the surrounding environment at a smaller scale (60).

As for the reliability, no study evaluated UCR-DP precision, interrater error or combined standard uncertainty of the measurement (136,137). Validations assessing the agreement between two techniques with the well standardised Bland-Altman technique (68) are not conclusive if precision is not independently assessed for both techniques through repeated measurements of the same variable on the same specimen.

Indeed, an apparent lack of agreement, or poor agreement, shown by UCR-DP with a reference technique could be the artifactual effect of the measurement imprecision in UCR-DP, in the reference technique, or in both (139). Indeed, data from the present research, and illustrated in the next chapter, showed a higher precision for UCR-DP compared to osteometry.

### Limits

The limitations of the review could be related to an incomplete retrieval of identified research due to the lack of terminology standardisation and an improper definition of the technique, still frequent in the literature. However, the inclusion in the search query of several terms inappropriately used for referring to the technique, along with the backward and forward citation analyses of selected studies, should have reduced such risk. Considering the outcome level of the studies, risk of bias could be linked to the frequently observed poor agreement to basic photographic principles, incomplete description of the protocol, limited sample size, and choice of inadequate statistical techniques.



## Conclusions

UCR-DP offers many significant advantages over other 3D scanning techniques: greater versatility in terms of application range and technical implementation, scalability, and photorealistic restitution. Further benefits include reduced requirements relating to hardware, labour, time, and cost, especially when applying cloud-based and free for academic use solutions. The technique is, therefore, an attractive option for capturing 3D spatial datasets in skeletal anthropology.

However, despite growing interest, UCR-DP still represents the least used method for three-dimensional reconstruction in skeletal anthropology. Related studies remain mainly of methodological concern, while there are not many actual applications. Most authors used commercial software packages and an offline approach. The sharing of 3D models was uncommon.

Furthermore, current research is still quite heterogeneous concerning methods, terminology, and quality of results. The protocols for 3D models production and the relative hardware are poorly described and not always in agreement with photographic principles and best practices. Indeed, besides some efforts, standardisation of UCR-DP methodologies and protocols, including the cloud-based approach, is still lacking.

Despite the insightful contribution of the reviewed studies, there is still the need for robust validation of UCR-DP, assessing both intra- and interrater accuracy and precision against a standardised reference technique, such as CT-scanning. Furthermore, the validation of software packages other than Photoscan, which is obsolete, and that of the cloud-based approach, are entirely lacking.

The application of standardised protocols, along with improved adherence to basic photographic principles during data collection, would level outcome accuracy and reproducibility of future research similar to the best practice studies.

Simultaneous analysis of UCR-DP, osteometry, and CT-scanning, performed on the same skeletal sample, under osteometric standards, involving multiple observers, repeated measurements, and different types of landmarks, along with the appropriate statistical procedures, would probably be conclusive for the technique reliability.

The cloud-based approach could further facilitate the production and open access sharing of extensive collections for research and communication purposes. Such effectiveness is highly relevant given the amount of undocumented prehistoric and historic skeletal material and sites, especially in low and middle-income countries.

## A NEW APPROACH: CLOUD-BASED UCR-DP

### Offline versus cloud computing for UCR-DP

Virtual anthropology studies human anatomical data through three-dimensional representations produced via several techniques (20). In general, the most accurate techniques involve expensive equipment, trained operators (21,22,60) and, therefore, are difficult to be applied to skeletal collections and large samples. Ultra close-range digital photogrammetry (UCR-DP) (27) enables photorealistic 3D reconstructions from photographs of the specimen taken from different perspective views, and is applicable to subjects about the size of the human body. It also offers significant advantages over other 3D scanning techniques, including greater versatility in terms of application range, technical implementation, and scalability, reduced hardware requirements, and photorealistic restitution of the specimens.

The most widespread software packages for UCR-DP, such as the former PhotoScan, now [MetaShape](#) (*Agisoft, Russia*), use an offline approach (27), i.e. they run on the hardware provided by the user. In this way, they usually require a good amount of computational time on powerful workstations and frequent operator intervention to produce a single 3D model at a time and, therefore, they are time-consuming and difficult to apply to large samples.

New cloud-based software environments host the processing logic and data storage capabilities into remote servers operated by a third-party services provider (Figure 21), thus enabling 3D models to be obtained via the Internet without high-end workstations and operator supervision. The input photographs are uploaded without prior masking and the three-dimensional outcome is downloaded almost effortlessly at the end of the processing.

Even though the application of the cloud-based approach could facilitate the preservation, study, and dissemination of large skeletal samples and collections, studies using it in skeletal anthropology are still the exception (42), while relatively few studies use UCR-DP at all (27).

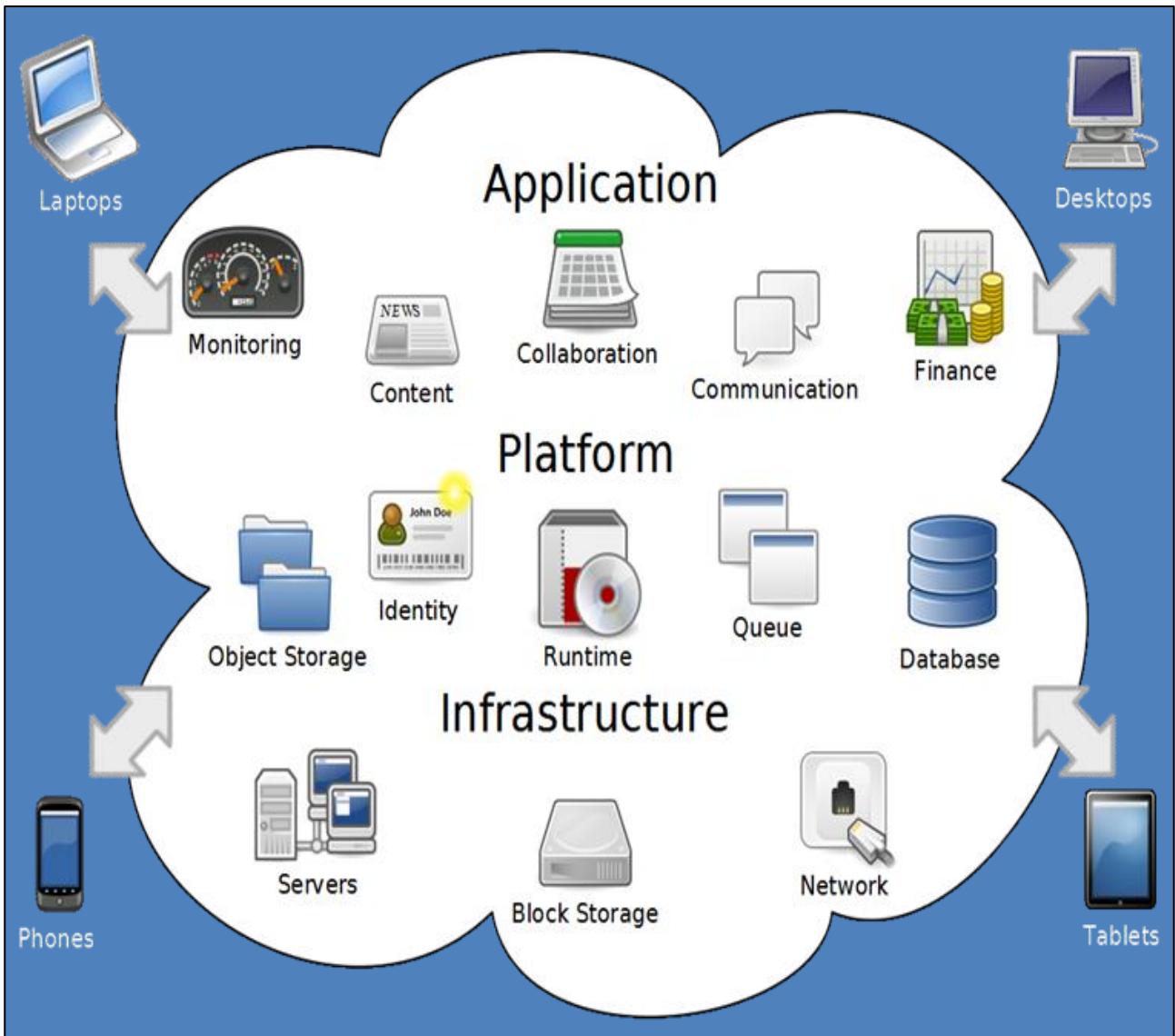


**Figure 21.** In a cloud-based software environment the processing logic, including the hardware infrastructure and the software services, is hosted into remote servers operated by a third-party services provider. Users access the services via their local hardware and an Internet connection. Original image by Sam Johnston, licensed under [CC BY-SA 3.0](https://creativecommons.org/licenses/by-sa/3.0/); modified by [Paolo Lussu](#).

Indeed, the application of cloud-based UCR-DP to skeletal anthropology has been hampered by the absence of specific protocols, while only recently a protocol for the application of the offline approach to cranial bones has been proposed (68).

Besides, although a few studies assessed UCR-DP accuracy with respect to osteometry (29,52,65,68), 3D coordinate digitiser (65), laser scanning (66,129), or microtomography (46), the sample size and measurement variety have usually been limited, reliability was rarely studied, and interrater data

had not been investigated yet (27). In addition, validation of software packages other than Photoscan, and of a cloud-based approach, is completely lacking (27).

This chapter aims to propose a protocol for the application of cloud-based UCR-DP to skeletal anthropology and to validate its accuracy and reliability, with respect to osteometry and CT-scanning, under osteometric standards, involving two observers, repeated measurements, and different types of landmarks and tools.

### Materials and methods

Ten well-preserved human crania, including individuals diagnosed of both sexes, and one infant, all dating back to the XIX century, were selected from the osteological collection of the Museo Sardo di Antropologia ed Etnografia ([MuSAE, Università degli Studi di Cagliari](#), Italy) (101).

A total of 40 3D models were created independently by 2 raters: 20 via CT-scanning and 20 using UCR-DP. To account for accuracy, each rater performed the same set of 12 measurements on the crania and the corresponding UCR-DP and CT-scanning 3D models. To account for reliability, each measurement was taken 3 times, with a minimum interval of 24 hours between repetitions.

**Table 5.** Study design – Sample and measurements.

Sample	Measurement technique	Reference technique	Measurements	Raters	Replications
10 crania	<b>Osteometry</b>	–	9 standard osteometric <sup>2</sup> 3 arbitrary <sup>3</sup>	2	3
20 CT-scanning 3D models <sup>1</sup>	<b>Virtual osteometry</b>	Osteometry			
20 UCR-DP 3D models <sup>1</sup>	<b>Virtual osteometry</b>	Osteometry CT-scanning			

<sup>1</sup> Ten for each rater. <sup>2</sup> Of which one could not be completed on CT-scanning 3D models. <sup>3</sup> Parallel to the body axes.

### Shooting protocol

The proposed shooting protocol has specifically been designed under photographic principles (27,44,67,69,78) for UCR-DP recording of skeletal remains.

Crania were placed in front of two cameras, on a turntable inside a lightbox (Figure 22).

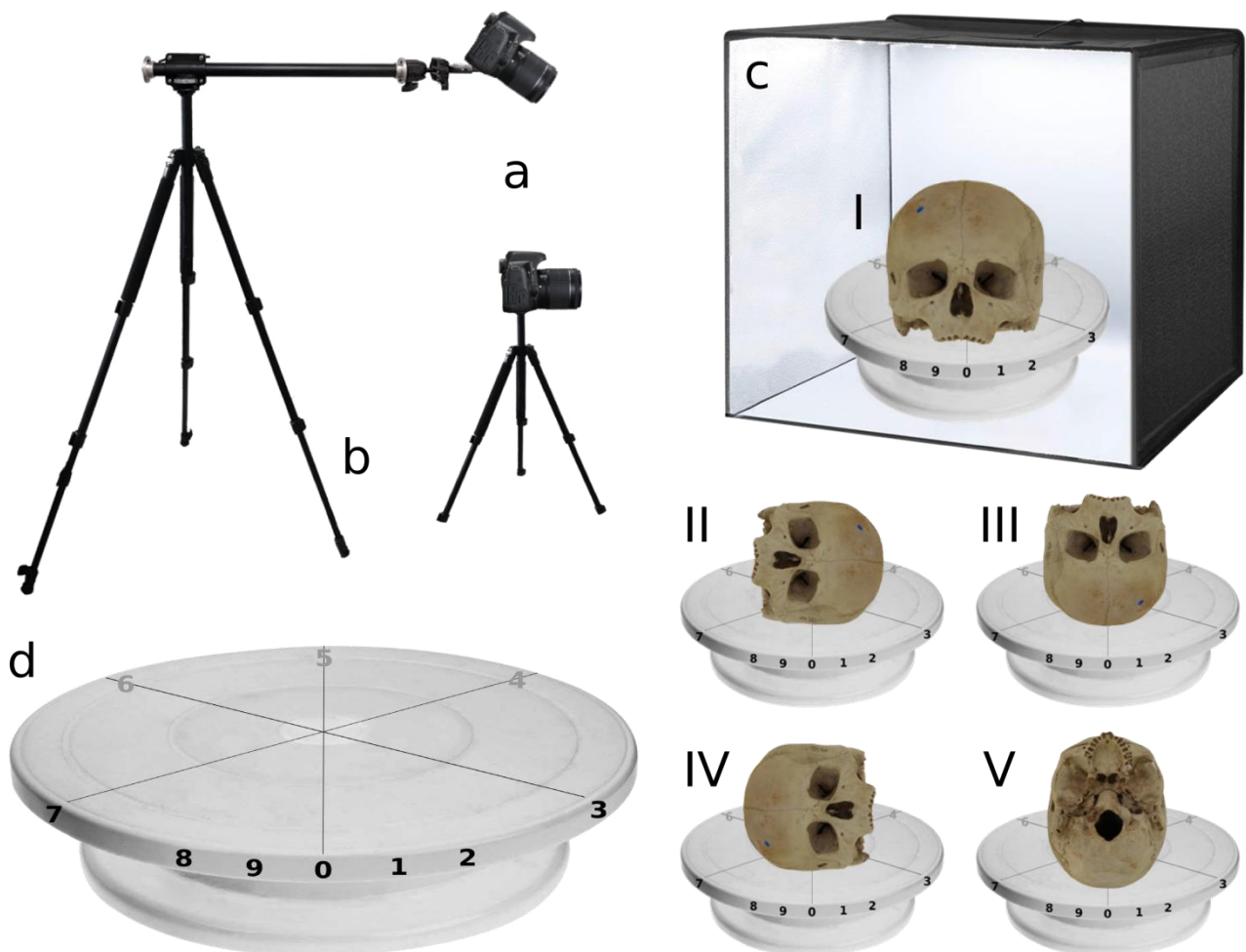


**Figure 22.** Studio equipment, specimen installation and perspective changes for 3D model acquisition through UCR-DP. <sup>a</sup> EOS 1200D digital single-lens reflex cameras (Canon Inc., Tokyo, Japan). <sup>b</sup> Camera tripods (Manfrotto, Italy) on which cameras were installed at different heights (0 cm and 50 cm) and tilts (0° and 35°) with respect to the specimen centre. <sup>c</sup> Lightbox. <sup>d</sup> Turntable with planned poses. <sup>I-V</sup> Specimen positioning. <sup>0-9</sup> Turntable poses acquired for each specimen position.

To enhance the actual image resolution and maximise its signal-to-noise ratio we used digital single-lens reflex (DSLR) cameras with APS-C CMOS sensors and 50 mm prime lenses; ISO sensitivity was set to 100 ISO, the minimum allowed by the cameras, and blur was prevented using a tripod mount and remote shutter release.

To increase the depth of field the lens diaphragm was closed until the whole specimen was in focus, at f/22 aperture. In fact, any further increase would have only reduced resolution and introduced unwanted geometrical features from the surrounding environment in the frame. Cameras were set to aperture priority mode (A or Av), where the shutter speed is chosen accordingly to the diaphragm aperture, returning proper exposure based on the lighting conditions.

A recording distance between 50 and 75 cm was chosen and adjusted to match the specimen's apparent maximum dimension with the camera frame size, so as to acquire the maximum detail while taking the necessary precautions to avoid any cropping.

As for the shooting environment, a plain and out of focus background was used to isolate the subject. Moreover, a lightbox and three softboxes (with 5500 K colour temperature, similar to daylight), two placed above the lightbox and one in front of it, beside the cameras, were used to ensure uniform, indirect lighting. White balance was adjusted accordingly to ensure colour accuracy.

The precautions mentioned above ensure that the maximum number of in-focus features of the specimen are captured, while avoiding the need to mask the shots and removing any unwanted geometry before passing the photographs into the 3D reconstruction software.

Sequential and continuous shooting sessions were applied to obtain a single complete mesh combining at once all the acquired perspective views. The DSLRs were oriented towards the specimens with different tilts, enabling the capture of two perspective views at once.

The perspective change was achieved by installing the specimen in 5 different positions (I to V), and then rotating it using a white turntable with planned poses (Figure 22, numbered from 0 to 9). After the installation in *position I*, with the prosthion aligned with the 0, the specimen was rotated to achieve 10 perspective views from each camera. The procedure was repeated after changing the specimen to positions *II*, *III*, *IV* and *V*, thus resulting in the complete coverage of its external surface. A total of 100 photographs were acquired for each specimen. Coverage was denser for the front and basal standards (i.e. poses numbered from 8 to 2).



### 3D models production

*Cloud UCR-DP.* Photographs were taken following the newly proposed protocol, detailed in APPENDIX: UCR-DP PROTOCOL, page 157. The cameras were connected to a notebook PC via USB 3.0 cables and hub. Image acquisition was controlled via [digiCamControl](#), thus enabling multiple camera management for sequential shooting sessions (27) and automatic image indexing and storage. The resulting photographs were processed employing [ReCap Photo](#) (Autodesk Inc., USA) cloud services. UCR-DP 3D models were scaled to their real dimensions using [ReCap Photo Scale by Value](#) function.

*CT-scanning.* The crania were placed to lie on their base and scanned by a [SOMATOM Definition Flash](#) 128-slice CT-scanner (Siemens, Germany), with a slice thickness of 0.75 mm, at 120 kVp, convenient for bone tissue detection (Figure 23). Data resulted in a Digital Imaging and Communications in Medicine ([DICOM](#)<sup>®</sup>) dataset (48). Segmentation to produce the 3D models was performed using the open-source software package [3D Slicer](#) 4.10.2 (140). The segmentation threshold was adjusted to return an external surface of the 3D model the most similar to the one of the specimens. The result was saved in OBJ file format.



**Figure 23.** The sample at the [Istituto di Radiologia ed Ecografia Deriu](#) (Cagliari, Italy) just minutes before the start of the CT-scanning.

## Measurements

In accordance with Martin & Saller (141), a set of 9 standard measurements widely used in osteometry (Table 6; Figure 24) was chosen, involving a variety of digital and analogue tools, and landmarks. In particular, we considered 4 *type I* landmarks (bregma, dacryon, nasion, lambda), defined by juxtaposition of discrete structures; 3 *type II* (*basion*, *ectoconchion*, *opistion*), identified by the maximum curvature of a single structure, and 4 *type III* (*glabella*, *opisthocranium*, *eurion*, *zygion*), defined by the extreme points of a structure (142,143) (Table 6).

**Table 6.** Summary of the osteometric and arbitrary measurements performed on specimens and 3D models.

Type	Instrument (division)	#	Measurement (reference # (141))	Landmarks <sup>1</sup>
Osteometric	Analogue spreading calliper ( $\pm 0.05$ cm)	1	Skull length (#1)	gl – op
		2	Skull breadth (#8)	eu – eu
		3	Skull total height (#17)	ba – br
		4	Total face breadth (#45)	zy – zy
	Digital sliding calliper ( $\pm 0.01$ cm)	5	Biorbital breadth (#44)	ec – ec
		6	Interorbital breadth (#50)	d – d
		7	Frontal chord (#29)	n – br
		8	Parietal chord (#30)	br – l
		9	Occipital chord (#31)	l – o
Arbitrary (scaling)		10	Calibration baseline, parallel to the sagittal plane	$a - b$ <sup>2</sup>
		11	Calibration check line, parallel to the coronal plane	$c - d$ <sup>2</sup>
		12	Calibration check line, parallel to the long. body axis	$e - f$ <sup>2</sup>

<sup>1</sup> *gl*, glabella; *op*, opisthocranium; *eu*, eurion; *ba*, basion; *br*, bregma; *zy*, zygion; *ec*, ectoconchion; *d*, dacryon; *n*, nasion; *l*, lambda; *o*, opistion. <sup>2</sup> Measurement between precisely pinpointable arbitrary landmarks.

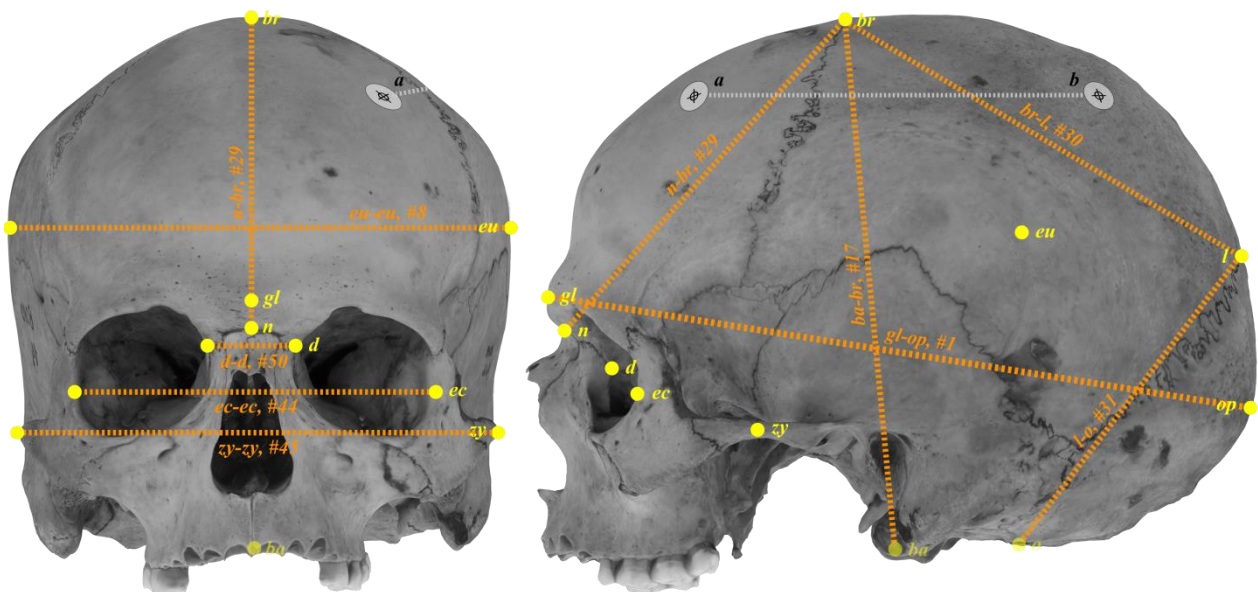


**Figure 24.** Summary of the anthropometric measurements taken in front and lateral views. The linear length  $a-b$  was defined on each specimen between two arbitrary landmarks and used for UCR-DP 3D model scaling.

Scaling measurements considered arbitrary landmarks, each pinpointed with small, circular marking label with two intersecting lines printed on its centre to ensure the maximum precision in locating them. The linear length  $a - b$  (Table 6: landmarks  $a, b$ ; Figure 24: length from  $a$  to  $b$ ), of approximately 10 cm, parallel to the sagittal plane, was defined as the calibration baseline. Here, the average of three measurements was used as a calibration baseline and data value for the *Scale by Value* function in [ReCap Photo](#). Arbitrary lengths along two other directions parallel to the coronal (Table 6: landmarks  $c, d$ ) and the longitudinal planes (Table 6: landmarks  $e, f$ ) were used to verify the scaling consistency. Such precautions were fundamental because an incorrect scaling would affect the accuracy of all subsequent measurements carried out on the digitalised specimens.

*Osteometry.* Specimens were mounted in a craniophor and oriented following the Frankfurt plane. Linear measurements were taken with a digital sliding calliper (to the nearest hundredth/100th of a millimetre) or with an analogue spreading calliper (to the nearest half of a millimetre) (Table 6).

*CT-scanning and UCR-DP.* 3D models derived from CT and UCR-DP both underwent the same virtual osteology standardised measurement protocol using [ReCap Photo](#). Furthermore, the 3D model production time was registered for CT (scan, production, and downloading) and UCR-DP (shooting, data uploading, data downloading, and scaling).

#### *Statistical analysis*

*Descriptive statistics.* Mean, variance, standard deviation and coefficient of variation were calculated for each set of measurements. The Kolmogorov-Smirnov (144) and D'Agostino-Pearson tests (145) were performed, and frequency histograms were drawn, to confirm whether the observed differences between the alternative techniques followed a normal distribution.

*Accuracy.* According to the observed variances, paired sample homoscedastic t-tests for two-tailed distributions were performed to verify whether average measurements taken with alternative techniques were significantly different.

In accordance with Bland & Altman (139,146), and using [MedCalc](#) 12.7 (MedCalc Software Ltd, Belgium), plots were drawn to analyse the consistency between the alternative techniques. One interrater and two intrarater plots were produced for each measurement and comparison (UCR-DP vs. osteometry; UCR-DP vs. CT-scanning; CT-scanning vs. osteometry). Bias was defined as the mean difference between measured values. The 95% limits of agreement (LOA = bias  $\pm$  1.96 SD) were calculated considering the effect of the replicated measurements. The bias and LOA percentage values were calculated with respect to the mean measured value.

Furthermore, one interrater plot was produced for each osteological measurement and technique comparison to take into account the single repetitions on each specimen, and analyse possible size-related effects on accuracy by drawing the linear regression graph for the differences between the techniques, along with its confidence interval.

Lastly, one interrater and two intrarater plots were drawn, for each technique comparison, including all osteological measurements, grouped by measurement, rater, and specimen, so as to summarise the agreement between the techniques in a wide range of application.

One similar interrater plot was produced for each technique comparison to show the scatter of the single osteological measurements, and analyse any overall size-related effect on accuracy by drawing the linear regression graph for the differences between the techniques, along with its confidence interval.

*Reliability.* The intra- and interrater reliabilities were estimated using the intra-class correlation coefficients (ICC) – (2,1) and (2,2) models, respectively – with absolute agreement [24]. The Currier (147) criterion was used to evaluate the ICC results: 0.90–0.99, high reliability; 0.80–0.89, good reliability; 0.70–0.79, fair reliability; less than 0.69, poor reliability.

The percent coefficient of variation (CV%) and the standard error of measurement (SEM =  $\sqrt{1-ICC}$ ) were also calculated and a paired sample homoscedastic t-test for two-tailed distributions was run to confirm whether differences in CV% between the techniques were significant.

## Results

### *3D model production and measurement*

To produce the 3D models using the newly proposed cloud UCR-DP protocol, users are only required to upload the photographs, without prior masking, and to download the three-dimensional outcome at the end of the processing.

The cloud UCR-DP software environment allowed the processing of multiple 3D models at once. 3D model production took between 14 and 21 minutes for each specimen, including the shooting session, scaling and post-processing. The 10 3D models produced by UCR-DP by rater 2 were made available online (148).

Remarkably, only landmarks defined by geometric features, which are detectable in the three-dimensional space independently by the specimen appearance, can be identified using 3D models derived from CT-scanning data.

For instance, some type I (142,143) landmarks (e.g., bregma, nasion, lambda) were variably visible, depending on the level of closure of the sutures. Conversely, the dacryon was consistently undetectable and, therefore, the interorbital breadth #50 had to be excluded from the comparative analysis.

### *Descriptive statistics*

The Kolmogorov-Smirnov and D'Agostino-Pearson tests agreed that differences between UCR-DP and osteometry and between CT-scanning and osteometry were normally distributed. Differences between UCR-DP and CT-scanning were normally distributed according to the Kolmogorov-Smirnov test, but not for D'Agostino-Pearson's.

However, the frequency histograms showing the differences between the mean measurements obtained with all the techniques were unimodal, and visually approximated a normal distribution (Figure 25).

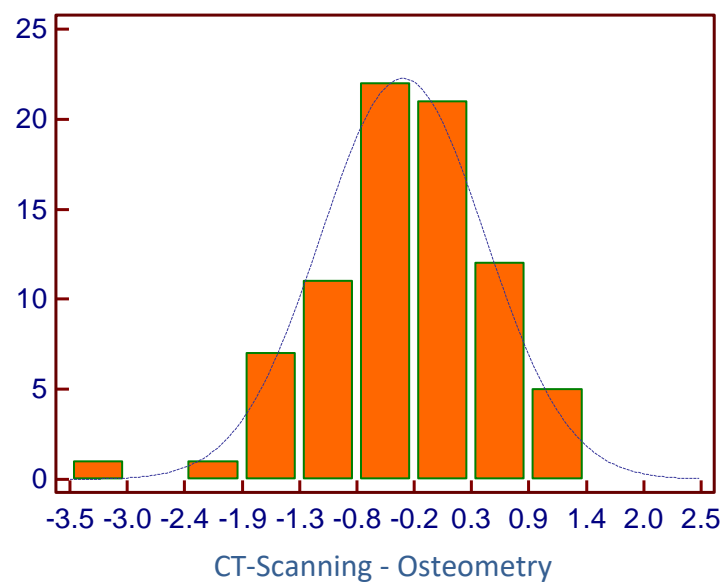
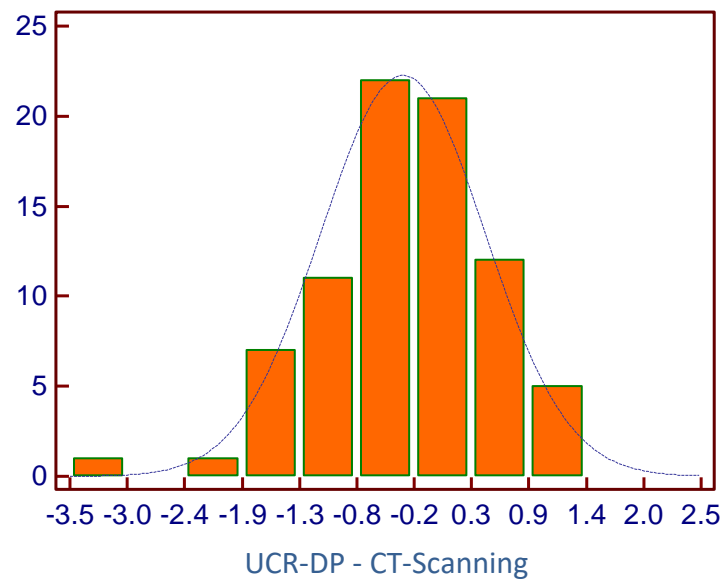
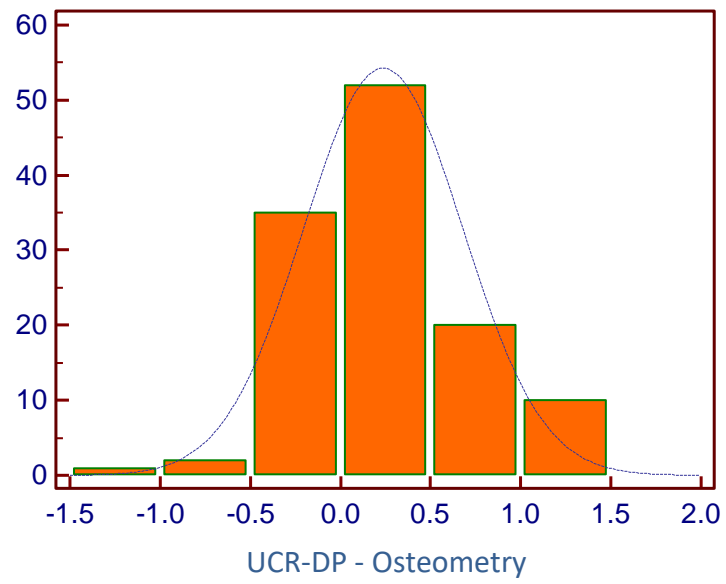


**Figure 25.** Frequency histograms showing the differences between interrater mean measurements carried out with the alternative techniques under study.

### *Accuracy*

The t-tests confirmed that the mean difference between the paired measurements taken with the alternative techniques is, in any case, significantly different from 0 ( $p < 0.0001$  for UCR-DP - osteometry, UCR-DP - CT-scanning, and CT-scanning - osteometry).

Interrater data (Table 7) concerning the osteological measurements considered altogether showed an average UCR-DP bias of 0.35 mm (0.27%) referring to osteometry and -0.3 mm (0.3%) to CT-scanning (Figure 26 and Figure 27, top). Accordingly, CT-scanning showed an average bias of 0.7 mm (0.5%) referring to osteometry (Figure 28, top). The plots showing the differences between the techniques as a percentage, the scatter of the measured values for any kind of osteological measurement, and the linear regression line, along with its confidence interval, are displayed at the bottom.

The interval defined between the upper and lower LOA% showed an amplitude of 2.77% between UCR-DP and osteometry, of 3.83% between UCR-DP and CT-scanning, and 3.88% between CT-scanning and osteometry (Table 7). Overall, when considering each osteometric measurement separately, the LOA% was narrower for UCR-DP compared to CT-scanning in most cases.

The LOA% amplitude observed for the agreement between UCR-DP and osteometry was found significantly different from that observed for the agreement between CT-scanning and osteometry ( $p = 0.0434$ ).

When considering specific osteometric measurements, the interrater agreement is shown in Figure 29, Figure 30, and Figure 31 for UCR-DP and osteometry; in Figure 32, Figure 33, and Figure 34 for UCR-DP and CT-scanning, and in Figure 35, Figure 36, and Figure 37 for CT-scanning and osteometry.

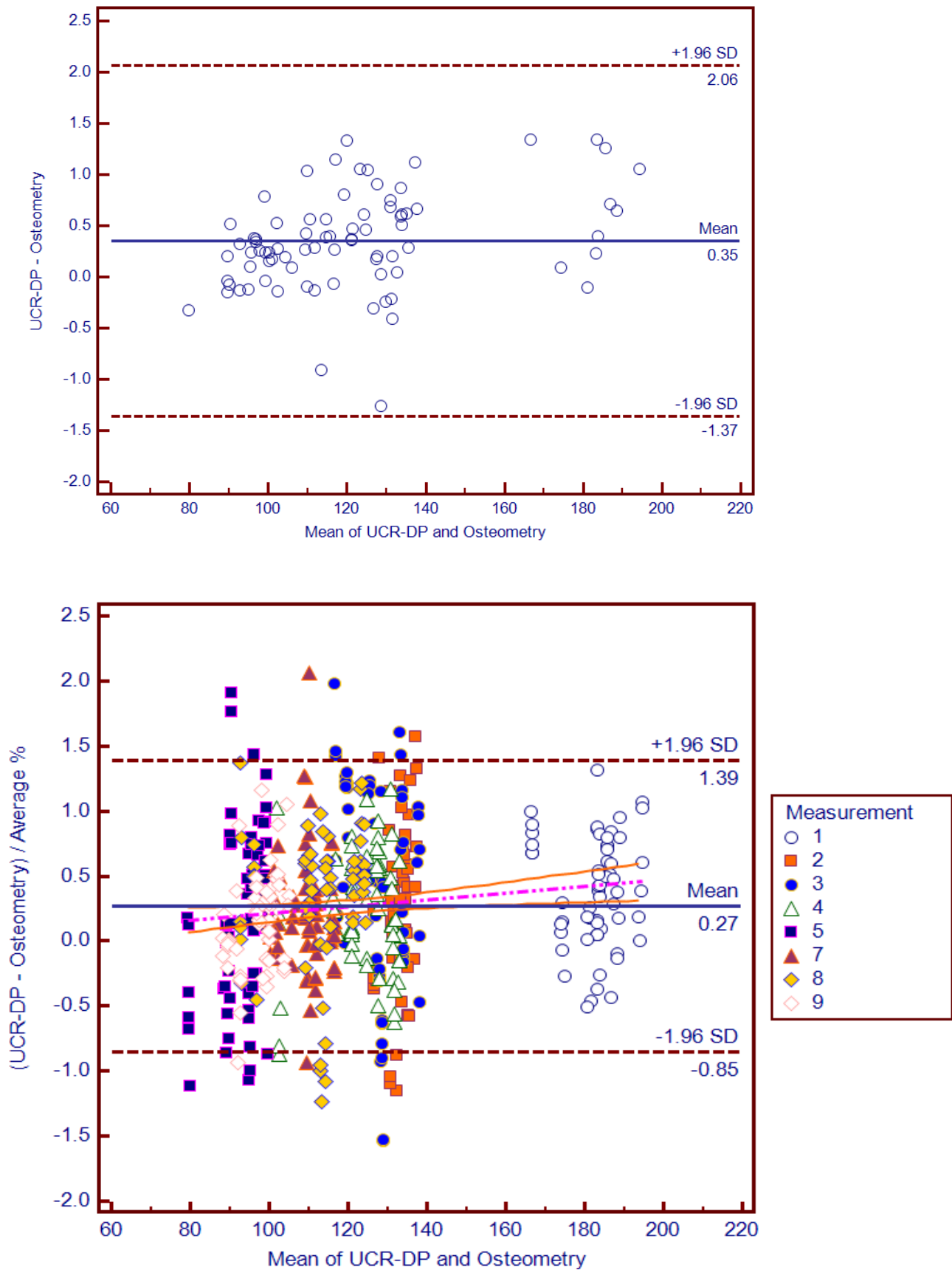
In such figures, the 95% limits of agreement ( $LOA = \text{bias} \pm 1.96 \text{ SD}$ ) calculated considering the effect of the replicated measurements are shown in the upper graph. The lower graph shows, instead, the scatter of the single measurements and the linear regression plot.

Table 7. Accuracy of UCR-DP with respect to osteometry and CT-scanning in measuring human crania.

Measurement	UCR-DP against OSTEOMETRY						UCR-DP against CT-SCANNING						CT-SCANNING against OSTEOMETRY						
	Rater 1		Rater 2		Interrater		Rater 1		Rater 2		Interrater		Rater 1		Rater 2		Interrater		
	Bias	LoA	Bias	LoA	Bias	LoA	Bias	LoA	Bias	LoA	Bias	LoA	Bias	LoA	Bias	LoA	Bias	LoA	
Anatomical landmarks	gl-op (1) mm	0.52	[-0.68, 1.72]	0.88	[-0.77, 2.53]	-0.70	[-0.81, 2.21]	-0.72	[-2.71, 1.27]	-1.30	[-4.90, 2.30]	-1.00	[-4.00, 2.00]	1.20	[-0.80, 3.30]	2.10	[-0.60, 4.90]	1.70	[-0.90, 4.30]
		%	0.28	[-0.37, 0.94]	0.48	[-0.42, 1.38]	-0.38	[-0.44, 1.21]	-0.39	[-1.48, 0.69]	-0.71	[-2.67, 1.25]	-0.54	[-2.18, 1.09]	0.66	[-0.44, 1.80]	1.14	[-0.33, 2.67]	0.93
	eu-eu (8) mm	0.55	[-1.18, 2.28]	0.12	[-1.32, 1.56]	0.30	[-2.30, 2.90]	0.27	[-1.70, 2.24]	-1.00	[-5.40, 3.40]	-0.40	[-3.80, 3.00]	0.30	[-1.90, 2.50]	1.20	[-3.20, 5.50]	0.70	[-2.40, 3.90]
		%	0.41	[-0.89, 1.72]	0.09	[-1.00, 1.18]	0.23	[-1.73, 2.19]	0.20	[-1.28, 1.68]	-0.75	[-4.07, 2.56]	-0.30	[-2.86, 2.26]	0.23	[-1.43, 1.88]	0.90	[-2.41, 4.14]	0.53
	ba-br (17) mm	0.01	[-1.71, 1.73]	1.08	[-0.64, 2.80]	0.54	[-1.34, 2.43]	-0.30	[-1.17, 0.57]	0.19	[-0.83, 1.21]	-0.06	[-1.06, 0.95]	0.31	[-1.23, 1.86]	0.89	[-0.33, 2.10]	0.60	[-0.98, 2.18]
		%	0.01	[-1.34, 1.36]	0.85	[-0.50, 2.20]	0.42	[-1.05, 1.91]	-0.24	[-0.92, 0.45]	0.15	[-0.65, 0.95]	-0.04	[-0.83, 0.75]	0.24	[-0.97, 1.46]	0.70	[-0.26, 1.65]	0.47
	zy-zy (45) mm	0.03	[-1.07, 1.13]	0.53	[-0.48, 1.53]	0.28	[-0.86, 1.42]	-0.45	[-1.20, 0.30]	-0.38	[-1.40, 0.63]	-0.42	[-1.34, 0.50]	0.48	[-0.61, 1.57]	0.91	[-0.30, 2.11]	0.69	[-0.46, 1.85]
		%	0.02	[-0.86, 0.91]	0.43	[-0.39, 1.24]	0.23	[-0.70, 1.15]	-0.36	[-0.97, 0.24]	-0.31	[-1.13, 0.51]	-0.33	[-1.08, 0.40]	0.39	[-0.49, 1.27]	0.74	[-0.24, 1.70]	0.56
	ec-ec (44) mm	0.34	[-0.95, 1.62]	0.03	[-1.15, 1.21]	0.19	[-1.25, 1.62]	-0.20	[-2.20, 1.80]	0.31	[-0.89, 1.50]	0.06	[-1.79, 1.90]	0.53	[-0.89, 1.96]	-0.27	[-1.62, 1.08]	0.13	[-1.46, 1.72]
		%	0.37	[-1.02, 1.74]	0.03	[-1.24, 1.30]	0.20	[-1.34, 1.74]	-0.21	[-2.36, 1.93]	0.33	[-0.96, 1.62]	0.06	[-1.92, 2.04]	0.57	[-0.96, 2.10]	-0.29	[-1.75, 1.16]	0.14
	d-d (50) mm	0.06	[-1.15, 1.27]	0.07	[-0.79, 0.92]	0.06	[-1.63, 1.75]												
		%	0.27	[-5.14, 5.68]	0.32	[-3.60, 4.19]	0.27	[-7.36, 7.90]											
	n-br (29) mm	0.07	[-0.62, 0.76]	0.38	[-0.83, 1.60]	0.23	[-0.96, 1.41]	-0.70	[-3.30, 2.00]	0.10	[-2.50, 2.70]	-0.30	[-2.90, 2.30]	0.70	[-2.20, 3.70]	0.30	[-2.50, 3.00]	0.50	[-2.30, 3.30]
		%	0.06	[-0.57, 0.70]	0.35	[-0.76, 1.46]	0.21	[-0.88, 1.29]	-0.64	[-3.01, 1.82]	0.09	[-2.28, 2.46]	-0.27	[-2.65, 2.10]	0.64	[-2.01, 3.38]	0.27	[-2.28, 2.74]	0.46
	br-l (30) mm	0.36	[-0.68, 1.40]	0.41	[-1.01, 1.84]	0.39	[-1.22, 1.99]	0.10	[-2.90, 3.20]	-0.40	[-3.90, 3.20]	-0.10	[-3.40, 3.20]	0.20	[-2.60, 3.10]	0.80	[-3.00, 4.60]	0.50	[-2.80, 3.80]
		%	0.32	[-0.61, 1.25]	0.37	[-0.90, 1.64]	0.35	[-1.09, 1.78]	0.09	[-2.58, 2.85]	-0.36	[-3.47, 2.85]	-0.09	[-3.03, 2.85]	0.18	[-2.32, 2.77]	0.71	[-2.67, 4.10]	0.45
	l-o (31) mm	0.08	[-0.44, 0.61]	0.21	[-0.65, 1.06]	0.14	[-1.64, 1.93]	-1.10	[-3.80, 1.70]	0.10	[-2.00, 2.20]	-0.50	[-2.70, 1.80]	1.20	[-1.60, 3.90]	0.10	[-2.10, 2.30]	0.60	[-1.70, 2.90]
		%	0.08	[-0.45, 0.63]	0.22	[-0.67, 1.09]	0.14	[-1.69, 1.98]	-1.13	[-3.90, 1.74]	0.10	[-2.05, 2.25]	-0.51	[-2.77, 1.84]	1.23	[-1.64, 4.00]	0.10	[-2.15, 2.36]	0.62
Arbitrary landmarks	Coronal mm	-0.09	[-0.41, 0.24]	-0.17	[-0.47, 0.13]	-0.13	[-0.55, 0.29]												
		%	-0.14	[-0.66, 0.38]	-0.27	[-0.75, 0.21]	-0.21	[-0.88, 0.46]											
	Sagittal mm	0.01	[-0.18, 0.20]	0.01	[-0.14, 0.16]	0.01	[-0.41, 0.43]												
		%	0.01	[-0.21, 0.24]	0.01	[-0.16, 0.19]	0.01	[-0.48, 0.51]											
	Vertical mm	0.14	[-0.25, 0.54]	0.08	[-0.22, 0.38]	0.11	[-0.32, 0.55]												
		%	0.24	[-0.42, 0.91]	0.13	[-0.37, 0.64]	0.18	[-0.54, 0.92]											
Summary	Anatomical landmarks <sup>1</sup> mm	0.24	[-1.01, 1.50]	0.45	[-1.01, 1.92]	0.35	[-1.37, 2.06]	-0.40	[-2.60, 1.90]	-0.30	[-3.20, 2.60]	-0.30	[-2.80, 2.20]	0.60	[-1.60, 2.90]	0.70	[-2.20, 3.70]	0.70	[-1.80, 3.20]
		%	0.19	[-0.85, 1.23]	0.35	[-0.83, 1.53]	0.27	[-0.85, 1.39]	-0.30	[-2.40, 1.70]	-0.20	[-2.50, 2.10]	-0.30	[-2.40, 1.90]	0.50	[-1.50, 2.50]	0.50	[-1.90, 2.90]	0.50
	Arbitrary landmarks <sup>2</sup> mm	0.02	[-0.34, 0.38]	-0.03	[-0.36, 0.30]	0.00	[-0.35, 0.34]												
%	0.04	[-0.55, 0.63]	-0.05	[-0.61, 0.52]	0.00	[-0.58, 0.58]													

<sup>1</sup> Summary of all measurements between anatomical landmarks, except for measurement d - d (50), which could not be carried out on CT-scanning 3D models. <sup>2</sup> Summary of all scaling measurements between arbitrary landmarks, taken with a digital sliding calliper.





**Figure 26.** Bland & Altman plots describing the interrater agreement between **UCR-DP and osteometry** for all measurements. Above, the plot showing the absolute differences. Each point identifies the mean of the three repetitions concerning any combination of osteometric measurement, specimen, and rater. Below, the plot showing the differences as a percentage. Here, measurements are grouped through a different point style. **1**, skull length (#1). **2**, skull breadth (#8). **3**, skull total height (#17). **4**, total face breadth (#45). **5**, biorbital breadth (#44). **7**, frontal chord (#29). **8**, parietal chord (#30). **9**, occipital chord (#31).

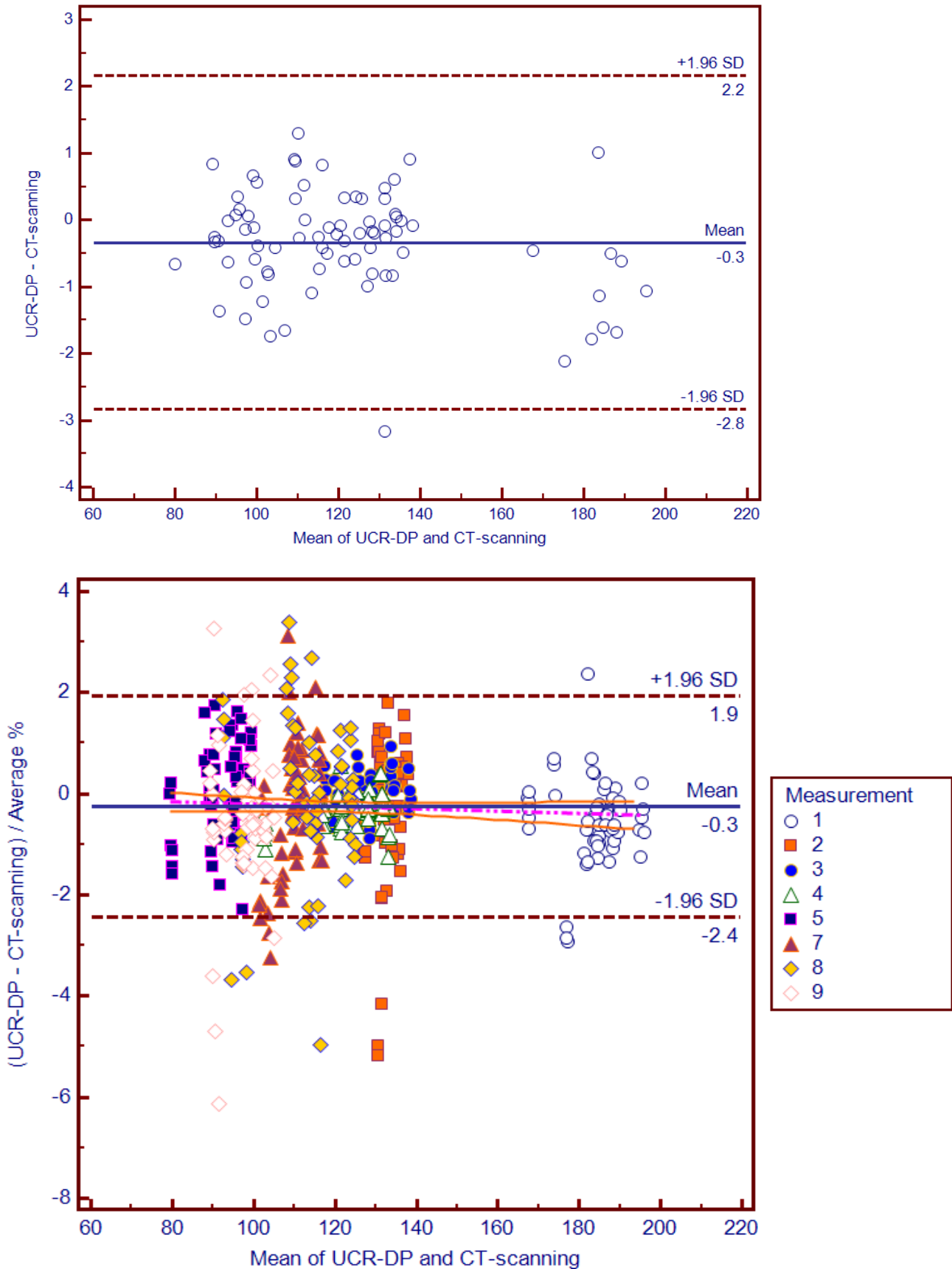


**Figure 27.** Bland & Altman plots describing the interrater agreement between **UCR-DP and CT-scanning** for all measurements. Above, the plot showing the absolute differences. Each point identifies the mean of the three repetitions concerning any combination of osteometric measurement, specimen, and rater. Below, the plot showing the differences as a percentage. Here, measurements are grouped through a different point style. 1, skull length (#1). 2, skull breadth (#8). 3, skull total height (#17). 4, total face breadth (#45). 5, biorbital breadth (#44). 7, frontal chord (#29). 8, parietal chord (#30). 9, occipital chord (#31). (141).

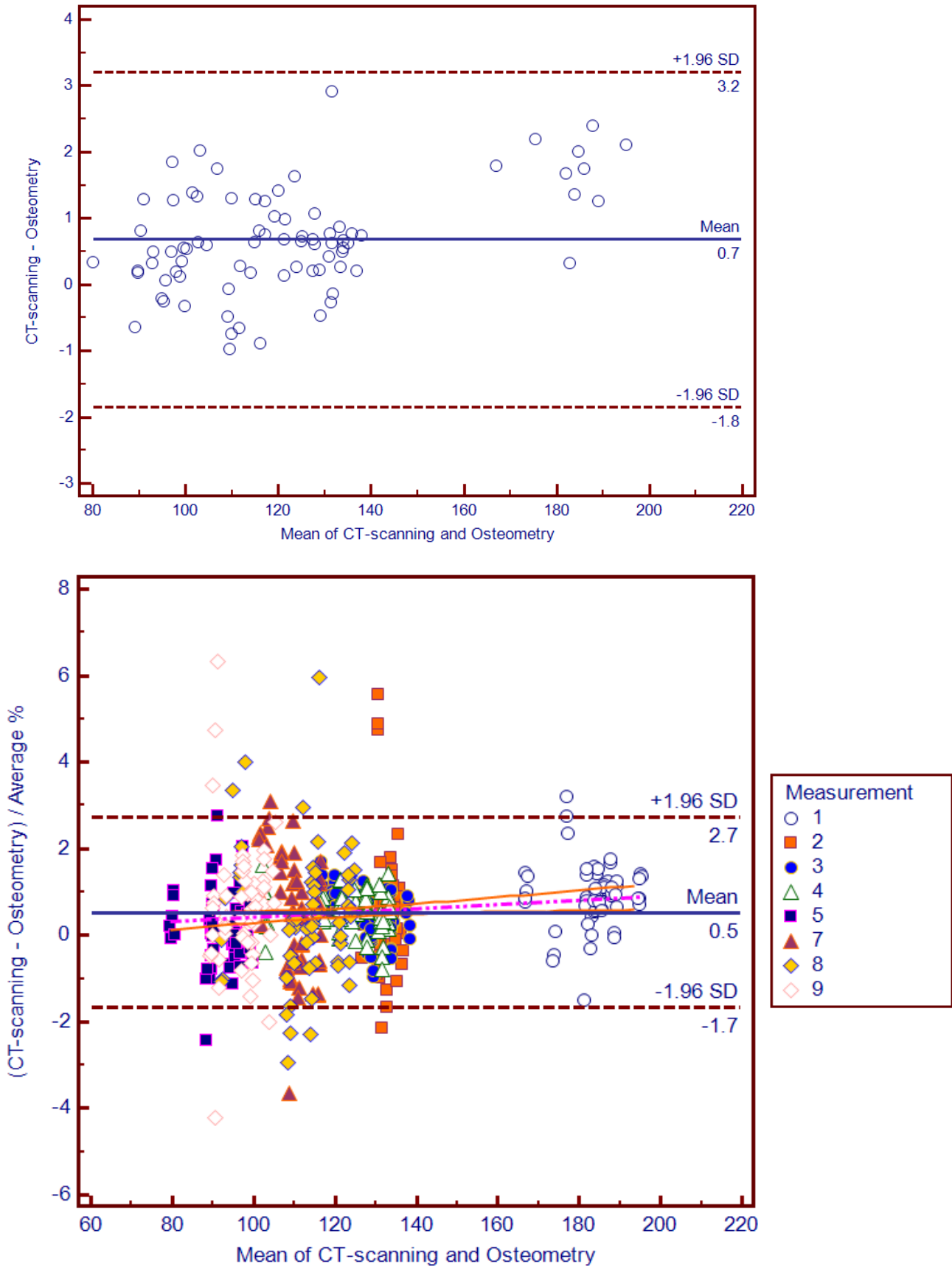


**Figure 28.** Bland & Altman plots describing the interrater agreement between **CT-scanning and osteometry** for all measurements. Above, the plot showing the absolute differences. Each point identifies the mean of the three repetitions concerning any combination of osteometric measurement, specimen, and rater. Below, the plot showing the differences as a percentage. Here, measurements are grouped through a different point style. **1**, skull length (#1). **2**, skull breadth (#8). **3**, skull total height (#17). **4**, total face breadth (#45). **5**, biorbital breadth (#44). **7**, frontal chord (#29). **8**, parietal chord (#30). **9**, occipital chord (#31). (141).

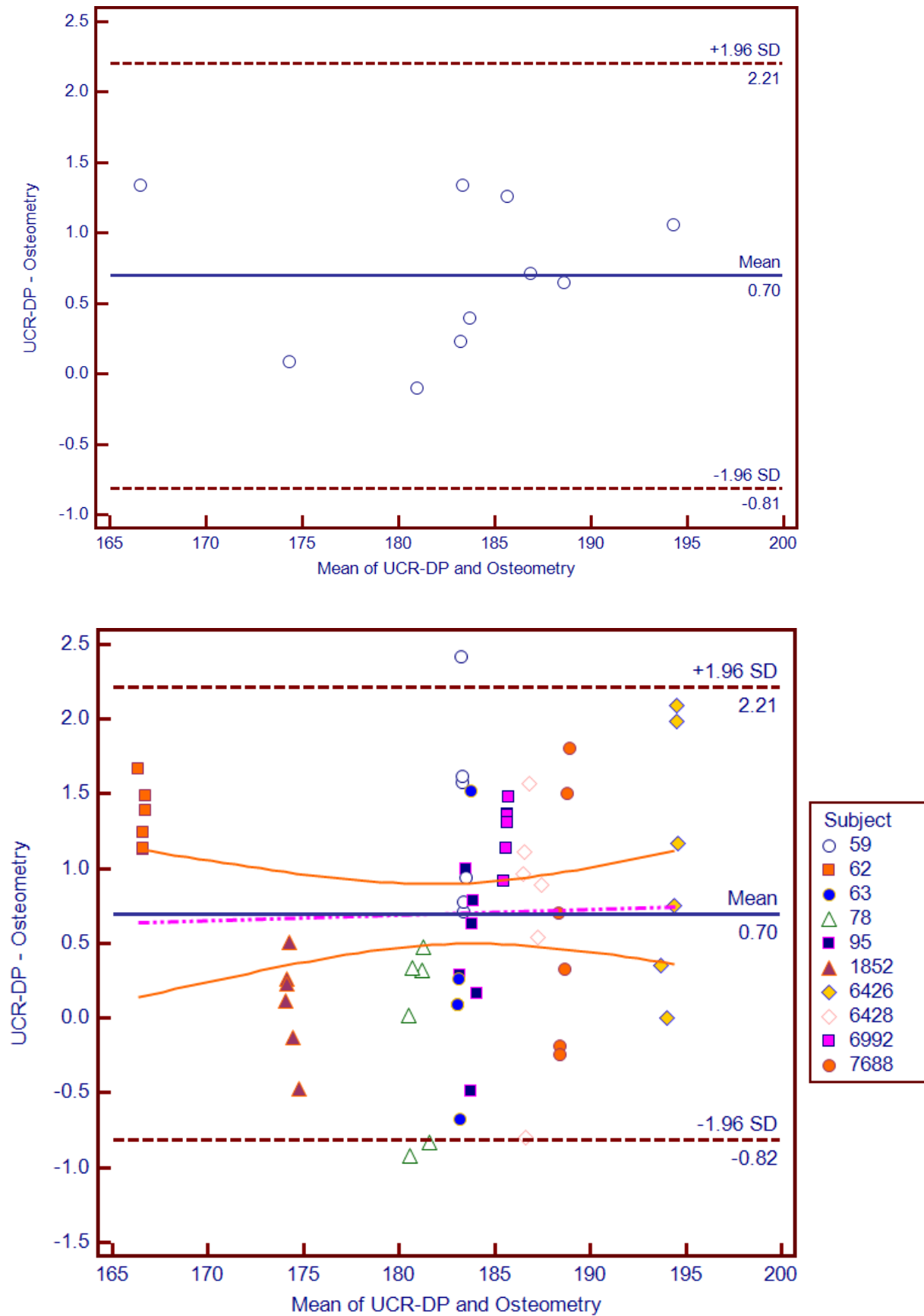


**Figure 29.** Bland & Altman plots describing the interrater agreement between **UCR-DP and osteometry** for measurement 1, **skull length (#1)** (141). Above, the plot showing the absolute differences between the mean measured values for each specimen. Below, the plot showing the scatter of the measured values for each specimen (subjects from 59 to 7688); here, the regression line for the differences between the techniques is drawn in light violet, and its confidence interval in light red.

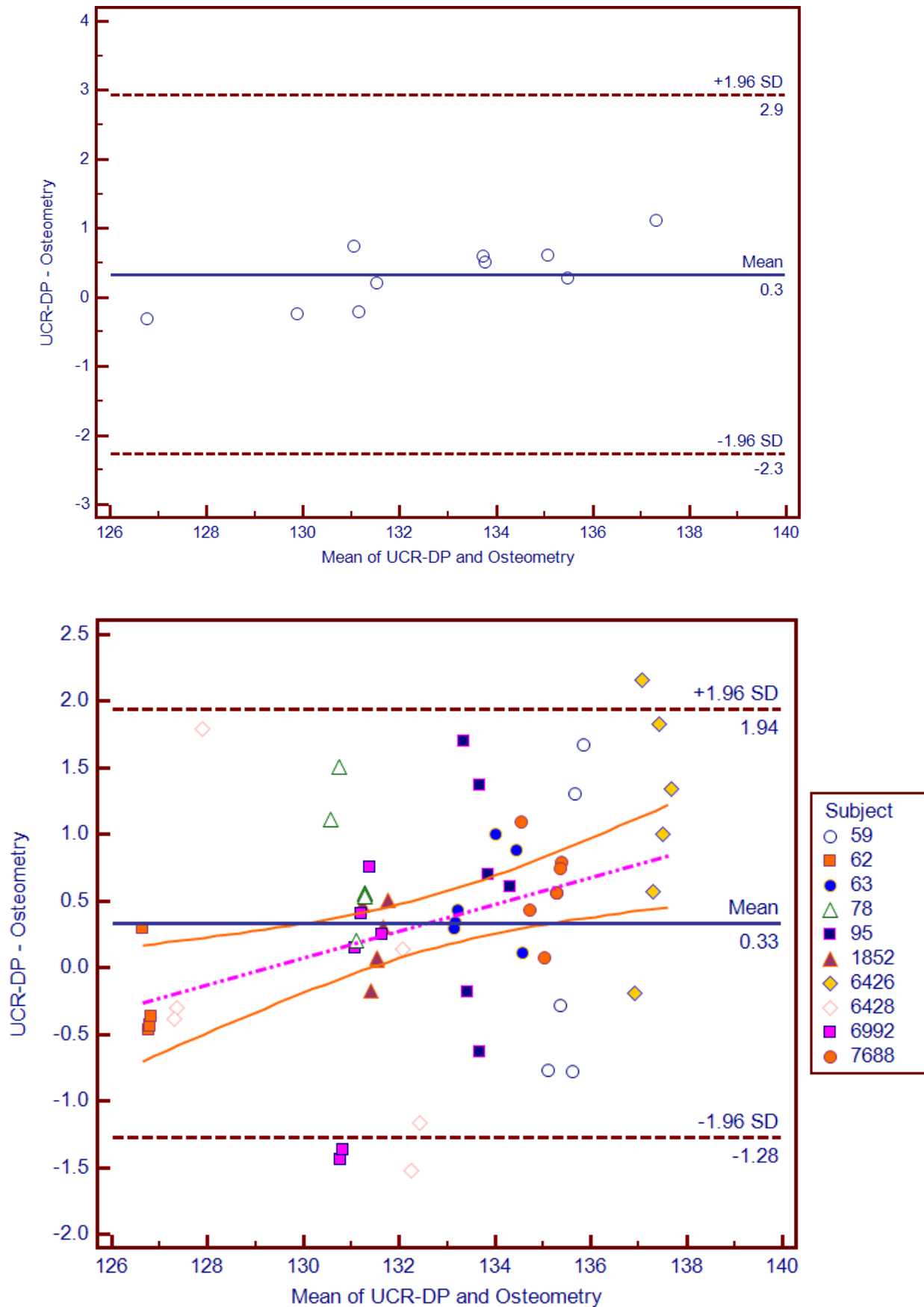


**Figure 30.** Bland & Altman plots describing the interrater agreement between **UCR-DP and osteometry** for measurement 2, **skull breadth (#8)** (141). Above, the plot showing the absolute differences between the mean measured values for each specimen. Below, the plot showing the scatter of the measured values for each specimen (subjects from 59 to 7688); here, the regression line for the differences between the techniques is drawn in light violet, and its confidence interval in light red.

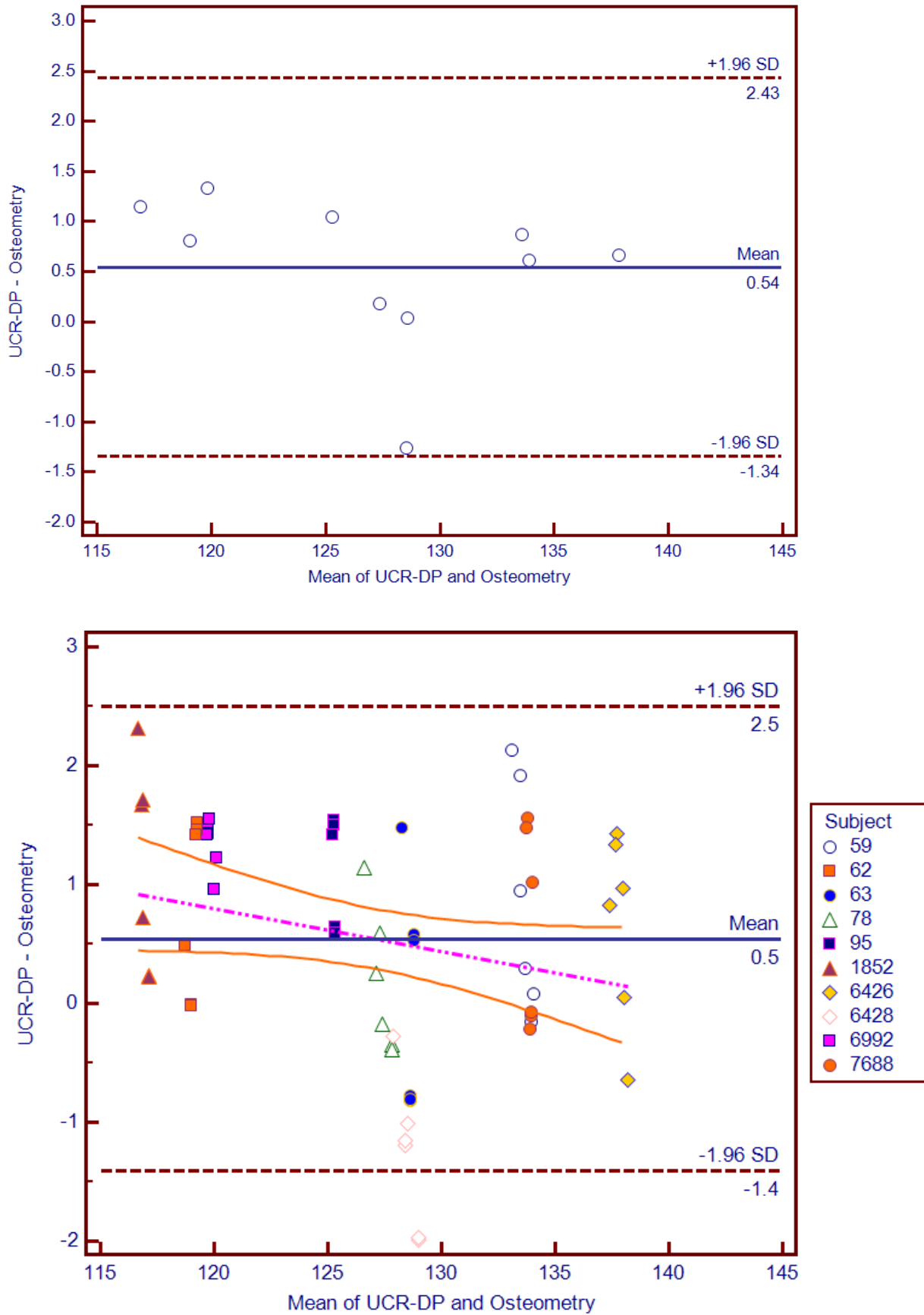


**Figure 31.** Bland & Altman plots describing the interrater agreement between **UCR-DP and osteometry** for measurement 3, **skull total height (#17)** (141). Above, the plot showing the absolute differences between the mean measured values for each specimen. Below, the plot showing the scatter of the measured values for each specimen (subjects from 59 to 7688); here, the regression line for the differences between the techniques is drawn in light violet, and its confidence interval in light red.

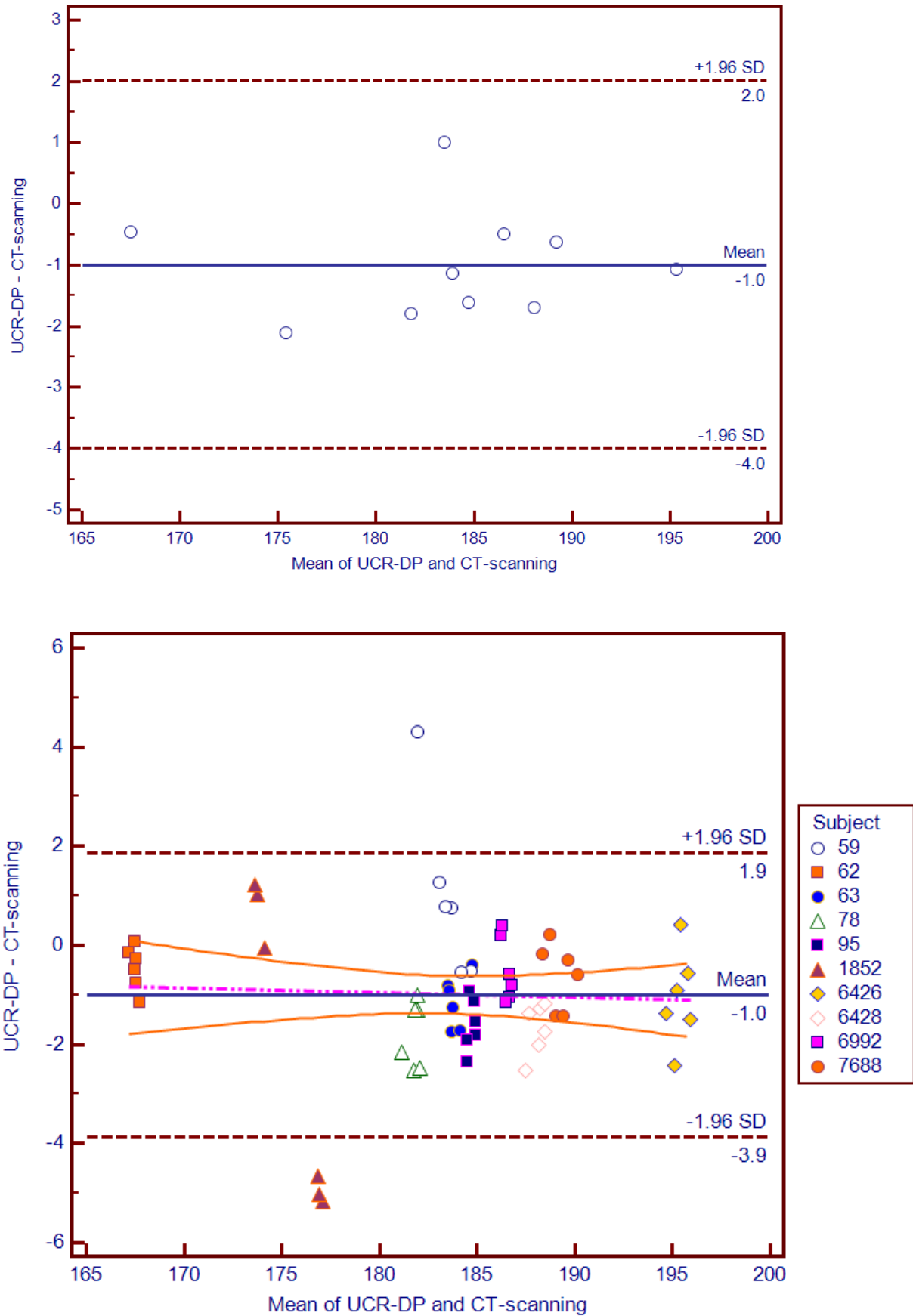


**Figure 32.** Bland & Altman plots describing the interrater agreement between **UCR-DP and CT-scanning** for measurement 1, **skull length (#1)** (141). Above, the plot showing the absolute differences between the mean measured values for each specimen. Below, the plot showing the scatter of the measured values for each specimen (subjects from 59 to 7688); here, the regression line for the differences between the techniques is drawn in light violet, and its confidence interval in light red.

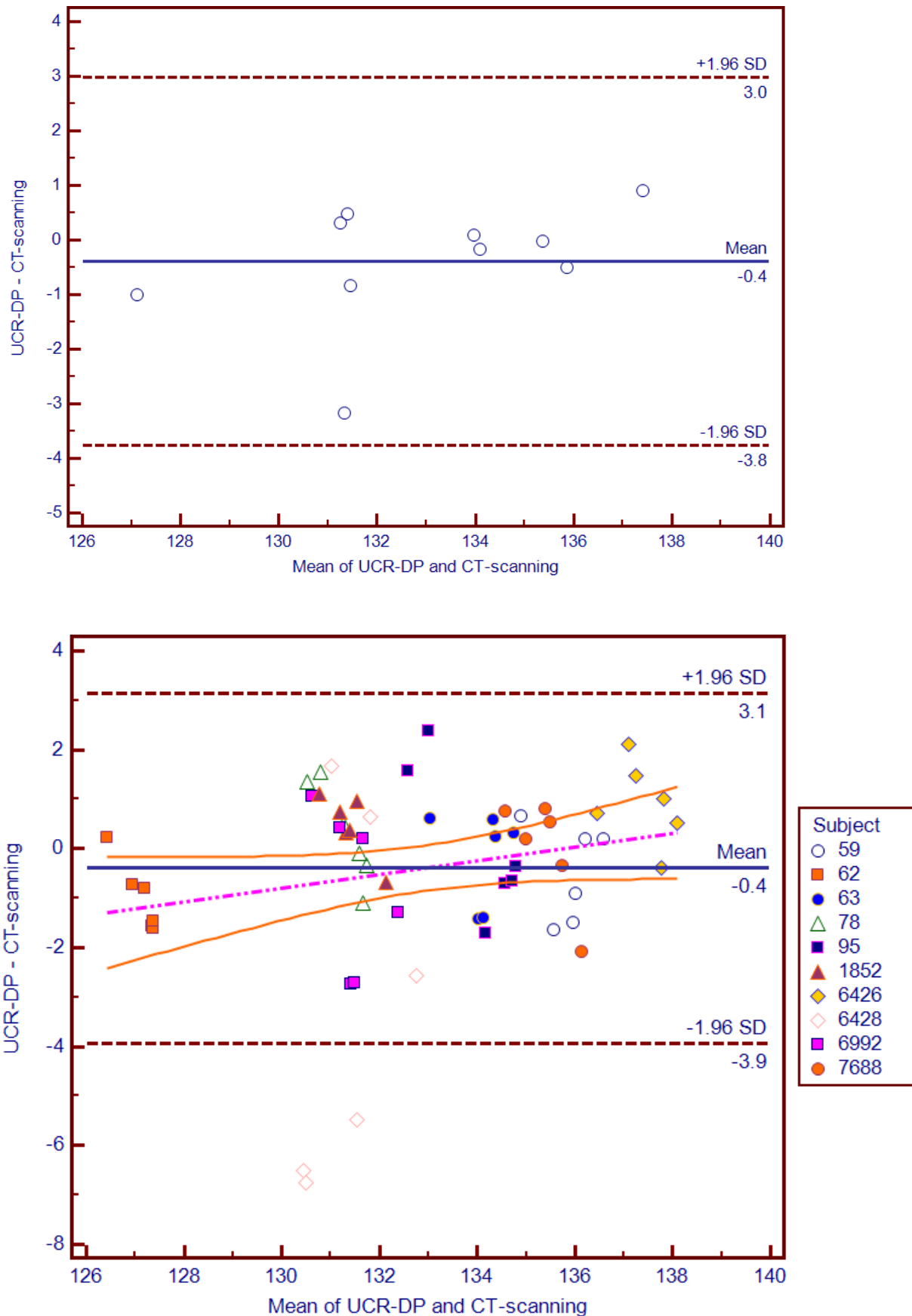


**Figure 33.** Bland & Altman plots describing the interrater agreement between **UCR-DP** and **CT-scanning** for measurement 2, **skull breadth (#8)** (141). Above, the plot showing the absolute differences between the mean measured values for each specimen. Below, the plot showing the scatter of the measured values for each specimen (subjects from 59 to 7688); here, the regression line for the differences between the techniques is drawn in light violet, and its confidence interval in light red.



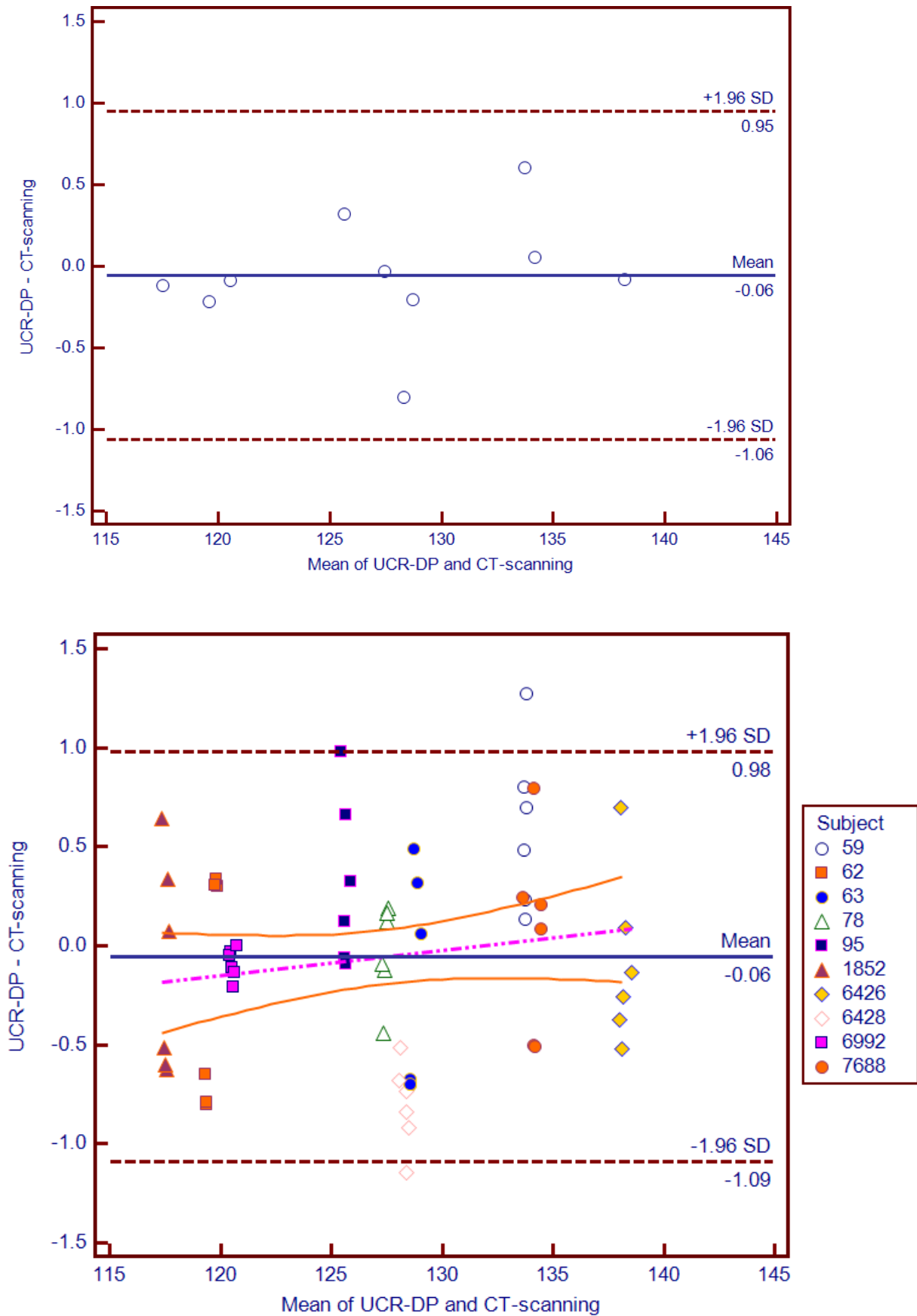


**Figure 34.** Bland & Altman plots describing the interrater agreement between **UCR-DP and CT-scanning** for measurement 3, **skull total height (#17)** (141). Above, the plot showing the absolute differences between the mean measured values for each specimen. Below, the plot showing the scatter of the measured values for each specimen (subjects from 59 to 7688); here, the regression line for the differences between the techniques is drawn in light violet, and its confidence interval in light red.

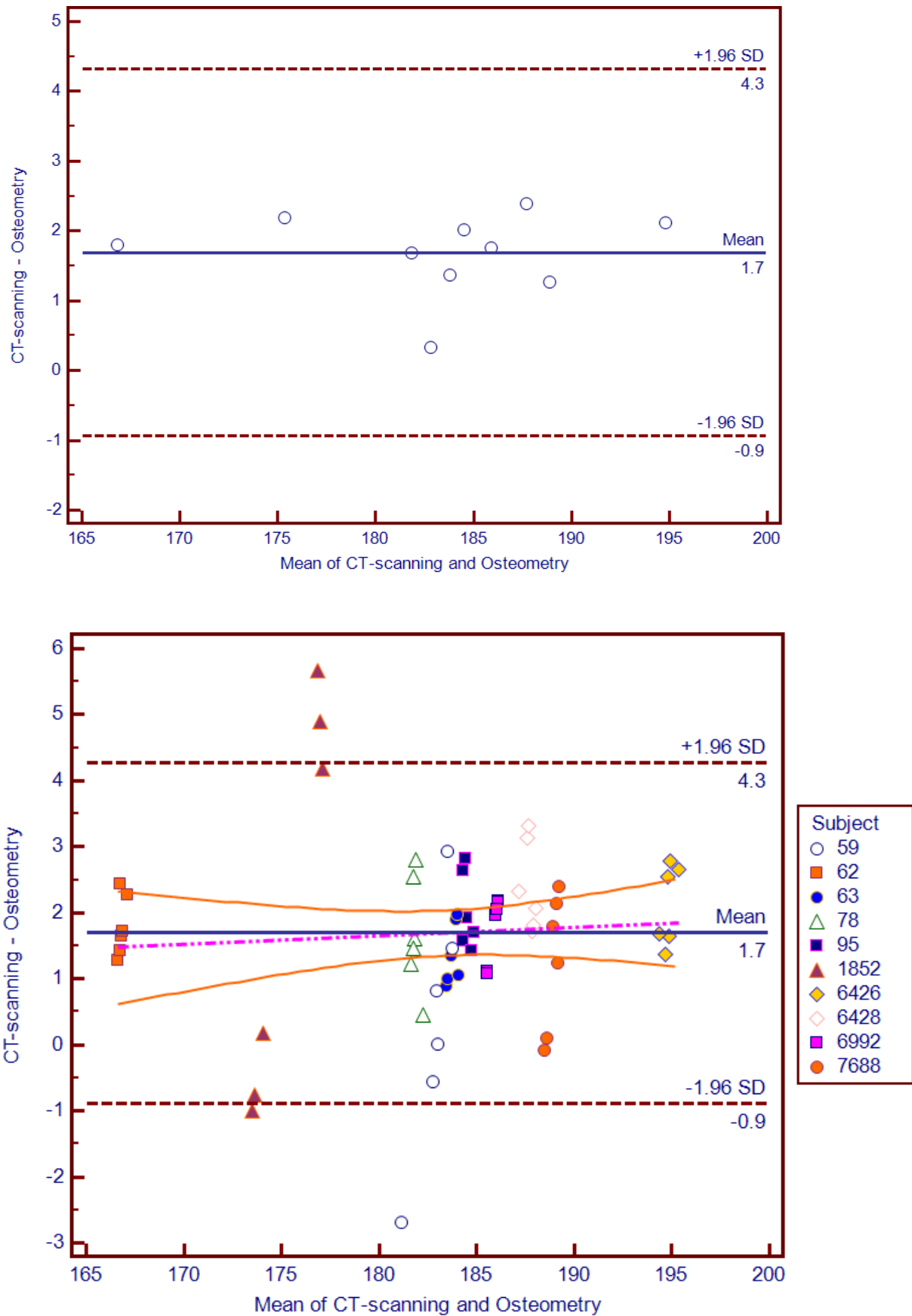


**Figure 35.** Bland & Altman plots describing the interrater agreement between **CT-scanning and osteometry** for measurement 1, **skull length (#1)** (141). Above, the plot showing the absolute differences between the mean measured values for each specimen. Below, the plot showing the scatter of the measured values for each specimen (subjects from 59 to 7688); here, the regression line for the differences between the techniques is drawn in light violet, and its confidence interval in light red.

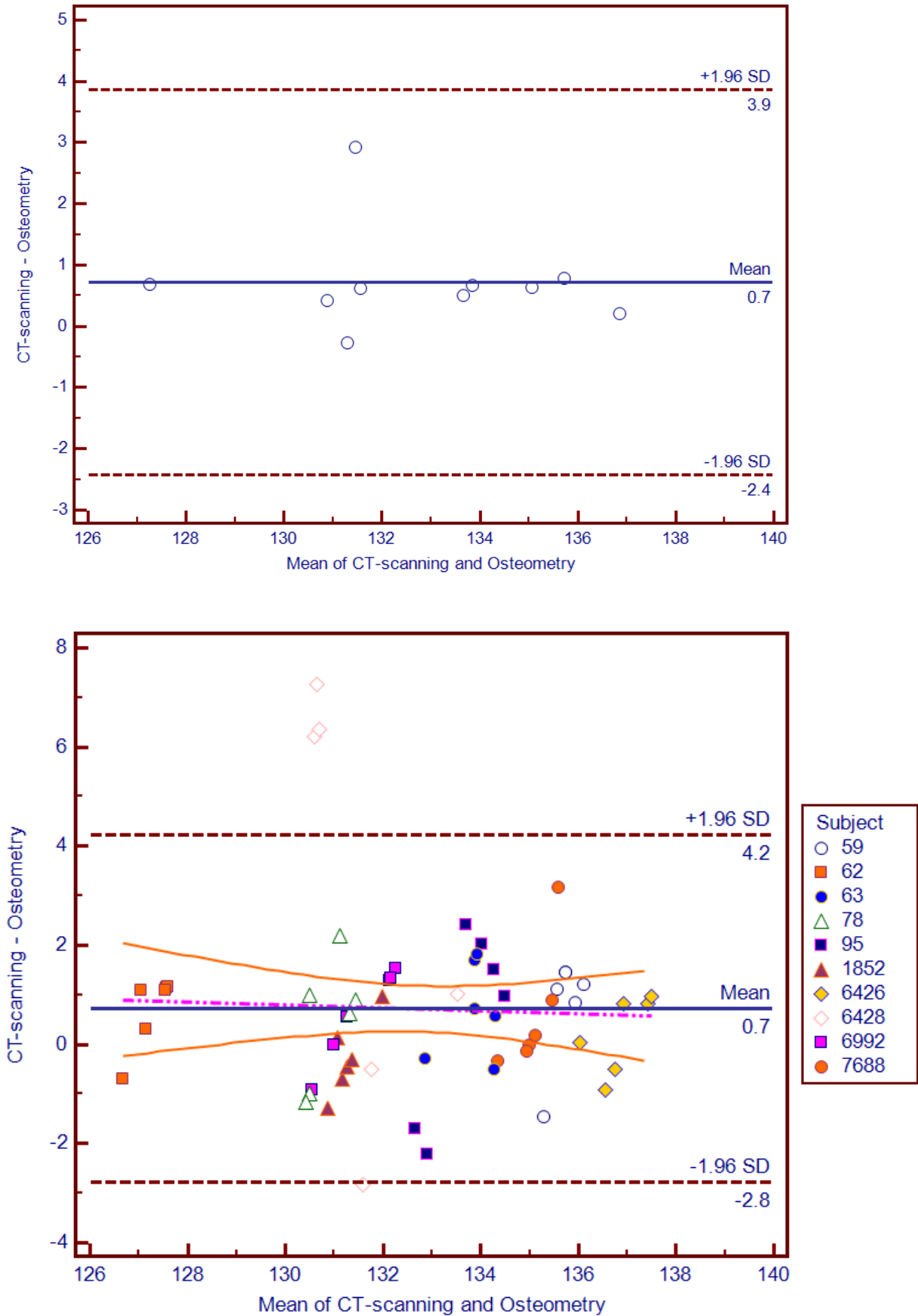


**Figure 36.** Bland & Altman plots describing the interrater agreement between **CT-scanning and osteometry** for measurement 2, **skull breadth (#8)** (141). Above, the plot showing the absolute differences between the mean measured values for each specimen. Below, the plot showing the scatter of the measured values for each specimen (subjects from 59 to 7688); here, the regression line for the differences between the techniques is drawn in light violet, and its confidence interval in light red.

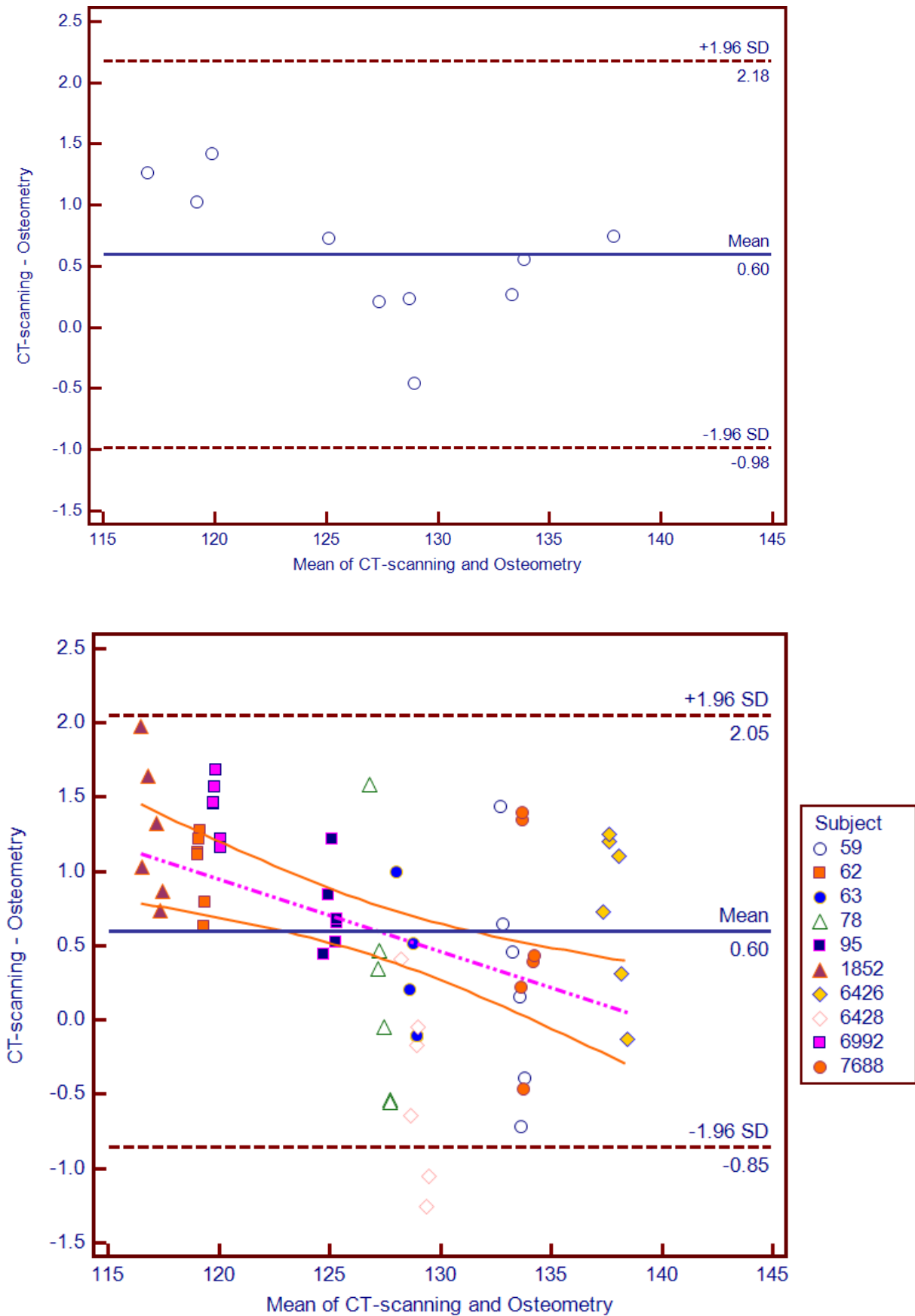


**Figure 37.** Bland & Altman plots describing the interrater agreement between **CT-scanning and osteometry** for measurement 3, **skull total height (#17)** (141). Above, the plot showing the absolute differences between the mean measured values for each specimen. Below, the plot showing the scatter of the measured values for each specimen (subjects from 59 to 7688); here, the regression line for the differences between the techniques is drawn in light violet, and its confidence interval in light red.

Interrater UCR-DP scaling measurements showed, overall, no bias with respect to osteometry. Intra- and interrater bias was consistently under 0.2 mm and 0.27% with respect to osteometry. In particular, the measurements along the sagittal plane, which were used to scale UCR-DP 3D models, showed a bias of no more than 0.1 mm and 0.1%, which was assessed as negligible ( $p = 0.9922$ ).

Intrarater data (Table 7) showed an absolute UCR-DP bias, with respect to osteometry, of less than 1 mm in all measurements except for #17 (ba-br) performed by rater 2. The absolute bias of UCR-DP with CT-scanning was less than 1 mm in all measurements except for #31 (l-o) performed by rater 1 and #1 (gl-op) and #8 (eu-eu) performed by rater 2. The absolute bias of CT-scanning with osteometry was over 1 mm in measurements #1 (gl-op) performed by both raters, measurement #31 (l-o) performed by rater 1, and measurement #8 (eu-eu) performed by rater 2.

#### *Reliability*

Interrater data (Table 8) for the osteological measurements considered altogether showed an average CV% of 0.350% for UCR-DP, 0.364% for osteometry, and 0.638% for CT-scanning. This picture is confirmed for both the observers, although CV% is higher for Rater 2.

Differences in CV% between UCR-DP and osteometry were not significant ( $p = 0.7112$ ) and likewise for those between CT-scanning and osteometry ( $p = 0.0515$ ). Conversely, differences between UCR-DP and CT-scanning were found to be significant ( $p = 0.0252$ ).

Interrater ICCs for measurements and techniques were always above the threshold defined by Currier (147) for good reliability. For the osteological measurements considered altogether, ICCs were 1.000 for the three techniques. Where considering specific osteometric measurements separately, ICCs range of variation was slightly narrower for osteometry (from 0.981 to 1.000) and UCR-DP (from 0.968 to 1.000) than for CT-scanning (from 0.954 to 1.000).

Table 8. Reliability of UCR-DP, osteometry, and CT-scanning in measuring human crania.

Measurements		Rater 1						Rater 2						Interrater			
		Mean $\pm$ SD (mm)			CV%	SEM	ICC	Mean $\pm$ SD (mm)			CV%	SEM	ICC	Mean $\pm$ SD (mm) All replicates	CV%	SEM	ICC
		Replicate 1	Replicate 2	Replicate 3				Replicate 1	Replicate 2	Replicate 3							
<b>UCR-DP</b>																	
Anatomical landmarks	gl-op (1)	182.87 $\pm$ 7.49	183.03 $\pm$ 7.67	182.96 $\pm$ 7.52	0.103	0.032	0.999	183.17 $\pm$ 7.80	183.24 $\pm$ 7.85	183.28 $\pm$ 7.85	0.181	0.055	0.997	183.09 $\pm$ 7.37	0.231	0.045	0.998
	eu-eu (8)	133.07 $\pm$ 3.26	133.19 $\pm$ 3.26	133.23 $\pm$ 3.35	0.176	0.089	0.992	132.10 $\pm$ 3.39	132.41 $\pm$ 3.56	132.40 $\pm$ 3.34	0.336	0.158	0.975	132.73 $\pm$ 3.25	0.500	0.192	0.963
	ba-br (17)	127.15 $\pm$ 6.81	127.22 $\pm$ 6.89	127.16 $\pm$ 6.82	0.037	0.000	1.000	127.55 $\pm$ 6.78	127.55 $\pm$ 6.81	127.53 $\pm$ 6.85	0.068	0.000	1.000	127.36 $\pm$ 6.53	0.223	0.032	0.999
	zy-zy (45)	123.71 $\pm$ 9.15	123.81 $\pm$ 9.17	123.66 $\pm$ 9.02	0.094	0.000	1.000	123.93 $\pm$ 9.16	123.84 $\pm$ 9.23	123.80 $\pm$ 9.17	0.209	0.032	0.999	123.79 $\pm$ 8.76	0.196	0.000	1.000
	ec-ec (44)	93.10 $\pm$ 6.05	93.36 $\pm$ 6.01	93.21 $\pm$ 6.09	0.347	0.071	0.995	93.04 $\pm$ 6.09	93.00 $\pm$ 6.03	92.94 $\pm$ 5.96	0.188	0.032	0.999	93.11 $\pm$ 5.78	0.516	0.084	0.993
	d-d (50)	22.39 $\pm$ 2.92	22.38 $\pm$ 2.91	22.39 $\pm$ 2.88	0.312	0.032	0.999	21.99 $\pm$ 3.44	22.01 $\pm$ 3.37	21.94 $\pm$ 3.43	0.670	0.045	0.998	22.18 $\pm$ 3.04	2.311	0.179	0.968
	n-br (29)	109.28 $\pm$ 5.16	109.31 $\pm$ 5.20	109.27 $\pm$ 5.16	0.090	0.032	0.999	109.66 $\pm$ 5.01	109.62 $\pm$ 5.12	109.71 $\pm$ 5.11	0.126	0.032	0.999	109.48 $\pm$ 4.91	0.326	0.063	0.996
	br-l (30)	112.34 $\pm$ 10.62	112.26 $\pm$ 10.71	112.36 $\pm$ 10.60	0.149	0.000	1.000	112.23 $\pm$ 10.51	112.18 $\pm$ 10.55	112.13 $\pm$ 10.67	0.154	0.000	1.000	112.25 $\pm$ 10.15	0.336	0.032	0.999
	l-o (31)	97.02 $\pm$ 5.13	97.00 $\pm$ 5.18	97.05 $\pm$ 5.14	0.064	0.000	1.000	97.70 $\pm$ 4.97	97.72 $\pm$ 5.04	97.70 $\pm$ 4.97	0.138	0.032	0.999	97.36 $\pm$ 4.86	0.470	0.105	0.989
Arbitrary landmarks	Coronal	62.34 $\pm$ 8.31	62.35 $\pm$ 8.31	62.37 $\pm$ 8.31	0.042	0.000	1.000	62.51 $\pm$ 8.34	62.51 $\pm$ 8.35	62.51 $\pm$ 8.34	0.038	0.000	1.000	62.43 $\pm$ 7.97	0.194	0.000	1.000
	Sagittal	84.76 $\pm$ 8.18	84.75 $\pm$ 8.17	84.77 $\pm$ 8.20	0.038	0.000	1.000	84.97 $\pm$ 8.07	84.97 $\pm$ 8.07	84.97 $\pm$ 8.08	0.017	0.000	1.000	84.87 $\pm$ 7.78	0.166	0.000	1.000
	Vertical	59.58 $\pm$ 11.80	59.57 $\pm$ 11.80	59.55 $\pm$ 11.80	0.059	0.000	1.000	59.70 $\pm$ 11.82	59.69 $\pm$ 11.83	59.69 $\pm$ 11.83	0.036	0.000	1.000	59.63 $\pm$ 11.30	0.170	0.000	1.000
Summary	Anatomical landmarks <sup>1</sup>				0.133	0.000	1.000				0.175	0.000	1.000				
	Arbitrary landmarks <sup>2</sup>				0.046	0.000	1.000				0.030	0.000	1.000				
<b>OSTEOMETRY</b>																	
Anatomical landmarks	gl-op (1)	182.45 $\pm$ 7.69	182.45 $\pm$ 7.82	182.40 $\pm$ 7.71	0.127	0.045	0.998	182.20 $\pm$ 7.57	182.40 $\pm$ 7.62	182.45 $\pm$ 7.61	0.165	0.045	0.998	182.39 $\pm$ 7.34	0.182	0.032	0.999
	eu-eu (8)	132.45 $\pm$ 2.60	132.55 $\pm$ 2.84	132.85 $\pm$ 2.83	0.262	0.148	0.978	132.15 $\pm$ 3.18	132.15 $\pm$ 3.43	132.25 $\pm$ 3.40	0.176	0.100	0.990	132.40 $\pm$ 2.94	0.502	0.307	0.906
	ba-br (17)	127.25 $\pm$ 7.26	127.10 $\pm$ 7.29	127.15 $\pm$ 6.97	0.216	0.055	0.997	126.55 $\pm$ 6.91	126.40 $\pm$ 7.09	126.45 $\pm$ 6.88	0.280	0.063	0.996	126.82 $\pm$ 6.77	0.425	0.032	0.999
	zy-zy (45)	123.65 $\pm$ 8.96	123.80 $\pm$ 9.01	123.65 $\pm$ 8.91	0.176	0.032	0.999	123.45 $\pm$ 9.36	123.45 $\pm$ 9.17	123.10 $\pm$ 9.04	0.261	0.032	0.999	123.52 $\pm$ 8.69	0.318	0.000	1.000
	ec-ec (44)	92.86 $\pm$ 5.74	92.91 $\pm$ 5.83	92.89 $\pm$ 5.79	0.216	0.045	0.998	92.96 $\pm$ 6.03	92.92 $\pm$ 5.92	93.00 $\pm$ 5.59	0.370	0.071	0.995	92.92 $\pm$ 5.57	0.385	0.032	0.999
	d-d (50)	22.28 $\pm$ 3.05	22.37 $\pm$ 2.96	22.35 $\pm$ 2.97	0.616	0.077	0.994	21.84 $\pm$ 3.45	21.95 $\pm$ 3.41	21.96 $\pm$ 3.37	1.134	0.084	0.993	22.12 $\pm$ 3.08	2.380	0.138	0.981
	n-br (29)	109.27 $\pm$ 5.26	109.22 $\pm$ 5.18	109.17 $\pm$ 5.19	0.111	0.032	0.999	109.38 $\pm$ 4.99	109.30 $\pm$ 5.17	109.16 $\pm$ 5.12	0.212	0.055	0.997	109.25 $\pm$ 4.93	0.269	0.055	0.997
	br-l (30)	112.00 $\pm$ 10.53	111.95 $\pm$ 10.35	111.93 $\pm$ 10.53	0.171	0.032	0.999	112.02 $\pm$ 10.56	111.55 $\pm$ 10.58	111.73 $\pm$ 10.45	0.322	0.032	0.999	111.86 $\pm$ 10.05	0.381	0.032	0.999
	l-o (31)	96.97 $\pm$ 5.10	96.96 $\pm$ 5.12	96.88 $\pm$ 5.22	0.101	0.032	0.999	97.39 $\pm$ 4.62	97.64 $\pm$ 4.75	97.46 $\pm$ 4.76	0.242	0.063	0.996	97.22 $\pm$ 4.73	0.452	0.114	0.987
Arbitrary landmarks	Coronal	62.44 $\pm$ 8.29	62.46 $\pm$ 8.34	62.42 $\pm$ 8.30	0.129	0.000	1.000	62.67 $\pm$ 8.29	62.74 $\pm$ 8.27	62.64 $\pm$ 8.28	0.156	0.000	1.000	62.56 $\pm$ 7.94	0.273	0.000	1.000
	Sagittal	84.77 $\pm$ 8.23	84.77 $\pm$ 8.16	84.71 $\pm$ 8.17	0.118	0.000	1.000	84.93 $\pm$ 8.08	84.99 $\pm$ 8.08	84.97 $\pm$ 8.07	0.094	0.000	1.000	84.86 $\pm$ 7.78	0.201	0.000	1.000
	Vertical	59.42 $\pm$ 11.86	59.42 $\pm$ 11.85	59.43 $\pm$ 11.80	0.118	0.000	1.000	59.59 $\pm$ 11.88	59.60 $\pm$ 11.83	59.66 $\pm$ 11.80	0.230	0.000	1.000	59.52 $\pm$ 11.32	0.262	0.000	1.000
Summary	Anatomical landmarks <sup>1</sup>				0.173	0.000	1.000				0.254	0.000	1.000				
	Arbitrary landmarks <sup>2</sup>				0.122	0.000	1.000				0.160	0.000	1.000				

<sup>1</sup> Summary of all measurements between anatomical landmarks, except for d - d (50), which could not be carried out on CT-scanning 3D models. <sup>2</sup> Summary of all scaling measurements between arbitrary landmarks.

Measurements	Rater 1							Rater 2						Interrater					
	Mean $\pm$ SD (mm)			CV%	SEM	ICC	Mean $\pm$ SD (mm)			CV%	SEM	ICC	Mean $\pm$ SD (mm)	CV%	SEM	ICC			
	Replicate 1	Replicate 2	Replicate 3				Replicate 1	Replicate 2	Replicate 3				All replicates						
<b>CT-SCANNING</b>																			
Anatomical landmarks	<b>gl-op (1)</b>	183.53 $\pm$ 8.19	183.94 $\pm$ 7.92	183.55 $\pm$ 7.81	0.214	0.045	0.998	184.16 $\pm$ 7.53	184.73 $\pm$ 7.58	184.60 $\pm$ 7.49	0.328	0.130	0.983	184.09 $\pm$ 7.44	0.486	0.122	0.985		
	<b>eu-eu (8)</b>	132.69 $\pm$ 2.78	132.84 $\pm$ 3.34	133.15 $\pm$ 3.17	0.536	0.285	0.919	133.11 $\pm$ 2.86	133.37 $\pm$ 2.94	133.56 $\pm$ 2.73	0.691	0.383	0.853	133.12 $\pm$ 2.86	0.784	0.214	0.954		
	<b>ba-br (17)</b>	127.45 $\pm$ 6.66	127.48 $\pm$ 6.74	127.51 $\pm$ 6.79	0.094	0.032	0.999	127.36 $\pm$ 6.74	127.37 $\pm$ 6.78	127.33 $\pm$ 6.75	0.193	0.045	0.998	127.42 $\pm$ 6.45	0.172	0.000	1.000		
	<b>zy-zy (45)</b>	124.20 $\pm$ 9.14	124.25 $\pm$ 8.89	124.09 $\pm$ 8.94	0.248	0.045	0.998	124.12 $\pm$ 8.97	124.39 $\pm$ 9.11	124.21 $\pm$ 9.17	0.190	0.032	0.999	124.21 $\pm$ 8.65	0.267	0.000	1.000		
	<b>ec-ec (44)</b>	93.29 $\pm$ 5.66	93.61 $\pm$ 5.68	93.36 $\pm$ 5.74	0.412	0.084	0.993	92.62 $\pm$ 6.18	92.73 $\pm$ 6.01	92.70 $\pm$ 5.61	0.492	0.089	0.992	93.05 $\pm$ 5.58	0.642	0.045	0.998		
	<b>d-d (50)</b>	<i>Unrecognisable landmarks</i>																	
	<b>n-br (29)</b>	109.80 $\pm$ 4.22	110.02 $\pm$ 4.37	110.03 $\pm$ 4.31	0.361	0.100	0.990	109.92 $\pm$ 4.90	108.91 $\pm$ 4.84	109.81 $\pm$ 4.42	0.854	0.219	0.952	109.75 $\pm$ 4.34	0.754	0.095	0.991		
	<b>br-l (30)</b>	112.45 $\pm$ 10.50	112.09 $\pm$ 10.46	112.03 $\pm$ 10.97	0.699	0.084	0.993	112.57 $\pm$ 11.08	112.75 $\pm$ 11.00	112.38 $\pm$ 9.23	1.405	0.176	0.969	112.38 $\pm$ 10.10	1.232	0.071	0.995		
	<b>l-o (31)</b>	98.19 $\pm$ 4.72	98.04 $\pm$ 5.18	98.07 $\pm$ 4.35	0.668	0.167	0.972	97.84 $\pm$ 4.91	97.24 $\pm$ 5.23	97.65 $\pm$ 5.29	0.709	0.161	0.974	97.84 $\pm$ 4.76	0.768	0.084	0.993		
Arbitrary landmarks	<b>Coronal</b>	<i>Unrecognisable landmarks</i>																	
	<b>Sagittal</b>																		
	<b>Vertical</b>																		
Summary	<b>Anatomical landmarks<sup>1</sup></b>				0.404	0.000	1.000				0.608	0.032	0.999				0.364	0.000	1.000
	<b>Arbitrary landmarks<sup>2</sup></b>	<i>Unrecognisable landmarks</i>																	

<sup>1</sup> Summary of all measurements between anatomical landmarks, except for d - d (50), which could not be carried out on CT-scanning 3D models. <sup>2</sup> Summary of all scaling measurements between arbitrary landmarks.



Intrarater ICCs for measurements and techniques were always above the threshold defined by Currier (147) for high reliability, except for measurement #8 (eu-eu) performed with CT-scanning by rater 2, which fell into the range for good reliability.

Apart from a few measurements, inter- and intrarater ICCs were consistently higher for UCR-DP compared to CT-scanning, while the reliability of UCR-DP was in general comparable to that of osteometry.

Interrater SEM was 0 for the three techniques. However, intrarater SEM was different from 0 for CT-scanning measurements taken by Rater 2.

## Discussion

The newly proposed cloud UCR-DP approach is characterised by fast data collection, single-step automated workflow for geometry and texture reconstruction, and the adoption of a free for academic use software environment which allowed the processing of multiple 3D models at once, leading to a low-cost, quick and effective 3D production.

### *Shooting protocol*

The shooting protocol illustrated in the present chapter is suitable for both cloud-based and offline approaches to UCR-DP.

The indirect and uniform illumination coming from every direction through the lightbox and softboxes fills any shade and penetrates any hollow space over the specimen's surface. As a result, the shade pattern is kept constant while moving the specimen, avoiding any apparent non-corresponding image features between the shots, and preventing the loss of geometric information due to dark areas. Lastly, setting the cameras for the appropriate white balance ensures faithful restitution of surface colours and texture.

An accurate choice concerning the depth of field and recording distance keeps both the closest and farthest points of the specimen in focus at the same time. It also helps, along with the use of a white turntable in a white, plain, and out of focus background, to isolate the subject, thus excluding any extraneous geometrical features.

In this way, the need for masking interventions on the single photographs, a cumbersome task that could take on average about 1 min per image (66), and therefore approximately 100 minutes for each specimen of the present research, is prevented. Because the turntable surface is not detected by the reconstruction software, the need for the removal of any unwanted geometry in the outcomes is reduced.

Furthermore, matching the specimen's dimensions with the camera frame size by finding an adequate shooting distance allows for the acquisition of the maximum detail. Indeed, the sub-optimal performance reported by some authors on relatively small specimens could be due to their small size compared to that of the frame, particularly where macro lenses have not been adopted (65).

Adopting sequential shooting sessions and controlling data acquisition with [digiCamControl](#) reduces the possibility of errors in organising the files and the time demand and cost of the process. Previous research (27) found that sub-optimal performances could arise from the use of discrete shooting sessions (51,65).

Using a turntable with planned poses improves the repeatability in the outcomes and allows for a more dense image coverage of the front and basal views, where most of the geometrical features of the cranium are, maximising the geometric information acquired with the given number of poses.

One hundred shots were sufficient to describe in detail the geometry of a cranium, despite the 120-320 shots recommended by other recent research on offline UCR-DP (42,46,59,65,68).

### *3D models production and measurement*

As for the scaling, the adoption of a long linear length between precisely pinpointable landmarks, and the repetition of the measurement for 3 times with a digital sliding calliper accounted for reduced relative error and increased precision. Incorrect scaling could be one of the causes of the relatively loose agreement found by some studies between UCR-DP and osteometry (27) .

In literature the most used solution (27) for mesh scaling is [MeshLab](#) (Visual Computing Lab, [ISTI-CNR](#), Italy) (98,99), which allows independent scaling, i.e. the use of a different scaling factor, for the three axes. Regrettably, mesh scaling based on an arbitrary length is cumbersome with [MeshLab](#), while [ReCap Photo](#), used in the present research, can identify the landmarks more easily and precisely.

### *Offline UCR-DP accuracy*

Despite the potential of the application, studies using UCR-DP in skeletal anthropology are scanty and mainly used offline software packages (27), where cloud-based applications are still the exception (42). Validation studies – particularly those detailing the shooting and scaling protocols, and performed following osteometric protocols (141,149) – are also limited. Furthermore, they all used an offline approach, based on Photoscan, while none considered the validation of a cloud-based one (27).

Some research assessed the accuracy of close-range digital photogrammetry against linear measurements taken on mannequin heads (150,151). More recently some insightful studies have provided quantitative data on UCR-DP accuracy with respect to other techniques such as osteometry (29,52,65,68), 3D coordinate digitiser (65), laser scanning (66,129), or microtomography (46). Here, UCR-DP bias was generally under 2% and the 2 mm threshold (46,66,68,129), that is considered an acceptable error in osteometry (138). Furthermore, frequency histograms for UCR-DP measurements were unimodal and normally distributed, meaning that

errors were basically random (68). Performance was slightly worse in the application to relatively small specimens (65) or in situ (29,52).

Overall, the majority of previous studies (29,46,52,65,66,68,79,129), with only one exception (43), agree that UCR-DP results are comparable to those produced by osteometry (65,66,68), CT-scanning (46,68), laser scanning (66,68,79,129), or structured light scanning (79). Some skeletal areas are more prone to having artifacts (66,68).

Differently to CT, MRI, and some range techniques, the presence of a photorealistic texture is of invaluable help in locating landmarks and fine structures even if, when acquiring a human cranium with standard lenses, meshes obtainable via UCR-DP are less dense than those derived from a CT-scan (27). Therefore, although the detail appears adequate to describe human crania, it could be insufficient to study smaller structures. More research is needed on the subject.

Indeed, the sub-optimal performance reported by some authors on relatively small specimens could be due to their size compared to that of the frame, particularly where macro lenses have not been adopted (65), or due to the use of discrete shooting sessions (51,65).

Nonetheless, in relation to recent research, the sample size and measurement variety have usually been limited, reliability comparing repeated measurements of the same variable on the same specimen was rarely studied, and the coefficient of variation, intraclass correlation coefficient, standard error of measurement, along with interrater data, have not been investigated yet (27).

A recent insightful study applied osteometric techniques and the well standardised Bland-Altman technique (139,146) to assess the agreement between UCR-DP and osteometry (68), finding a high level of agreement and bias under 0.48 mm for the 3D models obtained with the *high detail* setting. Furthermore, models created with more photographs and on higher settings tend to display better agreement with osteometry (68).

The aforementioned findings are similar to those available for CT-scanning, which demonstrated negligible differences in measurements compared to skeletal samples, with a slight tendency to overestimate measurements taken on CT-scanning derived 3D models (25).

However, not all the results of the latter two studies (25,68) can be considered conclusive without the assessment of measurement reliability. Indeed, an apparent poor agreement could be the artifactual effect of the measurement imprecision in one or both the techniques under study (139). Hence the utility of the present simultaneous analysis of UCR-DP, osteometry, and CT-scanning, performed under osteometric standards, involving multiple observers, repeated measurements, and different types of landmarks, along with the appropriate statistical procedures.

#### *Descriptive statistics*

The differences between the measurements obtained with the techniques were normally distributed according to the Kolmogorov-Smirnov test, as expected when systematic effects are negligible. Conversely, the D'Agostino-Pearson test failed to validate the hypothesis of a normal distribution of the differences between UCR-DP and CT-scanning. This could be because the average measurement lengths are not normally distributed, but form at least two subgroups, with one group including measurements between 80 and 140 mm, and another group including measurements between 170 and 200 mm (Table 8). In any case, the frequency histograms showing the differences between the techniques visually approximate a normal distribution.

#### *Accuracy*

The inter- and intrarater bias between the measurements taken with the alternative techniques was not caused by random effects, and therefore was significant. Interrater data showed a slight tendency for UCR-DP to overestimate over osteometry and underestimate over CT-scanning. Accordingly, CT-scanning showed a more pronounced tendency for overestimation with respect to osteometry.

However, the observed UCR-DP bias is undoubtedly significantly under 2% and the 2 mm threshold that is considered an acceptable error in osteometry (138) and so is, in most cases, the 95% LOA. Even when considering specific osteometric measurements, the average bias of UCR-DP with any reference techniques was considerably under the acceptable error.

In general, intra- and interrater Bland & Altman plots showed a quite homogeneous distribution of the coordinates close to the mean, and the absence of relevant systematic and size-related effects. The linear regression plots concerning the differences between the techniques do not show steep slopes, which suggests the absence of any relevant size-related effect across the range of the measurements.

What appears to be a slight size-effect has been observed in measuring skull breadth (#8) with UCR-DP and skull total height (#17) with both UCR-DP and CT-scanning, when compared to osteometry. This result is not conclusive, as it could be caused by any of the three techniques under study.

Nevertheless, it is noteworthy that when measuring skull total height the angular coefficient for the regression line related with UCR-DP is of the same sign of that of CT-scanning, and therefore such effect is common to the two techniques. Furthermore, the effect appears more pronounced for CT-scanning. In any case, the confidence interval for the regression lines is narrow, and compatible with the acceptable error in osteometric practice (138).

Scaling measurements were substantially unbiased. Actually, because inter- and intrarater UCR-DP bias in scaling measurements was consistently under 0.1 mm and 0.1%, it can be interpreted as a *background noise* of the measurement process, a random effect which amplitude is undoubtedly insignificant, and cannot be prevented. The remaining observed bias is thus due to operator error, which is considered the biggest source of error in computer-aided measurement (13), and systematic effects.

The fact that CT-scanning returns larger dimensions compared both to UCR-DP and osteometry could be due to the segmentation step, and more precisely to a phenomenon that could be called the *segmentation threshold effect*.

CT-scanning data come as stacks, i.e. sets of sequential images which can be rendered as a volume by software. However, to achieve and save a 3D surface from such data, a threshold value should be inputted into the software to identify what part of the volume is bone tissue and discard the surrounding matter (e.g., the air).

For the present study, the threshold was adjusted for each specimen and by each rater so that the 3D surface appearance matched that of the actual cranium, i.e. so that no additional volume was included and no bone tissue appeared to be lacking.

Because a threshold slightly higher than optimal results in the evident lack of bone tissue during the segmentation interactive visualisation step, the operator could have decreased the threshold to values slightly lower than optimal, thus increasing the volume of the resulting segmented 3D model.

Recent research carried out on CT data acquired from primate skulls found that during visual-based segmentation procedures users generally select a global threshold where no scanning artifacts can be seen and bony regions are as visible as possible, thus resulting in a lower threshold and, therefore, a more inflated surface, particularly in high-density anatomical regions (63).

Because CT-scanning is currently considered the gold standard for the three-dimensional description of skeletal samples, and in general of bone tissue (21,25), more research on the segmentation step as a possible cause for biased 3D models, and source of uncertainty of the measurement process, is advisable.



### *Reliability*

When the two techniques were compared to osteometry, the interval defined between the upper and lower LOA% was significantly narrower for UCR-DP than for CT-scanning. This was observed for the osteological measurements considered altogether, and also, in most cases, when considering specific osteometric measurements.

As stressed by Bland & Altman (139), a looser agreement such as the one between UCR-DP and CT-scanning could be caused by a lack of precision in one or both of the techniques being compared. Because CT-scanning shows significantly wider LOAs with respect to osteometry than UCR-DP, this brings to the conclusion that the increased imprecision in CT-scanning measurements, which is likely due to the lack of a photorealistic texture, is the primary cause for the observed weak agreement between UCR-DP and CT-scanning, and also between CT-scanning and osteometry.

To confirm this picture, while differences in CV% between UCR-DP and osteometry were not significant, those between UCR-DP and CT-scanning were found to be significant, and therefore UCR-DP is more reliable than CT-scanning when replicating standard osteometric measurements.

Interrater ICCs for measurements and techniques were always above the thresholds defined by Currier (147) for good and high reliability. For the osteological measurements considered altogether, ICCs were 1.000 for the three techniques.

Furthermore, among the three techniques UCR-DP showed the highest ICC values in measurements #8 (eu-eu) and #45 (zy-zy), while in measurement #30 the score was identical for UCR-DP and osteometry. Osteometry showed the highest values for measurements #1 (gl-op), #44 (ec-ec), and #29 (n-br). Finally, CT-scanning showed the highest ICC value for measurements #17 (ba-br) and #31 (l-o). Again, scaling measurements showed very high ICCs for both UCR-DP and osteometry, along all directions. ICCs range of variation was slightly narrower for osteometry and UCR-DP than for CT-scanning.

Intrarater ICCs for measurements and techniques were always above the threshold defined by Currier (147) for high reliability, except for measurement #8 (eu-eu) performed with CT-scanning by rater 2, which fell into the range for good reliability.

### Copyright issues

The Autodesk software licensing agreement considers both commercial and educational licenses.

The former is subject to the payment of fees and allows general use of the so called *work product*, i.e. the 3D models produced using the software, and of other data created under the licensing agreement, including professional or any other for-profit purposes.

The latter is intended for the so-defined *educational licensees* – i.e. qualified educational institutions, faculties, students, or other authorised licensees recognised by Autodesk – and are free only for academic, educational, and non-commercial use.

Unfortunately, while middle schools and high schools, junior colleges, colleges, universities and technical schools are recognised as educational licensees, non-accredited educational institutions, training centres, churches, hospitals, healthcare systems and research laboratories, libraries and museums are expressly excluded ([Autodesk terms of use](#), retrieved on 20<sup>th</sup> April 2020).

Educational licenses include the *individual stand-alone*, the *multi-seat stand-alone*, and the *network*.

The individual license allows the licensee to install a copy of the software environment on to two computers, while the multi-seat one allows installing copies on up to the permitted number of computers. Both authorise access on a stand-alone basis. On the other hand, the network license allows the installation on a single file server to be accessed from multiple connected computers on a networked basis.

Educational licenses are granted for the fixed term of thirty-six months from installation, unless otherwise specified or authorised in writing by Autodesk. They permit access to the software solely by educational licensees and solely for educational purposes, i.e. purposes directly related to learning, teaching, training, research, and development. Commercial, professional or any other for-profit purposes are explicitly excluded, except as designated in the [Autodesk terms of use](#) or otherwise authorised in writing by Autodesk.

In fact, the work product and other data created under educational license conditions should be used for educational or personal learning purposes. If any work product or other data created with such licensed materials is combined or linked with work product or other data otherwise created, then such other work product or data will also be affected by the same limitations. However, the Autodesk software licensing agreement clearly states that the user should maintain ownership of and responsibility for any files, designs, models, data sets, images, documents or similar material uploaded to the cloud service by the user, and any specific output generated from such data.

Indeed, educational licenses allow for a wide and free use among the educational community. However, work product and other data created under Autodesk's educational license provisions are not suitable for skeletal material belonging to institutions such as museums, nor can be distributed under any of the [Creative Commons](#) licenses. Furthermore, it is still not clear what type of license could be obtained by a university museum.

### Limits

While developing the shooting protocol for the present research, most of the precautions to enhance photographic image resolution were adopted. However, the additional use of a full-frame sensor camera, a self-timer, and mirror lock-up could have improved it further (27,69,78).

Furthermore, UCR-DP validation would benefit from the application of the procedures suggested by the International Standard Organization (ISO) (136,137) to assess the combined standard uncertainty for the measurement process carried out with alternative techniques, so as to identify and include in their assessment all sources of uncertainty.

Lastly, validation and comparison of UCR-DP with respect to other surface scan techniques, such as the new generation of 3D surface scanners - e.g. the [Spider](#) (*Artec 3D, Luxembourg*) (26), is still lacking despite its potential interest. Indeed, some 3D surface scanners have become extremely handy and enable fast high-resolution three-dimensional scanning with photorealistic textures.

## Conclusions

In summary the newly proposed protocol showed accuracy and reliability comparable to both osteometry and CT-scanning. Its effective, quick, and photorealistic three-dimensional production, along with the reduced requirements concerning hardware, labour, and cost make it an attractive option for producing 3D datasets in skeletal anthropology for research, teaching and dissemination.

Promising topics for future research include improving the image resolution by using full-frame sensor cameras, self-timers, and mirror lock-ups; the assessment of the combined standard uncertainty for the measurement process, and the comparison of the technique outcomes with those from high-end laser and structured light scanning solutions.

Lastly, the comparison between UCR-DP and CT-scanning emphasised some limitations of the latter technique, particularly in relation to the effects of segmentation. Because CT-scanning is the gold standard for the three-dimensional description of bone tissue, more research on the segmentation step as a possible cause for biased 3D models, and source of uncertainty of the measurement process, is advisable.

## THE DIGITALISED SAMPLE

### The Osteological Collection

The osteological collections of the *Museo Sardo di Antropologia ed Etnografia* ([MuSAE](#), [Università degli Studi di Cagliari](#), Italy) were chosen to collect the data needed for the present study. Such choice was driven by the fact that the collections host some 12,000 skeletal specimens about the Sardinian population, from Neolithic to modern times, of which more than 900 are related to crania, and most of them are in good condition (101).

From the anatomical point of view, the cranium was chosen to start the digitalisation process because it is a district of the skeleton showing several anatomical features. Yet, it is the most studied in detail (141,149), thus representing a convenient choice to collect data with a view to addressing a future population study based on the anatomical characteristics.

The study of the collection has involved several sources, many of which had already been reviewed by Sanna in his monography *Il popolamento della Sardegna e le origini dei Sardi* (103). A census of the Sardinian skeletal material, including all the known collections from Prehistory to the Middle Ages, was completed in 2009 and the related information published online repository [Anthroponet](#) (104).

Both Sanna's work and [Anthroponet](#) are useful sources to start any investigation on the biological characterisation of Sardinians and the pattern of Sardinia settlement over time.

Lastly, the [MuSAE](#) skeletal material was recently reviewed, and organised into five main categories: *Modern Collection* (Modern times); *Historical Collection* (Punic, Roman and Medieval times); *Prehistoric Collection* (Early Neolithic – Iron Age); *Other Maxia discoveries* (unknown periods); *Teaching Collection* (unknown periods) (101).

### The reconstructed sample


The reconstructed study sample (from now on referred to as *the sample*) includes 27 sites and 534 3D models representing all the intact crania from the Prehistoric Collection (138 specimens), a significant part of the Historical Collection (98 crania from the Iron Age and 54 from the Middle Ages), and the majority of the Modern Collection (244 specimens). The remaining Medieval crania, alongside those from the Other Maxia discoveries and the Teaching collections, were pro-tempore excluded from the sample respectively because they were represented by a single site or lacked any chronological dating. Because most of the crania in the sample are not associated with their corresponding mandible, the latter was not reconstructed; likewise for any isolated cranial bones or fragmented material.

The data was collected using two DSLRs equipped with a standard lens and following the protocol developed for UCR-DP validation (see chapters A NEW APPROACH: CLOUD-BASED UCR-DP and APPENDIX: UCR-DP PROTOCOL). However, the crania from the Upper Neolithic necropolis of San Benedetto (101,152), being the earliest investigated specimens, were reconstructed with a previous version of the protocol (153,154) in which specimens were hung on to a rotating platform instead of being placed on a turntable.

The composition of the reconstructed sample is illustrated in Table 9, and its geographical distribution in Figure 38.

The temporal and spatial distribution of the retrieval sites is indicative of the high representativity of the sample. To the author's knowledge, no previous single study in the world has ever achieved the reconstruction of such a large skeletal sample. Regarding the study of the biology of the Sardinians, the previous study with the most comprehensive sample is that of Germanà (105).

**Table 9.** The reconstructed sample, including links to Google Maps and [Anthroponet](#) (104).

Collection	Period ( <i>Culture or civilisation</i> ) <sup>1</sup>	#. Site ( <i>municipality</i> )	Crania	Links
Prehistoric	Middle Neolithic	1. Grotta di San Bartolomeo ( <i>Cagliari</i> )	13	
	Upper Neolithic ( <i>Ozieri</i> )	2. San Benedetto ( <i>Iglesias</i> )	30	
	Early Bronze Age ( <i>Bonnanaro A</i> )	3. Concali Corongiu 'Acca cave ( <i>Villamassargia</i> )	2	
		4. Santa Maria 'e Turri ( <i>Senis</i> ) <sup>2</sup>	2	
	Middle Bronze Age ( <i>Nuragic I</i> )	5. Cannisonis – Is Bituleris – Gastea ( <i>Seùlo</i> )	10	
		6. Capo Pecora ( <i>Fluminimaggiore</i> )	17	
		7. Perdalba ( <i>Sardara</i> )	9	
		8. Su Cungiareddu de Serafini ( <i>Carbonia</i> )	30	
		9. Li Muri ( <i>Arzachena</i> )	3	
	Final Bronze Age ( <i>Nuragic III</i> )	10. Lu Maccioni ( <i>Alghero</i> )	20	
		11. Motrox 'e Bois ( <i>Usellus</i> )	2	
Historical	Iron age ( <i>Púnica – Roman</i> )	12. <i>Barumini</i>	10	
		13. <i>Bithia (Chia)</i>	38	–
		14. <i>Cornus (Cuglieri)</i>	19	
		15. <i>Donori</i>	1	
		16. <i>Poetto (Cagliari)</i>	1	
		17. <i>Su Sercone (Orgosolo)</i>	5	
		18. <i>Tratalias</i>	3	
		19. <i>Tharros (Cabras)</i>	21	
		20. <i>Dolianova</i>	24	
Medieval	21. Chiesa di San Lucifero ( <i>Cagliari</i> )	30 <sup>3</sup>		
	19 <sup>th</sup> century	22. Chiesa di San Michele ( <i>Bono</i> )	9 <sup>4</sup>	
Modern	20 <sup>th</sup> century	23. <i>Ghilarza</i>	100	
		24. <i>Samugheo</i>	15	
		25. <i>Seui</i>	22	
		26. Chiesa delle Anime Purganti ( <i>Iglesias</i> ) <sup>5</sup>	8	
		27. Chiesa di Santa Maria ( <i>Oliena</i> ) <sup>5</sup>	90	
<b>Total</b>			<b>534</b>	

<sup>1</sup> According to Sanna (103) and Sarigu et al. (101) unless differently noted. As reported by Sarigu et al., for the Prehistoric and the Historical collections the chronological dating according to Tykot (1994) (155) has been followed.

<sup>2</sup> Referred to as *Prenuragic* or *Nuragic* in the Museo Sardo di Antropologia ed Etnografia collection catalogue.

<sup>3</sup> Out of 259 specimens; sampling is in progress. <sup>4</sup> Out of 177 specimens; sampling is in progress. <sup>5</sup> Uncertain period.



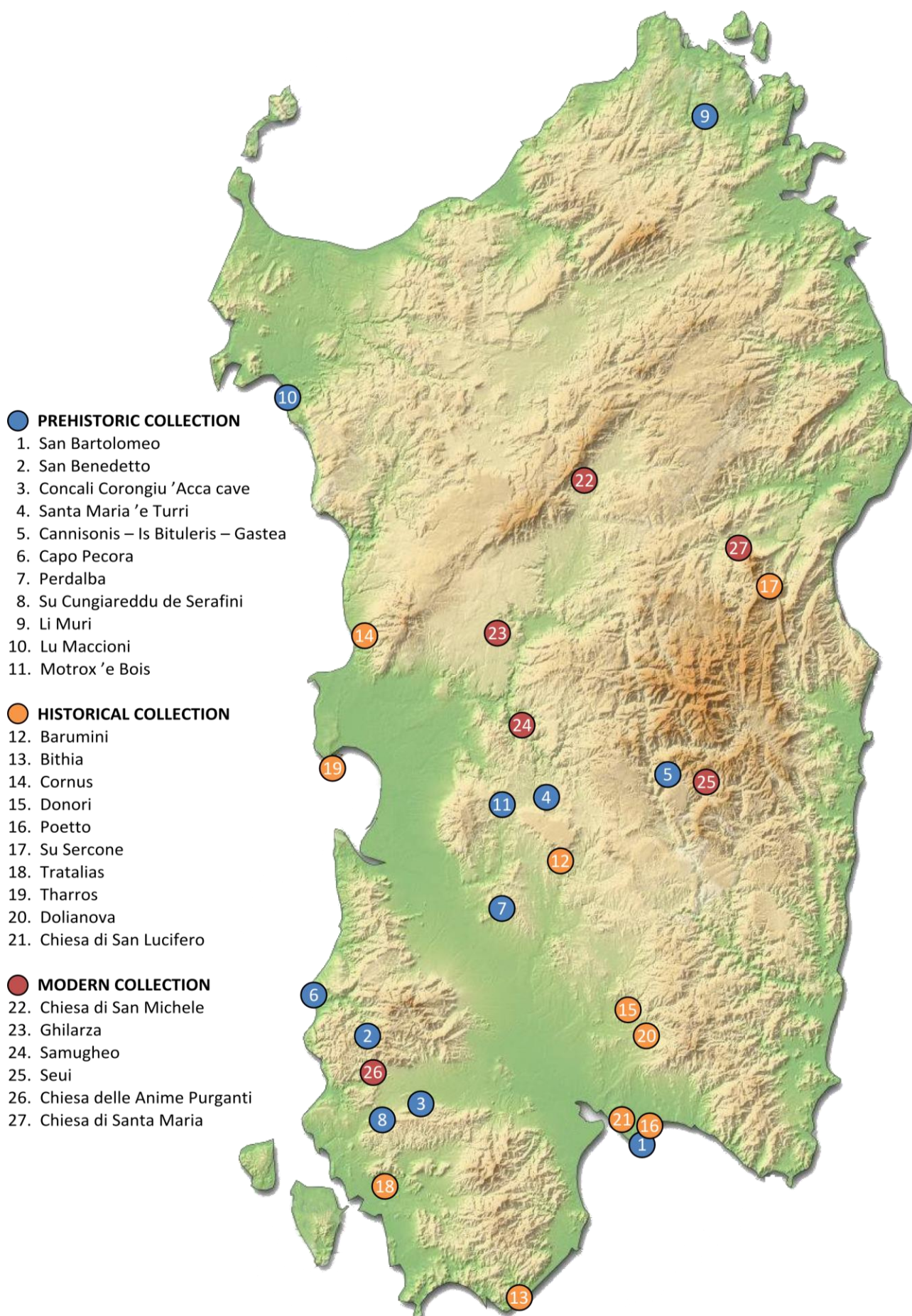


**Figure 38.** Geographic and temporal distribution of the retrieval sites.



## The Prehistoric Collection

The Prehistoric Collection includes thirteen sites dated from the Early Neolithic to the Iron Age, several of which are provided with absolute dating by  $^{14}\text{C}$  (103). Eleven sites are included in the sample. While Taramelli performed the earliest excavation in 1904 in Sant'Elia promontory near Cagliari, most of the specimens were retrieved between the 1930s and the 1970s, mainly from burial caves, graves and *Domus de Janas*, a type of chamber tombs that are unique to Sardinia.

Various geographical areas of Sardinia are represented in the Collection, allowing for a somewhat complete geographical coverage (Figure 38). However, because early excavators tended to recover only well-preserved specimens, the sample for such findings is usually biased or incomplete. The Prehistoric Collection has been recently investigated to provide more information about fragmentary material, leading to a revision of the number of excavated individuals (101).

Figure 39, Figure 40, and Figure 41 show details and a complete 3D model from the reconstructed material. The high level of detail makes it possible to fully appreciate the structure and condition of the specimens: Figure 39 shows tooth decay, Figure 40 shows the result of a cranial trepanation, and Figure 41 shows the cranial sutures and a maxillary third molar which was still enclosed within the soft tissue of the gum, or had only partially erupted at death.



**Figure 39.** MSAE 3612 from Su Cungiareddu de Serafini (Carbonia), attributed to the Middle Bronze Age (Nuragic I).

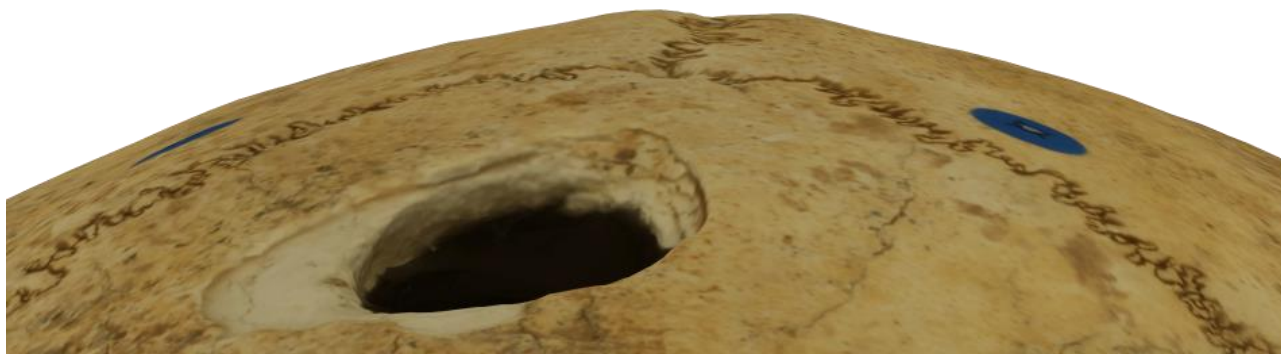


**Figure 40.** MSAE 3611 from Su Cungiareddu de Serafini (Carbonia), attributed to the Middle Bronze Age (Nuragic I).



**Figure 41.** MSAE 3621 from Su Cungiareddu de Serafini (Carbonia), attributed to the Middle Bronze Age (Nuragic I).

### The Historical Collection

The Historical Collection is comprised of thirteen sites dating from the Punic-Roman to the Mediaeval times, of which ten were included in the sample. The skeletal material comes from excavations and recoveries (101).



**Figure 42.** MSAE 6830 from Su Sercone (Orgosolo) – Roman.



c



**Figure 43.** MSAE 6450 from Cornus (Cuglieri, Riola Sardo) – Púnic-Roman.

### The Modern Collection

The twenty-two sites of the Modern Collection include recoveries, excavations of cemeteries and ossuaries dating back to the 16<sup>th</sup> century (101). The collection also contains eighteen skulls from Moravia (Czech Republic), which were excluded from the sample.

Indeed, modern material comes almost exclusively from charnel houses associated with cemeteries and churches.

### Other reconstructed material

Besides the aforementioned cranial sample, specimens of different size and nature were reconstructed. Smaller skeletal specimens such as the vertebra MSAE 1061 (Figure 44) and the male lower jaw MSAE 6438 (Figure 45) could be reconstructed in detail through the same protocol, decreasing the shooting distance and using macro lenses.



**Figure 44.** MSAE 1061 vertebra.



Figure 45. MSAE 6438 male lower jaw.

The dry anatomical specimen of a newborn was also reproduced (Figure 46). However, because the Autodesk [ReCap Photo](#) educational license was used for three-dimensional reconstruction, only one-hundred photographs were allowed for upload despite the three-hundred collected. Possibly due to the size (~55 cm), complexity, and relatively dark surface of the specimen, the outcome proved to be suitable for dissemination, but not for research.



**Figure 46.** Anatomical specimen of a newborn from the 19<sup>th</sup> century.



## UCR-DP APPLICATIONS AND CASE STUDIES

### Skeletal three-dimensional dataset applications

In cultural heritage, 3D reconstructions play a primary role in the conservation and preservation of artefacts and specimens and, via online public dissemination, in their communication.

The broad applicability and scalability of close- and ultra close-range digital photogrammetry (CR-DP and UCR-DP) enables the digitisation of objects ranging from entire archaeological excavations, mounds, tel sites, and historic buildings, to relatively small objects which include not only osteological remains but also pottery, artefacts, and lithic pieces. Indeed, because of their ease of production, and photorealistic textures, CR-DP and UCR-DP 3D models are particularly suitable for a wide range of applications requiring the creation of large datasets and their online interactive use (27,154).

In particular, cloud-based UCR-DP is applicable to overcome one of the main limitations of the existing 3D model collections which, being mainly based on resource-intensive techniques, still include only a few specimens (27). Removing such limitation enables for comprehensive comparison and population studies of potentially enormous impact.

Furthermore, the open science and FAIR (Findability, Accessibility, Interoperability, and Reusability) principles allow the widespread online exploitation of such extensive collections. In fact, such digital collections, made available under an open license, could be accessed from almost anywhere in the world thus enabling current use, e.g. virtual labs to be delivered in face-to-face or even distance learning lessons, and also have still unforeseen future possibilities of reuse.

Furthermore, the application of values-led participatory design principles and practices (33,35–39) to wide and photorealistic collections of human osteo-archaeological materials can undoubtedly help in making existing museological exhibitions more valuable by developing interactive tools to attract visitors' interest, and build cultural heritage engagement.



Such interactive experiences could be given in situ or online and could include, among others, virtual (fragmented) specimen reconstruction, geographic localisation, and investigation on the cause of death, age at death, sexual dimorphism, palaeopathology, and taphonomy.

Lastly, whenever user experience is assessed after collecting appropriate feedback, nature and limits of the osteoarchaeological knowledge and perception of the public could also be investigated.

A striking example of cloud-base UCR-DP application to skeletal anthropology exhibitions to attract visitors' interest is represented by the [African Fossils Project](#) (42), featuring a virtual lab in which 3D embedded UCR-DP models of specimens from the National Museums of Kenya and the Turkana Basin Institute can be explored, downloaded, or shared by social media functions. However, unfortunately, the 3D models were made available in low resolution only.

#### [Digital skeletal collections to serve comparative and population studies](#)

Cloud-based UCR-DP is suitable to collect large osteological samples to benefit comparative and population studies.

Methodologies for comparing 3D models include the well-established geometric morphometrics (50–52), which is a landmark-based approach, and the new dense cloud and mesh-to-mesh strategies (47,50) using the entire surface of the 3D models to assess specimen distance.

Geometric morphometrics enables the investigator to identify specific landmarks, or areas, of interest to the comparison. However, this approach usually requires a high number of landmarks to describe the geometry of, for instance, an entire skull. Because artificial intelligence technology is still relatively unreliable in locating such landmarks automatically, whenever the sample is vast, it is difficult to be studied with the geometric morphometrics approach.

On the other hand, dense cloud and mesh-to-mesh strategies compare the outer surface of the specimen, or part of it, point-to-point, returning an average measure of the specimen distance. This latter approach allows researchers to study a more significant amount of morphological data and therefore is possibly suitable for large samples (47,50). However, some caution is needed, and more research is advisable on the subject, as the two approaches have recently been compared in a study on hominin mandibular variation (50), returning slightly different group membership estimates.

### Guiding principles for preserving and disseminating digital collections

Several principles and guidelines have already been produced to create, manage and use digital collections. Going forward from general to particular, the most general principles are those related to open science.

#### *Open science*

Open science involves making and communicating research in a collaborative, transparent, and reproducible way that takes advantage of current IT networks and data sharing capabilities. The stress is on achieving the free production and validation of scientific knowledge, and on making it freely verifiable, usable and reusable by everyone, thus facilitating scientific progress and science openness to citizens.

Open science involves several practices to be carried out at any stage of the scientific venture (Figure 47). The basic instances of open science are the following ones.

- Open data, i.e. making any *input* and *raw materials* involved in the scientific process public and easily usable and reusable, including not only the experimental data, but also the associated metadata and paradata, the experimental protocols, and the best practices.
- Open access, i.e. making any *output* and *outcomes* of the scientific process freely available.
- Open processes, i.e. supporting collaborative, independent, and transparent tools – such as open peer review, to achieve and assess scientific output.

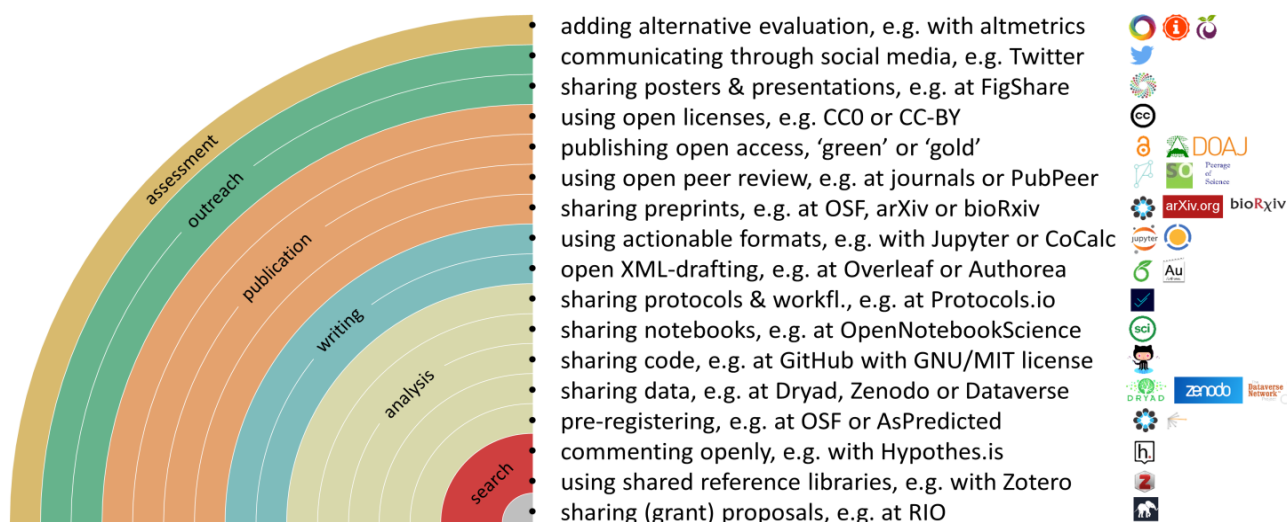


**Figure 47.** (Bianca Kramer & Jeroen Bosman, <https://101innavations.wordpress.com>; DOI: 10.5281/zenodo.1147025).

While open science bases were conceived as social practices among the scientific community to help scientific advancement, they also enhance the impact of the publication and the visibility and use of a researcher's work.

### *The FAIR guidelines*

After those related to open science, the most general principles which could be applied to digital skeletal collections are the FAIR (Findability, Accessibility, Interoperability, and Reusability) guidelines (11), intended to support discovery by the facilitation of present, and future data use and reuse both by machines and people.

The key concept is that data use should not end with the validation and publication processes. To enable further use, the FAIR guidelines aim at enhancing the ability of machines to automatically find and integrate scientific data, thus producing new knowledge by maximising the impact of the current information. Furthermore, by producing data in agreement with such principles, it is also possible to support its reuse by individuals.

Following FAIR, data findability, be it by machines or individuals, is greatly improved by its indexing in a searchable resource and the use of a persistent identifier (PID), i.e. a long-lasting reference to

objects and subjects, e.g. webpages, specimens, collections, papers, and authors. The most widespread PIDs among the scientific community are the well-known *Digital Object Identifier* (DOI) and the *Open Researcher and Contributor ID* (ORCID).

The DOI is the standard mechanism based on a code to permanently and uniquely identify and retrieve the data object itself and any related metadata, for instance, the protocol and paper describing object production and characteristics, or the license providing the allowed data use. The ORCID is based on a similar concept to permanently and uniquely identify scientific contributors.

When dealing with digital skeletal collections, individual DOIs should be assigned to each 3D model, and to any paper quoting them, while the authors' ORCID should be made explicit. As for metadata, it should clearly and explicitly include the identifier of the data it describes to allow unique access to it.

Findability and accessibility are also influenced by choice of a suitable online data repository. Numerous general-purpose data repositories are emerging (11). However, because they accept a wide range of data types and formats, they generally do not attempt to integrate them or allow for their interactive experience, thus limiting their usability.

Therefore, when archiving 3D datasets, the use of a specific 3D data repository is advisable, especially if it allows permanent storage and libre open access to the dataset, thus enabling the sharing of 3D models without the need for the creation and maintenance of a dedicated website. Here, the preferred repositories are those that support online interactive 3D model use, along with their easy download and embedding capabilities.

The choice of a repository should be made so as to ensure long-lasting access to the dataset. Indeed, the durability of a repository is a function of several factors such as its aim, openness to open science principles, property, and funding sources. Repositories for scientific purposes, owned,

kept and ordinarily funded by national or international public organisations, are the preferred choice compared to those which are owned, kept, or funded by private enterprises, and therefore, are subject to fluctuating conditions linked to the property, the investors, and the market.

As for skeletal collections, several online repositories are available for 3D data (Table 10) (27). However, none show all the aforementioned characteristics. It is noteworthy that the transnational [ARIADNEplus project](#) is integrating archaeological data infrastructures in Europe to serve the research community that studies the past. As stated, the latter includes palaeoanthropologists, bioarchaeologists, and environmental archaeologists involved in all periods of human presence from the appearance of hominids to present times.

It is, therefore, possible, and very desirable, that in the future a long-lasting and internationally recognised 3D data repository will emerge as a project development, conceivably based on the previous experience of the [ARIADNE Visual Media Service \(VMS\)](#) (135).

For the time being, among the existing 3D data repositories, [MorphoSource](#) is the world's most popular one for research purposes (19), while [Sketchfab](#) is considered a de-facto standard for sharing 3D content on the web (31,135).

[MorphoSource](#) publishes under [Creative Commons](#) licences, although it lacks the immediacy of use and interactivity not allowing the material to be manipulated nor visualised online, or embedded into external websites.

On the other hand, [Sketchfab](#) is a commercial solution, with an extensive community of users, and supporting 3D model online visualisation, embedding, and download (31). However, it lacks the flexibility to meet the diversified needs of the cultural heritage field; furthermore, it uses lossy compression, and consequently, most of the 3D models found there are drastically simplified in their geometry (135).

**Table 10.** Online repositories for skeletal 3D models sharing.

Repository			Data				Functions <sup>a</sup>					
Name <i>website</i>	Main aim	Field	Access rights	Licensing	3D scanning technologies	UCR-DP models	Contr	View	Down	Share	Embed	Muse
<b>3D Cad Browser</b> <a href="http://www.3dcadbrowser.com">http://www.3dcadbrowser.com</a>	Commercial	Various	Open, or for a fee	Chosen by contributor	Various	Some	✓	✓	✓	✗	✗	✗
<b>3D Virtual Museum</b> <sup>b</sup> <a href="http://www.3d-virtualmuseum.it">http://www.3d-virtualmuseum.it</a>	Non-commercial	cultural heritage	Open	Chosen by contributor	UCR-DP, LS, SLS	Some	✓	✓	✗	✓	✓	✗
<b>Africanfossils</b> <sup>c</sup> <a href="https://africanfossils.org">https://africanfossils.org</a>	Non-commercial	Palaeontology	Open	CC BY-NC-SA	UCR-DP, SLS	Most	✗	✓	✓	✓	✓	✓
<b>ARIADNE Visual Media Service</b> <sup>d</sup> <a href="http://visual.ariadne-infrastructure.eu">http://visual.ariadne-infrastructure.eu</a>	Non-commercial	cultural heritage	Open	CC BY-NC	Various	Most	✓	✓	✓	✓	✓	✗
<b>Digimorph</b> <a href="http://www.digimorph.org">http://www.digimorph.org</a>	Non-commercial	Biology	Open for personal use	Chosen by contributor	CT	–	✓	✓	✓	✗	✗	✗
<b>Digital Archive of Fossil Hominoids</b> <a href="https://www.virtual-anthropology.com/virtual-anthropology/share/digital-archive-of-fossil-hominoids">https://www.virtual-anthropology.com/virtual-anthropology/share/digital-archive-of-fossil-hominoids</a>	Commercial	Palaeoanthropology	For a fee	–	CT	–	✗	✗	✗	✗	✗	✗
<b>Digital Morphology Museum, KUPRI</b> <a href="http://dmm.pri.kyoto-u.ac.jp/dmm">http://dmm.pri.kyoto-u.ac.jp/dmm</a>	Non-commercial	Primates	Open for educational and research purposes	–	CT, MRI	–	✗	✓	✓	✗	✗	✗
<b>Dryad</b> <sup>d</sup> <a href="https://datadryad.org">https://datadryad.org</a>	Non-commercial	Various	Open	Chosen by contributor	Various	Some	✓	✗	✓	✗	✗	✗

<b>Figshare</b> <sup>d</sup> <a href="https://figshare.com">https://figshare.com</a>	Non-commercial	Various	Open	Chosen by contributor	Various	Some	✓	✓	✓	✓	✓	✗
<b>GB3D Type Fossils</b> <sup>e</sup> <a href="http://www.3d-fossils.ac.uk">http://www.3d-fossils.ac.uk</a>	Non-commercial	Palaeontology	Open	CC BY-NC-SA	Various	Some	✓	✓	✓	✗	✗	✗
<b>MorphoMuseum</b> <sup>d</sup> <a href="https://morphomuseum.com/collections">https://morphomuseum.com/collections</a>	Non-commercial	Vertebrates	Open for educational and research purposes	CC BY-NC	Various	–	✓	✓	✓	✗	✗	✗
<b>MorphoSource</b> <a href="https://www.morphosource.org">https://www.morphosource.org</a>	Non-commercial	Biology	Open	CC BY-NC <sup>f</sup>	Various	Some	✓	✓	✓	✓	✗	✗
<b>Nespos</b> <sup>g</sup> <a href="https://www.nespos.org">https://www.nespos.org</a>	Non-commercial	Primates	Open	Chosen by contributor	CT	–	✓	✗	✗	✗	✗	✗
<b>Phenome10</b> <a href="https://phenome10k.org">https://phenome10k.org</a>	Non-commercial	Biology	Open	CC BY-NC	Various	–	✓	✓	✓	✗	✗	✗
<b>Sketchfab for cultural heritage</b> <sup>d</sup> <a href="https://sketchfab.com/museums">https://sketchfab.com/museums</a>	Hybrid	Various	For a fee	Chosen by contributor	Various	Some	✓	✓	✓	✓	✓	✓
<b>Smithsonian Natural History Museum</b> <sup>h</sup> <a href="http://humanorigins.si.edu/evidence/3d-collection">http://humanorigins.si.edu/evidence/3d-collection</a>	Non-commercial	Biology	Open	–	Various	Some	✗	✓	✓	✗	✗	✗
<b>SpineWeb</b> <sup>g</sup> <a href="http://spineweb.digitalimaginggroup.ca">http://spineweb.digitalimaginggroup.ca</a>	Non-commercial	Human spine	Open for research purposes	Chosen by contributor	X-ray, CT, MRI	–	✓	✗	✗	✗	✗	✗
<b>Turbosquid</b> <a href="http://www.turbosquid.com">http://www.turbosquid.com</a>	Commercial	Various	Open, for a fee	Royalty-free	Various	–	✓	✗	✓	✗	✗	✗
<b>Virtual Fossils</b> <sup>b</sup> <a href="http://www.virtualfossils.com">http://www.virtualfossils.com</a>	Non-commercial	Palaeontology	Open	CC-BY	CT, mostly	–	✓	✓	✗	✓	✓	✗
<b>Zenodo</b> <sup>b</sup> <a href="https://zenodo.org">https://zenodo.org</a>	Non-commercial	Various	Open	Chosen by contributor	Various	–	✓	✗	✓	✓	✗	✗

<sup>a</sup> Detail of the functions allowed for three-dimensional data: CONTR, contribution; VIEW, online viewing; DOWN, downloading; SHARE, social media sharing; EMBED, embedding in external websites; MUSE, virtual museum online. <sup>b</sup> Database links to Sketchfab resources. <sup>c</sup> Example of a virtual museum, linking to Autodesk online resources. <sup>d</sup> Suitable for research purposes. <sup>e</sup> Restricted to reference specimens for species description. <sup>f</sup> Recommended licensing. <sup>g</sup> Database links to external repositories. <sup>h</sup> Download allowed upon request. <sup>i</sup> After contributor's agreement.

Platforms specifically suitable in skeletal anthropology include the [ARIADNE Visual Media Service](#) (VMS) (135), as mentioned earlier, which is aimed at supporting cooperative work in archaeology by sharing large visual data, and [MorphoMuseuM](#) (156), which is meant to improve the knowledge of vertebrate fine anatomy.

They are both based on [3DHOP](#) (3D Heritage Online Presenter, Visual Computing Lab, [ISTI-CNR](#), Italy) (96,135), an open-source software for the online presentation of data in the cultural heritage field.

[3DHOP](#) is very flexible, being based on the efficient multi-resolution Nexus format, which allows the online use of full-resolution models (31,96,135). [3DHOP](#) also supports different presentation layouts and interaction modes (31), the orthographic visualisation, and tools to slice and measure the specimens which are fundamental in skeletal anthropology.

Because the [ARIADNE VMS](#) (135) is not intended as a data repository, and its persistence depends on future developments of the [ARIADNEplus project](#), [MorphoMuseuM](#) is currently a more suitable option for sharing 3D datasets.

An alternative to [3DHOP](#) is represented by the open-source project [Aton](#), which is based on the same open-source library as [Sketchfab](#), focusing on scene-graph concepts and implementing multi-resolution Level Of Detail (LOD) management in order to present and visualise complex 3D datasets such as vast terrains.

The front-end provides support for mobile browsers and multi-touch devices and offers several options for camera manipulation, spherical panorama support, rich annotation and immersive virtual reality capabilities (31).



Interoperability is the ability of data or tools from non-cooperating resources to integrate or work together with minimal effort (11). Indeed, to be interoperable, data and metadata should use a formal, accessible, shared, and broadly applicable language for knowledge representation and include qualified references to other (meta)data to establish univocal relationships between different resources.

Therefore, specific open access thesauri of current widespread application within the scientific community should be used, such as Getty Art & Architecture Thesaurus ([Getty AAT](#)) for cultures, styles, materials, and other concepts related to cultural heritage; Getty Thesaurus of Geographic Names ([Getty TGN](#)), [Geonames](#) and [Pleiades](#) for current and ancient geographical information; [PeriodO](#) period gazetteer and [iDAI.ChronOntology](#) to refer to period terms and datings.

Existing data and metadata impact is increased by its reuse for new aims, e.g. in integrative analyses, constituting the bulk of contemporary e-Science; the creation of derived content for teaching, dissemination, and cultural enjoyment; specimen reproduction or restoration.

The most crucial factor affecting reusability is the presence of a rich data and metadata description with a plurality of accurate and relevant attributes associated with detailed provenance (31).

Lastly, reuse is greatly facilitated by choice of open licenses, such as the [Creative Commons](#). In skeletal anthropology, for instance, the [CC BY-NC-SA 4.0](#) license is particularly suitable because it enables material in any medium or format to be copied, redistributed, transformed and built upon.

Appropriate credit must be recognised to the original source and whether any changes are made they are to be made clear and distributed under the same agreement as the original data. Nevertheless, the [CC BY-NC-SA 4.0](#) license excludes any commercial purposes, avoiding that sensitive material like a skeletal sample is used for, e.g., videogames or advertising.

### *The London Charter*

In the field of cultural heritage, several general guidelines have already been proposed explicitly for digital data creation, preservation, and dissemination, and they could be applied to the related management of digital skeletal collections.

The [London Charter](#) (157) addresses six fundamental principles about the use of computer-based visualisations in the study and communication of cultural heritage. It was developed following two symposiums on the subject *Making 3D visual research outcomes transparent*, convened at The British Academy and King's College in 2006, in London.

Its updated version (2.1, February 2009) has been translated into many languages. Because of its general approach, the [London Charter](#) is still current.

Regarding the six principles, the first three relate to project planning (1<sup>st</sup>), data capture (2<sup>nd</sup>), and data creation (3<sup>rd</sup>). The last three principles are of particular interest in UCR-DP application to skeletal anthropology because they relate to data documentation, formats for preservation, and formats and methods for data dissemination.

The *documentation* (4<sup>th</sup>) principle advises on what information should be documented during the development process of 3D content to facilitate understanding and use of 3D visualisations. The principle states that *sufficient information should be documented and disseminated to allow computer-based visualisation methods and outcomes to be understood and evaluated in relation to the contexts and purposes for which they are deployed* (157).

Subsequently, documentation strategies should be developed to:

- enhance the visualisation activity by encouraging, and helping to structure, thoughtful practice;
- enable rigorous, comparative analysis and evaluation of computer-based visualisations;
- assist in the management of Intellectual Property Rights or privileged information.

As for the computer-based visualisation of skeletal collections, per the [London Charter](#) documentation principle, adequate information should be provided and disseminated on:

- any research sources used, along with their provenance;
- the creative process, e.g. the relationships between research sources, implicit knowledge, explicit reasoning, and visualisation-based outcomes;
- the method, including the rationale for choosing a computer-based visualisation method while rejecting other ones, the method description, and its current and proposed applications;
- the dependency relationships; hypothetical dependency relationships between elements should be clearly identified by users and the reasoning underlying such hypotheses explicated;
- formats and standards, including graphical, textual, video, audio, and numerical, according to best practice and in such a way that facilitates content inclusion in relevant citation indexes.

Following the 4<sup>th</sup> principle, sufficient metadata should be documented and disseminated to allow computer-based visualisation methods and outcomes to be understood and evaluated concerning the contexts and purposes for which they are deployed.

The *sustainability* (5<sup>th</sup>) principle addresses the planning of long-term sustainability and usability of 3D content. *Strategies should be planned and implemented to ensure the long-term sustainability of cultural heritage-related computer-based visualisation outcomes and documentation, in order to avoid loss of this growing part of human intellectual, social, economic and cultural heritage* (157).

Therefore, it is advised that:

- the most reliable and sustainable form of archiving should be identified and implemented;
- digital preservation strategies should aim to preserve the data, rather than the medium;
- sufficient information to enable future data use should be provided to allow a long-lasting utility through migration to different formats or software emulation, or to allow reuse in research and dissemination.

Lastly, the *access* (6<sup>th</sup>) principle advises on planning the effective dissemination of 3D visualisations. *The creation and dissemination of computer-based visualisation should be planned in such a way as to ensure that maximum possible benefits are achieved for the study, understanding, interpretation, preservation and management of cultural heritage* (157).

In the case of 3D models obtained via UCR-DP from skeletal collections, the application of the [London Charter](#) principles could be done implementing the following actions or steps.

First of all, data and metadata should refer to any phase of the 3D model production and use, and should be both published in a durable repository to allow for their potential persistent use and reuse.

To allow metadata survival in case of repository failure, it could be incorporated into the data files themselves, before being associated at the repository level; for instance, the OBJ files accept data descriptions as human-readable comment lines. Whether a [Creative Commons](#) license is provided, optional machine-readable metadata could be specified.

Raw or intermediate data concerning the 3D model production process should be provided too under the same license of 3D data. In fact, the provision of the original photographs both in TIFF and JPEG file formats allows for the future reconstruction of the geometry by newly developed algorithms. This would enable the recovery of the 3D models in case they are lost, or their file format cannot be read or migrated to a new software environment anymore. Furthermore, because UCR-DP software accuracy in reconstructing 3D geometry is limited by the performance of current computer systems and algorithms, and both are continuously improved, such provision enables the possibility of future three-dimensional reconstructions from the original photographs with new software and improved accuracy.

It is also advised that additional images or video files are captured. Such files allow a convenient preview or overview of the geometry and appearance of the 3D model and may preserve elements of 'look and feel' that may be difficult to retain in the available preservation formats (31).

## Planning durable online use and reuse

To better gain an understanding of best practices for the effective and durable online management and dissemination of large 3D datasets, and form guidance for museological collections in the cultural heritage field, including skeletal collections, a short term scientific mission (STSM) named *Durable online dissemination of large 3D datasets from museological collections* was carried out between January 28<sup>th</sup> and March 30<sup>th</sup>, 2020.

The mission took place at the [Archaeology Data Service](#) (ADS), Department of Archaeology, University of York (the United Kingdom), within COST Action [CA18128](#) – Saving European Archaeology from the Digital Dark Age ([SEADDA](#)).

The ADS is the only accredited digital repository in the United Kingdom for heritage data. Together with [Digital Antiquity](#) (Tempe, the United States), they have written several good practice guidelines including digital data and metadata planning, 3D model use in archaeology, and close-range photogrammetry (31).

COST Action SEADDA has been conceived by ADS members and includes proposers from twenty-six COST and four COST-associated international partner countries. It aims at bringing together an interdisciplinary network of archaeologists, computer scientists, and experts in archaeological data management and open data dissemination and reuse. Thus, developing common guidelines and appropriate, persistent repositories for making archaeological data open and freely accessible across Europe.

SEADDA is working to establish a priority research area in the archiving, dissemination and open access reuse of archaeological data and creating publications and materials that will set out the state of the art for archaeological archiving across Europe and recommendations to mitigate the crisis.

As a result of the mission, the ways to achieve an effective, durable, and low-cost online dissemination of digital data were detailed. The following key aspects were considered: 3D model file formats, selection of project data and metadata, suitable licensing, and existing durable repositories.

### *3D model file formats*

As highlighted by McHenry et al. (94), the range of available 3D file formats is vast, with each format storing various types of data in different ways. Furthermore, software environments and file formats dealing with 3D data evolve, become obsolete and cease to be supported at a high pace. Besides, preferred formats, i.e. those suggested for specific uses, vary according to the archival aim. Therefore, making the appropriate choices for the durable preservation and use of 3D datasets can be daunting. File formats suitable for UCR-DP data storage, including the output point clouds or meshes, and the input images, are considered here.

In general, the most stable formats for preserving 3D data and making them usable and reusable also in the future are those which are openly documented and text-based. Indeed, they allow access to data independent of specific software. Software specific, proprietary, commercial, or binary formats, such as 3DS, MAX, SKP, or BLEND, are usually not suitable for long-term storage (31).

On the other hand, the OBJ file format is particularly suitable for specimen documentation as it is open access, of current widespread use, and its structure is simple. Its geometry description can be saved as human-readable ASCII text and read using a simple text reader software application. Furthermore, a texture can be stored in a separate image, accessible through visualisation or editing software packages (31); this feature is essential as UCR-DP output comes with a photorealistic texture of the object. Lastly, a copy of any associated metadata, including scale information, could be saved in the data file itself as human-readable comment lines. From an open science and FAIR perspective, these characteristics maximise the chances of an effective conservation and reuse, even in a more or less distant future.

The PLY file format is inspired by OBJ and appears to be suitable for the strategies mentioned above too. However, PLY is less widespread and supported. Moreover, it can incorporate extensions that are supported by specific software programs, but not by others. In the latter case, when opening specific files some properties may not be displayed and, in case of reuse and adaptation of the original data, could be permanently lost. Therefore, in general, the OBJ is preferred with a view to storing, interoperating and reusing data.

Where the main application is dissemination, the 3D PDF file format could also be considered (29), as it can be read by [Reader DC](#) (Adobe Inc., the United States), a globally widespread software package, thus avoiding the installation of specific visualisation software, such as [MeshLab](#) (28,56,58). Indeed, the PDF format supports the incorporation of 3D models in the U3D and PRC formats and can additionally integrate text, images, and links alongside the 3D data. What's more, users can apply measurement and annotation tools to measure distances, radii and angles (31). However, 3D PDF file sizes may be substantial, and the models often require a large amount of RAM, which may not be available on every system. As a result, the 3D PDF format is better used to disseminate lower resolution or down-sampled versions of 3D models (31). Last but not least, a commercial software licence is needed to generate 3D PDF files (27), the format is not open-source, and it is not readable by most software programs for 3D models analysis.

The [Nexus](#) (NXS, Visual Computing Lab, [ISTI-CNR](#), Italy) format is open access, multi-resolution, and used by [3DHOP](#), and therefore is recommended when the primary purpose of a project is online use and dissemination. In fact, it has been specifically designed for the efficient web-based fruition of extensive 3D reconstructions, and supporting their lossless compression, embedding, and streaming. [Nexus](#) is currently not recommended for preservation (31). However, its possibly increased diffusion in the future could make it suitable also for archival purposes.

Whether 3D models are intended both for research and dissemination, again the PLY and OBJ file formats appear the most suitable. Online systems based on 3DHOP such as the [ARIADNE Visual Media Service](#) (135) and [MorphoMuseuM](#) (156) (Table 10), automatically convert data from OBJ and PLY sources into [NXZ](#), a compressed version of NXS, for their online display. Therefore, the OBJ, which is suitable for preservation, is also easily converted for online dissemination.

In certain circumstances, where data migration proves difficult, it is also advised that the original formats be retained and that source files (textures, visualisations) or problematic elements of a model be captured separately and stored in a suitable archival format (31).

#### *Selection of project data and metadata*

According to the *Guides to Good Practice* (31) project and data documentation can exist on many levels, chiefly if the creation of 3D models is part of a larger project involving other methods of data collection and analysis. At a minimum, all datasets will be part of a larger project and as such require the so-called *top-level metadata* regarding the focus, dates, and people and organisations involved. Important information that should be recorded includes the sources consulted to create the 3D model, the processes that were undertaken during the developmental stages, the applied methods, and a description of the relationships and dependencies between its different components.

The selection of 3D data for archiving should be done, within the broader context of the project's data workflow, to document any steps at which data is created, collected, or significantly changed, and include any primary intermediary data or results (31). Indeed, any well-documented workflow step, called *preservation intervention point*, would encourage future data reuse, and even data restoration or new processing. For instance, while following a UCR-DP workflow the original untrimmed and unmodified photographs should be provided in a separate archive as both proprietary camera raw and TIFF files, the latter being the currently preferred format for long-lasting preservation (31). Furthermore, pre-processing 3D models should be preserved too. These archives should be provided under the same license as the disseminated post-processed 3D



models. The precautions above would enable not only the effective preservation of the data, but also the possibility of reprocessing the original photograph to create 3D models with future and possibly more accurate and advanced algorithms.

Where 3D datasets are generated as part of a complex workflow incorporating multiple acquisitions and processing stages, important information to record includes: the type of device used for producing the initial raw sampling; the software tools used to process the sampled data; the kind of processing applied to the reconstructed model (e.g. holes filling, surface smoothing, surface simplification). Furthermore, documentation and metadata can be used to record information relating to the model's geometry, appearance, and scene information, as well as documenting derived objects such as image and video files (31).

In some cases, file formats will allow the storage of specific metadata within the file structure. Nevertheless, such metadata must be recorded separate to the file and externally deposited so that elements can be checked against the file's content.

The metadata for UCR-DP 3D models listed below (Table 11) (31) should be considered as the minimum requirement at the file level and in addition to that described at the project level.

**Table 11.** Suggested five-level metadata for UCR-DP 3D models (31).

Element	Description
Number of vertices	The number of vertices (points) in the model
Number of polygons	The number of polygons describing the model surface
Geometry type	The type of geometry used within the model, i. e. vertex-based wire-frame
Scale	What scale is existent, resp. what is represented by a single unit
Coordinate system	Does the model use a real-world or arbitrary coordinate system?
Master or processed model	Is the model the master model produced just after raw data processing, or is it derived?
Level of Detail (LOD)	How detailed is the model, what is the resolution of the scan
Material	Information about the material properties of the model and whether they match the physical properties of the actual object
Colour and texture	Does the model contain colour or texture information? How is this stored? If raster texture files are used, then these should be archived separately
Light source(s)	Number and accuracy of light sources used in the model
Shader	Have specialised or extended shaders been used?
External files	List of external files required to correctly open the 3D model (e.g. texture or material files)

## Values-led participatory designs to share skeletal collections

Participatory design, sometimes referred as co-design, co-creation, or open design, is a creative practice approach enabling a wide range of people to contribute to the formulation and solution of a problem (35,36). Participatory design is led by a focus upon participants' values (36).

Indeed, participants are often users of the product or service that is being designed, and are involved as *experts* of their own experience. One or more facilitators provide ways for people to engage with each other, communicate, be creative, share insights and test out new ideas.

The entire process leads to improved knowledge of user needs, the immediate validation of ideas or concepts, a high degree of originality and, therefore, more efficient decision making, lower development costs, and reduced development time (35).

A wide range of tools and techniques are available to support the creative process, including brainstorming sessions, SWOT analysis, scripting, storyboarding, shared and multiauthored online documents, rapid prototyping, co-operative prototyping, and making and tinkering workshops. Potential solutions can be tested through prototyping and scenario generation techniques (35,37).

When participatory design began, nearly four decades ago, in Scandinavia, it was developed with a commitment to values (37). Values are enduring beliefs that we hold concerning desirable modes of conduct or end-state of existence in different situations, societies and cultural contexts, such as caring for loved ones, being active and healthy, and a preference for a peaceful life or democracy (37).

In the context of a project, shared values emerge from the collaboration, dialogue, and negotiation between researchers and project designers. These emergent values then lead the project development (37). Participatory design has been recognised as a way to effectively promote cultural heritage assets by involving digital data (33,35,38,39).

### Open science and FAIR case study: the Teaching Collection of the University

To put into practice open science and FAIR recommendations an article (148) describing a UCR-DP [3D dataset](#) relating to the teaching collection was submitted to [MorphoMuseum](#) journal, along with the dataset itself (148) which was published online on [MorphoMuseum](#) repository (156).

The [3D dataset](#) contains ten 3D models of human crania (Figure 48) dating back to the XIX century, and selected from the Teaching Collection of the Museo Sardo di Antropologia ed Etnografia ([MuSAE](#), [Università degli Studi di Cagliari](#), Italy).



**Figure 48.** The 3D model sample from the Teaching Collection preserved at the [MuSAE](#).

The sample includes specimens from Bono and Laconi (Sardinia, Italy) which inventory numbers are: MSAE 59, MSAE 62, MSAE 63, MSAE 78, MSAE 95, MSAE 1852, MSAE 6426, MSAE 6428, MSAE 6992, and MSAE 7688. The [3D dataset](#) was produced via cloud-based UCR-DP (27) and exported in OBJ format. The post-processing was performed with [ReCap Photo](#) (mesh cleaning and hole filling) and [Krita](#) (texture editing).

The [sample](#) (148) was made available in agreement with FAIR principles (11). Each model was exported in OBJ file format and assigned a separate [DOI](#). The sample was published in the [MorphoMuseum](#) (156) online repository, whose interactive visualisation features are based on [3DHOP](#) (96,135), under the Attribution-NonCommercial-ShareAlike 4.0 International [Creative Commons \(CC BY-NC-SA 4.0\)](#), hence allowing the creation of derivative works of educational value, while banning any commercial exploitation, which is undesirable when dealing with human remains.

### [Open science and FAIR reuse case study: a virtual laboratory of physical anthropology](#)

The reuse of the Teaching collection [3D dataset](#) (Figure 48) already published online was implemented to allow virtual labs of physical anthropology, in accordance with Open science and FAIR principles.

The application was first inspired, and then driven, by the necessity of organising distance learning practical activities for the students of the Physical Anthropology course at the University of Cagliari. In fact, between the end of 2019 and the start of 2020, the coronavirus disease (COVID-19) outbreak caught the world by surprise. Italy was severely affected, and several draconian measures had to be put in place to contain and delay the contagion. A Decree of the President of the Council of Ministers, in force since March 5<sup>th</sup>, suspended face-to-face didactic activities in all schools and higher education institutions, and the [Università degli Studi di Cagliari \(UniCa\)](#) rushed to convert their activities to distance learning.

Indeed digital technologies have demonstrated effectiveness in supplementing learning resources, although with some type of performance penalty (158). However, 3D models – especially those with photorealistic textures – have not been widely used to facilitate distance learning yet, although some universities have activated online courses including 3D models of skeletal material (see for example the *Forensic Archaeology and Anthropology* course developed by Durham University, UK). A recent paper discussed the potential of digital technology for producing and printing 3D anatomical models to be used for research, teaching and museum exhibitions (159).

The [3D model sample](#) (148) comprised individuals of both sexes and various ages at death and was used to demonstrate cranial anatomy, measurement, and variability during physical anthropology labs.

The theoretical lessons were produced in collaboration with the E-learning For didactic Innovation Service centre (EFIS) of the [Università degli Studi di Cagliari](#) and carried out using the [Connect](#) (Adobe Inc., San Jose, the United States) and [TEAMS](#) (Microsoft Corporation, Redmond, the United States) web conferencing environments.

The [3D model sample](#) (148) was used to discuss with the students the basics of the osteological investigation, the main cranial features, and the most common measurements. Hence, the students were asked to use the online visualisation features provided by [MorphoMuseuM](#) and [3DHOP](#) to see and measure the 3D models (Figure 49).



**Figure 49.** A measurement being carried out online in [MorphoMuseuM](#) using [3DHOP](#) interface. The glabella - opisthocranium length is being taken on MSAE 6426.

A series of exercises, dealing with cranial anatomy, landmarks and measurements, sex diagnosis, age at death assessment, was also proposed (Table 12). The 3D sample and the associated teaching material has been shared online on a dedicated [MuSAE teaching web page](#) (Figure 50).

The photorealistic appearance of UCR-DP models proved to be of invaluable utility in osteological analyses. Indeed, it improves the representation of details such as suture closure and dental wear and facilitates the localisation of landmarks and the assessment of sex and age at death, which would be much more difficult, and in some cases impossible, with CT-scanning 3D models without texture, as shown during the present research. [MorphoMuseuM](#) and [3DHOP](#) enabled easy specimen exploration, measurement, and download.

The online published 3D cranial sample is freely available for similar purposes, and the use of [3DHOP](#) enables online interactive use through a web browser, without the need for locally installed software packages.

**Table 12.** Interactive exercises to engage students. In parenthesis the measurement number of Martin and Saller (141).**Exercise 1**

Using one 3D cranial model, pinpoint the following structures and landmarks:

- a. frontal, parietal, temporal, occipital, sphenoid, ethmoid, nasal, lacrimal, and zygomatic bones, along with the maxilla;
- b. zygomatic, mastoid, and styloid processes;
- c. coronal, sagittal, lambdoid, and squamous sutures;
- d. glabella (gl), opisthocranion (op), eurion (eu), basion (ba), bregma (br), zygon (zy), ectoconchion (ec), dacryon (d), nasion (n), lambda (l), and opistion (o) landmarks.

**Exercise 2**

Measure the maximum cranial length (#1) and breadth (#8), the basion-bregma height (#17), the bizygomatic breadth (#45), and the frontal (#29), parietal (#30), and occipital (#31) chords of five 3D models included in the sample. Calculate their cranial index.

**Exercise 3**

Using the combined method (160) and considering the guidelines of the European Anthropologists (161), estimate the sex of all the individuals represented in the sample.

**Exercise 4**

Using the methods based on occlusal dental wear (according to Brothwell (162) and Lovejoy (163)) and ectocranial sutures closure (according to Meindl and Lovejoy (164)), estimate the age-at-death of all the individuals represented in the sample.



- Museo
- Avvisi
- Collezioni
- Didattica**
- Tour 3D
- Visite

UniCa > Museo Sardo di Antropologia ed Etnografia > Didattica

## Didattica

### Un laboratorio di Antropologia scheletrica virtuale

Il laboratorio di Antropologia virtuale pubblicato in questa sezione offre la possibilità di interagire con modelli tridimensionali di reperti scheletrici (Marini e Lussu, submitted). Come esempio applicativo, vengono illustrati alcuni esercizi pensati per gli studenti dell'Università degli Studi di Cagliari (Tabella 1), che possono essere utilizzati per attività pratiche di apprendimento interattivo a distanza in diversi contesti educativi.

Il laboratorio si basa su un campione di 10 modelli 3D di crani della collezione museale, risalenti al XIX secolo e variabili per sesso ed età alla morte. I modelli 3D, esportati in formato OBJ, sono stati pubblicati sulla piattaforma online MorphoMuseum (Lebrun e Orliac, 2016), con una licenza di distribuzione ad accesso aperto (CC BY-NC-SA 4.0), che ne consente il libero utilizzo, con il solo vincolo di citare la fonte, evitare qualsiasi sfruttamento commerciale, e distribuire allo stesso modo lo stesso materiale, o eventuali opere derivate (Lussu e Marini, 2020a).

La ricostruzione tridimensionale è stata realizzata con la fotogrammetria digitale a distanza ravvicinata, una tecnica relativamente semplice e a basso costo, utilizzando un protocollo validato nel Laboratorio di Antropologia virtuale dell'Università degli Studi di Cagliari (Lussu e Marini, 2020; Lussu et al., 2020). Si tratta di modelli molto accurati, la cui superficie ha un aspetto fotorealistico che risulta estremamente utile nelle analisi osteologiche. Sono infatti ben distinguibili i dettagli anatomici, come ad esempio le suture craniche e la superficie occlusale dei denti, necessari per la localizzazione dei punti di repere e per la valutazione del sesso e dell'età alla morte.

L'interazione con i modelli può essere effettuata attraverso l'interfaccia di 3DHOP (Visual Computing Lab, ISTI - CNR, Italia) (Potenziani et al., 2015) e il proprio browser Web, senza quindi la necessità di software installati localmente.

Le attività di laboratorio sono pensate per studenti che abbiano già acquisito conoscenze di base sulle principali caratteristiche anatomiche, le più comuni misurazioni, i metodi per l'analisi del sesso e dell'età alla morte. I modelli possono essere manipolati liberamente, facilitando così l'acquisizione delle conoscenze teoriche e di abilità pratiche.

#### Tabella 1

**Esercizio 1**  
Utilizzando cinque modelli cranici 3D, individuare le seguenti strutture e punti di riferimento:

- a. ossa frontali, parietali, temporali, occipitali, sfenoidi, etmoidali, nasali, lacrimali e zigomatiche, insieme alla mascella;
- b. processi zigomatici, mastoidei e stiloidei;
- c. suture coronali, sagittali, lambdoidee e squamose;
- d. glabella (gl), opisthocranion (op), eurion (eu), basion (ba), bregma (br), zygon (zy), ectoconchion (ec), dacryon (d), nasion (n), lambda (l), e opistion (o) punti di riferimento.

**Esercizio 2**  
Dopo aver selezionato l'opzione "orthographic camera" e poi attivato "measure tool", misura la lunghezza cranica massima (n. 1) e la larghezza (n. 8), l'altezza basion-bregma (n. 17), la larghezza bizigomatica (n. 45) e quella frontale (n. 29), parietale (n. 30) e occipitale (# 31) dei cinque modelli 3D inclusi nel campione. Calcola l'indice cranico. Tra parentesi il numero di misurazione secondo Martin e Saller (1957).


**Esercizio 3**  
Utilizzando il metodo combinato (Acsádi e Nemeskéry, 1970) e considerando le linee guida degli antropologi europei (Ferembach et al., 1980), fornire una diagnosi di sesso per ciascun individuo rappresentato nel campione.

**Esercizio 4**  
Utilizzando i metodi basati sull'usura dentale (secondo il metodo indicato da Brothwell, 1981, e Lovejoy, 1985) e sul grado di obliterazione delle suture ectocraniche (secondo Meindl e Lovejoy, 1985), stimare l'età alla morte di ciascun individuo rappresentato nel campione.

### INIZIA ORA LA SESSIONE INTERATTIVA CON I MODELLI 3D

**MSAE 59 - cranio, Bono, Sardegna, Italia**  
Museo Sardo di Antropologia ed Etnografia, MuSAE, University of Cagliari, Sardinia, Italy


Vedi il modello in 3D



MSAE 59

**MSAE 62 - cranio, Bono, Sardegna, Italia**  
Museo Sardo di Antropologia ed Etnografia, MuSAE, University of Cagliari, Sardinia, Italy

Vedi il modello in 3D



MSAE 62

**Figure 50.** The title of the [MuSAE teaching webpage](#) sharing the 3D sample and the associated teaching material.



## Open science and FAIR case study: the sharing of the San Benedetto Collection

The Upper Neolithic necropolis of [San Benedetto](#) (Iglesias, Sardinia, Italy) is a site framed in the Ozieri culture and dated about 4900 B.P. (101,103,152) (Figure 51). To document and preserve the specimens retrieved there, thirty 3D models of crania (Figure 52) from the inviolate *Tomba 2* and preserved at the Museo Sardo di Antropologia ed Etnografia ([MuSAE](#), [Università degli Studi di Cagliari](#), Italy) (101) were produced using ultra close-range digital photogrammetry (UCR-DP) (27).

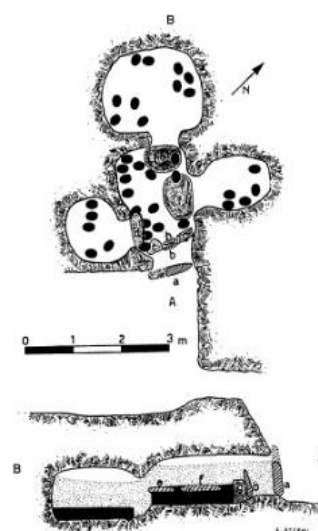


**Figure 51.** The entrance (left) and two drawings (right) showing the planimetry and a cross-section of the Tomba II (San Benedetto necropolis, Iglesias, Italy). Photograph and drawings from Atzeni (2001) (152).

Meta-description was carried out following the guidelines as mentioned earlier. Post-processing included solving 3D surface problems and applying 3D model orientation along the Frankfurt Plane and was carried out employing of [ReCap Photo](#) and [MeshLab](#) (98,99) (Figure 53).

The choices related to metadata management, [Creative Commons](#) licensing, and durable online repositories were addressed to make of the publication a case study for best practice in virtual skeletal anthropology. The manuscript is currently being written jointly with the [Archaeology Data Service](#) (ADS) staff.



**Figure 52.** The 3D model sample from San Benedetto Neolithic necropolis (Iglesias, Italy). Original image by Davide Bratzu; modified by [Paolo Lussu](#) and reprinted with the author's permission.



**Figure 53.** 3D model orientation with [ReCap Photo](#) (Autodesk Inc., USA).

### Value led participatory design case study: the MuSAE

To explore best practices in the application of values-led participatory design principles (35–37) of human osteoarchaeological materials (33), and to design an interactive exhibition for the Museo Sardo di Antropologia ed Etnografia (MuSAE, Università degli Studi di Cagliari, Italy) (101), featuring to raise awareness of how it is possible to learn about humans in the past through their skeletal remains, a second STSM had been planned within *COST Action CA15201 (Arkwork)*, to be carried in the near future at the School of Humanities, University of Glasgow (the United Kingdom).

The STSM was named *Experiencing bones – I was what you are*, because the fundamental value which could be related to skeletal collections is empathy.

Other values that could be identified as highly related to skeletal collections are the respect due to human remains and the enrichment for the society that comes from human diversity and cultural heritage.

During the planning of the mission, the fundamental principles to make the exhibitions more useful, understandable, and enjoyable were pointed out to form guidance for future application and a case study in designing a digital or digital+ museum-based physical display was studied.

*Audience-, institution-, and feedback- oriented questions* were explored through brainstorming sessions, SWOT analysis, scripting, storyboarding, and shared and multiauthored online documents. Some examples are reported below.

*Audience-oriented questions.* What audiences are to be addressed? How could the needs and desires of the audience be met? What does the anthropological material allow to be experienced by the audience? Is it preferable to allow guided or unguided experience?

*Institution-oriented questions.* What message and underlying concepts should be communicated? How can such communication be made useful, understandable, and enjoyable, following a hierarchy of design-led value in the context of working with human skeletal remains? What amount of design is relevant? What equipment (hardware and software) is suitable?

*Feedback-oriented questions.* How is it possible to collect preliminary feedback on the exhibition experience and assess target behaviour during real use? What message have visitors taken away?

Following the initial study, the principles and values thus identified were put into practice to design an interactive exhibition for the skeletal collections preserved at the [MuSAE](#), featuring to raise awareness of how it is possible to learn about humans in the past through their skeletal remains.

During the first planning sessions of the interactive exhibition, it was clear that emphasis should be given on evoking empathic reflections in the visitor (34) by delivering the message, or suggesting, that what is now a bone was once a person living in the same area, yet possibly under very diverse circumstances. Furthermore, showing a history of succeeding populations and human diversity will help build cultural heritage engagement and respect of human remains.

Indeed, human remains belong to people who were part of communities with a possible alternative set of values, or religion. They may show skull features which today are unusual in the same area. Moreover, several diverse communities may have occupied pro tempore the area in the past.

The prototyping of an operational design for the interactive exhibition is based on the previously described 3D model samples that have already been produced using cloud-based UCR-DP (27). The 3D models were partially shared via the online repository [MorphoMuseuM](#) (156).

The result was the conception of a number of reference stations, along with an interactive and immersive installation to allow the experience of the 3D models to groups of people. The installation of the exhibit began last March 2020. However, it had to be interrupted because of the pandemic outbreak.

The planned reference stations will include four vertical display screens (Figure 54; Table 13), each placed in one of the main rooms of the museum. These touch screen stations will show interactive hypertextual content. Furthermore, they will have the ability to recognise simple vocal questions, search the museum's database, and provide relevant information as an answer. To do so, they will incorporate a built-in microphone and the Speech Recognition app of Google Chrome.



**Figure 54.** The vertical display screen to be placed in the four main rooms of the [MuSAE](#).



**Table 13.** Facilities, components and specifications of the multimedia experience at the [MuSAE](#).

Facility	Component	Specifications
Reference stations (in number of 4) (Figure 54)	Vertical display touch screen	40" diagonal (approx. 102 cm) or wider Anti-glare screen Integrated Windows or Android Integrated microphone for voice recognition Integrated speakers or audio output
	Vertical display stand (whether not integrated)	Steel made Stabilising base to support the previous vertical display touch screen 45 Kg payload or more
Interactive station	Multi touch screen	65" diagonal (approx. 165 cm) or wider Anti-glare screen, 4K Ultra HD resolution 20 simultaneous touches Integrated Windows or Android Integrated microphone for voice recognition Built-in speakers or audio output
	Tilt & table display stand (Figure 55)	Steel made Stabilising base to support the previous multi touch screen 90° tilt or more, so that the supported screen can be placed both vertically (tilt position) and horizontally (table position). 90 Kg payload or more
Immersive environment	Concave led display screen (in number of 2)	Assembled from 256x128 mm modules Adjustable curvature 3mm pixel pitch 4 mm 62,500 dots/sqm
	Sound system	7 + 1 audio sound system Wall-mounted
Logic	Desktop computer	3.2 GHz 8-core Intel® Core™ i7 CPU (or similar) 12 GB system RAM NVIDIA GTX 1660 graphics card (or similar) 6 GB video RAM 4 video outputs including 1 HDMI and 3 DisplayPort interfaces 2 TB Hard Disk, 512 GB SSD disk DVD-RW optical drive Windows 10 operating system

The interactive and immersive station will be placed in a dedicated museum room enclosed by black velvet curtains. It will comprise of an interactive station in the centre and an immersive environment. Its function is to reproduce the atmosphere and sounds of the archaeological sites in which the specimens illustrated in the interactive station were found, thus allowing an engaging and immersive experience that can be experienced by groups up to 20 people altogether.

The interactive equipment, which has already been installed, comprises a 65" multi-touch screen supporting 20 simultaneous touches and therefore can show four 3D models at once, each of them independently usable through a dedicated interactive web page. The screen is supported by a tilt and table display stand (Figure 55;

Table 13), allowing it to be placed both vertically (tilt position) and horizontally (table position).

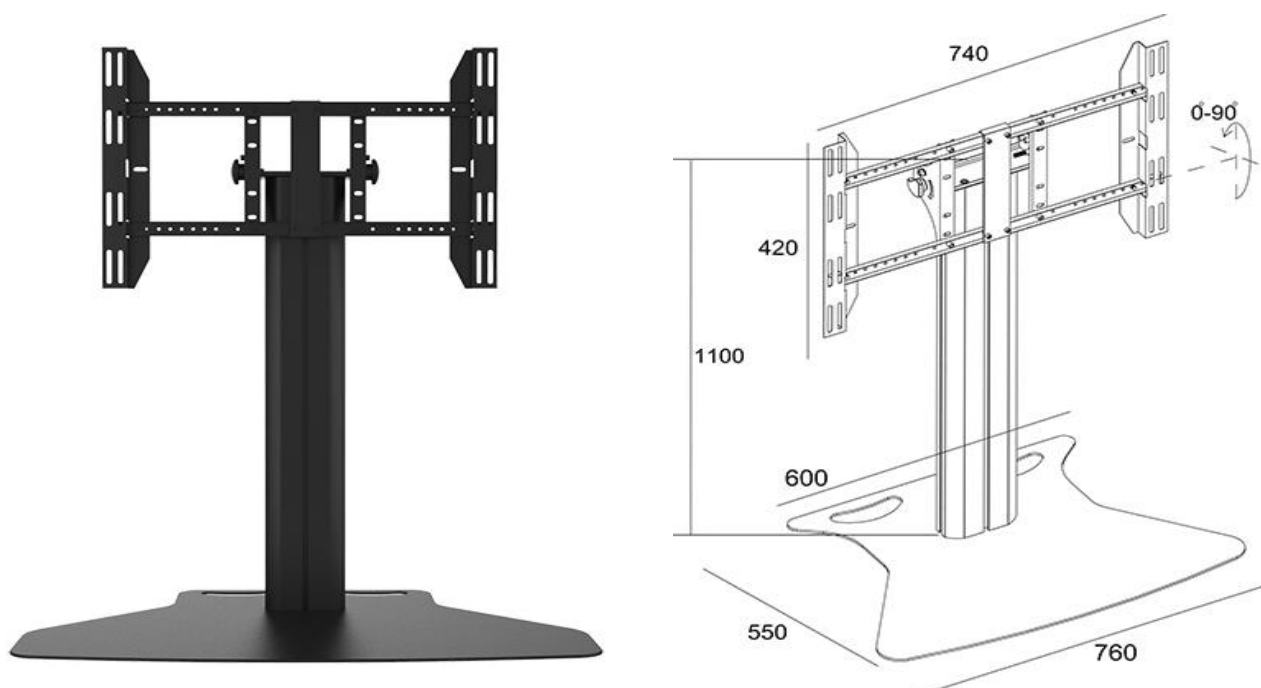


**Figure 55.** Detail of the display stand allowing both tilt and table positions for the touch screen of the interactive station.

Activities and workshops involving the audience will be conceived to suggest that behind bones are life stories. Furthermore, to attract visitors' interest and to encourage them to learn the basics of osteoarchaeological investigation, the interactive experiences will include virtual specimen

measurement and slicing, virtual (fragmented) specimen reconstruction, geographic localisation, and an inquiry into the cause of death, age at death, sexual dimorphism, palaeopathology, and taphonomy.

The immersive environment will include a concave led display screen of the type shown in Figure 56 (Table 13), creating a 300° field view around the interactive station and showing a 360° movie of the retrieval site of the specimens, e.g. a field, a hill, a cave, or a church. A 7 + 1 audio sound system will reproduce the sound of the retrieval environment.



**Figure 56.** Concave led display screen suggested for the immersive environment at the [MuSAE](#). Public domain image.

To engage visitors on the website, a 360° interactive and clickable [virtual tour](#) of the [MuSAE](#) was produced and published online using [Google Tour Creator](#) (Figure 57). It includes six scenes in which the visitor can navigate and is listed among the other virtual tours of Google (Figure 58) around the world. The virtual tour is compatible with [Google Expeditions](#).



Lastly, a clickable map linking the 3D models of the specimens to their retrieval location has been planned. As a future research object, user feedback will also be obtained to assess their experience.

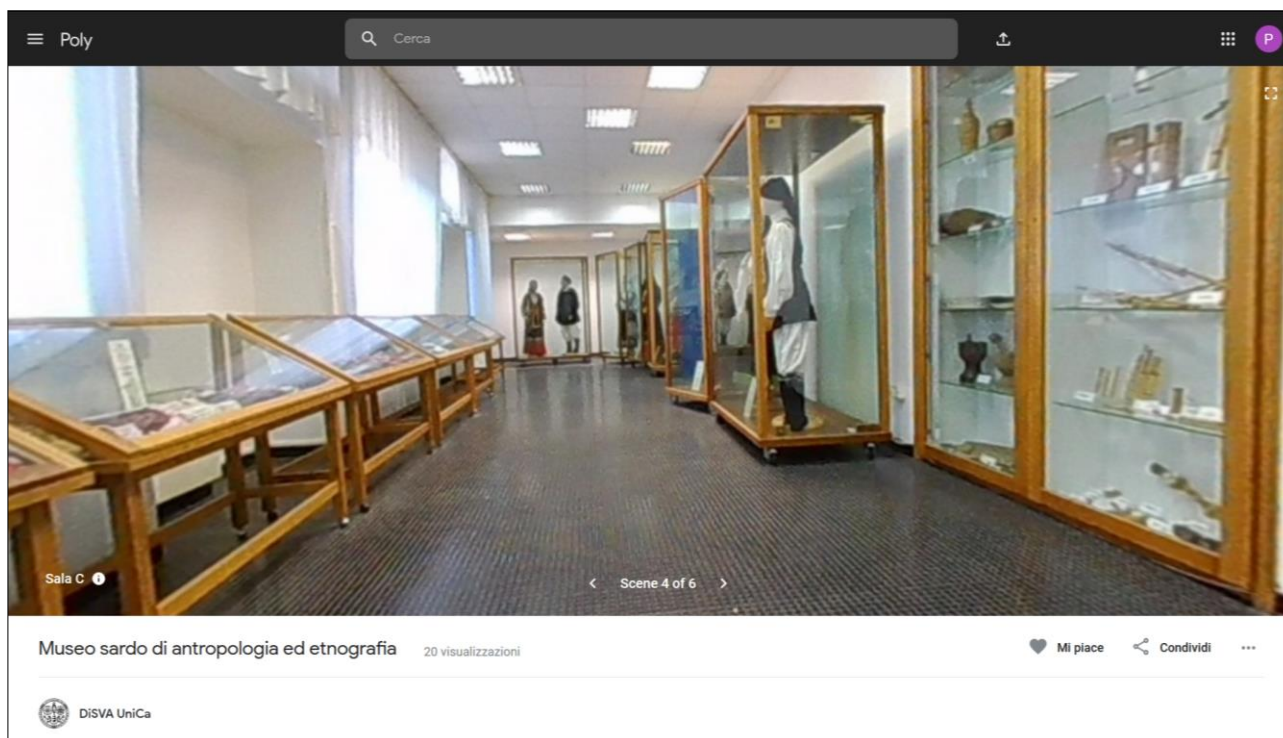


Figure 57. 360° interactive and clickable view of the MuSAE.

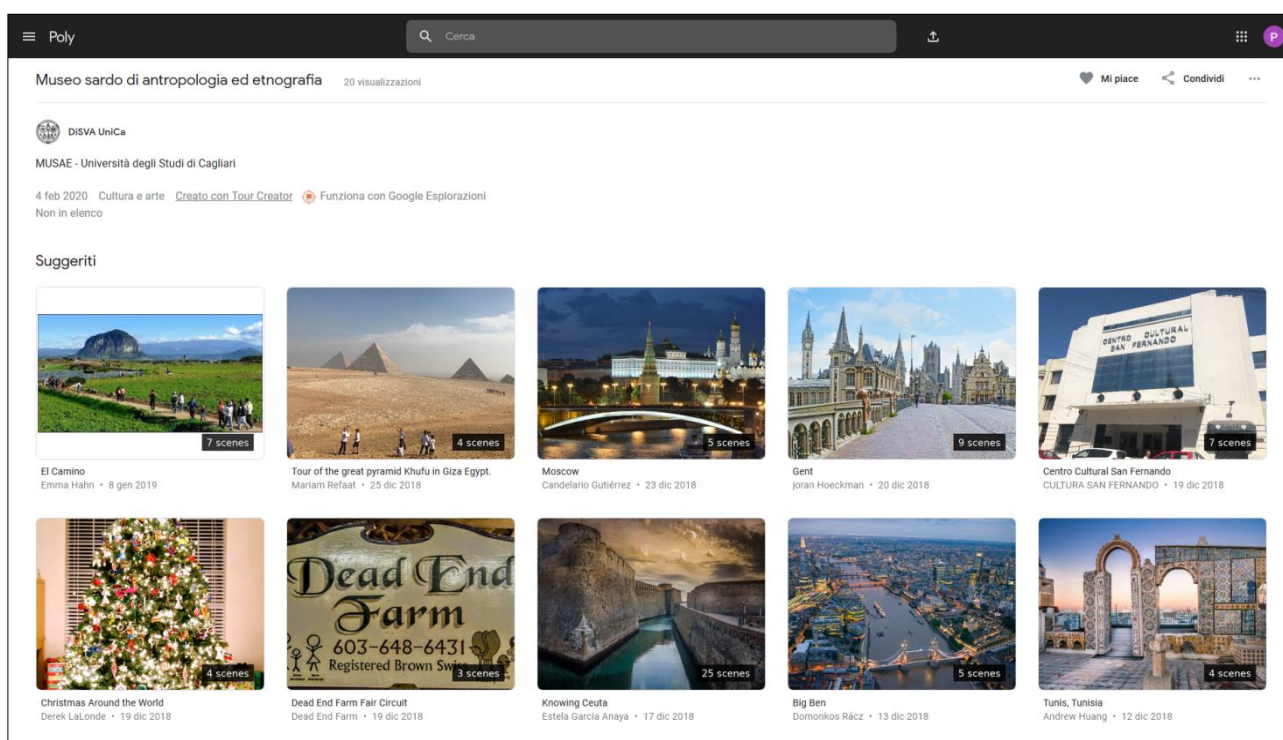


Figure 58. The other virtual tours of Google.

## CONCLUSIONS

Skeletal collections represent a source of interest with extraordinary value that should be exploited. Virtual anthropology provides several ways to do so using digital three-dimensional reconstructions. Thus, enabling the long-lasting preservation of the sample, its detailed study in comparative and population research, and engaging dissemination, both in situ and online, through interactive and immersive experiences.

Nevertheless, extensive digital collections are still challenging to be retrieved online. Constraints limiting the availability of digital specimens arise from the use of resource-intensive reconstruction technologies, intellectual property rights, ethical and political issues, and the lack of enthusiasm of most scholars, thus restraining the potential for scientific knowledge evolution.

Most of the limitations mentioned above could be overcome by using a straightforward technique for 3D reconstruction, and by following open science principles and FAIR guidelines to share the outcomes.

Ultra close-range digital photogrammetry (UCR-DP) offers many significant advantages over other 3D scanning techniques: greater versatility in terms of application range and technical implementation, scalability, and photorealistic restitution.

The proposed cloud-based approach and protocol showed accuracy and reliability comparable to those of osteometry and CT-scanning. Significant benefits include the use of remote servers to compute the 3D models and automate the sampling, thus leading to further reduced hardware, labour, time, and cost requirements.

Indeed, cloud-based UCR-DP was successfully used to reconstruct the widest 3D digital sample to date, including 534 well-preserved crania from 27 Sardinian sites.

The application of open science and FAIR principles to such a comprehensive digital sample has enabled several uses among the scientific community, demonstrated by case studies, and is expected to facilitate future, long-lasting data use and reuse.

The sample reconstructed during the present research is suitable for a future study on the patterns of morphological variation in space and time in the biological characteristics of the Sardinians from Neolithic to modern times.

On the other hand, the application of a values-led participatory design could be successfully used to plan and implement interactive and immersive exhibits featuring, at the same time, the skeletal remains and the environmental images and sounds of their retrieval site.

In conclusion, virtual anthropology has demonstrated great, yet largely unexplored, potential in skeletal anthropology, where UCR-DP appears to be an ideal choice for documenting and valuing large samples and collections.

Railroads networks were developed about two centuries ago, and modern rocket technology started about one century ago. Indeed, virtual anthropology is much more recent – after only about two decades from its first significant applications we are still at the dawn of this technology.

It is likely that, in the near future, vast online virtual specimen databases will spread, and their content will be classified by artificial intelligence, just like it already happens with digital photographs.

While it is difficult to anticipate further developments, it is certainly possible to apply UCR-DP following open science and FAIR principles for describing data in a complete, general, and lasting way.

Indeed, if such description is clear, its message will travel far away through space and time to allow vast, and still unforeseen, possibilities of future reuse and scientific advancement.

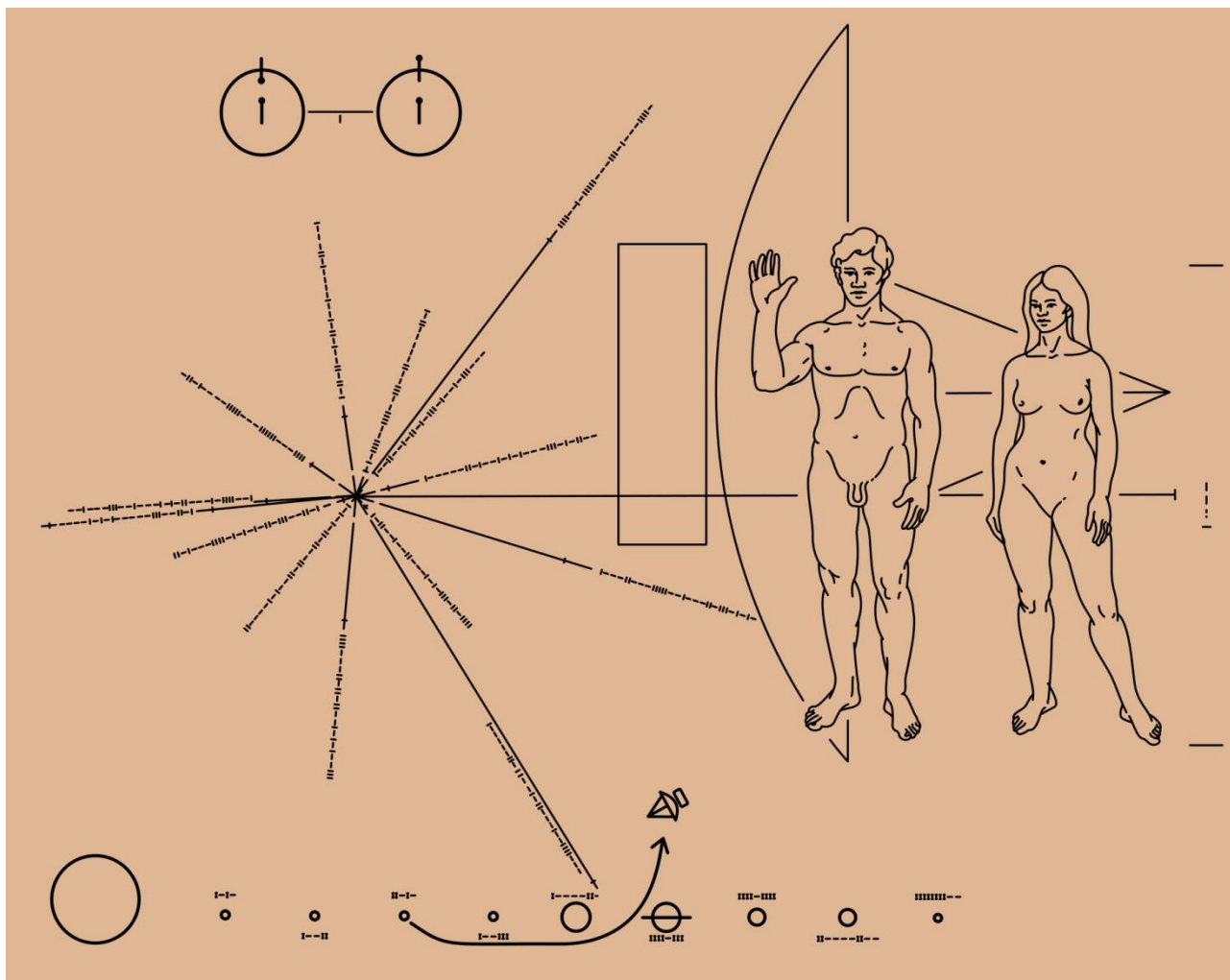


**Figure 59.** Gold-anodized aluminum plate installed on both Pioneer 10 and 11 space probes, launched in 1972 and 1973 respectively. The plate features a pictorial message intended to be intelligible to the intelligent life that could intercept it. It includes basic information about the Solar System, the trajectory of the spacecraft, the appearance and relative size of the humans, and the position of the Sun relative to 14 pulsars. By Vectors by Oona Räisänen (Mysid); designed by Carl Sagan & Frank Drake; artwork by Linda Salzman Sagan – Vectorized in CorelDRAW from NASA image GPN-2000-001623. Public Domain.

## APPENDIX: UCR-DP PROTOCOL

The appendix illustrates the materials (software and hardware), the settings, and the detailed procedure applied during the present research to achieve a cloud-based ultra close-range digital photogrammetry (UCR-DP) three-dimensional reconstruction.

Before to start a UCR-DP project, it is advisable to gather basic knowledge of the photographic principles (78) and to refer both to previous methodological studies which reported the best practices for three-dimensional reconstruction (27,60,67–69), and to the *Autodesk knowledge network* dedicated [web page](#).

### Software setup

- Two software packages are required to follow the proposed UCR-DP protocol. Autodesk ReCap Pro includes [ReCap Photo](#), which is used for cloud-based three-dimensional reconstruction and post-processing. [digiCamControl](#) is an open-source project, which enables multiple camera management for sequential shooting sessions (27) and automatic image indexing and storage.

### Autodesk ReCap Pro and ReCap Photo

#### *Obtaining the software environment*

- Autodesk ReCap Pro and [ReCap Photo](#) software environment can be installed and used by anyone for a 30-day free trial period. Professors and university students are entitled to a 3-year free use license for non-commercial study or research purposes, as detailed in *Copyright issues*, page 106. To obtain the license, the creation of an *Autodesk account* is required. This is, unfortunately, a complicated task.

- Visit the page <https://accounts.autodesk.com/authentication> and press *CREATE ACCOUNT*, then fill in the required fields, accept the conditions of the service and press, again, *CREATE ACCOUNT*. On the next page press *CLOSE* to access the personal profile, then *MODIFY PROFILE*. At the bottom, in the *Professional information box*, select the *Education sector* and then *SAVE PROFILE*.
- On the personal profile page, click on *Manage products and downloads*, re-entering the authentication data (e-mail and password) if required.
- A *verify request* message appears: *The email address has not been verified for Autodesk*; press on *EXECUTE E-MAIL VERIFICATION*, then access the user personal mailbox and click on the link to verify the account in the email that has just been sent by Autodesk.
- If no e-mail has been received, check the spam folder and the correctness of the e-mail address specified at the beginning of the registration process.
- Upon verifying the e-mail address, the user is redirected to the page of his Autodesk account.
- Visit the page <https://www.autodesk.com/education/free-software/featured> and, in the *Free education license products* tab select *ReCap Pro*. On the new page select *SIGN IN*, then authenticate.
- On the following page, complete the profile by entering the country (e.g., *Italy*), the teaching role (e.g., *Student*) and the date of birth.
- On the next page, enter the name of the affiliate institution (e.g., *University of Cagliari*) and tick the study area (e.g., *Others*). It is required to specify the enrollment date and the indicative expected date for the end of the course (month, year). Since the license for study and research purposes has a potential duration of three years, if in doubt, it is preferable to enter a realistic end date. Click on *NEXT*.

- At this point, the account necessary to download the software has been opened. The message *Your account has now been updated to access the Autodesk Education Community* appears.
- Press on *CONTINUE* to access the download page and select the desired software version (e.g., *ReCap Pro 2020*), the operating system and the desired language.
- At this point, license details appear on the screen and are also sent by e-mail.
- If an updated installation package has already been downloaded, it is possible to skip this step. Otherwise, at the bottom of the same page, press the arrow on the *INSTALL NOW* button and then on *BROWSER DOWNLOAD* to permanently save a copy of the software, which can be used if necessary for subsequent installation on other devices.

#### *Installing Autodesk ReCap Pro and ReCap Photo*

- The license is valid for installation on a maximum of two devices in total, so it is a good idea to accurately choose the computer where to install the software.
- Click on the downloaded file to start the installation procedure. After being asked the directory for temporary files extraction, press *OK* to confirm.
- Once the extraction is complete, if the installation does not start automatically open the file extraction directory, then start the *setup.exe* program. Press *INSTALLATION*, then accept the license agreements and press *NEXT*. Verify that both Autodesk ReCap and Autodesk [ReCap Photo](#) installations are selected, and press *INSTALL* again.
- The file extraction directory can be deleted once the installation is complete.
- An update may be requested the first time the software is started. Press *UPDATE* to run it, accept any information and then press *START* and then, again, *UPDATE* next to the most recent update package in the list. All necessary updates will be automatically installed.



## digiCamControl

### *Obtaining and installing the software package*

- Visit the software homepage <http://digidcamcontrol.com>, then download the installation archive from the page <http://digidcamcontrol.com/download> and install it following on-screen instructions.
- The page <http://digidcamcontrol.com/#features> describes the main features of the software, while the user manual is found at page <http://digidcamcontrol.com/doc/>.

### *Setting up digiCamControl*

- Start the program. The *Help* menu provides access to the documentation. Press *F1* for *Quick Help*.
- Follow the next steps to configure the program for the acquisition from two cameras connected through USB ports.

File > Settings > Advanced.

> Activate *Use parallel file transfer*.

> Activate *Sync camera date time on camera connect*.

> Deactivate *Automatically send usage statistics*.

Connect the bottom camera via USB cable and turn it on.

Menu at the top of the interface > Camera > Camera property.

*Camera name*: prefix the string *Lower\_* to the existing camera identifier.

Connect the upper camera via USB cable and turn it on.

Menu at the top of the interface > Camera > Camera property.

*Camera name*: prefix the string *Upper\_* to the existing camera identifier.

Repeat the previous three steps to identify unambiguously any other camera to be connected.

- Follow the next steps to create a work session whose settings can be recovered later using the session drop-down menu. In this way, each photograph acquired will be saved in the specified folder with a name formed by the name of the session, the specific capture (e.g., the inventory code of the museum exhibit) and by a progressive three-digit number (e.g., *MSAE\_3609\_001*).



Window to the right of the interface > Session.

> *Session name* MSAE (or any other name related to our project).

> *Folder* D:\3D\_MODELS\MSAE\ (or other directories for saving the acquired photos).

> *File name template* [Session Name] \_ [Capture Name] \_ [Counter 3 digit].

> *Capture name* > 4-digit inventory code of the finding (or any other unique identifier).

- Follow the next steps to configure all cameras according to the shooting protocol, and to check that the settings are consistent among all cameras and during the entire shooting session.

Menu at the top of the interface > Camera > Camera property.

> *Mode*: Av (Aperture value, i.e., aperture priority) .

> *Aperture*: 22.0 (or as advised).

> *ISO*: 64 ISO (or as low as supported).

> *White balance*: manual (set directly in the camera).

> *Transfer*: Save to PC only.

- Associate the 'b' key as a command to shoot a photograph with all connected cameras at the same time.

## Hardware setup

### *Cameras and lenses*

- Two (or more) digital single-lens reflex cameras with full-frame CMOS sensor, supporting 64 ISO sensitivity or lower, aperture priority mode, custom white-balance setting, remote shutter release, self-timer, operativity while connected to AC supply, and USB or wifi direct data connection to a PC.
- Two (or more) bright, high-resolution, low distortion and high quality standard prime lenses with a focal length of 50 mm or higher and focusing distance of 50 cm or less.
- For small specimens, the use of macro lenses is more indicated over standard ones to allow the image of the specimen to occupy the greatest part of the photo frame.

### *Camera installation*

- To prevent any blur and to be remotely controlled, the two cameras should be installed on tripod mounts, equipped with remote shutter release and self-timer, and connected to a notebook PC via USB 3.0 cables and hub.
- The two cameras should be oriented towards the specimen at different heights (e.g., 0 cm and 50 cm) and tilts with respect to the specimen centre (e.g., 0° and 35°), thus enabling the capture of two perspective views at once (Figure 22, page 73).
- The recording distance between the camera and the specimen (e.g., 50 cm) should be adjusted to match the specimen's apparent maximum dimension with 80% of the camera frame size, so as to acquire the maximum detail while taking the necessary precautions to avoid any cropping.

### *Shooting environment*

- A plain and out of focus background should be set used to isolate the subject.
- Uniform, indirect lighting should be diffused in every direction around the specimen.
- The use of a lightbox and two or more softboxes is, therefore, highly recommended (Figure 22, page 73).
- The softboxes, and any other source of indirect illumination used during data collection, should have a 5500 K colour temperature, similar to daylight, and camera white balance should be adjusted accordingly to ensure colour accuracy.

## Preliminary settings

### *Specimen preparation*

- Scaling measurements consider arbitrary landmark pinpointed with small, circular marking labels (5-8 mm diameter) with two intersecting lines printed on their centre. The marking labels can be bought off-the-shelves and the symbol  $\oplus$  can be printed on them.

- The following steps allow data acquisition for the subsequent scaling of the three-dimensional model.
  - > Identify, on the specimen, the calibration baseline as an arbitrary linear length  $a - b$  (similar to that shown in Figure 24, page 76: length from  $a$  to  $b$ ), approximately 10 cm long.
  - > The calibration baseline should be measurable as the crow flies using a digital sliding calliper.
  - > The calibration baseline should be as long as possible to reduce the relative measurement error.
  - > Use the labels to pinpoint the arbitrary landmarks of the calibration baseline, while avoiding to hide any anatomical landmarks or structures that could be of interest to the study.
  - > Measure the calibration baseline three times with a digital sliding calliper and take note of the results reporting them in millimetres, to the hundredth of a millimetre.
  - > Before each measurement, check the correct zeroing of the calliper gauge.
  - > During the measurement, check that the extremes of the calliper measurement gauge both correspond with the points on the labels where the two lines of the symbol  $\oplus$  cross.
  - > Find the average calibration baseline and round the result to the nearest hundredth of a millimetre and take note of the result.
  
- It is fundamental to pay maximum attention to the scaling process any error would affect the accuracy of all subsequent measurements carried out on the digitalised specimens.

#### *Specimen installation*

- Install the specimen in its first recording position, on a circular turntable, inside a lightbox, in front of the two cameras (Figure 22, page 73).
- The turntable has planned poses identifying all the specimen orientations which should be photographically recorded (e.g., those numbered from 0 to 9, Figure 22, page 73).
- For specimens with an approximate spherical symmetry, the poses could be equally spaced along the perimeter of the turntable.
- For specimens with bilateral symmetry, or with specific morphological assets, the poses should be denser for the regions showing more complex geometry, e.g. holes, depressions, and minute structures.

### *Shot settings*

- Set the camera to operate in aperture priority (A) mode, a.k.a. aperture value (Av) mode, at the lowest supported ISO sensitivity.
- In Av mode the shutter speed is chosen accordingly to the diaphragm aperture, returning proper exposure based on the lighting conditions. Low values for ISO sensitivity increase photograph resolution by maximising its signal-to-noise ratio.
- The lenses diaphragm aperture should be the minimum which ensures that both the closest and farthest point of the specimen are in focus at the same time. Any further decrease of the aperture would reduce resolution and extend the focus to unwanted geometrical features from the surrounding environment.
- Photographs should be saved in the highest-resolution uncompressed file format available and should not be trimmed at any stage.

---

*Summary.* Av mode, minimum ISO, specimen distance adjusted to fit the frame, diaphragm aperture adjusted to focus the entire specimen, , white balance custom setting.

*Example.* Av mode, 64 ISO, 50 cm recording distance, f/22, TIFF as a file format for photographs.

---

## Data acquisition

### *Shooting*

- Connect a remote wireless controller with USB interface, such as any wireless presenter, to the computer where the software package [digiCamControl](#) has already been installed and configured.
- Start [digiCamControl](#), turn the cameras on, and check that they all appear in the software interface.

- Use [digiCamControl](#) to configure automatic image acquisition and archiving, and to check that the specimen is correctly framed by each camera. Repeat the procedure for every new specimen that needs to be recorded.

- > Check the frame by each camera with the *Live View function*.

- > In the window to the right of the interface, select the *MSAE* session (or other previously assigned name related to the project) and associate the numeric code of the specimen (e.g., a four-digit inventory number) as *Capture name* and *Series*.

- > Reset the shot counter in the session settings (gear wheel image).

- > At the top of the interface, select *Multiple camera control* and check that the settings of all cameras correspond to those provided in the shooting protocol.

- Use sequential and continuous shooting sessions, i.e. a continuous series of shots to obtain a single complete mesh directly, (27) to obtain a single complete mesh combining at once all the acquired perspective views.

- The perspective change could be achieved by installing the specimen in different positions, and then stopping the turntable for photographic recording in any of the planned poses.

- Use [digiCamControl](#) to control image acquisition by pressing the *next slide* button (which is read as the keyboard 'b' key by the software) on the wireless presenter; [digiCamControl](#) has already been configured to acquire photographs with all the connected cameras at once when a 'b' key is pressed.

- After photographic acquisition, rotate or change the position of the specimen. Repeat the procedure until a complete image coverage is achieved. Ensure adequate horizontal and vertical image overlap (27).

- > In the left side menu of the *Multiple camera control*, viewable by clicking on the tab, press *Capture photos* to take a photo with each of the connected cameras, then rotate the turntable to the next planned pose.

- > Repeat the operation until completing the poses and positions provided by the protocol.
- > After any change in specimen position, use the *Live View* function to check that the specimen is correctly framed by each camera.
- > Additional shots should be acquired for regions with a more complex geometry: e.g. the front and basal views of a cranium.
- > At least 40 shots should be acquired to allow cloud-based UCR-DP reconstruction.
- > Exit *Multiple camera control* and restart the procedure from the beginning to document any additional specimen.

---

*Example for cranial specimens.* After the installation in *position I* (Figure 22, page 73), with the prosthion aligned with the 0, the specimen should be rotated to achieve 10 perspective views from each camera. The procedure should be repeated after changing the specimen to positions *II, III, IV* and *V*, thus resulting in the complete coverage of its external surface. Coverage should be denser for the front and basal standards (i.e., for poses numbered from 8 to 2, Figure 22, page 73).

---

## Data processing and post-processing

### *Mesh processing*

- Start [ReCap Photo](#) and upload to the cloud the photographs to be processed.
  - > Select Create 3D > Object, and press in the centre of the new window to locate the photographs of the specimen which have previously been saved locally.
  - > Select the photographs by clicking on the first and then extending the selection, for example using *SHIFT + DOWN ARROW*.
  - > Click on *OPEN* and then on *CREATE*. Enter the Project name (e.g., *MSAE\_7639*), tick *Auto-crop* and then press *START*.
  - > *My Cloud Drive* displays the percentage of uploading photos of the project to the cloud.

- Once the photos have been uploaded, the percentage of 3D model processing completed is displayed. The processing takes place in *batch mode*, whereby the Autodesk server devotes some machine time to the processing of the 3D model before moving on to others and, possibly, returning to the uploaded data until processing is complete. Thus, a model is completed after a few hours, depending on the congestion of the service.

Yet, it is possible to process several sets of photographs at once.

- Sometimes, in [ReCap Photo](#), the photo upload progress indicator, or the processing progress indicator, freezes due to a software bug. However, the three-dimensional models would still be produced after a few hours, and accessible from the page <https://recap360.autodesk.com>.
- To view a 3D model previously completed and available in the cloud, it must first be downloaded locally in the proprietary RCM format, from the *My Cloud Drive* section, by clicking on the download icon (arrow at the bottom right displayed on the project icon).
- Once downloaded, the 3D model appears in *My Computer* section, from where it can be viewed simply by pressing on it.
- From the visualisation interface it is possible to export a 3D model locally in OBJ or PLY file format by selecting *Export > Export model* and then *Export* again. From the same menu, it is also possible to export images and videos of the model.
- Scale the resulting 3D models to their real dimensions using [ReCap Photo Scale by Value](#) function, inputting the preliminarily recorded calibration baseline average length.

#### *Mesh post-processing*

- Create a working copy of proprietary RCM file to be post-processed.
- Start [ReCap Photo](#) and load the RCM file to be post-processed in the editor.

- Detect any topological issues in the geometry of the 3D model by applying *Analyze > Detect and fix model issues > Detect issues*. Wait for the analysis to be completed.
- Solve the highlighted problems, then repeat the analysis and solve any further detected problem recursively, until the message *Detect issues (no defects)* appears.



## ACKNOWLEDGEMENTS

I would like to thank:

- Prof.ssa Elisabetta Marini, Prof.ssa Simona Distinto, Prof. Stefano Benazzi, and Prof. Damiano Marchi for their guidance, and support, during the development of the present research;
- Valeria Basciu, Davide Bratzu, Marco Casula, Alessio Garau, Nicol Andrea Peddis, Paolo Stara, and Roberto Tronci for contributing to the experiments within their curricular activities at the [Corso di Laurea in Scienze Naturali – Università degli Studi di Cagliari](#);
- Dott.ssa Valeria Succa, Dott. Marco Melis, and Sandro Piludu for facilitating my research at any time;
- Dott. Paolo Deriu, Dott. Corrado Amatiello, and Alessandro Caschili of the [Istituto di Radiologia ed Ecografia Deriu](#) (Cagliari, Italy) for allowing, performing and facilitating the CT-scans;
- The [Department of Archaeology](#) at the University of York and the [Archaeology Data Service](#) team – particularly Professor Julian Richards, Dr Tim Evans, Dr Ray Moore, Dr Holly Wright, and Kieron Niven – for helping my understanding of online sharing, use, and reuse of digital data;
- Dominick John Tompkins for proofreading;
- My family for supporting me at any time.

## REFERENCES

### Bibliography

1. MacKinnon M. Osteological research in classical archaeology. *Am J Archaeol.* 2007;111(3):473–504.  
Available from: <http://www.jstor.org/stable/40027080>
2. Pievani T. *Homo sapiens*. Le nuove storie dell'evoluzione umana. Libreria Geografica; 2017.
3. Manzi G. *Ultime notizie sull'evoluzione umana*. Il Mulino; 2017.
4. Manzi G. *Il grande racconto dell'evoluzione umana*. Il Mulino; 2018.
5. Marchi D. *Il mistero di Homo naledi*. Arnoldo Mondadori Editore; 2013.
6. Luongo G, Perrotta A, Scarpati C. Impact of the AD 79 explosive eruption on Pompeii, I. Relations amongst the depositional mechanisms of the pyroclastic products, the framework of the buildings and the associated destructive events. *J Volcanol Geotherm Res.* 2003;126(3):201–23.  
Available from: <http://www.sciencedirect.com/science/article/pii/S037702730300146X>
7. Luongo G, Perrotta A, Scarpati C, De Carolis E, Patricelli G, Ciarallo A. Impact of the AD 79 explosive eruption on Pompeii, II. Causes of death of the inhabitants inferred by stratigraphic analysis and areal distribution of the human casualties. *J Volcanol Geotherm Res.* 2003;126(3):169–200.  
Available from: <http://www.sciencedirect.com/science/article/pii/S0377027303001471>
8. Gostner P, Pernter P, Bonatti G, Graefen A, Zink AR. New radiological insights into the life and death of the Tyrolean Iceman. *J Archaeol Sci.* 2011;38(12):3425–31.  
Available from: <http://www.sciencedirect.com/science/article/pii/S0305440311002731>

9. Oegg K, Kofler W, Schmidl A, Dickson JH, Egarter-Vigl E, Gaber O. The reconstruction of the last itinerary of “Ötzi”, the Neolithic Iceman, by pollen analyses from sequentially sampled gut extracts. *Quat Sci Rev.* 2007;26(7):853–61.  
Available from: <http://www.sciencedirect.com/science/article/pii/S0277379106003465>
10. Kutschera W, Rom W. Ötzi, the prehistoric Iceman. *Nucl Instruments Methods Phys Res Sect B Beam Interact with Mater Atoms.* 2000;164–165:12–22.  
Available from: <http://www.sciencedirect.com/science/article/pii/S0168583X99011969>
11. Wilkinson MD, Dumontier M, Aalbersberg IJ, Appleton G, Axton M, Baak A, et al. Comment: The FAIR guiding principles for scientific data management and stewardship. *Sci Data.* 2016;3:1–9.
12. Galletta L, Stephens NB, Bardo A, Kivell TL, Marchi D. Three-dimensional geometric morphometric analysis of the first metacarpal distal articular surface in humans, great apes and fossil hominins. *J Hum Evol.* 2019;132:119–36.  
Available from: <http://www.sciencedirect.com/science/article/pii/S0047248418300964>
13. Friess M. Scratching the surface? The use of surface scanning in physical and paleoanthropology. *J Anthropol Sci.* 2012;90:7–31.
14. Ross AH, Keegan WF, Pateman MP, Young CB. Faces divulge the origins of Caribbean prehistoric inhabitants. *Sci Rep.* 2020;10(1):1–9.
15. Sorrentino R, Belcastro MG, Figus C, Stephens NB, Turley K, Harcourt-Smith W, et al. Exploring sexual dimorphism of the modern human talus through geometric morphometric methods. *PLoS One.* 2020;15(2):e0229255–e0229255.  
Available from: <https://pubmed.ncbi.nlm.nih.gov/32059040>

16. Blessi GT, Grossi E, Sacco PL, Pieretti G, Ferilli G. The contribution of cultural participation to urban well-being. A comparative study in Bolzano/Bozen and Siracusa, Italy. *Cities*. 2016;50:216–26.  
Available from: <http://www.sciencedirect.com/science/article/pii/S0264275115001626>
17. Berggren Å, Dell'Unto N, Forte M, Haddow S, Hodder I, Issavi J, et al. Revisiting reflexive archaeology at Çatalhöyük: integrating digital and 3D technologies at the trowel's edge. *Antiquity*. 2015;89(344):433–48.
18. Davies TG, Rahman IA, Lautenschlager S, Cunningham JA, Asher RJ, Barrett PM, et al. Open data and digital morphology. *Proc R Soc B Biol Sci*. 2017;284(1852).
19. Dyani L. The fight for control over virtual fossils. *Nature*. 2019;567:20–3.
20. Weber GW, Bookstein FL. *Virtual anthropology*. Wien: Springer-Verlag / SpringerWienNewYork; 2011.
21. Garvin HM, Stock MK. The utility of advanced imaging in forensic anthropology. *Acad Forensic Pathol*. 2017;6(3):499–516. Available from: <https://doi.org/10.23907/2016.050>
22. Profico A, Bellucci L, Buzi C, Di Vincenzo F, Micarelli I, Strani F, et al. Virtual anthropology and its application in cultural heritage studies. *Stud Conserv*. 2018;64, 2019(6):323–36.
23. Di Vincenzo F, Churchill SE, Buzi C, Profico A, Tafuri MA, Micheli M, et al. Distinct among Neanderthals: the scapula of the skeleton from Altamura, Italy. *Quat Sci Rev*. 2019;217:76–88.
24. Historic England. *3D laser scanning for heritage: advice and guidance on the use of laser scanning in archaeology and architecture*. Swindon: Historic England; 2018.  
Available from: [https://www.bb.reading.ac.uk/bbcswebdav/pid-4178722-dt-content-rid-12904095\\_2/courses/CE1CES-18-9A/Laser scanning for heritage buildings%281%29.pdf](https://www.bb.reading.ac.uk/bbcswebdav/pid-4178722-dt-content-rid-12904095_2/courses/CE1CES-18-9A/Laser%20scanning%20for%20heritage%20buildings%281%29.pdf)

25. Robinson C, Eisma R, Morgan B, Jeffery A, Graham EAM, Black S, et al. Anthropological measurement of lower limb and foot bones using multi-detector computed tomography. *J Forensic Sci.* 2008 Nov 1;53(6):1289–95.  
Available from: <https://doi.org/10.1111/j.1556-4029.2008.00875.x>
26. Adams JW, Olah A, McCurry MR, Potze S. Surface model and tomographic archive of fossil primate and other mammal holotype and paratype specimens of the Ditsong National Museum of Natural History, Pretoria, South Africa. *PLoS One.* 2015 Oct 6;10(10):e0139800–e0139800. Available from: <https://pubmed.ncbi.nlm.nih.gov/26441324>
27. Lussu P, Marini E. Ultra close-range digital photogrammetry in skeletal anthropology: a systematic review. *PLoS One.* 2020;15(4):e0230948.  
Available from: <http://dx.doi.org/10.1371/journal.pone.0230948>
28. Ducke B, Score D, Reeves J. Multiview 3D reconstruction of the archaeological site at Weymouth from image series. *Comput Graph.* 2011;35(2):375–82.  
Available from: <http://dx.doi.org/10.1016/j.cag.2011.01.006>
29. Forte M. 3D archaeology. New perspectives and challenges — the example of Çatalhöyük. *J East Mediterr Archaeol Herit Stud.* 2014;2(1):1–29.
30. Forte M, Dell’Unto N, Jonsson K, Lercari N. Interpretation process at Çatalhöyük using 3D. In: Hodder I, Marciniak A, editors. *Assembling Çatalhöyük*. European Association of Archaeologists; 2015. p. 43–57.  
Available from: <http://e-archaeology.org/assembling-catalhoyuk-book/>
31. Archaeology Data Service and Digital Antiquity guides to good practice. [cited 2020 Apr 20].  
Available from: <https://guides.archaeologydataservice.ac.uk/g2gpwiki>

32. Hanke K. The photogrammetric contribution to archaeological documentation of prehistory. *Int Arch Photogramm Remote Sens.* 2000;33(B5/1; PART 5):355–7. Available from: [https://www.researchgate.net/profile/Klaus\\_Hanke/publication/236155245\\_The\\_photogrammetric\\_contribution\\_to\\_archaeological\\_documentation\\_of\\_prehistory/links/0deec5167d4e379d29000000.pdf](https://www.researchgate.net/profile/Klaus_Hanke/publication/236155245_The_photogrammetric_contribution_to_archaeological_documentation_of_prehistory/links/0deec5167d4e379d29000000.pdf)
33. Ciolfi L, Avram G, Maye L, Dulake N, Marshall MT, Van Dijk D, et al. Articulating co-design in museums: reflections on two participatory processes. *Proc ACM Conf Comput Support Coop Work CSCW.* 2016;27:13–25.
34. Williams H, Pudney C, Ezzeldin A, editors. *Public archaeology: arts of engagement.* Oxford: Archaeopress Publishing Ltd.; 2019.
35. Steen M, Manschot M, Koning N De. Benefits of co-design in service design projects. *Int J Des Vol 5, No 2.* 2011. Available from: <http://www.ijdesign.org/index.php/IJDesign/article/view/890/346>
36. Leong TW, Iversen OS. Values-led participatory design as a pursuit of meaningful alternatives. In: *Proceedings of the Annual Meeting of the Australian Special Interest Group for Computer Human Interaction.* New York, NY, USA: Association for Computing Machinery; 2015. p. 314–323. (OzCHI '15). Available from: <https://doi.org/10.1145/2838739.2838784>
37. Iversen OS, Halskov K, Leong TW. Values-led participatory design. *CoDesign.* 2012 Jun 1;8(2–3):87–103. Available from: <https://doi.org/10.1080/15710882.2012.672575>
38. McDermott F, Maye L, Avram G. Co-designing a collaborative platform with cultural heritage professionals. In: *iHCI Conference'14, September 1-2 2014.* Dublin; 2014.

39. Mason M. Prototyping practices supporting interdisciplinary collaboration in digital media design for museums. *Museum Manag Curatorsh*. 2015 Oct 20;30(5):394–426. Available from: <https://doi.org/10.1080/09647775.2015.1086667>
40. Sofaer JR. *The body as material culture: a theoretical osteoarchaeology*. Topics in Contemporary Archaeology. Cambridge: Cambridge University Press; 2006. Available from: <https://www.cambridge.org/core/books/body-as-material-culture/36F2A7641A05C85B38C3CE7193FFD1C6>
41. Flores JR. *Experimental archaeology: an ethnography of its perceived value and impact in archaeological research*. University of Exeter; 2012.
42. Leakey L, Dzambazova T. Prehistoric collections and 3D printing for education. In: Canessa E, Fonda C, Zennaro M, editors. *Low-Cost 3D Printing for Science, Education & Sustainable Development*. ICTP — The Abdus Salam International Centre for Theoretical Physics; 2013. p. 159–62.
43. Jurda M, Urbanová P. Three-dimensional documentation of Dolní Věstonice skeletal remains: can photogrammetry substitute laser scanning? *Anthropologie*. 2016;54(2):109–18.
44. Kullmer O. Benefits and risks in virtual anthropology. *J Anthropol Sci*. 2008;86:205–7.
45. Gunz P, Kozakowski S, Neubauer S, Le Cabec A, Kullmer O, Benazzi S, et al. Skull reconstruction of the late Miocene ape *Rudapithecus hungaricus* from Rudabánya, Hungary. *J Hum Evol*. 2020;138:102687. Available from: <http://www.sciencedirect.com/science/article/pii/S0047248419301265>
46. Buzi C, Micarelli I, Profico A, Conti J, Grassetti R, Cristiano W, et al. Measuring the shape: performance evaluation of a photogrammetry improvement applied to the Neanderthal skull *Saccopastore 1*. *Acta Imeko*. 2018;7(3):79–85.

47. Jurda M, Urbanová P. Sex and ancestry assessment of Brazilian crania using semi-automatic mesh processing tools. *Leg Med.* 2016;23:34–43.
48. NEMA PS3 / ISO 12052. Digital Imaging and Communications in Medicine (DICOM) Standard. Rosslyn, VA, USA: National Electrical Manufacturers Association; 2017.  
Available from: <http://medical.nema.org/>
49. Senck S, Coquerelle M. Morphological integration and variation in facial orientation in *Pongo pygmaeus pygmaeus*: a geometric morphometric approach via partial least squares. *Int J Primatol.* 2015;36(3):489–512. Available from: <https://doi.org/10.1007/s10764-015-9837-1>
50. Hassett BR, Lewis-Bale T. Comparison of 3D landmark and 3D dense cloud approaches to Hominin mandible morphometrics using structure-from-motion. *Archaeometry.* 2017;59(1):191–203.
51. Aramendi J, Maté-González MA, Yravedra J, Ortega MC, Arriaza MC, González-Aguilera D, et al. Discerning carnivore agency through the three-dimensional study of tooth pits: Revisiting crocodile feeding behaviour at FLK- Zinj and FLK NN3 (Olduvai Gorge, Tanzania). *Palaeogeogr Palaeoclimatol Palaeoecol.* 2017;488:93–102.  
Available from: <https://doi.org/10.1016/j.palaeo.2017.05.021>
52. Guyomarc'h P, Samsel M, Courtaud P, Mora P, Dutailly B, Villotte S. New data on the paleobiology of the Gravettian individual L2A from Cussac cave (Dordogne, France) through a virtual approach. *J Archaeol Sci Reports.* 2017;14:365–73.  
Available from: <http://dx.doi.org/10.1016/j.jasrep.2017.06.005>
53. Human inheritance exhibition featuring Ötzi the Iceman. 2020 [cited 2020 Jun 18].  
Available from: <https://dnalc.cshl.edu/programs/exhibition.html>



54. Wei-Haas M. An artist creates a detailed replica of Ötzi, the 5,300-year-old “Iceman”. 2016 [cited 2020 Jun 18]. Available from: <https://www.smithsonianmag.com/science-nature/artist-creates-detailed-replica-otzi-5300-year-old-iceman-180958151/>
55. Ulguim PF. Recording in situ human remains in three dimensions: applying digital image-based modeling. In: Errickson D, Thompson T, editors. *Human Remains: Another Dimension*. London: Elsevier Academic Press; 2017. p. 71–92.
56. Wilhelmson H, Dell’Unto N. Virtual taphonomy: a new method integrating excavation and postprocessing in an archaeological context. *Am J Phys Anthropol*. 2015;157(2):305–21.
57. Baier W, Rando C. Developing the use of structure-from-motion in mass grave documentation. *Forensic Sci Int*. 2016;261:19–25.  
Available from: <http://dx.doi.org/10.1016/j.forsciint.2015.12.008>
58. Santoro V, Lubelli S, De Donno A, Inchingolo A, Lavecchia F, Introna F. Photogrammetric 3D skull/photo superimposition: a pilot study. *Forensic Sci Int*. 2017;273:168–74.  
Available from: <http://dx.doi.org/10.1016/j.forsciint.2017.02.006>
59. Trizio I, Savini F, Giannangeli A. Integration of three-dimensional digital models and 3D GIS: the documentation of the medieval burials of amiternum (L’Aquila, Italy). *Int Arch Photogramm Remote Sens Spat Inf Sci - ISPRS Arch*. 2018;42(2):1121–8.
60. Randolph-Quinney PS, Haines SD, Kruger A. The use of three-dimensional scanning and surface capture methods in recording forensic taphonomic traces: issues of technology, visualisation, and validation. In: Barone PM, Groen WJM, editors. *Multidisciplinary Approaches to Forensic Archaeology: Topics Discussed During the European Meetings on Forensic Archaeology (EMFA)*. Cham: Springer International Publishing; 2018. p. 115–30.  
Available from: [https://doi.org/10.1007/978-3-319-94397-8\\_8](https://doi.org/10.1007/978-3-319-94397-8_8)

61. Luhmann T, Robson S, Kyle S, Boehm J. Close-range photogrammetry and 3D imaging. 2nd ed. Walter De Gruyter, editor. Berlin: De Gruyter; 2014.
62. Gershtein EC, Willis M, Black SL, Castañeda AM, Buonasera T, Koenig CW, et al. High-resolution mapping and analysis of shiny grooved rock surfaces: the case study of the Skiles Shelter, Lower Pecos, Texas. *Quat Int.* 2017;439:69–82.
63. Ito T. Effects of different segmentation methods on geometric morphometric data collection from primate skulls. *Methods Ecol Evol.* 2019 Nov 1;10(11):1972–84.  
Available from: <https://doi.org/10.1111/2041-210X.13274>
64. Buffa R, Mereu E, Lussu P, Succa V, Pisanu T, Buffa F, et al. A new, effective and low-cost three-dimensional approach for the estimation of upper-limb volume. *Sensors (Switzerland).* 2015;15(6):12342–57.
65. Bennani H, McCane B, Cornwall J. Three dimensional (3D) lumbar vertebrae data set. *Data Sci J.* 2016;15:9:1–15.
66. Katz D, Friess M. Technical note: 3D from standard digital photography of human crania - a preliminary assessment. *Am J Phys Anthropol.* 2014;154(1):152–8.
67. Mallison H, Wings O. Photogrammetry in paleontology – A practical guide. *J Paleontol Tech.* 2014;(12):1–31.
68. Morgan B, Ford ALJ, Smith MJ. Standard methods for creating digital skeletal models using structure-from-motion photogrammetry. *Am J Phys Anthropol.* 2019;169(1):152–60.  
Available from: <http://doi.wiley.com/10.1002/ajpa.23803>
69. Historic England. Photogrammetric applications for cultural heritage - Guidance for good practice. Swindon: Historic England; 2017.

70. Acacia S, Babbetto R, Casanova M, Macchioni E, Pittaluga D. Photogrammetry as a tool for chronological dating of fired bricks structures in Genoa area. *Int Arch Photogramm Remote Sens Spat Inf Sci - ISPRS Arch.* 2017;42(2W5):749–53.
71. Sapirstein P. Accurate measurement with photogrammetry at large sites. *J Archaeol Sci.* 2016;66:137–45. Available from: <http://dx.doi.org/10.1016/j.jas.2016.01.002>
72. Alsadik B, Gerke M, Vosselman G, Daham A, Jasim L. Minimal camera networks for 3D image based modeling of cultural heritage objects. *Sensors (Switzerland).* 2014;14(4):5785–804.
73. Lo Brutto M, Dardanelli G. Vision metrology and structure from motion for archaeological heritage 3D reconstruction: a case study of various roman mosaics. *Acta Imeko.* 2017;6(3):35–44.
74. Inzerillo L. Smart SfM: Salinas archaeological museum. *Int Arch Photogramm Remote Sens Spat Inf Sci - ISPRS Arch.* 2017;42(2W5):369–73.
75. Herries AIR, Murszewski A, Pickering R, Mallett T, Joannes-Boyau R, Armstrong B, et al. Geoarchaeological and 3D visualisation approaches for contextualising in-situ fossil bearing palaeokarst in South Africa: a case study from the ~2.61 Ma Drimolen Makondo. *Quat Int.* 2018;483:90–110. Available from: <https://doi.org/10.1016/j.quaint.2018.01.001>
76. Peng F, Lin SC, Guo J, Wang H, Gao X. The application of SfM photogrammetry software for extracting artifact provenience from palaeolithic excavation surfaces. *J F Archaeol.* 2017;42(4):326–36.
77. Fau M, Cornette R, Houssaye A. Apport de la photogrammétrie à la numérisation 3D d'os de spécimens montés: potentiel et limites. *Comptes Rendus - Palevol.* 2016;15(8):968–77. Available from: <http://dx.doi.org/10.1016/j.crvp.2016.08.003>

78. Langford M, Bilissi E. Langford's advanced photography. 8th ed. Focal Press; 2011.
79. Edwards J, Rogers T. The accuracy and applicability of 3D modeling and printing blunt force cranial injuries. *J Forensic Sci.* 2018;63(3):683–91.
80. Laussedat A. Mémoire sur l'emploi de la chambre claire dans les reconnaissances topographiques. Mallet-Bachelier; 1854.
81. Laussedat A. Mémoire sur l'emploi de la photographie dans la levée des plans. *Comptes rendus des séances l'Académie des Sci.* 1859;49:732–4.
82. Konecny G. Geoinformation - Remote sensing, photogrammetry, and geographic information systems. 2nd ed. Boca Raton: CRC Press - Taylor & Francis Group; 2014.
83. Vivian Thompson F. Stereo-photo surveying. *Geogr J.* 1908;31(5):534–49.
84. Jacobshagen B. The limits of conventional techniques in anthropometry and the potential of alternative approaches. *J Hum Evol.* 1981;10(8):633–7.
85. Hertzberg HT. E, Dupertuis CW, Emanuel I. Stereophotogrammetry as an anthropometric tool. *Photogramm Eng.* 1957;23(5):942–7.
86. Burke P., Beard HF. Stereophotogrammetry of the face. *Am J Orthod.* 1967;53(10):769–82.
87. Björn H, Lundqvist C, Hjelmström P. A photogrammetric method of measuring the volume of facial swellings. *J Dent Res.* 1954;33(3):295–308.  
Available from: <https://doi.org/10.1177/00220345540330030201>
88. Cuzzi JR, Herron RE, Hugg JE, Rouk KR. Calibration of a biostereometric system. In 1971. p. 26–8.  
Available from: <https://doi.org/10.1117/12.975338>
89. Liebelt RA, Herron RE. Stereometric analysis in the field of anatomy. In 1971. p. 24–6.  
Available from: <https://doi.org/10.1117/12.975333>

90. Berkowitz S, Cuzzi J. Biostereometric analysis of surgically corrected abnormal faces. *Am J Orthod.* 1977;72(5):526–38.
91. Jacobshagen B. Grenzen konventioneller Techniken und Möglichkeiten alternativer Ansätze in der Anthropometrie: mit einem Beispiel für den Einsatz der Biophotogrammetrie in der Schädelmeßtechnik. *Z Morphol Anthropol.* 1980;71(3):306–21.
92. Kearfott KJ, Juang RJ, Marzke MW. Implementation of digital stereo imaging for analysis of metaphyses and joints in skeletal collections. *Med Biol Eng Comput.* 1993;31:149–56.
93. Gaber O, Künzel KH. Man from the Hauslabjoch. *Exp Gerontol.* 1998;33(7–8):655–60.
94. McHenry K, Bajcsy P. An overview of 3D data content, file formats and viewers. Tech Rep Image Spat Data Anal Gr Natl Cent Supercomput Appl. 2008;(December 2008):21.  
Available from: <http://isda.ncsa.illinois.edu/peter/publications/techreports/2008/NCSA-ISDA-2008-002.pdf>
95. Callieri M, Dell'Unto N, Dellepiane M, Scopigno R, Soderberg B, Larsson L. Documentation and interpretation of an archeological excavation: an experience with dense stereo reconstruction tools. *VAST 11th Int Symp Virtual Reality, Archaeol Cult Herit.* 2011;33–40.  
Available from: <http://vcg.isti.cnr.it/Publications/2011/CDDSSL11>
96. Potenziani M, Callieri M, Dellepiane M, Corsini M, Ponchio F, Scopigno R. 3DHOP: 3D heritage online presenter. *Comput Graph.* 2015 Nov 1 [cited 2019 Oct 11];52:129–41. Available from: <https://www.sciencedirect.com/science/article/pii/S0097849315001041?via%3Dihub>
97. Potenziani M, Corsini M, Callieri M, Benedetto D, Ponchio F, Dellepiane M, et al. An advanced solution for publishing 3D content on the Web. 2014;

98. Callieri M, Ranzuglia G, Dellepiane M, Cignoni P, Scopigno R. Meshlab as a complete open tool for the integration of photos and colour with high-resolution 3D geometry data. *Comput Appl Quant Methods Archaeol*. 2012;406–16.
99. Cignoni P, Cignoni P, Callieri M, Callieri M, Corsini M, Corsini M, et al. MeshLab: an open-source mesh processing tool. *Sixth Eurographics Ital Chapter Conf*. 2008;129–36.
100. Ponchio F. Multiresolution structures for interactive visualization of very large 3D datasets. Clausthal University of Technology; 2009. Available from: <http://citeseerx.ist.psu.edu/viewdoc/download?doi=10.1.1.633.1318&rep=rep1&type=pdf>
101. Sarigu M, Floris GU, Floris R, Pusceddu V. The osteological collection of the University of Cagliari: from Early Neolithic to Modern Age. *HOMO-Journal Comp Hum Biol*. 2016. Available from: <http://dx.doi.org/10.1016/j.jchb.2016.03.001>
102. D'Amore G, Di Marco S, Floris G, Pacciani E, Sanna E. Craniofacial morphometric variation and the biological history of the peopling of Sardinia. *HOMO*. 2010;61(6):385–412. Available from: <http://www.sciencedirect.com/science/article/pii/S0018442X10001071>
103. Sanna E. *Il popolamento della Sardegna e le origini dei Sardi*. Cagliari: CUEC - Cooperativa Universitaria Editrice Cagliariitana; 2006.
104. Lodde M, Marini E. Anthroponet: il censimento del materiale scheletrico proveniente dagli scavi della Sardegna. *Antrocom, Online J Anthropol*. 2008;4(1).
105. Germanà F. *L'uomo in Sardegna dal Paleolitico all'Età nuragica*. Carlo Delfino editore; 1995.
106. Lerma JL, Navarro S, Seguí AE, Cabrelles M. Range-based versus automated markerless image-based techniques for rock art documentation. *Photogramm Rec*. 2014;29(145):30–48.

107. Fraile FJL, García LMG, Klink AC. 3D documentation and use of dstretch for two new sites with Post-Palaeolithic rock art in Sierra Morena, Spain. *Rock Art Res.* 2016;33(2):127–42.
108. McDonald J, Catacora A, de Koning S, Middleton E. Digital technologies and quantitative approaches to recording rock art in the Great Basin, USA. *J Archaeol Sci Reports.* 2016;10:917–30. Available from: <http://dx.doi.org/10.1016/j.jasrep.2016.03.052>
109. Davis A, Belton D, Helmholtz P, Bourke P, McDonald J. Pilbara rock art: laser scanning, photogrammetry and 3D photographic reconstruction as heritage management tools. *Herit Sci.* 2017;5(1):1–16.
110. Fernández-Lozano J, Gutiérrez-Alonso G, Ruiz-Tejada MÁ, Criado-Valdés M. 3D digital documentation and image enhancement integration into schematic rock art analysis and preservation: the Castrocontrigo Neolithic rock art (NW Spain). *J Cult Herit.* 2017;26:160–6. Available from: <http://dx.doi.org/10.1016/j.culher.2017.01.008>
111. Clini P, Frapiccini N, Mengoni M, Nespeca R, Ruggeri L. SFM technique and focus stacking for digital documentation of archaeological artifacts. *Int Arch Photogramm Remote Sens Spat Inf Sci - ISPRS Arch.* 2016;41(July):229–36.
112. Porter ST, Huber N, Hoyer C, Floss H. Portable and low-cost solutions to the imaging of Paleolithic art objects: a comparison of photogrammetry and reflectance transformation imaging. *J Archaeol Sci Reports.* 2016;10:859–63. Available from: <http://dx.doi.org/10.1016/j.jasrep.2016.07.013>
113. Maté González MÁ, Yravedra J, González-Aguilera D, Palomeque-González JF, Domínguez-Rodrigo M. Micro-photogrammetric characterization of cut marks on bones. *J Archaeol Sci.* 2015;62:128–42.

114. Courtenay LA, Yravedra J, Mate-González MÁ, Aramendi J, González-Aguilera D. 3D analysis of cut marks using a new geometric morphometric methodological approach. *Archaeol Anthropol Sci.* 2017;1–15.
115. Yravedra J, Diez-Martín F, Egeland CP, Maté-González MÁ, Palomeque-González JF, Arriaza MC, et al. FLK West (Lower Bed II, Olduvai Gorge, Tanzania): a new early Acheulean site with evidence for human exploitation of fauna. *Boreas.* 2017;46(4):816–30.
116. Maté-González MÁ, Palomeque-González JF, Yravedra J, González-Aguilera D, Domínguez-Rodrigo M. Micro-photogrammetric and morphometric differentiation of cut marks on bones using metal knives, quartzite, and flint flakes. *Archaeol Anthropol Sci.* 2018;10(4):805–16.
117. Otárola-Castillo E, Torquato MG, Hawkins HC, James E, Harris JA, Marean CW, et al. Differentiating between cutting actions on bone using 3D geometric morphometrics and Bayesian analyses with implications to human evolution. *J Archaeol Sci.* 2018;89:56–67.
118. Bennett MR, Falkingham P, Morse SA, Bates K, Crompton RH. Preserving the impossible: conservation of soft-sediment Hominin footprint sites and strategies for three-dimensional digital data capture. *PLoS One.* 2013;8(4):e60755.
119. Marzke MW, Tocheri MW, Steinberg B, Femiani JD, Reece SP, Linscheid RL, et al. Comparative 3D quantitative analyses of trapeziometacarpal joint surface curvatures among living catarrhines and fossil hominins. *Am J Phys Anthropol.* 2010;141(1):38–51.
120. Tanner JM, Weiner JS. The reliability of the photogrammetric method of anthropometry, with a description of a miniature camera technique. *Am J Phys Anthropol.* 1949;7(2):145–86.
121. Hunt EE, Giles E. An evaluation of the photo-metric camera. *Am J Phys Anthropol.* 1956;14(3):429–36.



122. Berbesque JC, Hoover KC. Frequency and developmental timing of linear enamel hypoplasia defects in Early Archaic Texan hunter-gatherers. *PeerJ*. 2018;6:e4367.  
Available from: <https://peerj.com/articles/4367>
123. Knyaz VA, Zheltov SY, Stepanyants DG. Automated photogrammetric system for photorealistic skull 3D reconstruction. *Proc SPIE - Int Soc Opt Eng*. 2001;4309:336–45.  
Available from: <https://www.scopus.com/inward/record.uri?eid=2-s2.0-0035058052&doi=10.1117%2F12.410892&partnerID=40&md5=6b982d6a780540741b2e5414767fc5de>
124. Knyaz VA, Gaboutchian A V. Photogrammetry-based automated measurements for tooth shape and occlusion analysis. *Int Arch Photogramm Remote Sens Spat Inf Sci - ISPRS Arch*. 2016;41(July):849–55.
125. Gaboutchian A V., Knyaz VA, Leybova NA. Measurements of cuspal slope inclination angles in palaeoanthropological applications. *ISPRS - Int Arch Photogramm Remote Sens Spat Inf Sci*. 2017;XLII-2/W4(May):185–91.
126. Cole G, Kingham E, Waldron T. Printing pathology: a case study in presenting pathological human skeletal remains for education and display. *J Inst Conserv*. 2018;42(1):18–33.  
Available from: <https://doi.org/10.1080/19455224.2018.1550431>
127. Moher D, Liberati A, Tetzlaff J, Altman DG, Altman D, Antes G, et al. Preferred reporting items for systematic reviews and meta-analyses: the PRISMA statement. *PLoS Med*. 2009;6(7).
128. Bertsatos A, Chovalopoulou M-E. A novel method for analyzing long bone diaphyseal cross-sectional geometry. A GNU Octave CSG Toolkit. *Forensic Sci Int*. 2019;297:65–71. Available from: <https://doi.org/10.1016/j.forsciint.2019.01.041>

129. Morales CA da C, Dias PEM, Melani RFH. Demonstration of protocol for computer aided forensic facial reconstruction with free software and photogrammetry. *JRD - J Res Dent.* 2014;2(1):77–90.
130. Micheletti N, Chandler JH, Lane SN. Structure from motion (SFM) photogrammetry. In: Clarke, LE and Nield, JM (Eds) *Geomorphological Techniques (Online Edition)*. London: British Society for Geomorphology; 2015.
131. Gonzalez-Aguilera D, López-Fernández L, Rodriguez-Gonzalvez P, Hernandez-Lopez D, Guerrero D, Remondino F, et al. GRAPHOS - Open-source software for photogrammetric applications. *Photogramm Rec.* 2018 Mar [cited 2019 Dec 10];33(161):11–29.  
Available from: <http://doi.wiley.com/10.1111/phor.12231>
132. Furukawa Y, Ponce J. Accurate, dense, and robust multi-view stereopsis. *IEEE Trans Pattern Anal Mach Intell.* 2010;32(8):1362–76.
133. Moulon P, Bezi A. Python Photogrammetry Toolbox: a free solution for three-dimensional documentation. *ArcheoFoss.* 2013;(June):1–12, hal-00834940.  
Available from: <http://hal-enpc.archives-ouvertes.fr/hal-00834940>
134. Chalás I, Urbanová P, Kotulanová Z, Jandová M, Králík M, Kozlíková B, et al. Forensic 3D facial identification software (FIDENTIS). In: *Proceedings of the 20th World Meeting of the International Association of Forensic Sciences.* 2014.
135. Scopigno R, Callieri M, Dellepiane M, Ponchio F, Potenzi M. Delivering and using 3D models on the web: are we ready? *Virtual Archaeol Rev.* 2017;8(17):1–9.
136. Joint Committee for Guides in Metrology. *Evaluation of measurement data — Guide to the expression of uncertainty in measurement.* International Organization for Standardization; 2008.

137. Joint Committee for Guides in Metrology. International vocabulary of metrology — Basic and general concepts and associated terms (VIM). 3rd ed. International Organization for Standardization; 2012.  
Available from: [http://www.bipm.org/utils/common/documents/jcgm/JCGM\\_200\\_2008.pdf](http://www.bipm.org/utils/common/documents/jcgm/JCGM_200_2008.pdf)
138. Bräuer G, Knußmann R. Grundlagen der osteometrie. In: Anthropologie Handbuch der Vergleichenden Biologie des Menschen. Stuttgart: Springer; 1988. p. 129–59.
139. Bland JM, Altman DG. Measuring agreement in method comparison studies. *Stat Methods Med Res.* 1999;8(2):135–60.
140. Fedorov A, Beichel R, Kalphaty-Cramer J, Finet J, Fillion-Robbin J-C, Pujol S, et al. 3D slicer as an image computing platform for the quantitative imaging network. *Magn Reson Imaging.* 2012;30(9):1323–41.
141. Martin R, Saller K. Lehrbuch der Anthropologie in Systematischer Darstellung mit Besonderer Berücksichtigung der Anthropologischen Methoden - Band I. Stuttgart: Gustav Fischer; 1957.
142. Bookstein FL. Morphometric tools for landmark data: geometry and biology. Cambridge: Cambridge University Press; 1991.  
Available from: [https://www.amazon.com/Morphometric-Tools-Landmark-Data-Geometry/dp/0521585988#reader\\_0521585988](https://www.amazon.com/Morphometric-Tools-Landmark-Data-Geometry/dp/0521585988#reader_0521585988)
143. Wärmländer SKTS, Garvin H, Guyomarc'h P, Petaros A, Sholts SB. Landmark typology in applied morphometrics studies: what's the point? *Anat Rec.* 2019;302(7):1144–53.
144. Neter J, Wasserman W, Kutner MH. Applied linear regression models. Irwin; 1989.
145. D'Agostino RB, Belanger A. A suggestion for using powerful and informative tests of normality. *Am Stat.* 1990 Jul 3;44(4):316–21. Available from: <http://www.jstor.org/stable/2684359>

146. Bland JM, Altman DG. Agreement between methods of measurement with multiple observations per individual. *J Biopharm Stat.* 2007;17(4):571–82.
147. Currier DP. *Elements of Research in Physical Therapy*, 3rd Edition. Wolters Kluwer; 1992.
148. Lussu P, Marini E. A photorealistic collection of *Homo sapiens* crania for research and dissemination. *MorphoMuseumM.* 2020;1–2.
149. Nikita E. *Osteoarchaeology: A Guide to the Macroscopic Study of Human Skeletal Remains*. Vol. 1, Forensic Anthropology. London: Academic Press; 2017.
150. Weinberg SM, Scott NM, Neiswanger K, Brandon CA, Marazita ML. Digital three-dimensional photogrammetry: evaluation of anthropometric precision and accuracy using a Genex 3D camera system. *Cleft Palate-Craniofacial J.* 2004;41(5):507–18.
151. Weinberg SM, Naidoo S, Govier DP, Martin RA, Kane AA, Marazita ML. Anthropometric precision and accuracy of digital three-dimensional photogrammetry: comparing the Genex and 3DMD imaging systems with one another and with direct anthropometry. *J Craniofac Surg.* 2006;17(3):477–83.
152. Atzeni E. La necropoli di cultura “Ozieri” a San Benedetto di Iglesias (CA). In: Alba L, Canino G, editors. *La collezione Pistis-Corsi e il patrimonio archeologico del comune di Iglesias*. Iglesias; 2001. p. 25–9.
153. Lussu P, Casula S, Bratzu D. Conference poster: Cloud-based 3D reconstruction of skeletal remains from San Benedetto necropolis (Sardinia, Italy). In: *1st Palaeontological Virtual Congress - Palaeontology in the virtual era*. Vicente D. Crespo, Esther Manzanares, Rafael Marquina-Blasco, Maite Suñer, José Luis Herráiz, Arturo Gamonal, Fernando Antonio M. Arnal, Humberto G. Ferrón, Francesc Gascó and Carlos Martínez-Pérez.; 2018. p. 50.  
Available from: <https://www.uv.es/palaeovc/Documentos /1stPVC BOOK OF ABTRACTS.pdf>

154. Lussu P, Casula S, Bratzu D. Conference poster: Cloud-based 3D reconstruction of skeletal remains from San Benedetto necropolis (Sardinia, Italy). In: 1st Palaeontological Virtual Congress -Palaeontology in the virtual era. 2018.  
Available from: [https://www.researchgate.net/publication/329702667\\_Cloud-based\\_3D\\_reconstruction\\_of\\_skeletal\\_remains\\_from\\_San\\_Benedetto\\_Necropolis\\_Sardinia\\_Italy](https://www.researchgate.net/publication/329702667_Cloud-based_3D_reconstruction_of_skeletal_remains_from_San_Benedetto_Necropolis_Sardinia_Italy)
155. Tykot RH. Radiocarbon dating and absolute chronology in Sardinia and Corsica. In: Skeates R, Whitehouse R, editors. Radiocarbon dating and Italian Prehistory. Rome: British School at Rome; 1994.
156. Lebrun R, Orliac MJ. MorphoMuseum: an online platform for publication and storage of virtual specimens. *Paleontol Soc Pap*. 2016 Sep 27 [cited 2019 Nov 12];22:183–95. Available from: [https://www.cambridge.org/core/product/identifier/S1089332617000146/type/journal\\_article](https://www.cambridge.org/core/product/identifier/S1089332617000146/type/journal_article)
157. The London Charter for the computer-based visualisation of cultural heritage (Draft 2.1). 2009.  
Available from: <http://www.londoncharter.org>
158. Hart CMD, Friedmann E, Hill M. Online course-taking and student outcomes in California community colleges. *Educ Financ Policy*. 2016 Jul 12;13(1):42–71.  
Available from: [https://doi.org/10.1162/edfp\\_a\\_00218](https://doi.org/10.1162/edfp_a_00218)
159. Bastir M, García-Martínez D, Torres-Tamayo N, Palancar CA, Fernández-Pérez FJ, Riesco-López A, et al. Workflows in a virtual morphology lab: 3D scanning, measuring, and printing. *J Anthropol Sci*. 2019;97:107–34.
160. Acsádi G, Nemeskéry J. History of human life span and mortality. Akadémiai Kiadó, Budapest. 1970.

161. Ferembach D, Schwidetzky I, Stloukal M. Recommendations for age and sex diagnoses of skeletons. *J Hum Evol.* 1980;9(7):517–49.  
Available from: <http://www.sciencedirect.com/science/article/pii/0047248480900615>
162. Brothwell DR. *Digging Up Bones*. 3rd ed. Ithaca. New York: Cornell University Press; 1981.
163. Lovejoy CO. Dental wear in the Libben population: its functional pattern and role in the determination of adult skeletal age at death. *Am J Phys Anthropol.* 1985 Sep 1;68(1):47–56.  
Available from: <https://doi.org/10.1002/ajpa.1330680105>
164. Meindl RS, Lovejoy CO. Ectocranial suture closure: a revised method for the determination of skeletal age at death based on the lateral-anterior sutures. *Am J Phys Anthropol.* 1985 Sep 1;68(1):57–66. Available from: <https://doi.org/10.1002/ajpa.1330680106>

## Figure index

<b>Figure 1.</b> Interactive visualisation of the ascending aorta from CT-scanning data of a living subject who gave explicit consent to this image publication.....	12
<b>Figure 2.</b> Interactive visualisation of three-dimensional data from a total-body CT-scan of a living subject: the author.....	13
<b>Figure 3.</b> Interactive visualisation of the skeletal system from a total-body CT-scan of a living subject: the author.....	13
<b>Figure 4.</b> Anatomical modules in a cranium of <i>Pongo pygmaeus pygmaeus</i> (Northwest Bornean orangutan). Blue surface and yellow landmarks: cranial base (sphenoid bone including basion); blue landmarks: orbital outline; orange surface and red landmarks: maxillary bone (49). Image by Sascha Senck and Michael Coquerelle. Reprinted with the authors' permission.....	14
<b>Figure 5.</b> Side-by-side comparison of Neanderthal and modern human skulls from the Cleveland Museum of Natural History. Original photo by Matt Celeskey, licensed under CC BY-SA 2.0; modified by DrMikeBaxter and Paolo Lussu. ....	15
<b>Figure 6.</b> Ötzi the Iceman's mummified corpse, as preserved in a cold room at the Südtiroler Archäologiemuseum (Museo Archeologico dell'Alto Adige, Bolzano/Bozen, Italy). Image credit: Südtiroler Archäologiemuseum. Public domain.....	16
<b>Figure 7.</b> Gary Staab's recreation of Ötzi the Iceman's mummified corpse on display at the DNA Learning Center (Cold Spring Harbor, New York, the United States). Public domain. ....	17
<b>Figure 8.</b> Application of the mathematical model of the central projection imaging to calculate the spatial coordinates of object point $x$ from its projected image points $p_1$ , $p_2$ , and $p_3$ and camera perspective centres $o_1$ , $o_2$ , and $o_3$ .....	20
<b>Figure 9.</b> The pioneering work of Hertzberg et al. (1956) (85) produced elevation contour maps of the human body.....	26

<b>Figure 10.</b> Point cloud with colour information. Public domain original image modified by Paolo Lussu. ...	30
<b>Figure 11.</b> Two over imposed triangular polygon meshes. Public domain original images modified by Paolo Lussu.....	30
<b>Figure 12.</b> Texture images (left) and their projection on a polygon mesh 3D model (right). In this way textures map point-to-point the colour of the object, as represented for the three-dimensional models of a toy (above) and of cranium MSAE-6230, reconstructed with digital photogrammetry (Museo Sardo di Antropologia ed Etnografia, MuSAE). Upper 3D model provided by Keenan Crane. Upper images by Warren Moore, modified by Paolo Lussu. Reprinted with the author's permission. ....	32
<b>Figure 13.</b> Figure 5: Effects of different Levels of Detail applied to the Stanford Bunny 3D model (left to right: 69451, 3851 and 948 polygons). Image by Federico Ponchio (100). Reprinted with the author's permission. ....	34
<b>Figure 14.</b> Some terms and acronyms variably associated with the photogrammetric technique, including obsolete (†) ones.....	41
<b>Figure 15.</b> Flow chart for the study identification. ....	44
<b>Figure 16.</b> Distribution of the publication journals within SCImago disciplinary areas. ....	47
<b>Figure 17.</b> Classification of reviewed studies according to their aim. Data up to December 31st, 2018. ...	48
<b>Figure 18.</b> Cloud-based UCR-DP (27) 3D model of a human vertebra obtained with macro lenses (left) compared with a specimen digitized with $\mu$ CT (right), the recognised standard for three-dimensional reconstruction of skeletal remains (60). ....	63
<b>Figure 19.</b> Cloud UCR-DP 3D model compared to: offline UCR-DP 3D model of Saccopastore 1 from Buzi et al. (2018) (46) (top of the page); 3D model segmented from a standard CT-scan with 0.7 mm slice thickness (bottom of the page). ....	64
<b>Figure 20.</b> Comparison between UCR-DP (left) and CT-scanning (right) in describing the cranium MSAE-6428 (MuSAE, Università degli Studi di Cagliari, Italy). a1-a2. Visual restitution of the whole	



specimen. b1-b2. Mesh density for the whole specimen. c1-c2. Mesh density detailing the geometry. UCR-DP data collection with two Canon EOS 1200D DSLRs at 100 ISO, using prime 50 mm f/1.8 lenses, 50 cm shooting distance, 5500 K light sources; 3D reconstruction via ReCap Photo cloud-based environment. CT data collection with a Siemens SOMATOM Definition Flash CT-scanner and 0.75 mm slice thickness; segmentation via 3D Slicer.....66

**Figure 21.** In a cloud-based software environment the processing logic, including the hardware infrastructure and the software services, is hosted into remote servers operated by a third-party services provider. Users access the services via their local hardware and an Internet connection. Original image by Sam Johnston, licensed under CC BY-SA 3.0; modified by Paolo Lussu..... 71

**Figure 22.** Studio equipment, specimen installation and perspective changes for 3D model acquisition through UCR-DP. <sup>a</sup> EOS 1200D digital single-lens reflex cameras (Canon Inc., Tokyo, Japan). <sup>b</sup> Camera tripods (Manfrotto, Italy) on which cameras were installed at different heights (0 cm and 50 cm) and tilts (0° and 35°) with respect to the specimen centre. <sup>c</sup> Lightbox. <sup>d</sup> Turntable with planned poses. <sup>I-V</sup> Specimen positioning. <sup>0-9</sup> Turntable poses acquired for each specimen position..... 73

**Figure 23.** The sample at the Istituto di Radiologia ed Ecografia Deriu (Cagliari, Italy) just minutes before the start of the CT-scanning..... 75

**Figure 24.** Summary of the anthropometric measurements taken in front and lateral views. The linear length a-b was defined on each specimen between two arbitrary landmarks and used for UCR-DP 3D model scaling..... 76

**Figure 25.** Frequency histograms showing the differences between interrater mean measurements carried out with the alternative techniques under study. ....80

**Figure 26.** Bland & Altman plots describing the interrater agreement between UCR-DP and osteometry for all measurements. Above, the plot showing the absolute differences. Each point identifies the mean of the three repetitions concerning any combination of osteometric measurement, specimen, and

rater. Below, the plot showing the differences as a percentage. Here, measurements are grouped through a different point style. 1, skull length (#1). 2, skull breadth (#8). 3, skull total height (#17). 4, total face breadth (#45). 5, biorbital breadth (#44). 7, frontal chord (#29). 8, parietal chord (#30). 9, occipital chord (#31). ..... 83

**Figure 27.** Bland & Altman plots describing the interrater agreement between UCR-DP and CT-scanning for all measurements. Above, the plot showing the absolute differences. Each point identifies the mean of the three repetitions concerning any combination of osteometric measurement, specimen, and rater. Below, the plot showing the differences as a percentage. Here, measurements are grouped through a different point style. 1, skull length (#1). 2, skull breadth (#8). 3, skull total height (#17). 4, total face breadth (#45). 5, biorbital breadth (#44). 7, frontal chord (#29). 8, parietal chord (#30). 9, occipital chord (#31). (141). ..... 84

**Figure 28.** Bland & Altman plots describing the interrater agreement between CT-scanning and osteometry for all measurements. Above, the plot showing the absolute differences. Each point identifies the mean of the three repetitions concerning any combination of osteometric measurement, specimen, and rater. Below, the plot showing the differences as a percentage. Here, measurements are grouped through a different point style. 1, skull length (#1). 2, skull breadth (#8). 3, skull total height (#17). 4, total face breadth (#45). 5, biorbital breadth (#44). 7, frontal chord (#29). 8, parietal chord (#30). 9, occipital chord (#31). (141). ..... 85

**Figure 29.** Bland & Altman plots describing the interrater agreement between UCR-DP and osteometry for measurement 1, skull length (#1) (141). Above, the plot showing the absolute differences between the mean measured values for each specimen. Below, the plot showing the scatter of the measured values for each specimen (subjects from 59 to 7688); here, the regression line for the differences between the techniques is drawn in light violet, and its confidence interval in light red. .... 86

**Figure 30.** Bland & Altman plots describing the interrater agreement between UCR-DP and osteometry for measurement 2, skull breadth (#8) (141). Above, the plot showing the absolute differences between the mean measured values for each specimen. Below, the plot showing the scatter of the measured values for each specimen (subjects from 59 to 7688); here, the regression line for the differences between the techniques is drawn in light violet, and its confidence interval in light red.....87

**Figure 31.** Bland & Altman plots describing the interrater agreement between UCR-DP and osteometry for measurement 3, skull total height (#17) (141). Above, the plot showing the absolute differences between the mean measured values for each specimen. Below, the plot showing the scatter of the measured values for each specimen (subjects from 59 to 7688); here, the regression line for the differences between the techniques is drawn in light violet, and its confidence interval in light red. ....88

**Figure 32.** Bland & Altman plots describing the interrater agreement between UCR-DP and CT-scanning for measurement 1, skull length (#1) (141). Above, the plot showing the absolute differences between the mean measured values for each specimen. Below, the plot showing the scatter of the measured values for each specimen (subjects from 59 to 7688); here, the regression line for the differences between the techniques is drawn in light violet, and its confidence interval in light red.....89

**Figure 33.** Bland & Altman plots describing the interrater agreement between UCR-DP and CT-scanning for measurement 2, skull breadth (#8) (141). Above, the plot showing the absolute differences between the mean measured values for each specimen. Below, the plot showing the scatter of the measured values for each specimen (subjects from 59 to 7688); here, the regression line for the differences between the techniques is drawn in light violet, and its confidence interval in light red. ....90

**Figure 34.** Bland & Altman plots describing the interrater agreement between UCR-DP and CT-scanning for measurement 3, skull total height (#17) (141). Above, the plot showing the absolute differences between the mean measured values for each specimen. Below, the plot showing the scatter of the

measured values for each specimen (subjects from 59 to 7688); here, the regression line for the differences between the techniques is drawn in light violet, and its confidence interval in light red.....91

**Figure 35.** Bland & Altman plots describing the interrater agreement between CT-scanning and osteometry for measurement 1, skull length (#1) (141). Above, the plot showing the absolute differences between the mean measured values for each specimen. Below, the plot showing the scatter of the measured values for each specimen (subjects from 59 to 7688); here, the regression line for the differences between the techniques is drawn in light violet, and its confidence interval in light red.....92

**Figure 36.** Bland & Altman plots describing the interrater agreement between CT-scanning and osteometry for measurement 2, skull breadth (#8) (141). Above, the plot showing the absolute differences. between the mean measured values for each specimen. Below, the plot showing the scatter of the measured values for each specimen (subjects from 59 to 7688); here, the regression line for the differences between the techniques is drawn in light violet, and its confidence interval in light red.....93

**Figure 37.** Bland & Altman plots describing the interrater agreement between CT-scanning and osteometry for measurement 3, skull total height (#17) (141). Above, the plot showing the absolute differences between the mean measured values for each specimen. Below, the plot showing the scatter of the measured values for each specimen (subjects from 59 to 7688); here, the regression line for the differences between the techniques is drawn in light violet, and its confidence interval in light red.....94

**Figure 38.** Geographic and temporal distribution of the retrieval sites..... 112

**Figure 39.** MSAE 3612 from Su Cungiareddu de Serafini (Carbonia), attributed to the Middle Bronze Age (Nuragic I). ..... 113

**Figure 40.** MSAE 3611 from Su Cungiareddu de Serafini (Carbonia), attributed to the Middle Bronze Age (Nuragic I). ..... 114

<b>Figure 41.</b> MSAE 3621 from Su Cungiareddu de Serafini (Carbonia), attributed to the Middle Bronze Age (Nuragic I).....	114
<b>Figure 42.</b> MSAE 6830 from Su Sercone (Orgosolo) – Roman.....	115
<b>Figure 43.</b> MSAE 6450 from Cornus (Cuglieri, Riola Sardo) – Púnic-Roman.....	116
<b>Figure 44.</b> MSAE 1061 vertebra. ....	117
<b>Figure 45.</b> MSAE 6438 male lower jaw. ....	118
<b>Figure 46.</b> Anatomical specimen of a newborn from the 19 <sup>th</sup> century. ....	119
<b>Figure 47.</b> (Bianca Kramer & Jeroen Bosman, <a href="https://101innovations.wordpress.com">https://101innovations.wordpress.com</a> ; DOI: 10.5281/zenodo.1147025).....	123
<b>Figure 48.</b> The 3D model sample from the Teaching Collection preserved at the MuSAE. ....	139
<b>Figure 49.</b> A measurement being carried out online in MorphoMuseum using 3DHOP interface. The glabella - opisthocranion length is being taken on MSAE 6426. ....	141
<b>Figure 50.</b> The title of the MuSAE teaching webpage sharing the 3D sample and the associated teaching material. ....	144
<b>Figure 51.</b> The entrance (left) and two drawings (right) showing the planimetry and a cross-section of the Tomba II (San Benedetto necropolis, Iglesias, Italy). Photograph and drawings from Atzeni (2001) (152)..	145
<b>Figure 52.</b> The 3D model sample from San Benedetto Neolithic necropolis (Iglesias, Italy). Original image by Davide Bratzu; modified by Paolo Lussu and reprinted with the author’s permission. ....	146
<b>Figure 53.</b> 3D model orientation with ReCap Photo (Autodesk Inc., USA).....	146
<b>Figure 54.</b> The vertical display screen to be placed in the four main rooms of the MuSAE. ....	149
<b>Figure 55.</b> Detail of the display stand allowing both tilt and table positions for the touch screen of the interactive station. ....	151
<b>Figure 56.</b> Concave led display screen suggested for the immersive environment at the MuSAE. Public domain image.....	152

<b>Figure 57.</b> 360° interactive and clickable view of the MuSAE. ....	153
<b>Figure 58.</b> The other virtual tours of Google. ....	153
<b>Figure 59.</b> Gold-anodized aluminum plate installed on both Pioneer 10 and 11 space probes, launched in 1972 and 1973 respectively. The plate features a pictorial message intended to be intelligible to the intelligent life that could intercept it. It includes basic information about the Solar System, the trajectory of the spacecraft, the appearance and relative size of the humans, and the position of the Sun relative to 14 pulsars. By Vectors by Oona Räisänen (Mysid); designed by Carl Sagan & Frank Drake; artwork by Linda Salzman Sagan – Vectorized in CorelDRAW from NASA image GPN-2000-001623. Public Domain.....	156

## Table index

<b>Table 1.</b> Summary of the reviewed articles. ....	45
<b>Table 2.</b> Shooting protocol summary.....	51
<b>Table 3.</b> Software used for mesh processing, post-processing, and analysis.....	55
<b>Table 4.</b> Summary of literature on UCR-DP accuracy and reliability. ....	62
<b>Table 5.</b> Study design – Sample and measurements. ....	72
<b>Table 6.</b> Summary of the osteometric and arbitrary measurements performed on specimens and 3D models. ....	76
<b>Table 7.</b> Accuracy of UCR-DP with respect to osteometry and CT-scanning in measuring human crania. ....	82
<b>Table 8.</b> Reliability of UCR-DP, osteometry, and CT-scanning in measuring human crania.....	96
<b>Table 9.</b> The reconstructed sample, including links to Google Maps and Anthroponet (104).....	111
<b>Table 10.</b> Online repositories for skeletal 3D models sharing.....	126
<b>Table 11.</b> Suggested five-level metadata for UCR-DP 3D models (31).....	137
<b>Table 12.</b> Interactive exercises to engage students. In parenthesis the measurement number of Martin and Saller (141). ....	143
<b>Table 13.</b> Facilities, components and specifications of the multimedia experience at the MuSAE. ....	150